

2013

Mechanistic Studies on the Effect of Additives in SmI₂-Mediated Reactions

Kimberly Ann Choquette
Lehigh University

Follow this and additional works at: <http://preserve.lehigh.edu/etd>

 Part of the [Chemistry Commons](#)

Recommended Citation

Choquette, Kimberly Ann, "Mechanistic Studies on the Effect of Additives in SmI₂-Mediated Reactions" (2013). *Theses and Dissertations*. Paper 1457.

This Dissertation is brought to you for free and open access by Lehigh Preserve. It has been accepted for inclusion in Theses and Dissertations by an authorized administrator of Lehigh Preserve. For more information, please contact preserve@lehigh.edu.

Mechanistic Studies on the Effect of Additives in SmI₂-Mediated Reactions

by

Kimberly A. Choquette

Presented to the Graduate and Research Committee
of Lehigh University
in Candidacy for the Degree of
Doctor of Philosophy

In

Department of Chemistry

Lehigh University

May 20, 2013

© 2013 Copyright

Kimberly A. Choquette

Approved and recommended for acceptance as a dissertation in partial fulfillment
of the requirements for the degree of Doctor of Philosophy

Kimberly A. Choquette

Mechanistic Studies on the Effect of Additives in SmI₂-Mediated Reactions

April 3, 2013

Defense Date

Dr. Robert A. Flowers, II, Chair
Dissertation Director

Approved Date

Committee Members:

Dr. Ned Heindel, Member

Dr. Natalie Foster, Member

Dr. Patrick Wernett, Outside
Member

Acknowledgements

I would like to give a very sincere thank you to my advisor, Dr. Flowers. I will always appreciate the support you gave me, even at times when I was struggling in classes or in the lab. The confidence you had in me helped me build that confidence in myself, and grow into a research chemist. I could never thank you enough for that. I also have to thank Sada, who trained me and mentored me in my first years in the Flowers group. Thank you for your patience and kindness toward me, I am certain I would not have gotten through my first years at Lehigh without you helping me through the millions of questions I had. The camaraderie and sense of community in the Flowers' group is incredible, and I learned so much from all of the grad students I have had the opportunity to work in lab with: Brian, Jim, Sherri, Todd, Niki, Gaby, Esther, Rajni, Godfred and Teshia. I am very grateful to have had my graduate career in a lab where all of the students were genuinely interested in each other's work, and instead of competition, we all helped each other rise up to greater standards. Also, thanks for making life at Lehigh fun and not just a job. I don't know how I could have shown up every day if I didn't know that if I needed to take a break from the lab that someone would be happy to escape and walk to the bookstore with me. Thank you to Brian Casey, for helping me so much, keeping me sane in lab, and being a great friend.

Thank you very much to my husband, Matthew. You have always showed unwavering support for all my decisions, in and before grad school, and I could not be more grateful for how much you are always there for me. For my Dad and Mom, who raised two strong-willed women, I don't think I would have gotten through any of my schooling without the work ethic you instilled in me. Dad, I will never forget your advice

to “reach higher than you might think you can, what’s the worst that can happen?” Your guidance is what led me believe I could give grad school a shot, and you were right! To my Choquette family: thank you for always being so patient and understanding with my schedule all of these years. You are all always so supportive, I couldn’t ask for a more loving family.

To my very best friend, Kim Bucha, thank for always being there for me and being an ear to listen to my problems. Kim and Katie Young, thank you for forcing me to go on weekend adventures with you and giving me time to laugh and relax. Chrissy, thank you for being a great friend and sister, calming me down when I’m stressed out and helping me get by all of these years. You always make me know how proud you are of me, and that is an amazing feeling that I will never take for granted.

And really, I think this is all due to Mrs. Graeca, who made PJAS and science seem so cool to a 7th grader. Thanks, Coach.

Table of Contents

Acknowledgements.....	iv
Table of Contents.....	vi
List of Figures.....	xii
List of Tables.....	xv
List of Schemes.....	xvii
Solvent Abbreviations.....	xxii
Abstract.....	1
Chapters	
1. Introduction to SmI ₂ as a single electron reductant	
1.1 Samarium Diiodide.....	3
1.2 Role of Additives.....	4
1.2.1 Coordinating Additives.....	4
1.2.1.1 Hexamethylphosphoramide.....	6
1.2.1.2 DMPU and TMU.....	9
1.2.1.3 Glycols and Ethers.....	12
1.2.2 Proton Sources.....	15
1.2.2.1 Alcohols.....	16
1.2.2.2 SmI ₂ and Water.....	23
1.2.3 Transition Metal Salts.....	31
1.3 SmI ₂ in Organic Synthesis.....	35
1.3.1 Organosamarium Intermediates.....	35
1.3.2 Grignard and Barbier Reaction.....	38

1.3.3 Reformatsky-Type Reactions.....	42
1.3.4 Ketyl-Olefin Coupling.....	48
1.3.5 Halide-Olefin Coupling.....	52
1.3.6 Pinacol Coupling.....	53
1.4 Project Goals.....	59
2. SmI ₂ Reduction of an Aldehyde vs. α,β -Unsaturated Ester	
2.1 Background and Significance.....	60
2.1.1 SmI ₂ Reduction of Various Functional Groups.....	60
2.1.2 SmI ₂ in Cascade Syntheses.....	65
2.1.3 Selective Cyclization of Functionalized Dialdehyde Compounds...69	
2.2 Experimental.....	72
2.2.1 Materials.....	72
2.2.2 Instrumentation.....	72
2.2.3 Methods.....	73
2.2.3.1 Synthesis of 3-butyl-3,6,6-trimethylcyclohex-1-ene methylcarboxylate.....	73
2.2.3.2 General Procedure for SmI ₂ Reduction.....	75
2.2.3.3 General Procedure for Stopped-Flow Studies.....	75
2.3 Results.....	76
2.3.1 Kinetic Data.....	76
2.3.1.1 Pseudo-First Order Rates.....	77
2.3.1.2 Radical Traps.....	79
2.3.1.3 Initial Rates.....	82

2.3.2 Computational Data.....	84
2.4 Conclusions.....	86
3. Impact of HMPA on the Samarium Barbier Reaction	
3.1 Background and Significance.....	89
3.1.1 SmI ₂ and HMPA in Organic Reactions.....	89
3.1.2 Samarium-Barbier Reaction.....	93
3.2 Experimental.....	99
3.2.1 Materials.....	99
3.2.2 Instrumentation.....	100
3.2.3 Methods.....	100
3.2.3.1 General Procedure for the Samarium Barbier Reaction..	100
3.2.3.2 General Procedure for Stopped-Flow Studies.....	101
3.2.3.3 General Procedure for NMR Experiments.....	102
3.3 Results.....	102
3.3.1 Kinetic Analysis of Samarium Barbier Reagents.....	102
3.3.2 DFT Calculations.....	106
3.3.3 NMR Titration Experiments.....	107
3.3.4 Proposed Mechanism of the Samarium Barbier Reaction with HMPA.....	110
3.3.4.1 Derivation of Rate Equation.....	110
3.3.4.2 Derived Equation Fit to Saturation Plots.....	112
3.3.4.3 Proposed Mechanism.....	115

3.3.5	Samarium Barbier Reaction with Secondary and Tertiary Alkyl Halides.....	116
3.3.5.1	Kinetic Analysis of Samarium Barbier Reagents.....	117
3.3.5.2	NMR Titration Experiments.....	120
3.4	Conclusions.....	121
4.	Catalytic Ni(II) in SmI ₂ Reactions: Sm(II) or Ni(0) Chemistry?	
4.1	Background and Significance.....	122
4.1.1	Transition metal salts in SmI ₂ reactions.....	122
4.2	Experimental.....	126
4.2.1	Materials.....	126
4.2.2	Instrumentation.....	127
4.2.3	Methods.....	128
4.2.3.1	General Procedure for the Samarium Barbier Reaction with Ni(II).....	128
4.2.3.2	General Procedure for Stopped-Flow Studies.....	128
4.2.3.3	Procedure for the Preparation of TEM Samples.....	129
4.3	Results.....	129
4.3.1	UV-Vis Identification of Ni(0).....	129
4.3.2	TEM Images of Ni Nanoparticles.....	131
4.3.3	Kinetic Data: Reaction Progress Kinetic Analysis.....	131
4.3.4	Proposed Mechanism.....	143
4.4	Conclusions.....	144
5.	Sm-H ₂ O—Reduction of Lactones	

5.1 Background and Significance.....	145
5.1.1 SmI ₂ -H ₂ O Reduction Systems.....	146
5.1.2 SmI ₂ -H ₂ O Reduction of Lactones.....	148
5.2 Experimental.....	157
5.2.1 Materials.....	157
5.2.2 Instrumentation.....	157
5.2.3 Methods.....	158
5.2.3.1 General Procedure for Lactone Reduction with SmI ₂ - H ₂ O.....	158
5.2.3.2 General Procedure for Stopped-Flow Studies.....	158
5.3 Results.....	159
5.3.1 Lactone Reductions.....	159
5.3.2 Kinetic Analysis of SmI ₂ -H ₂ O Reduction of Lactones.....	161
5.4 Conclusions.....	166
6. Sm-H ₂ O-Amine Reduction System	
6.1 Background and Significance.....	168
6.1.1 SmI ₂ -H ₂ O and SmI ₂ -Amine Additive Systems.....	168
6.1.2 SmI ₂ -H ₂ O-Amine Reduction Systems.....	171
6.2 Experimental.....	181
6.2.1 Materials.....	181
6.2.2 Instrumentation.....	181
6.2.3 Methods.....	181
6.2.3.1 General Procedure for reduction with SmI ₂ -H ₂ O-amine.....	181

6.2.3.2 General Procedure for Stopped-Flow Studies.....	182
6.3 Results.....	183
6.3.1 Synthetic Results.....	184
6.3.2 Kinetic Results.....	186
6.3.2.1 Pseudo-First Order Rates.....	186
6.3.2.2 Impact of H ₂ O.....	188
6.3.2.3 Impact of the Basicity of Amines.....	190
6.3.2.4 Kinetic Isotope Effects.....	191
6.3.2.5 Activation Parameters.....	192
6.3.3 Proposed Mechanism.....	194
6.3.4 Derived Rate Expression.....	197
6.3.4 Conclusions.....	200
7. Concluding Remarks.....	201
References.....	205
8. Appendix	
8.1 SmI ₂ Reduction of an Aldehyde vs. α,β -Unsaturated Ester.....	216
8.2 Impact of HMPA on the Samarium Barbier Reaction.....	231
8.3 Catalytic Ni(II) in SmI ₂ Reactions: Sm(II) or Ni(0) Chemistry?.....	271
8.4 Sm-H ₂ O—Reduction of Lactones.....	278
8.5 Sm-H ₂ O-Amine System.....	290
Curriculum Vitae.....	299

List of Figures

1.1 Crystal structure of SmI ₂ in THF.....	5
1.2 (a) SmI ₂ in THF with low concentrations of HMPA, [SmI ₂ (HMPA) ₄] (b) SmI ₂ in THF with 10equiv HMPA, [Sm(HMPA) ₆ I ₂].....	8
1.3 SmI ₂ -HMPA coordination complexes.....	9
1.4 (a) [Sm(DMPU) ₃ (THF)I ₂] (b) [Sm(DMPU) ₆]I ₂	11
1.5 TMU coordinated to Sm metal center, [Sm(THF) ₂ (TMU) ₂ I ₂].....	11
1.6 (a) <i>cis</i> -SmI ₂ [O(CH ₂ CH ₂ OMe) ₂] ₂ , {SmI ₂ (diglyme) ₂ }; (b) SmI ₂ [(CH ₃ OCH ₂ CH ₂ OCH ₃) ₃], {SmI ₂ (glyme) ₃ }; (c) Sm[(OCH ₂ CH ₂ OCH ₂ CH ₂ O) ₃]I ₂ , {[Sm(DG) ₃]I ₂ }; (d) [Sm(OCH ₂ CH ₂ OCH ₂ CH ₂ OMe) ₃]I ₂ , {[Sm(DGME) ₃]I ₂ }.....	4
1.7 Shift in UV band of SmI ₂ with the addition of MeOH.....	18
1.8 Absorption spectra of SmI ₂ (2.5 mM) in THF in the presence of increasing amount of H ₂ O. Inset shows the absorption spectra of SmI ₂ upon the addition of larger amounts of H ₂ O.....	26
1.9 Absorption spectra of SmI ₂ in THF (dot) and DME (solid) containing 1.25 M H ₂ O. Inset shows the absorption spectra of SmI ₂ in (a) THF and (b) DME.....	27
2.1 Rate order of n-butyl acrylate under low concentration pseudo-first order.....	79
2.2 α,β-unsaturated ester substrate “dimer” tethered to Sm metal.....	83
2.3 Cyclic α,β-unsat. ester: 3-butyl-3,6,6-trimethylcyclohex-1-ene methyl carboxylate..	84
3.1 Equivalents of HMPA versus k _{obs} for the reduction of 1 in the presence and absence of 3	104
3.2 HMPA-alkyl halide complex proposed by Wigfield.....	105
3.3 Calculated gas phase complex between HMPA and bromoethane.....	106

3.4 Iodoethane ^1H NMR shifts.....	109
3.5 Iodoethane ^{13}C NMR shifts.....	109
3.6 Bromoethane ^1H NMR shifts.....	109
3.7 Bromoethane ^{13}C NMR shifts.....	110
3.8 Michaelis-Menten saturation plot.....	113
3.9 Relationship between rate expression 3.10 and Michaelis-Menten saturation kinetics.....	113
3.10 Fit of saturation plot of iodododecane (1).....	114
3.11 Fit of saturation plot of bromodecane (2).....	114
3.12 Proposed complex formations with HMPA and (a) primary alkyl halides, (b) secondary alkyl halides and (c) tertiary alkyl halides.....	120
4.1 UV-vis spectra of SmI_2 in THF containing increasing amounts of NiI_2	130
4.2 TEM image of nanoparticles.....	131
4.3 Time-resolved UV-vis spectrum of the reduction of $\text{Ni}(\text{DPPE})_2\text{Cl}_2$ by SmI_2	132
4.4 Plot of initial rates vs. $[\text{SmI}_2]$ for the reduction of $\text{Ni}(\text{DPPE})_2\text{Cl}_2$ by SmI_2	133
4.5 Rate vs $[\text{SmI}_2]$ for same excess experiments, 1 mol% $\text{Ni}(\text{DPPE})_2$	137
4.6 Rate vs $[\text{SmI}_2]$ for same excess experiments, 3 and 5 mol% $\text{Ni}(\text{DPPE})_2$	138
4.7 Plot of rate vs $[\text{SmI}_2]$ for different excess experiment, order of 4	139
4.8 Plot of rate vs $[\text{SmI}_2]$ for different excess experiment, order of 5	140
4.9 Turn-over frequency of $\text{Ni}(\text{II})$ in the samarium Barbier reaction.....	141
4.10 Rate order of SmI_2 in the $\text{Ni}(\text{II})$ catalyzed samarium Barbier reaction.....	141
4.11 Rate constant of $\text{Ni}(\text{DPPE})_2\text{Cl}_2$ in the samarium Barbier reaction.....	142
5.1 SmI_2 chelation through ketyl radical and pendant ester carbonyl.....	164

6.1 Ligands attempted in the reduction of 4-phenyl-2-butanone with SmI ₂ -H ₂ O.....	176
6.2 Plot of k_{obs} vs [hydrocinnamic methylester].....	187
6.3 Plot of k_{obs} vs [H ₂ O].	189
6.4 UV-Vis of SmI ₂ with pyrrolidine and pyrrolidine-H ₂ O.....	191
6.5 Eyring plot from the reduction of hydrocinnamic acid methyl ester with (a) SmI ₂ - H ₂ O-Et ₃ N and (b) SmI ₂ -H ₂ O-pyrrolidine.....	193
6.6 Transition state images of (a) highly ordered H ₂ O coordinated to SmI ₂ in THF (b) hydrogen bond elongation as Et ₃ N deprotonates coordinated H ₂ O (c) hydrogen bond elongation as pyrrolidine carries out a more facile deprotonation of coordinated H ₂ O.....	195

List of Tables

1.1 Oxidation Potentials of SmI ₂ with increasing amounts of HMPA.....	9
1.2 Oxidation potentials determined vs. Ag/AgNO ₃	10
1.3 Impact of proton donor source on SmI ₂ reduction of β–hydroxy ketones.....	17
1.4 Observed rate constant, reaction order and k _H /k _D for reduction of acetophenone by SmI ₂ and proton donors.....	19
1.5 Reductive Sm-mediated 4- <i>exo-trig</i> cyclization.....	21
1.6 Intramolecular Sm-Barbier reaction with Fe(III) cat.....	33
1.7 Variety of haloketones and carbonyl substrates in the Reformatsky reaction.....	47
1.8 Largo carbocycles from Sm- Reformatsky reaction.....	47
1.9 Coupling of N-sulfinyl imine with aldehydes to form β–amino alcohols.....	57
2.1 Pseudo first order rates for the reduction of octanal and <i>n</i> -butyl acrylate by SmI ₂	78
2.2 Radical scavengers reacted with octanal and <i>n</i> -butyl acrylate.....	81
2.3 Initial rates for the reduction of octanal and <i>n</i> -butyl acrylate by SmI ₂	82
2.4 Energy calculations for starting substrates and their corresponding radical anions...	85
3.1 Rate orders for alkyl halide, 3-pentanone, SmI ₂ and HMPA.....	103
3.2 NMR shifts of primary alkyl halides in the presence of HMPA.....	108
3.3 Fit of experimental data to equation 3.11, shown in Figures 3.12 and 3.13.....	115
3.4 Rate orders of the reagents in the samarium Barbier reaction.....	118
3.5 Fit of experimental data to equation 3.11.....	119
4.1 Various transition metal salts in the samarium Barbier reaction.....	123
4.2 Reaction of 4 and 5 with SmI ₂ and/or various Ni additives.....	134
4.3 Same excess RPKA reaction conditions.....	136

4.4 Same excess RPKA conditions.....	138
4.5 Conditions for different excess experiments to determine reaction orders of the substrates 4 and 5	139
4.6 Reaction orders for the reagents in the Ni(II)-catalyzed Barbier reaction.....	142
5.1 SmI ₂ -H ₂ O-mediated reduction of lactones with directing groups.....	160
5.2 Lactone substrates in kinetic analysis.....	162
6.1 Effect of nitrogen-containing ligands on reduction and radical cyclization.....	170
6.2 Reduction of benzoic acid with SmI ₂ in a basic environment.....	172
6.3 Reaction conditions for the reduction of hydrocinnamic acid methyl ester by SmI ₂ - H ₂ O-amine.....	185
6.4 Esters reduced to alcohols by SmI ₂ -H ₂ O-Et ₃ N.....	186
6.5 Results from Pseudo-first order rate experiments.....	187
6.6 Rate of reduction with different amines in the reduction of hydrocinnamic methyl ester.....	190
6.7 Kinetic isotope effects with Et ₃ N and pyrrolidine.....	192
6.8 Activation parameters with SmI ₂ -H ₂ O-amine.....	193

List of Schemes

1.1	Synthesis of SmI ₂ in THF.....	3
1.2	Cross coupling of iodomethyl silyl ether with aldehydes with SmI ₂ -TMU.....	12
1.3	Sm-mediated reductive cyclization with <i>t</i> BuOH.....	17
1.4	Reduction and protonation of acetophenone with SmI ₂ -proton source	20
1.5	Alteration of reduction and cyclization pathways with SmI ₂ -proton sources.....	22
1.6	Product distribution of cyclized products based on the proton sources used in the SmI ₂ reduction.....	23
1.7	Reduction of <i>o</i> -allyloxyiodobenzene radical trap with SmI ₂ and SmI ₂ -H ₂ O.....	24
1.8	Single electron reduction of carbonyl containing substrates with SmI ₂	25
1.9	Reduction of alkyl halides through single electron transfer with SmI ₂	25
1.10	Dynamic equilibrium of H ₂ O coordinating with SmI ₂ in THF. R= H.....	30
1.11	Coupling of imines with ketones using SmI ₂ -NiI ₂	31
1.12	Formation of diamines with SmI ₂ -Ni(II).....	32
1.13	Synthesis of natural product Sequosempervirin A.....	33
1.14	Intramolecular Sm-Barbier reaction with Fe(III) cat.....	34
1.15	Radical and organosamarium coupling	36
1.16	SmI ₂ coupling quenched with D ₂ O or an electrophile.....	37
1.17	Synthesis of 1,2- <i>trans</i> -C-glycosides with SmI ₂	37
1.18	Radical cyclization followed by organocuprate addition.....	38
1.19	Samarium Barbier reaction.....	39
1.20	Tandem samarium Barbier reactions with selective reduction of the halides.....	39

1.21 Intramolecular samarium Barbier reaction for the formation of 10-isocyano-4-cadinene.....	40
1.22 Ring-closing samarium Barbier reaction in the synthesis of (-)-kendomycin.....	41
1.23 Samarium Barbier reaction with NiI ₂ in the total synthesis of variecolin.....	42
1.24 SmI ₂ -mediated Reformatsky reaction.....	42
1.25 Reformatsky reaction—ketyl radical followed by β-elimination.....	43
1.26 Reformatsky reaction with esters.....	43
1.27 Reformatsky reaction—Sm(III) coordination.....	44
1.28 Reformatsky coupling of ethyl bromopropionate and cyclohexanone.....	44
1.29 Stereo controlled Reformatsky reaction.....	45
1.30 Sm(II) chelation in the Reformatsky reaction.....	45
1.31 Sm-enolates in Reformatsky reactions.....	46
1.32 Reformatsky reaction in the synthesis of Taxol®.....	48
1.33 Ketyl-olefin coupling—ketyl radical formed first.....	49
1.34 “Alkene-first” mechanism in ketyl-olefin couplings.....	49
1.36 3- <i>Exo-trig</i> cyclizations of β,γ-unsaturated carbonyl compounds.....	50
1.37 Ketyl-olefin cyclization in the synthesis of englerin A.....	51
1.38 Halide-olefin cyclization.....	52
1.39 Halide-olefin cyclization followed by tandem Barbier reaction.....	53
1.40 Stereoselective syntheses of <i>cis</i> -hydrindane cores.....	53
1.41 Pinacol coupling with two aldehydes or ketones.....	54
1.42 Potential pathways for Sm-mediated pinacol coupling.....	54
1.43 Intramolecular pinacol reductive coupling.....	55

1.44	Ketyl-radical cyclization to form caryose.....	56
1.45	Intramolecular pinacolization for the bicyclic ring system of Taxol®.....	56
1.46	Pinacol coupling to form 14-membered ring of diazonamide A.....	58
1.47	Pinacol homocoupling of imines.....	59
2.1	Ketyl-olefin radical cyclization to form lactones.....	62
2.2	Relative rates of reduction by SmI ₂	63
2.3	Rate constants for the reduction by SmI ₂	64
2.4	Sm-mediated cascade for the synthesis of (±)-hypnophilin.....	66
2.5	Tandem intramolecular radical cyclization, Sm-Barbier coupling.....	67
2.6	Synthesis of a <i>Strychnos</i> alkaloid.....	67
2.7	Radical-anionic cascade for the synthesis of the BCD ring structure of penitrem D.....	68
2.8	Sm-mediated ring closure in the total synthesis of Mucocin.....	69
2.9	Proposed intermediate for cyclization.....	71
2.10	Possible mechanistic pathways for cyclization	71
2.11	Homocoupling of octanal.....	78
2.12	Reductive coupling SmI ₂ reduction of <i>n</i> -butyl acrylate.....	78
2.13	Thiophenol as radical trap in SmI ₂ reduction of an aldehyde.....	80
2.14	Possible mechanistic pathways for the reductive cyclization.....	88
3.1	(a) ketyl-olefin and (b) halide-olefin cyclizations promoted with SmI ₂ -HMPA.....	90
3.2	HMPA post-electron transfer role in pinacol coupling.....	91
3.3	Sm-HMPA in ketyl-olefin cyclization.....	91
3.4	Post-electron transfer role of HMPA in ketyl-olefin cyclization.....	93
3.5	Samarium Barbier reaction.....	94

3.6	Possible mechanisms of the samarium Barbier reaction.....	95
3.7	Radical vs. organosamarium pathways.....	97
3.8	Intermolecular examples of Sm-Barbier reaction.....	98
3.9	Samarium Barbier reaction with primary alkyl halides.....	102
3.10	Rate limiting step of the samarium Barbier reaction with HMPA.....	110
3.11	Proposed mechanism of the Sm-Barbier reaction with HMPA.....	116
3.12	Samarium Barbier reaction with secondary and tertiary alkyl halides.....	117
4.1	Samarium Barbier reaction with catalytic amount of FeCl ₃	122
4.2	Catalytic amount of NiI ₂ used in SmI ₂ reactions.....	123
4.3	Intramolecular Barbier reaction with catalytic NiI ₂	124
4.4	Halide-olefin cyclization with NiI ₂	125
4.5	Ni(II) catalyzed samarium Barbier reaction.....	133
4.6	Catalytic cycle of Ni(0)-mediated Barbier coupling.....	144
5.1	SmI ₂ -H ₂ O reduction of aromatic carboxylic acids.....	147
5.2	Ring-opening reduction of lactones by SmI ₂ -H ₂ O.....	149
5.3	Competition studies for the reduction of lactones by SmI ₂ -H ₂ O.....	150
5.4	Proposed pathway for the reduction of six-membered lactones by SmI ₂ -H ₂ O.	151
5.5	Competition studies with 6-membered lactone and 2-oxabicyclo[2,2,2]octan-3-one.....	152
5.6	Use of lactone intermediate in the selective reduction of aliphatic diesters.....	153
5.7	Proposed mechanism for the reduction of 1,3-diesters with SmI ₂ -H ₂ O.....	154
5.8	Radical cyclization cascade initiated through lactone reduction by SmI ₂ -H ₂ O.....	154
5.9	Retrosynthesis analysis of stolonidiol through triol a	155

5.10	Proposed pathway for the cascade cyclization through $\text{SmI}_2\text{-H}_2\text{O}$ reduction.....	156
5.11	Reductive cyclizations of lactones using $\text{SmI}_2\text{-H}_2\text{O}$ enabled by directing group effect.....	161
6.1	Reduction of substituted benzoic acid with $\text{SmI}_2\text{-H}_2\text{O-KOH}$	173
6.2	Reductions carried out with $\text{Sm-H}_2\text{O-amine}$	175
6.3	Proposed mechanism for the reduction of ketones by $\text{Sm-H}_2\text{O-amine}$	178
6.4	Proposed mechanism for the reduction of alkyl halides by $\text{Sm-H}_2\text{O-amine}$	179
6.5	Proposed mechanism for the reduction of benzyl alcohol by $\text{Sm-H}_2\text{O-amine}$	180
6.6	(a) Ketyl radicals formed through SmI_2 reduction of aldehydes or ketones (b) radical anion from ester single-electron reduction.....	184
6.7	Proposed transition state mechanism of the $\text{SmI}_2\text{-H}_2\text{O-amine}$ system.....	196
6.8	Deleterious effect of high concentrations of H_2O with $\text{SmI}_2\text{-H}_2\text{O-amine}$	197
6.9	Initial rate determining steps of the reduction of esters by $\text{SmI}_2\text{-H}_2\text{O-amine}$	198
6.10	Pathway of ester reduction by $\text{SmI}_2\text{-H}_2\text{O-amine}$	199

Abbreviations List:

Tetrahydrofuran	THF
Acetonitrile	MeCN
Hexamethylphosphoramide	HMPA
Cyclic Voltammetry	CV
Ethyl acetate	EtOAc
Tertiary butanol	<i>t</i> BuOH
Methanol	MeOH
Trifluoroethanol	TFE
Diethylene glycol	DG
Diethylene glycol monomethyl ether	DGME
1,2-dimethoxyethane	DME or glyme
Bis(2-methoxyethyl)ether	diglyme
equiv	equivalents

Abstract

Samarium diiodide (SmI_2) was first introduced to synthetic chemists in 1980. Although initially considered an esoteric compound, SmI_2 is now a standard reductant in organic laboratories and its use in synthesis is featured in nearly 100 publications a year. The unique place held by SmI_2 in the arsenal of synthetic chemists is a result of its versatility in mediating numerous, fundamentally important reactions in organic synthesis including reductions, reductive couplings, and cascade reactions. While numerous reactions have been developed for SmI_2 , its scope in synthesis has not been fully realized as new applications for this reagent are steadily being discovered.

One of the intriguing features of SmI_2 is that the addition of cosolvents or additives can be used to control the chemo- and diastereoselectivity of reactions. In fact, nearly all synthetic procedures utilize additives that are critical for the success of reactions initiated by SmI_2 . Additives commonly utilized to alter reactions of SmI_2 are typically classified into three major groups: (1) Lewis bases, including HMPA and other electron donor ligands and chelating ethers, (2) proton sources (predominantly water and alcohols), and (3) inorganic additives (NiI_2 , FeCl_3 , etc.).

The research presented in this defense focuses on studying well-established SmI_2 -additive systems to gain mechanistic information on the role of the additive in SmI_2 reactions. Within the systems studies we determined: (a) relative rates of reduction between α,β -unsaturated esters and aldehydes, (b) the dual role of HMPA as a cosolvent in the samarium Barbier reaction, (c) the change in the reaction pathway when catalytic

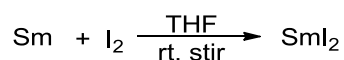
amounts of Ni(II) salts are added to SmI₂ reactions, (d) the impact of H₂O added to the Sm-mediated ring opening reduction of lactones, and (e) the mechanism of action of the powerful Sm-H₂O-amine additive system in the unprecedented reduction of esters. The systematic study of SmI₂-additive systems has led to a deeper understanding of the chemistry of SmI₂ reagent systems, providing a profound impact on their applications in organic synthesis and the development of general approaches to making the chemistry of SmI₂ more efficient.

Chapter 1. Introduction to SmI₂ as a single electron reductant

1.1 Samarium Diiodide

Samarium diiodide (SmI₂) is a versatile single-electron reductant which can reduce various functional groups under mild reaction conditions and facilitate radical and anionic carbon-carbon bond forming events. Over 2,000 publications can be found on new synthetic adaptations and detailed mechanistic studies of this single-electron reductant. While numerous reactions have been developed utilizing SmI₂, its scope in synthesis has not been fully realized as new applications and selective methods for the synthesis of multifunctional targets are steadily being discovered.

Samarium, a lanthanide metal, is most stable in its +3 oxidation state. Formation of a stable divalent samarium reagent results in a powerful single electron reductant. The most widely used Sm(II) reagent is SmI₂, which is easily made by reacting Sm metal with 1,2-diiodoethane or I₂ in THF (Scheme 1.1).¹ Homogeneous reactions with the divalent reductant can be carried out at room temperature, under inert atmosphere.



Scheme 1.1 Synthesis of SmI₂ in THF

Kagan introduced SmI₂ as a useful, soluble, and mild single-electron reductant in 1979,¹ and since has been expanded well beyond its initial label of being a “specialized” reagent. In the years following his seminal report, Kagan and others extended the breadth of substrate applications by demonstrating the ability of SmI₂ to efficiently carry out

deoxygenations,^{1,2} reduce sulfoxides and sulfones,^{3,4} phosphine oxides,^{3,4} epoxides,^{5,6} alkyl and aryl halides,⁶⁻¹² carbonyls,^{1,13,14} and conjugated double bonds.^{15,16} The rate at which SmI₂ reduces the different functional groups varies significantly. As a consequence, SmI₂ can be used to selectively reduce functional groups for follow-up bond-forming reactions in complex substrates.

1.2 Role of Additives

One of the unique features of SmI₂ is that the addition of cosolvents or additives can augment or control its reactivity. Remarkable changes in the rate, diastereoselectivity, and chemoselectivity of organic reactions initiated by SmI₂ can be achieved through addition of suitable additives to the reductant. In fact, nearly all Sm-mediated reactions in the literature utilize additives that are crucial for the success of the reaction. Additives commonly used in SmI₂ reactions can be classified into three groups: (1) Lewis bases, including HMPA and other electron donor ligands and chelating ethers, (2) proton sources (predominantly water and alcohols), and (3) inorganic additives (NiI₂, FeCl₃).

1.2.1 Coordinating Additives

The ionic radius of samarium is influenced by many different factors. Lanthanides experience the “lanthanide contraction” which arises from ineffective shielding of the 4f electrons, resulting in an increase in the effective nuclear charge and causing the atomic radius to decrease in size across the lanthanide series. The ionic radius of Sm is also

influenced by its oxidation number. Sm(III) has an ionic radius of 1.098 Å; however, Sm(II) is larger, at 1.36 Å.¹⁷ The increased ionic radius enables Sm(II) to accommodate up to 12 ligands in the coordination sphere, although coordination numbers of 6-8 are more common, depending on the ligand size. Since the f-orbital is buried beneath the p- and d-orbitals, the interaction of lanthanides with ligands is dominated by steric and electrostatic interactions.¹⁷

Lanthanides have a tendency to fill their coordination sphere by sequestering solvent. Crystallographic studies by Evans and coworkers showed that when SmI₂ is made in THF, the solvated structure is SmI₂(THF)₅, where the oxygen atoms of THF ligate to the very oxophilic Sm-metal center (Figure 1.1).¹⁸ Later studies by Flowers employing vapor pressure osmometry also established that SmI₂ is monomeric in THF solutions.^{19,20}

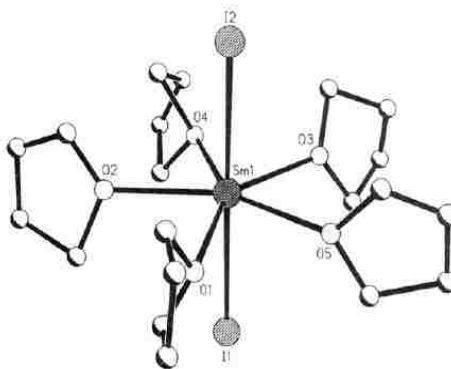


Figure 1.1 Crystal structure of SmI₂ in THF

A great deal of synthetic and mechanistic work has been carried out with SmI₂ in different solvents and cosolvent systems to determine the effect they have on the

coordination sphere of the lanthanide metal. Sm is very oxophilic, so the metal has a tendency to interact with oxygen-containing additives, solvent, and substrates. The affinity Sm has for the ligands dictates the complex that forms, and the coordinated ligands have been found to play an essential role in mediating the mechanistic features critical for the success of the reaction.^{3,4,21-23} A collection of mechanistic studies on these systems has shown that coordinating additives control divalent samarium reactivity through two main avenues: (1) changing the thermodynamic redox potential of samarium,^{6,8-12} and (2) controlling the steric bulk around the divalent metal center,^{19,24,25} which dictates the degree of interaction Sm(II) has with the substrate or the solvent.

1.2.1.1 Hexamethylphosphoramide

Lewis bases containing basic oxygen or nitrogen atoms are important promoters of reactions initiated by SmI₂. The most commonly utilized Lewis base in SmI₂ transformations is hexamethylphosphoramide (HMPA). The addition of HMPA to SmI₂ changes the characteristically navy blue solution of SmI₂ to a deep purple color and has a profound impact on the reactivity and selectivity of the reductant.²⁶ The use of HMPA with SmI₂ was first reported by Inanaga in 1987, in which he showed that the additive drastically accelerated the rate of reduction of a range of alkyl and aryl halides.⁶ Since this seminal report, the SmI₂-HMPA reducing system has played an important role in the development of SmI₂ chemistry given that it accelerates a broad range of functional group conversions and enhances the stereochemical control of bond-forming reactions (see section 1.3, and Chapter 3).

While HMPA has numerous positive synthetic attributes when used with SmI_2 , the additive is a suspected human carcinogen,^a so the advances made in the application of SmI_2 -HMPA in synthetic reactions will inevitably be truncated due to toxicity concerns. Since it has already been established in many SmI_2 reactions that HMPA is required to achieve the desired transformations, an in depth understanding of the role HMPA plays within these mechanisms will allow for alternative additive systems to be designed to have the constructive attributes without the toxicity concerns.

Crystallographic studies by Hou provided insight into the structure of the SmI_2 -HMPA complex. While SmI_2 in THF exists with 5 solvent molecules coordinated to the oxophilic metal center as $\text{SmI}_2(\text{THF})_5$, crystal studies indicate that upon addition of 4 equiv of HMPA, THF is displaced to form $[\text{SmI}_2(\text{HMPA})_4]$ (Figure 1.2, a).^{27,28} Careful examination of the complex shows that the samarium-iodide bond distance is dramatically increased upon the addition of HMPA. Hou also found that upon the addition of a 10 equiv or greater excess of HMPA to SmI_2 , $[\text{Sm}(\text{HMPA})_6]\text{I}_2$ was produced (Figure 1.2, b), saturating the metal with HMPA ligands and displacing the iodide ions to the outer sphere.^{27,28}

^a HMPA toxicity was studied through HMPA dosage on mice specimen in their drinking water as well as solutions of HMPA introduced through the nose.¹⁹⁹ Within the nasal studies, lesions were observed in the anterior regions of the nasal cavity. They identified this result as most likely due to HMPA metabolized by P450s to formaldehyde (by demethylation), which is known to produce nasal tumors in rats. Another study hypothesizes that the presence of the oxygen atom on the phosphorus appears to be a prerequisite for the genotoxic activity of HMPA since the study showed that derivatives lacking the oxygen are only weakly mutagenic in *Drosophila*.¹⁹⁹ According to the SCOEL/SUM/156 report overview done in 2010 there is still no firm evidence for HMPA toxicity in humans, and that the leading theory for the toxic behavior seen in rats is due to the formation of formaldehyde when HMPA is metabolized in the nasal cavities. This metabolic pathway has some differences in humans.²⁰⁰

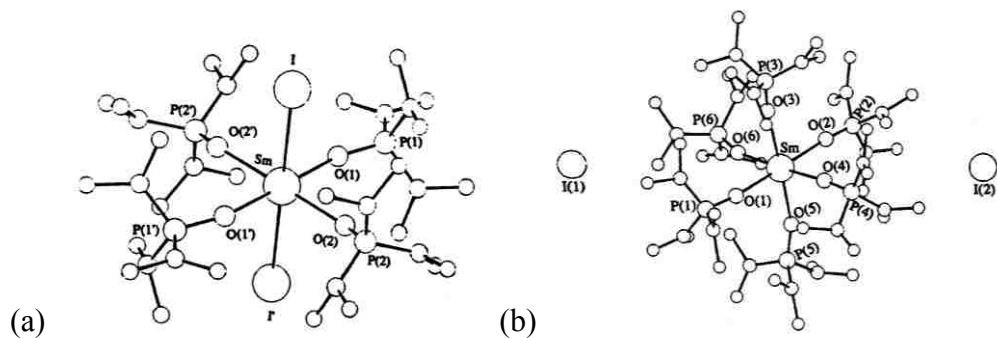


Figure 1.2 (a) SmI_2 in THF with low concentrations of HMPA, $[\text{SmI}_2(\text{HMPA})_4]$ (b) SmI_2 in THF with 10equiv HMPA, $[\text{Sm}(\text{HMPA})_6]\text{I}_2$.

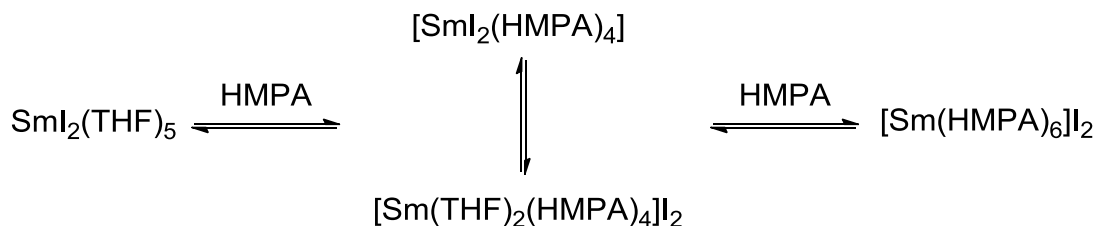
Conductance studies by Daasbjerg and Skrydstrup²⁹ in conjunction with linear sweep voltammetry studies by Flowers illustrate that a great deal of complexity is possible for the SmI_2 -HMPA system.³⁰ Conductance studies demonstrated that upon the addition of 4 equiv of HMPA to SmI_2 in THF, the iodide ions are displaced, suggesting that in solution the structure may be best represented as $[\text{Sm}(\text{THF})_2(\text{HMPA})_4]\text{I}_2$. The conductance studies also provide further evidence that with the addition of greater than 10 equiv of HMPA $[\text{Sm}(\text{HMPA})_6]\text{I}_2$ is produced.²⁹ Linear sweep voltammetry identified the reduction potential of $\text{Sm}(\text{III})/\text{SmI}_2(\text{II})$ in THF to be -1.33 V (Table 1.1). With increasing concentrations of HMPA with SmI_2 , the potential increased steadily to a maximum of -2.05 V (4 equiv HMPA). Further addition of 5 and 6 equiv displayed no change in potential, implying that the complex containing 4 equiv HMPA provides the greatest ground state reduction potential of $\text{Sm}(\text{II})$.^{13,25}

Table 1.1 Oxidation Potentials of SmI₂ with increasing amounts of HMPA

Equivalents of HMPA vs. SmI ₂ ^a	Oxidation Potential	
	V ^b	E, V (kcal)
0	-1.33	0
1	-1.43	0.10 (2.3)
2	-1.46	0.13 (3.0)
3	-1.95	0.62 (14.0)
4	-2.05	0.72 (16.6)
5	-2.05	0.72 (16.6)
6	-2.05	0.72 (16.6)

a) [SmI₂] 0.5 mM. b) vs. Ag/AgNO₃ reference electrode in THF.

Taken together, these studies concluded that the solution structure of SmI₂-HMPA in THF is a dynamic equilibrium of the ligands and solvent coordination with the metal (Figure 13). Additionally, coordination of HMPA to SmI₂ not only produces a more powerful reductant, but displacement of the iodide ligands to the outer sphere of Sm(II) creates open coordination sites for substrates.^{29,31,32} Synthetic examples of how HMPA impacts SmI₂ reactions can be found in section 1.3, as well as Chapter 2, section 2.

**Figure 1.3** SmI₂-HMPA coordination complexes

1.2.1.2 DMPU and TMU

Other Lewis bases such as 1,3-dimethyl-3,4,5,6-tetrahydro-2(1H)-pyrimidinone (DMPU) and tetramethyl urea (TMU) are known to coordinate to Sm(II), also producing

a more powerful reductant.³³ Measurements of oxidation potentials clearly show that as DMPU and TMU are added to SmI₂, the thermodynamic reducing power increases dramatically (Table 1.2). To achieve the increase in oxidation potential that is seen with HMPA, high concentrations of TMU are needed (60 equiv). Sm ligated by DMPU is not stable in solutions of THF, and with more than 30 equiv the Sm-DMPU complex is completely unstable and precipitates out of solution.³³ In acetonitrile the complex is stable, and an increase in the oxidation potential is observed, but not as drastic as observed with HMPA and TMU.^{20,33}

Table 1.2 Oxidation potentials determined vs. Ag/AgNO₃

Reductant	Standard Potential, V
SmI ₂ (THF)	-1.33
SmI ₂ - HMPA (THF) (4 equiv)	-2.05
SmI ₂ - TMU (THF) (60 equiv)	-2.04
SmI ₂ (acetonitrile)	-0.84
SmI ₂ - DMPU (acetonitrile)	-1.48

Crystal structures have identified that both DMPU and TMU coordinate to SmI₂, suggesting that electron donation through ligand coordination is the reason for the observed increase in oxidation potential. [Sm(DMPU)₃(THF)I₂] is formed with low concentrations of DMPU (2 equiv), while at higher concentrations (>6 equiv) forms a fully saturated [Sm(DMPU)₆]I₂, with the iodide ions displaced to the outer sphere (Figure 1.4).³⁴ This solvated Sm-DMPU complex differs from the Sm-HMPA complex in that it

has a distorted trigonal anti-prism structure as opposed to the octahedral structure seen with $\text{Sm}(\text{HMPA})_6$.

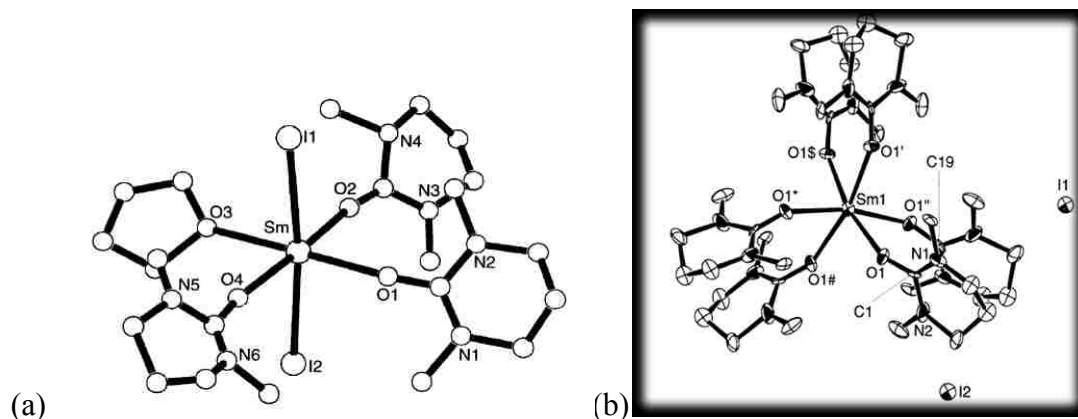


Figure 1.4 (a) $[\text{Sm}(\text{DMPU})_3(\text{THF})_2]\text{I}_2$ (b) $[\text{Sm}(\text{DMPU})_6]\text{I}_2$

TMU also coordinates to the Sm metal center in THF forming $[\text{Sm}(\text{THF})_2(\text{TMU})_2]\text{I}_2$ (Figure 1.5).³⁴ In contrast to HMPA and DMPU, a fully solvated complex does not form even at high concentrations of TMU.

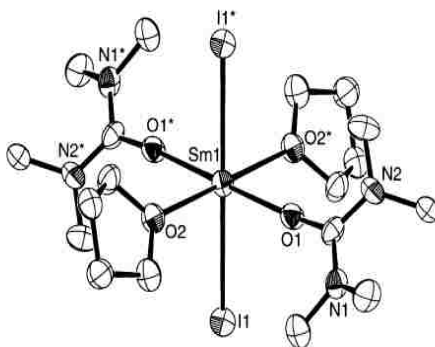
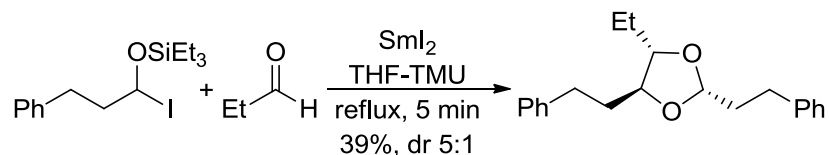


Figure 1.5 TMU coordinated to Sm metal center, $[\text{Sm}(\text{THF})_2(\text{TMU})_2]\text{I}_2$

While these cosolvents seem to be viable alternatives for HMPA, little synthetic success has been observed with them. Molander has shown instances in which the

addition of DMPU produces almost identical results to SmI_2 reduction in the absence of a cosolvent.³⁵ Curran observed that, while DMPU cannot be used in THF, with MeCN as the solvent, DMPU accelerated halide reduction and facilitated subsequent radical cyclization onto an olefin with a classic halide-olefin radical trap.³⁶ Without DMPU the reduction does not occur; however, HMPA still provided a faster reaction time as an additive (5 minutes with HMPA, 30 minutes with DMPU).³⁶

Only one report has used TMU with SmI_2 in a synthetic reaction, in the reductive coupling of iodomethyl silyl ethers with an aldehyde forming 1,3-dioxolanes (Scheme 1.2). This cross-coupling reaction is believed to proceed through stabilized carbonyl ylides of the silyl ethers.³⁷



Scheme 1.2 Cross coupling of iodomethyl silyl ether with aldehydes with SmI_2 -TMU

1.2.1.3 Glycols and ethers

Multidentate alcohols and ethers, such as glycols and dimethoxyethane (DME, or glyme), have also been used to accelerate the rate of SmI_2 reactions. Glycols were originally used as proton sources; however, they were also some of the first additives confirmed to coordinate to Sm through crystallization with SmI_2 .^{38,39}

Sen and Chebolu isolated *cis* and *trans* isomers of SmI_2 with bis(2-methoxyethyl)ether (diglyme, $\text{CH}_3\text{OCH}_2\text{CH}_2\text{OCH}_2\text{CH}_2\text{OCH}_3$), forming an 8-coordinate complex, $\text{SmI}_2[\text{O}(\text{CH}_2\text{CH}_2\text{OMe})_2]_2$ ³⁸ (Figure 1.6, a). The additive is tridentate, with all three oxygens in the ether coordinating to Sm. Another 8-coordinate Sm-complex was isolated with glyme ($\text{CH}_3\text{OCH}_2\text{CH}_2\text{OCH}_3$), in which each additive has two coordinating oxygens. Three glyme molecules chelate the metal center, forming $\text{SmI}_2[(\text{CH}_3\text{OCH}_2\text{CH}_2\text{OCH}_3)_3]$ ³⁹ (Figure 1.6, b). In both cases the glycols are multidentate, and the iodide ions are still coordinated to the metal center.

Flowers *et al.* obtained crystal structures of SmI_2 with chelating glycols. SmI_2 with diethylene glycol (DG, $\text{HOCH}_2\text{CH}_2\text{OCH}_2\text{CH}_2\text{OH}$) formed a 9-coordinate complex, $\text{Sm}[(\text{OCH}_2\text{CH}_2\text{OCH}_2\text{CH}_2\text{O})_3]\text{I}_2$ ⁴⁰ (Figure 1.6, c), in which all three oxygens in the glycol chelate to SmI_2 , and the iodide ions are displaced to the outer sphere. SmI_2 with diethylene glycol monomethyl ether (DGME, $\text{CH}_3\text{OCH}_2\text{CH}_2\text{OCH}_2\text{CH}_2\text{OH}$) also displaces the iodide ions to the outer sphere, forming the 8-coordinate complex $[\text{Sm}(\text{OCH}_2\text{CH}_2\text{OCH}_2\text{CH}_2\text{OMe})_3]\text{I}_2$ ⁴⁰ (Figure 1.6, d). In addition to the crystal structures, UV-Vis analysis showed a shift in SmI_2 absorbance bands as the glycols were added, which also illustrates the change in the coordination sphere from $\text{SmI}_2(\text{THF})_5$.⁴⁰

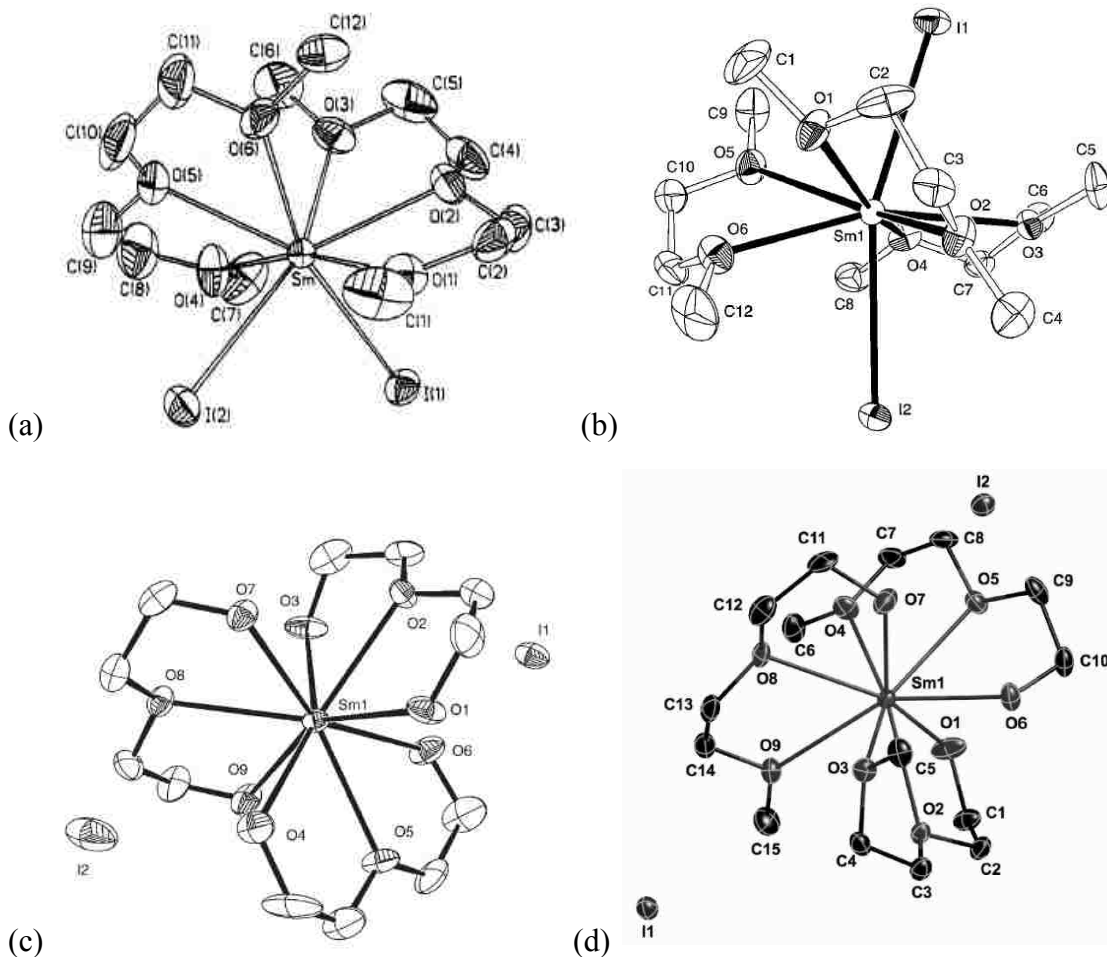


Figure 1.6 (a) $cis\text{-SmI}_2[\text{O}(\text{CH}_2\text{CH}_2\text{OMe})_2]_2$, $\{\text{SmI}_2(\text{diglyme})_2\}$; (b) $\text{SmI}_2[(\text{CH}_3\text{OCH}_2\text{CH}_2\text{OCH}_3)_3]$, $\{\text{SmI}_2(\text{glyme})_3\}$; (c) $\text{Sm}[(\text{OCH}_2\text{CH}_2\text{OCH}_2\text{CH}_2\text{O})_3]\text{I}_2$, $\{\{\text{Sm}(\text{DG})_3\}\text{I}_2\}$; (d) $[\text{Sm}(\text{OCH}_2\text{CH}_2\text{OCH}_2\text{CH}_2\text{OMe})_3]\text{I}_2$, $\{\{\text{Sm}(\text{DGME})_3\}\text{I}_2\}$.

Hilmersson used these coordinating alcohols to enhance the rate of SmI_2 reduction of 3-heptanone. Using glycols he found the rate of reduction was 2-4 times faster than reduction with MeOH as the additive, and 16 times faster than reduction with no proton source. Additionally, he concluded that the rate increase was proportional to the number of ethereal oxygens in the glycol.⁴¹

Rate and mechanistic studies by Flowers showed that the mechanistic role of glycols is complex. At low concentrations the rate of electron transfer is enhanced, while at higher concentrations the glycol ligands saturate the coordination sphere of Sm(II), producing a less reactive reductant.⁴⁰ In the Sm-mediated reduction of benzyl bromide, diglyme promoted the reduction of the substrate; however, bibenzyl was formed as the major product since the additive does not contain a labile hydrogen for protonation. Correspondingly, DG and DGME promoted the reduction, as well as acted as proton sources, forming toluene exclusively.⁴⁰ A full kinetic analysis of these additives with the reduction of the aryl halide led to some mechanistic conclusions on the systems. The Sm-glycol complexes carry out the reduction, and the rate increase from the additives followed the order DG > DGME > diglyme. This trend corresponds with the affinity of the additives for SmI₂ (based on the bond distances found in the crystal structures). Also, the ability of the additives to displace the iodide from SmI₂ substantially increased the rate of substrate reduction, suggesting the separation of iodide is required for the increased reactivity.⁴⁰

1.2.2 Proton Sources

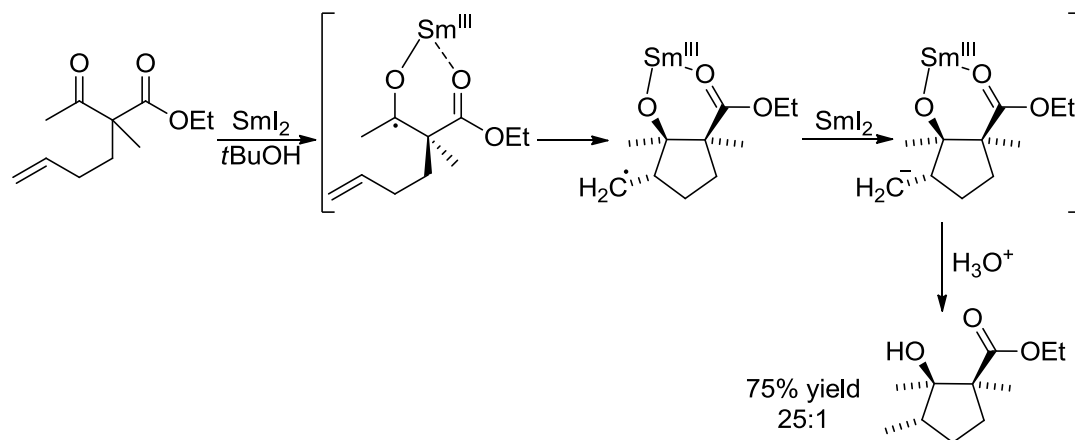
In addition to Lewis bases, many reactions initiated by SmI₂ require proton donors. The most commonly utilized proton donors are alcohols, glycols (*vide supra*), and water. It was long thought that the primary role of proton donors was to quench carbanions and alkoxides generated upon substrate reduction by SmI₂. It is now recognized that proton donors have a considerable impact on the regiochemical⁴² and

stereochemical⁴³ outcome of many SmI₂-mediated reactions, and often times changing the proton donor can have a profound impact on product distributions. The complicating feature of these systems is that oxygen-containing proton donors may coordinate to oxophilic SmI₂ as well as donate a proton to the reduced substrate through heterolytic cleavage of the O-H bond. For this reason, proton sources used with SmI₂ are usually put into two categories: those which form complexes with SmI₂, such as glycols, MeOH and H₂O, and those which do not, *t*BuOH and 2,2,2-trifluoro ethanol (TFE).

1.2.2.1 Alcohols

Low concentrations of alcohols (*t*BuOH and MeOH) were used in SmI₂ reductions in Kagan's seminal report. The addition of alcohols lowered the reaction times of the deoxygenation of sulfoxides and epoxides, and proved to be necessary in the reduction of carbonyl derivatives.¹ In other Sm-mediated methods, alcohols are added to simply protonate intermediate anions through the course of the reaction; however, their inclusion is often essential to proceed through the desired reaction.

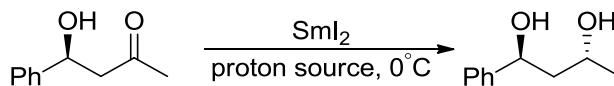
While carrying out reductive cyclizations of β -keto esters and β -keto amides (Schemes 1.3), Molander *et al.* noted that without the inclusion of a proton source, large amounts of unreacted starting material, as well as a mixture of unidentified products were recovered. With the addition of 2 equiv of either MeOH or *t*BuOH, the desired cyclized products were isolated in high yields.⁴⁴



Scheme 1.3 Sm-mediated reductive cyclization with *t*BuOH

Keck and coworkers examined the effect of different proton sources on the SmI₂-mediated reduction of β-hydroxy ketones.⁴³ The use of H₂O as a proton source provided high yields with moderate diastereoselectivities; however, an increase in H₂O concentration lowered the yield and resulted in a loss of the diastereoselectivity (Table 1.3, entries 1 and 2). Using MeOH in the reaction provided excellent yields and diastereoselectivity, while the best results came from high concentrations of MeOH (Table 1.3, entries 3 and 4). *t*BuOH as a proton source hindered the reduction.

Table 1.3 Impact of proton donor source on SmI₂ reduction of β-hydroxy ketones^a



Entry	Proton Source	Yield (%)	Ratio (<i>anti</i> / <i>syn</i>)
1	H ₂ O (2 equiv)	96	83:17
2	H ₂ O (10 equiv)	88	50:50
3	MeOH (2 equiv)	95	98:2
4	MeOH (10 equiv)	99	>99:1
5	<i>t</i> BuOH (2 equiv)	0	--

^aSmI₂ = 3 equiv. Reactions run for 1 h.

Mechanistic studies on the interaction of the alcohols with SmI_2 provided some insight into the differences observed between the proton donors. Through UV-Vis analysis, Hoz identified that MeOH coordinates to the Sm-metal center. As the concentration of MeOH was increased, the two absorbance bands associated with SmI_2 (555 and 615 nm) decreased in intensity and converged to one absorbance band at 584 nm (Figure 1.7).⁴⁵ These shifts were not found with other proton sources, such as propanol and trifluoroacetic acid, with SmI_2 .

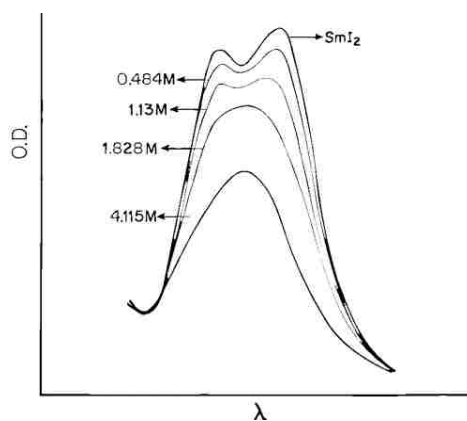


Figure 1.7 Shift in UV band of SmI_2 with the addition of MeOH

Through isotopic labeling, they also established that MeOH not only binds firmly to SmI_2 , but the labile proton, which participates in the protonation step, is from a coordinated alcohol. When equal amounts of MeOH and MeOD were added to the Sm-reduction of the olefin, a H/D incorporation ratio of 1.2 was found. Under the same reaction conditions, when MeOH and SmI_2 were pre-mixed, and then introduced to a solution of MeOD with the substrate, the incorporation ratio (H/D) increased to 7.15.⁴⁵ This significant increase clearly indicates that the coordination of MeOH to SmI_2 plays

an integral role in the mechanism of the reduction and protonation of the olefin by SmI₂-proton source.

Flowers *et al.* continued the mechanistic investigation of the role of proton donors with SmI₂, and identified a direct correlation between the rate of reduction of a ketone with the pK_a of the alcohol proton source.¹⁴ Kinetic studies identified that the reaction was first order in substrate and SmI₂; however, the order of the proton donor varied with the different additives used (Table 1.4). Both isopropyl alcohol and *t*BuOH had no effect on the rate of the reduction, even at high concentrations. A rate order of zero for these proton sources aligned with a k_H/k_D of one, indicating that the proton transfer is not rate-limiting. Conversely, H₂O, MeOH, EtOH, TFE and phenol all exhibited a rate order of one (within experimental error), and a kinetic isotope effect of approximately 2, indicating that the rate-limiting step in the reduction involved a proton transfer from the additives.

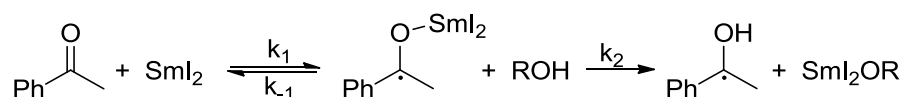
Table 1.4 Observed rate constant, reaction order and k_H/k_D for reduction of acetophenone by SmI₂ and proton donors

proton donor	k _{obs} (s ⁻¹) ^a	proton donor order	k _H /k _D
--	0.25 ± 0.02	--	--
H ₂ O	7.6 ± 0.2	1.4 ± 0.1	1.8
MeOH	1.0 ± 0.1	0.9 ± 0.1	1.9
EtOH	0.9 ± 0.1	0.8 ± 0.1	1.8
Isopropyl alcohol	0.33 ± 0.01	0	1.0
<i>t</i> BuOH	0.23 ± 0.01	0	1.0
TFE	1.4 ± 0.1	0.9 ± 0.1	2.0
phenol	1.7 ± 0.1	0.8 ± 0.1	1.9

^a[SmI₂] = 0.0025 M; [acetophenone] = 0.025 M; [proton donor] = 0.0625 M.

Based on these results, they proposed that with isopropyl alcohol and *t*BuOH, the alcohols are not strong enough donors to protonate the ketyl radical anion, and as a result

the first step of the reduction is rate-limiting. With the other proton sources, the protonation becomes the rate-limiting step (Scheme 1.4). Within the series of proton donors that had an impact on the rate, a plot of pK_a vs k_{obs} provided a correlation coefficient of 0.996, clearly indicating that the acidity of the proton donor dictated the rate of the reaction.¹⁴ These results explained the effects of the alcohols on the reduction, but the higher rate order for H_2O suggested there may be more to the role of H_2O in the system. A more in-depth look at how H_2O impacts SmI_2 reactions is described in a later section (1.2.2.2).

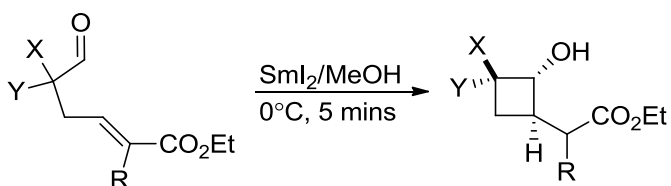


Scheme 1.4 Reduction and protonation of acetophenone with SmI_2 -proton source

Interesting synthetic impacts, based on the type of proton donor used in SmI_2 reductions, were observed by Procter *et al.* as they carried out the formation of functionalized cyclobutanols through a 4-*exo-trig* cyclization mechanism.⁴⁶ The reaction proceeded with moderate yields, forming *anti*-cyclobutanol products, with no trace of *syn*-products when MeOH was used as a cosolvent (Table 1.5, entries 1 and 2). It was reasoned that the observed selectivity was an effect of the cosolvent, which coordinates to the Sm metal center. With the Sm-coordination sites taken up by cosolvent interaction, the ability of oxophilic Sm to interact with both oxygen-containing functional groups on the substrate is disrupted, leading to an intermediate complex that favors the *anti*-configuration upon protonation. This supposition was verified by attempting the reaction

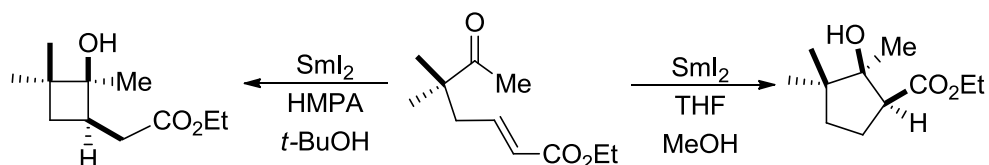
in the presence of other coordinating solvents such as HMPA (Table 1.5, entry 3) and H₂O (Table 1.5, entry 4). In these cases, the *anti*-configuration was obtained. When a non-coordinating proton source was used, such as EtOH, a 1:1 mixture of *anti:syn* diastereomers were formed.

Table 1.5 Reductive Sm-mediated 4-*exo-trig* cyclization



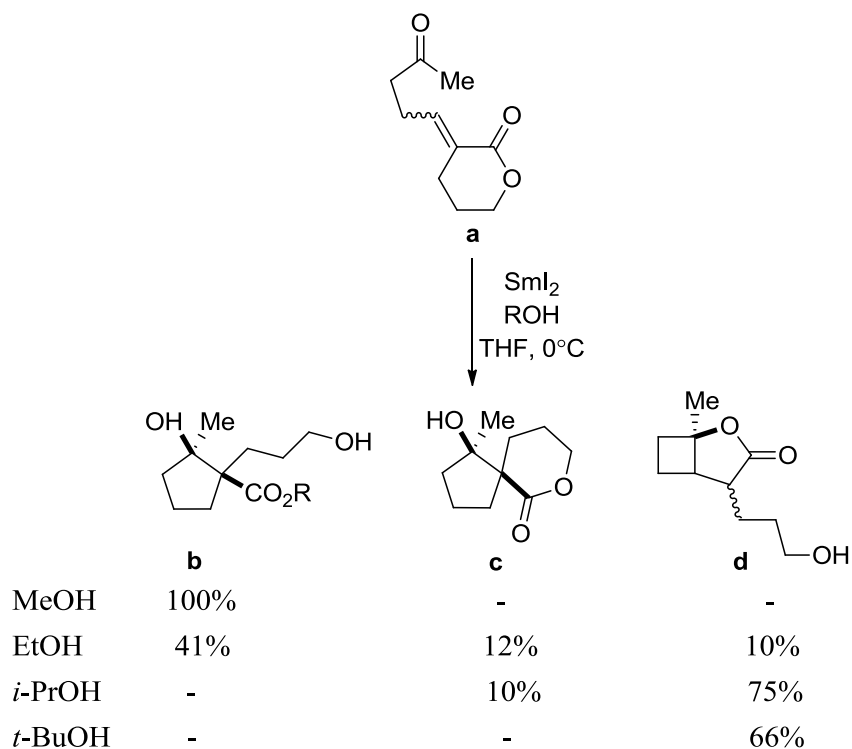
Entry	Additive	X	Y	R	Yield (%)
1	MeOH	CH ₃	CH ₃	H	65
2	MeOH	CH ₃	CH ₃	CH ₃	66
3	HMPA	OBn	CH ₃	H	57
4	H ₂ O	CH ₃	CH ₃	CH ₃	44

The study was then extended to ketones.⁴⁷ Instead of obtaining the cyclobutanol products through a 4-*exo-trig* cyclization, cyclopentanol products were unexpectedly obtained with MeOH as a cosolvent. With HMPA and non-coordinating *t*BuOH in the SmI₂ reaction, cyclobutanols were isolated through 4-*exo-trig* cyclization (Scheme 1.5). After a mechanistic study on the reaction,⁴⁷ Procter suggested that SmI₂ reduction in the presence of MeOH proceeds through a sequential reduction/intermolecular aldol process, to form the functionalized *syn*-cyclopentanols, while HMPA/*t*BuOH experiences a pathway similar to aldehyde reduction and cyclization.



Scheme 1.5 Alteration of reduction and cyclization pathways with SmI_2 -proton sources

The drastic effect on reactivity seen from the change in cosolvent was extended to other alcohols (Scheme 1.6), and an interesting conclusion was offered.⁴⁸ Procter proposed that the ability of the cyclization to go through a *4-exo-trig* or aldol spirocyclization is controlled by the ability of the cosolvent to protonate the intermediate. Because *t*BuOH has a slower rate of proton transfer, radical anion cyclization occurs first, forming the cyclobutanols (Scheme 1.6, **d**). MeOH efficiently protonates the intermediate anion, causing the radical to proceed through an aldol cyclization to form *syn*-cyclopentanol (Scheme 1.6, **b**). These results identify that the use of proton donors as additives in SmI_2 -mediated reactions can play an integral role in the process, drastically altering the outcome of the reaction.

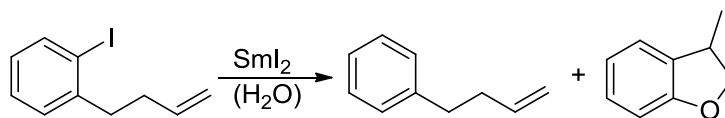


Scheme 1.6 Product distribution of cyclized products based on the proton sources used in the SmI₂ reduction

1.2.2.2 SmI₂ and Water

In Kagan's seminal report, he found that H₂O acted as a suitable proton source for the reduction of 2-octanone to 2-octanol.¹ Additionally, Inanaga carried out a coupling reaction of α,β -unsaturated esters with aqueous formaldehyde using Sm-HMPA to form lactones in high yields.⁴⁹ Based on this precedence, H₂O became an additive of choice in many reductions that required a strong protonating agent for organometallic intermediates. Due to the success of the reactions with H₂O, it was often speculated that the additive not only acted as a proton source, but also as a coordinating ligand.

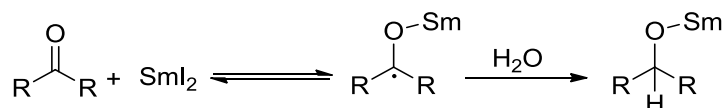
Work done by Curran identified that H₂O was not only useful as a proton source, but also accelerated the reduction of common functional groups used in SmI₂ reduction.³⁶ Curran *et al.* noted that as H₂O was added to solutions of SmI₂, a change in color was observed from deep blue to a wine purple/red color. This color change is reminiscent of what is observed when other coordinating solvents, such as HMPA and glycols, are added to SmI₂. When a ketone and α,β -unsaturated ester were reduced with SmI₂ (no additive) only starting material was recovered after 10 minutes. Adding 15 equiv H₂O to the reaction mixture allowed for nearly complete conversion to the reduced product for both substrates within the same reaction time. The reduction of sulfoxides and alkyl halides had a low conversion to reduced product with SmI₂ alone (34% in one minute and 12% conversion in 60 minutes respectively), and again with the addition of H₂O, the yields of the reduced products increased to 99% sulfane and 71% alkane. The effect of H₂O was observed with the Sm-mediated classic radical trap, *o*-allyloxyiodobenzene (Scheme 1.7). Without H₂O present, 20% of the cyclized product was obtained after 5 h. With the addition of water to the reaction mixture, 64% yield of the fused ring system along with 5% of the reduced product were obtained.



Scheme 1.7 Reduction of *o*-allyloxyiodobenzene radical trap with SmI₂ and SmI₂-H₂O

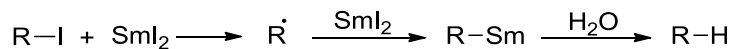
With carbonyl and sulfoxide containing substrates, it is generally accepted that the mechanism for the reduction of a carbonyl by SmI₂ proceeds through a ketyl radical,

which is likely rapid and reversible⁵⁰ (Scheme 1.8). In the absence of a proton source, the ketyl is consumed slowly and is susceptible to dimerization to the pinacolate.⁵¹ The addition of H₂O, acting as a proton source, protonates the ketyl radical, shifting the initial equilibrium to favor the formation of products. With this understanding of the reaction equilibrium, it is unclear if the increase in rate observed with the inclusion of H₂O is due to H₂O coordinating to SmI₂, or its action as a proton donor, favoring the shift in equilibrium.



Scheme 1.8 Single electron reduction of carbonyl containing substrates with SmI₂

The acceleration observed with SmI₂-H₂O in the reduction of alkyl halides provides insight into the role of H₂O as a coordinating ligand. SmI₂ is thought to reduce the iodide to its corresponding radical through dissociative electron transfer, followed by a facile second single electron transfer to form the intermediate organosamarium (see section 1.3.1) (Scheme 1.9). In this case, H₂O acting as a proton source in the reaction will not significantly impact the rate of the reduction, as was seen with the ketyl-radical equilibrium. Therefore, the rate increase observed by Curran suggests H₂O is acting as an accelerant in SmI₂ reactions.⁵⁰



Scheme 1.9 Reduction of alkyl halides through single electron transfer with SmI₂

UV-Vis analysis of SmI₂ in THF identified that the addition of H₂O shifts the UV-Vis spectrum, suggesting coordination of the additive to SmI₂. Closer examination of the interplay between H₂O and SmI₂ shows that as H₂O is added, the two absorption peaks of SmI₂ ($\lambda_{\text{max}} = 555$ and 618 nm) begin to converge to $\lambda_{\text{max}} = 570$ nm, indicating Sm- H₂O coordination (Figure 1.8). A second absorption peak is observed ($\lambda_{\text{max}} = 476$ nm) as H₂O concentration is increased, up to > 100 equiv, with an isosbestic point maintained between the two peaks (Figure 1.8, inset).⁵² The presence of two absorption peaks is mirrored by the color change observed in the solutions: a lower concentration of H₂O forms a deep purple color and high concentrations forms a bright red solution. These findings are consistent with two different Sm-H₂O complexes being formed in equilibrium with each other when high concentrations of H₂O are added. This study suggests that, after the addition of 50 equiv, H₂O effectively competes with the bulk solvent (THF), and a Sm-H₂O complex forms.

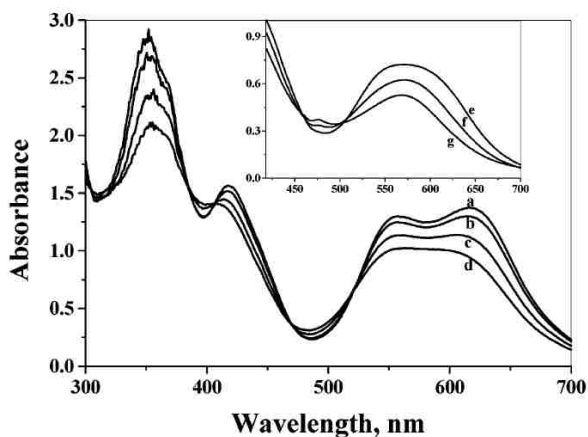


Figure 1.8 Absorption spectra of SmI₂ (2.5 mM) in THF in the presence of increasing amount of H₂O. (a) [H₂O] = 0.025 M, (b) [H₂O] = 0.05 M, (c) [H₂O] = 0.125 M, (d) [H₂O] = 0.188 M. Inset shows the absorption spectra of SmI₂ upon the addition of larger amounts of H₂O (e) [H₂O] = 0.15 M, (f) [H₂O] = 0.30 M, (g) [H₂O] = 0.45 M.

Further examination of the impact of H₂O on the coordination sphere of SmI₂ was carried out by observing the shift in the UV-Vis with SmI₂ in dimethoxyethane (DME). The UV-Vis spectra of SmI₂ in THF and DME are notably different (Figure 1.9, inset); however, when high concentrations of H₂O are added (1.25 M) both solutions exhibit $\lambda_{\text{max}} = 585$, and a smaller absorbance band at $\lambda_{\text{max}} = 476$ (Figure 1.9). As compared to the solution in THF, greater amounts of H₂O were needed before this spectra was observed in DME (500 equiv).⁵²

The observation of H₂O displacing solvent coordinated around SmI₂ is in agreement with the crystal structures found for SmI₂ in THF and DME. SmI₂-THF is surrounded by five THF molecules,^{18,53,54} while SmI₂ in DME has three bidentate DME molecules coordinated.⁵² Based on the concentrations of H₂O needed to affect the UV-Vis spectra and disrupt the inner coordination sphere of SmI₂, H₂O has greater affinity than THF or DME, but DME binds more tightly than THF.

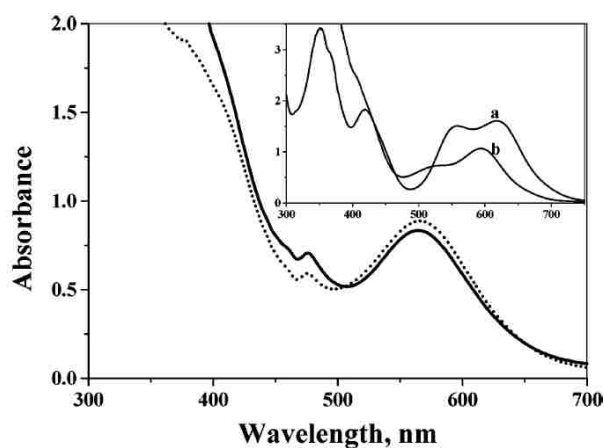


Figure 1.9 Absorption spectra of SmI₂ in THF (dot) and DME (solid) containing 1.25 M H₂O. Inset shows the absorption spectra of SmI₂ in (a) THF and (b) DME. [SmI₂] = 2.5 mM.

After studying the impact of H₂O on SmI₂ by UV-Vis, cyclic voltammetry (CV) studies were carried out to determine if the reduction potential of SmI₂ changes with the changing Sm-H₂O complex. SmI₂ in THF and DME display quasireversible^b voltammograms with identical redox potentials (within experimental error), with potentials of -1.5 ± 0.1 V vs a saturated Ag/AgNO₃ reference electrode.³⁰ As 60 equiv of H₂O was added to SmI₂ in THF, an irreversible cyclic voltammogram with an oxidation potential peak of -1.6 ± 0.1 V was observed. Further addition of H₂O (500 equiv) resulted in a more negative oxidation peak potential of -1.9 ± 0.1 V with a similar irreversible shape. Increasing the concentration of H₂O even more (1000 equiv, 5 M) had no further influence on the oxidation peak potential. These results are reminiscent of those observed with the Sm-HMPA complex. Solubility issues of the supporting electrolyte (tetraheptylammonium iodide) were encountered when CV studies were attempted on SmI₂ in DME with H₂O, however at high concentrations of H₂O (1000 equiv, 5 M) an irreversible voltammogram with a peak potential identical to SmI₂ in THF was found.⁵²

Conductance studies also showed that the addition of H₂O to solutions of SmI₂ (in THF) displace the iodide ions, presumably to the outer sphere.⁵⁵ Conductance is not observed until 20 equiv of H₂O is added to the solution. Taking this together with the

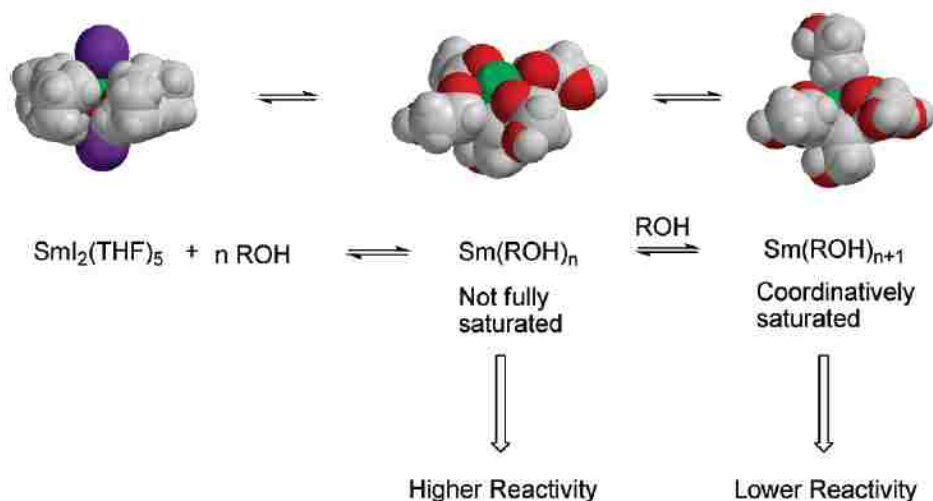
^b A reversible voltammogram infers that the electron transfer reaction at the electrode surface is so rapid that equilibrium conditions are maintained even with a substantial net current and a rapidly changing potential. A quasireversible voltammogram then, refers to a system in which the rate of the forward and backward equilibrium is not equal, but within the same order of magnitude over the potential range.²⁰¹

UV-Vis data, significant impact on the coordination sphere is not observed until 20-50 equiv of H₂O is added.

Based on the results of vapor pressure osmometry experiments, Flowers concluded that at the lower concentrations of H₂O (0.15 M) the complex formed is a monomer (in THF and DME); however, as high concentrations of H₂O are added (1.9-2.5 M), a complex mixture of a monomer-dimer equilibrium of Sm-H₂O complexes exists.⁵² High order aggregates are also supported by the fact that solutions of SmI₂ with high concentrations of H₂O tend to precipitate. As a large amount of precipitate forms, the solution loses the purple-red color. The resulting white solution implies Sm is no longer in its +2 oxidation state. Kinetic experiments also support the hypothesis that depending on the concentration of H₂O used, the Sm-H₂O complex exists in a monomer-dimer equilibrium.⁵² Experimentally, great caution must be taken when producing the SmI₂-H₂O solutions. If the H₂O is added neat, or too quickly, the solutions will lose color rapidly. A detailed procedure of how to carry out the formation of stable SmI₂-H₂O solutions in THF is described in Chapter 5, section 5.2.3.2.

In many cases, crystal structures were determined for Sm-additive complexes (i.e. HMPA, DMPU, TMU, glycols). While we use these data as evidence of the formation of coordinated complexes, crystallographic data does not always mirror solution structures, as solution chemistry is a dynamic process. Attempts to isolate crystals of SmI₂-H₂O have been unsuccessful, but based on the solution chemistry experiments described above, it is generally accepted that H₂O acts as a coordinating ligand with SmI₂. Rate

data from previous studies with DEG and related additives indicate that saturation of Sm typically leads to a decrease in Sm reactivity.⁴⁰ Work done by Procter has shown a number of synthetically important and unique reductions in which high concentrations of H₂O provide an increased reactivity of SmI₂⁵⁶ (see Chapter 5). Although the high H₂O concentrations increase the rate of reduction, SmI₂-H₂O complexes with high [H₂O] oxidize readily, and can be unstable, resulting in precipitation of Sm(III). These observations suggest there is a delicate balance in the dynamic equilibrium in which H₂O coordinates to SmI₂, liberating the iodide ions and providing open coordination sites, while not saturating the metal, as shown in Scheme 1.10.⁵⁷



Scheme 1.10 Dynamic equilibrium of H₂O coordinating with SmI₂ in THF. R= H.

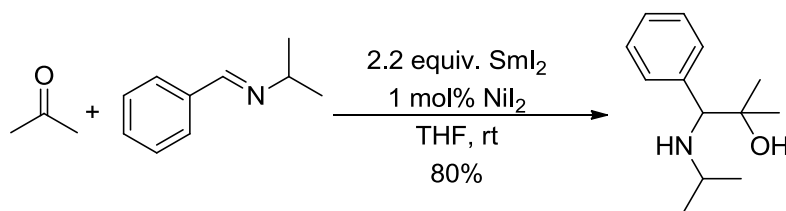
This result has been observed in many synthetic examples and can lead to interesting and fortuitous applications of SmI₂-mediated reactions. Synthetic uses of the

SmI₂-H₂O complex, as well as new experiments providing information on the power of SmI₂-H₂O in the reduction of lactones, are described in Chapter 5 of this dissertation.

1.2.3 Transition Metal Salts

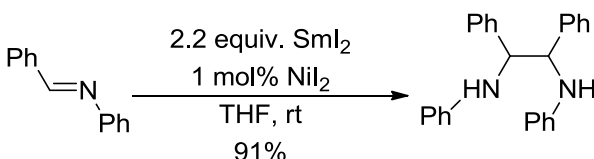
Inorganic salts can also be used to accelerate SmI₂-mediated reactions. The inorganic additives used with SmI₂ include lithium amide, lithium methoxide, lithium bromide, lithium chloride, and potassium hydroxide.^{58,59} In these reactions, it is likely that the anions displace iodide on Sm to produce a new reductant in solution.⁵⁸ Catalytic amounts of transition metal salts, such as NiI₂, FeCl₃, and CuCl₂, have also been shown to increase the efficiency of SmI₂-mediated reactions. Kagan has shown that in most instances, NiI₂ is superior to other transition metal salts.⁶⁰ As a consequence of these early studies, NiI₂ has become the additive of choice in reactions that require a transition metal to catalyze a bond-forming reaction.

Synthetically, examples of the use of Ni(II) in SmI₂ have been prevalent since Kagan and Namy's reports. Heterocoupling of an imine to a variety of ketones was accelerated with the addition of catalytic NiI₂ (Scheme 1.11).⁶¹



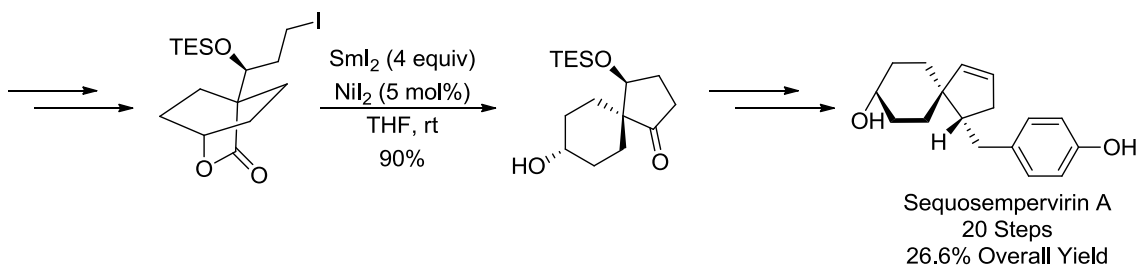
Scheme 1.11 Coupling of imines with ketones using SmI₂-NiI₂

Namy determined that the addition of catalytic amounts of NiI₂ also increased the efficiency of the coupling reaction of imines to form diamines (Scheme 1.12). In the absence of NiI₂, the reaction needed to be carried out at reflux for 6-16 hours for the reaction to go to completion.⁶¹



Scheme 1.12 Formation of diamines with SmI₂-Ni(II)

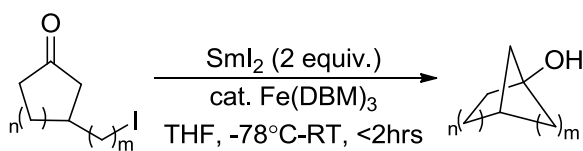
The use of NiI₂ in the samarium Barbier reaction was crucial in the synthesis of natural product Sequoempervirin A ((4R)-4-(4-hydroxybenzyl)spiro[4.5]dec-1-en-8-ol) (Scheme 1.13).⁶² A total synthesis of this compound was first presented in 2007 by Maity and Ghosh;⁶³ however, a mixture of regio- and stereoisomeric compounds were obtained due to reduction of ketone moieties in intermediate steps. Recently, Honda and coworkers⁶² circumvented this issue by using the samarium Barbier reaction in an intramolecular cyclization step, which they found to be most successful with the addition of 5 mol% NiI₂. This new stereocontrolled route for the synthesis was achieved in 20 steps with a 26.6% overall yield, improved from the 2% yield employing the 2007 method.



Scheme 1.13 Synthesis of natural product Sequosempervirin A

Iron salts were used to promote an intramolecular Barbier reaction in the construction of bridgehead bicyclic alcohols,⁶⁴ often integral in the carbon skeleton of complex pharmaceutical compounds and natural products. The Barbier procedure was successful over a broad range of compounds: cyclopentanone through cyclooctanone rings with halo alkyl side chains 1-4 carbon units long (Table 1.6). Optimization of the reaction conditions identified that the inclusion of an iron catalyst (FeCl_3 , FeCl_2 , $\text{Fe}(\text{acac})_3$, and $\text{Fe}(\text{DBM})_3$) resulted in the highest yields.

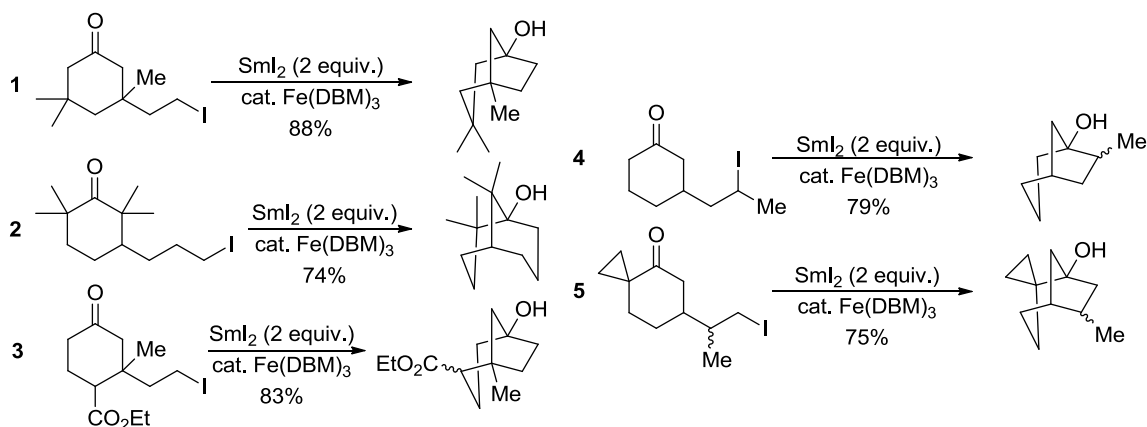
Table 1.6 Intramolecular Sm-Barbier reaction with Fe(III) cat.



Entry	<i>n</i>	<i>m</i>	Yield (%) ^a	Entry	<i>n</i>	<i>m</i>	Yield (%) ^a
1	1	1	66	7	2	3	73
2	1	2	71	8	2	4	15
3	1	3	54	9	3	2	73
4	1	4	22	10	3	3	76
5	2	1	77	11	4	2	86
6	2	2	69	12	4	3	87

^a: isolated yield.

These reactions were expanded using starting materials containing substitutions on the cycloalkanone ring (Scheme 1.14), all of which were still capable of proceeding through the Barbier reaction with high yields. Highly strained ring structures were synthesized (reactions 1 and 2), and secondary halides were also successful (reaction 4). It is important to note that this particular cyclization cannot be achieved with other typical reductants, such as butyl lithium compounds or activated magnesium, identifying the great benefit of SmI_2 as a reductant.



Scheme 1.14 Intramolecular Sm-Barbier reaction with Fe(III) cat.

Although NiI_2 has proven useful as an additive, its role in reactions has been unknown until recently. The mechanistic details for NiI_2 in SmI_2 reactions are described in Chapter 3.

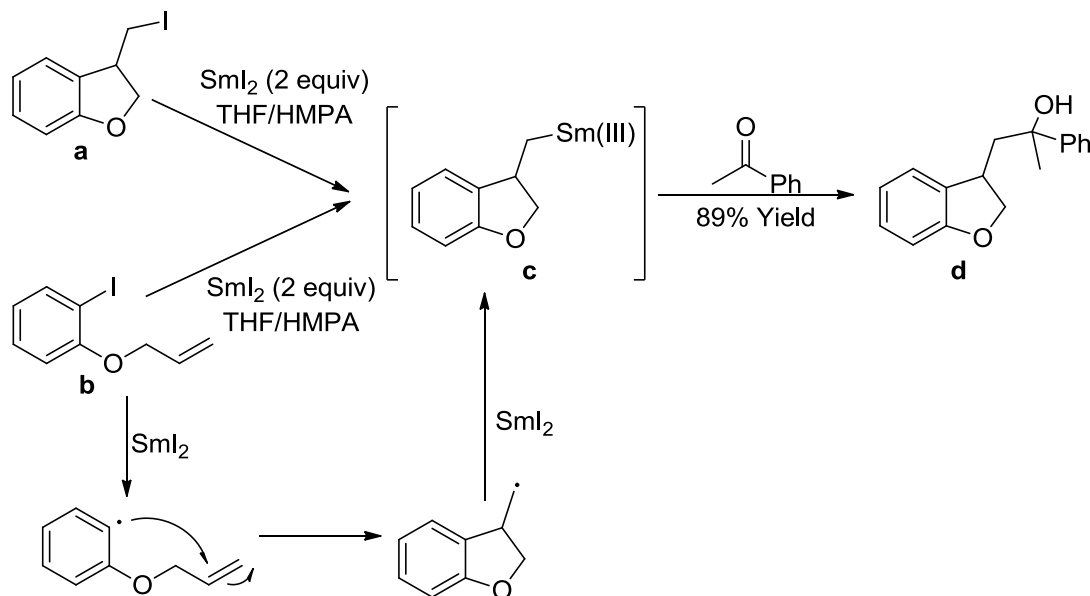
1.3 SmI₂ in Organic Synthesis

1.3.1 Organosamarium Intermediates

As shown in the above examples, a powerful aspect of SmI₂ in organic synthesis is the ability of the reductant to carry out the formation of new carbon-carbon and carbon-heteroatom bonds. Many of these reactions proceed through radical pathways initiated by the single electron reduction. In addition, reduction of the intermediate radical by SmI₂ leads to the formation of an intermediate anion often referred to as an organosamarium compound. Although organosamarium intermediates have not been isolated and characterized, their reactivity is similar to organometallic reagents. These intermediates behave as nucleophiles with carbonyls, can be protonated, and can also undergo transmetallation with other metals.

Intermediate organosamarium(III) compounds are likely the reactive intermediates in many coupling reactions labeled as “Sm(II)-mediated”. Curran examined the role of the organosamarium by distinguishing between pathways of radical or organosamarium intermediates in the Sm(II)-mediated coupling reaction of aryl halides and ketones.⁵⁰ In these reactions, it was noted that both starting halides (Scheme 1.15, a or b) produced the same product in almost identical yields in the presence of SmI₂-HMPA in THF.⁶⁵ Through this example and follow-up studies,^{66,67} Curran and coworkers proposed that an organosamarium intermediate (Figure 1.15, c) and not a radical intermediate was responsible for bond formation. No radical-radical coupling

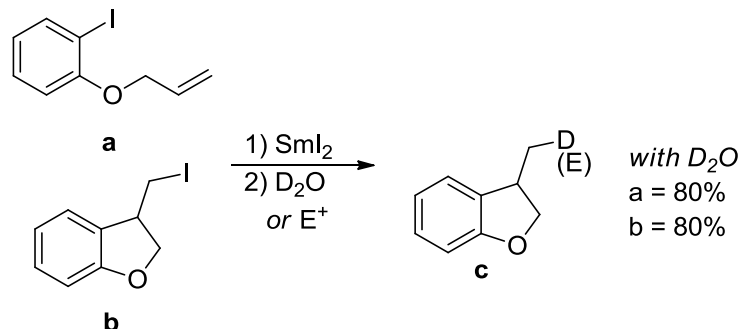
products were recovered, further implying the formation of the organosamarium intermediate occurs more rapidly than homocoupling of the radical.



Scheme 1.15 Radical and organosamarium coupling

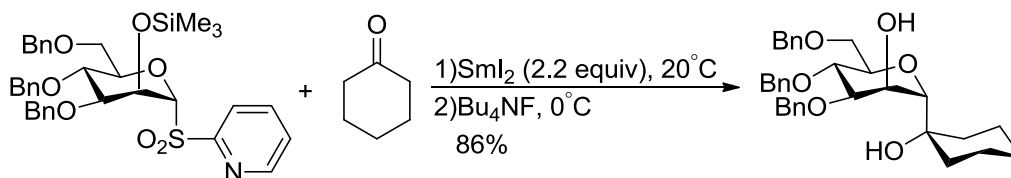
The presence of an organosamarium intermediate in reactions was also tested by withholding the ketone from the system and simply quenching the reduction of the alkyl halide with D_2O . The expected cyclic product (Scheme 1.16, **c**) was obtained with both the unsaturated and cyclic starting materials. Additionally, electrophiles were added after **a** or **b** were reduced by SmI_2 , and coupled products were obtained.⁶⁵ These studies were the first examples which described that electrophiles can react after pre-reduction of the alkyl halide by SmI_2 , providing evidence for the existence of the stable organometallic intermediate. The results described in these studies were further supported by rate and

mechanistic studies by Flowers, who showed that alkyl halides are reduced by SmI₂-HMPA several orders of magnitude faster than dialkyl ketones.⁶⁸



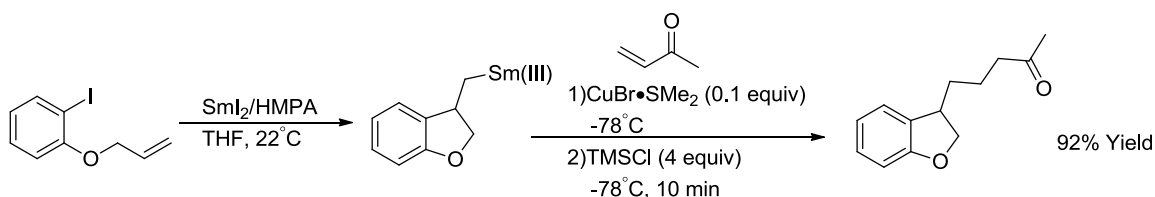
Scheme 1.16 SmI₂ coupling quenched with D₂O or an electrophile

The mechanistic underpinning of these reactions enabled the use of organosamarium intermediates in complex syntheses. An example of this approach is the synthesis of 1,2-*trans*-C-glycosides.⁶⁹ Glycosyl pyridyl sulfones were reduced by Sm(II), forming a glycosyl C1-organosamarium intermediate which then coupled with a carbonyl compound to form the C-glycoside (Scheme 1.17). The intermediate organosamarium displays considerable stability against β-elimination, suppressing the formation of the undesirable glucal side product.



Scheme 1.17 Synthesis of 1,2-*trans*-C-glycosides with SmI₂

Organosamarium transmetalation with catalytic Cu(I) has been employed in the synthesis of β -alkylated ketones from α,β -unsaturated carbonyl compounds.^{70,71} The initial single-electron transfer from SmI₂ forms an intermediate alkylsamarium via 5-*exo*-trig radical cyclization. Transmetalation with copper(I) salt (CuBr•SMe₂) produces an organocuprate that carries out conjugate addition in accordance with the general reactivity of organocuprates (Scheme 1.18). In the absence of Cu(I) salts, 1,2-additions of organosamarium reagents to carbonyl groups prevail.



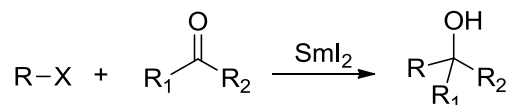
Scheme 1.18 Radical cyclization followed by organocuprate addition

The different types of SmI₂ reactions are often categorized by the type of organic transformations they carry out, albeit through radical or organosamarium pathways. Examples of these reactions are compiled below, many of which use the additives described in the first half of this chapter.

1.3.2 Grignard and Barbier Reactions

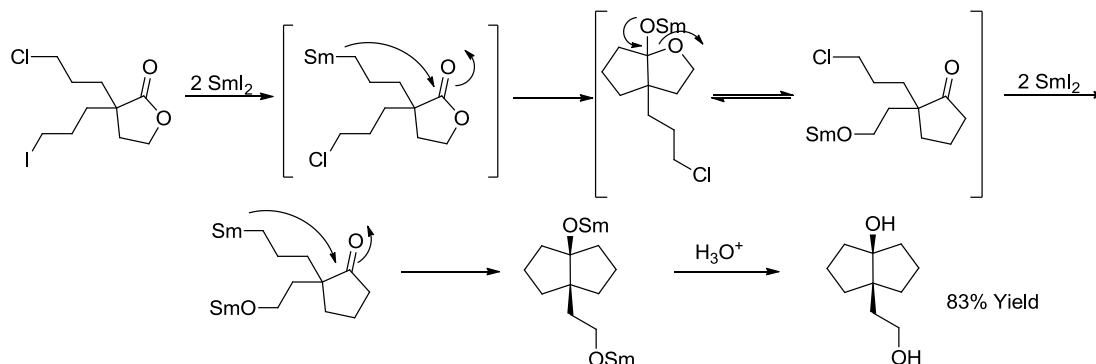
The Grignard and Barbier reactions couple an alkyl halide and ketone to form a new carbon-carbon bond in the coupled tertiary alcohol product (Scheme 1.19). Details on the differences between the two coupling reactions, and insight into their mechanisms can be found in Chapter 3 of this dissertation (3.1.2). It is generally believed that the reduction proceeds through initial reduction of the alkyl halide to an organosamarium

intermediate, which then nucleophilically adds to the carbon of the carbonyl, and upon protonation, via an *in situ* proton source or acidic work-up, the tertiary alcohol product is formed in high yields.⁵⁰



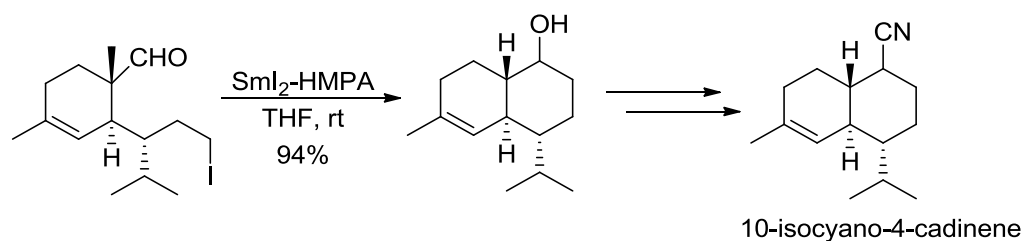
Scheme 1.19 Samarium Barbier reaction

Intramolecular samarium Barbier reactions have been used to produce a variety of compounds, especially complex ring systems. Due to the ability of SmI₂ to selectively reduce the alkyl halide over the carbonyl, the reductant effectively directs sequential cyclization processes. Molander explored this area with sequential intramolecular cyclizations with two pendant alkyl halide chains susceptible to SmI₂ reduction.⁷² SmI₂ preferentially reduces the iodide over the chloride, forming an organosamarium capable of nucleophilic attack into the carbonyl (Scheme 1.20). The formation of a wide range of bicyclic[m.n.0] and tricyclic[m.n.0] products was possible through SmI₂ reduction both in the presence and absence of HMPA.



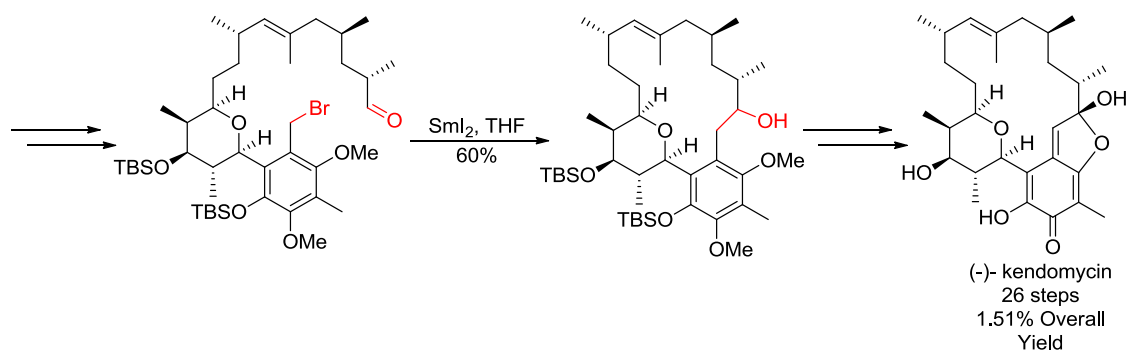
Scheme 1.20 Tandem samarium Barbier reactions with selective reduction of the halides

The samarium Barbier reaction was used in the total enantioselective synthesis of 10-isocyano-4-cadinene,⁷³ a marine sesquiterpene which is a lead compound for a nontoxic antifouling agent. The Barbier reaction was used to form the *trans*-decalin framework, closing the ring in high yield (Scheme 1.21). This was the first example of 10-isocyano-4-cadinene synthesized in its correct natural absolute configuration (1*S*, 6*S*, 7*R*, 10*S*).



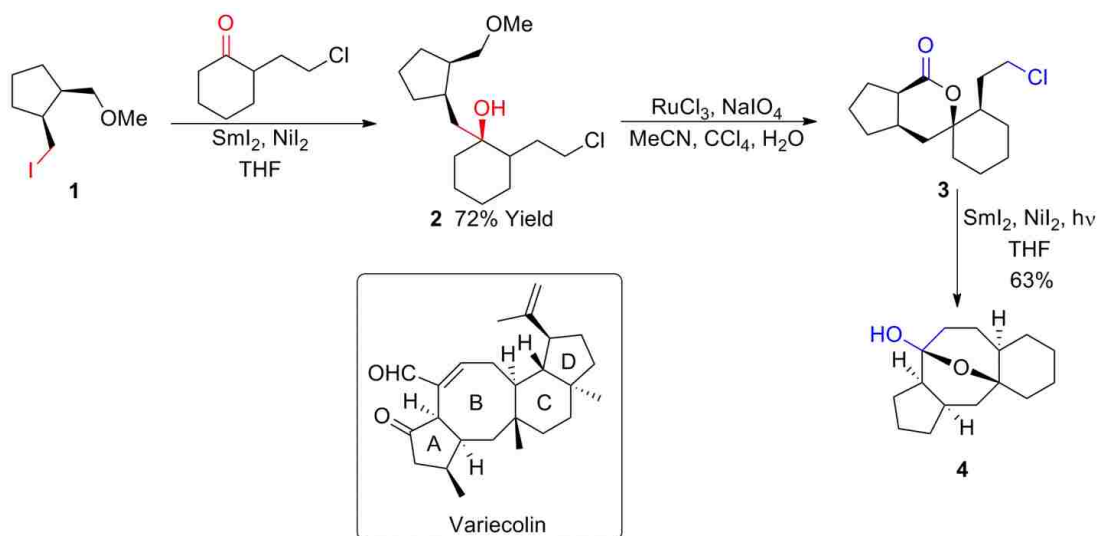
Scheme 1.21 Intramolecular samarium Barbier reaction for the formation of 10-isocyano-4-cadinene

An intramolecular samarium Barbier reaction was used for the macrocyclization of the natural product (-)-kendomycin, which was originally isolated from *streptomyces violaceuber*.⁷⁴ It is a potent antiosteoporotic agent, exhibits effective antibacterial activity against gram-positive and gram-negative strains and has enhanced cytotoxic activity toward several human tumor cell lines.^{75,76} An intramolecular samarium Barbier reaction is performed in the final stages of the synthesis, forming the strained 16-membered ring of the macrocycle in a single stereochemical configuration (Scheme 1.22). The macrocyclization step was completed in a 60% yield, and the final natural product was obtained in a 1.5% overall yield in 26 steps.



Scheme 1.22 Ring-closing samarium Barbier reaction in the synthesis of (-)-kendomycin

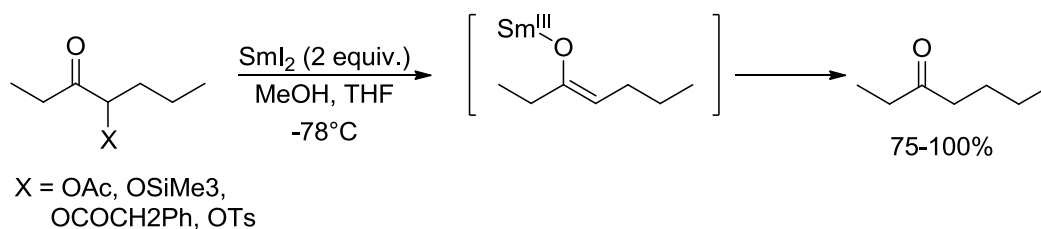
Control over the samarium Barbier reaction was exhibited in the synthesis of a variocolin model (Scheme 1.23, **4**). Variocolin is a sesterterpenoid natural product with known biological activities, such as immunosuppressant activity as well as being an antagonist of the angiotensin-II receptor. In the retrosynthetic analysis for the formation of variocolin model **4**, it was envisioned to proceed through two separate samarium Barbier reactions, achieved with the addition of catalytic NiI_2 (Scheme 1.23).⁷⁷ The first intermolecular Barbier reaction proceeded with complete recovery of the chloride on the molecule, eliminating the need for a protecting group. This reaction was then followed by Sharpless oxidation of **2** to its corresponding lactone in a high yield. The remaining pendant chloride was then cyclized through a second intramolecular Barbier reaction under photochemical Sm/Ni conditions to form the final intramolecular cyclooctane and complex four-ring system.



Scheme 1.23 Samarium Barbier reaction with NiI_2 in the total synthesis of variecolin

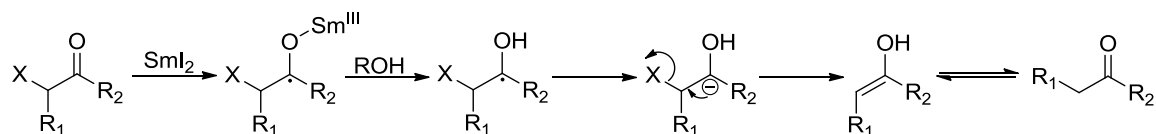
1.3.3 Reformatsky-type Reactions

SmI_2 has the ability to reduce α -heteroatom-substituted carbonyl compounds without over-reducing the carbonyl functionality (Scheme 1.24).²² These reductions are believed to proceed through an intermediate Sm(III) enolate which when generated can be used either as a nucleophile in coupling reactions, or could simply be protonated in solution.²²

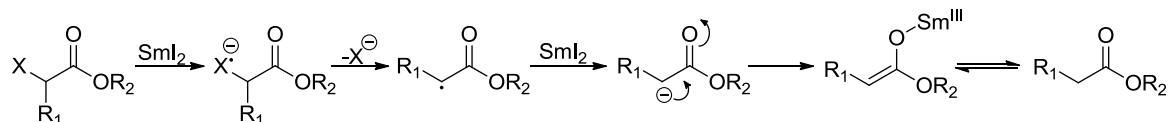


Scheme 1.24 SmI_2 -mediated Reformatsky reduction

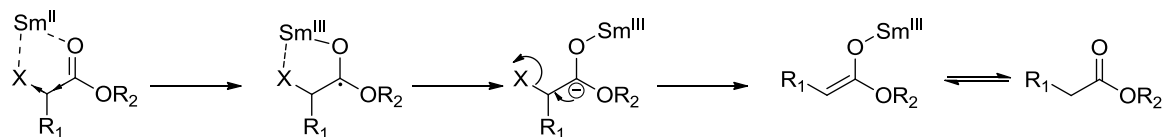
Two possible mechanisms for the formation of Sm-enolates have been proposed. In the first mechanism, Molander suggested that following single-electron transfer by SmI_2 , a ketyl radical is formed, which is quenched by an alcohol cosolvent.²² A subsequent reduction produces a carbanion which undergoes β -elimination to produce the enol tautomer of the final product ketone (Scheme 1.25). When esters are used as substrates, Molander proposed that electron transfer to the α -position generates a radical-anion, which undergoes fragmentation to produce a radical intermediate. A second reduction by SmI_2 produces the Sm-enolate, which can be protonated to form the final ester (Scheme 1.26). Another possible mechanism for ester reduction takes Sm coordination into consideration. The electron-withdrawing character of the α -heteroatom can facilitate the reduction of the ester carbonyl group to form the ketyl radical (Scheme 1.27). Once the activating heteroatom has been removed, no further ester reduction is possible.



Scheme 1.25 Reformatsky reaction—ketyl radical followed by β -elimination



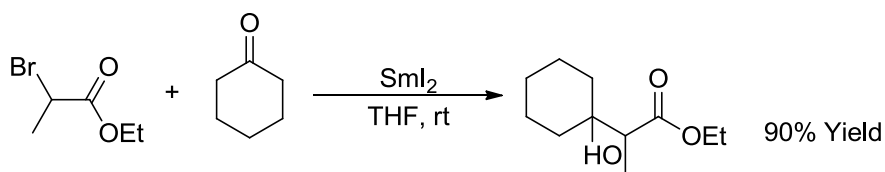
Scheme 1.26 Reformatsky reaction with esters



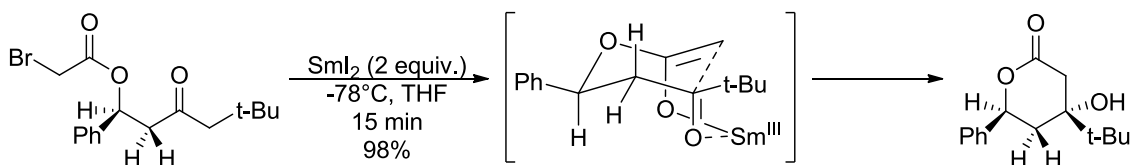
Scheme 1.27 Reformatsky reaction—Sm(III) coordination

When Sm-enolates are in solution with aldehydes or ketones they readily undergo an aldol reaction. More specifically, when an aldol condensation occurs with a Sm-enolate that was generated through the reduction of an α -halo carbonyl, the transformation is classified as a Reformatsky reaction. The reaction is carried out with a 1:1 mixture of the α -halo carbonyl and coupling partner, reacted with SmI_2 simultaneously.

The first intermolecular Reformatsky reaction was carried out in Kagan's seminal report, coupling an ethyl bromopropionate and cyclohexanone, achieving heterocoupling in a high yield under mild conditions (Scheme 1.28).¹ Soon thereafter, Molander performed intramolecular cyclizations utilizing the Reformatsky transformation,⁷⁸ achieving complete stereochemical control over a range of substituted starting materials (Scheme 1.29).

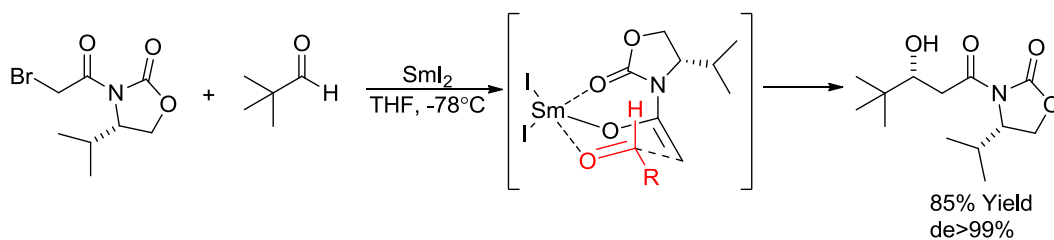


Scheme 1.28 Reformatsky coupling of ethyl bromopropionate and cyclohexanone



Scheme 1.29 Stereo controlled Reformatsky reaction

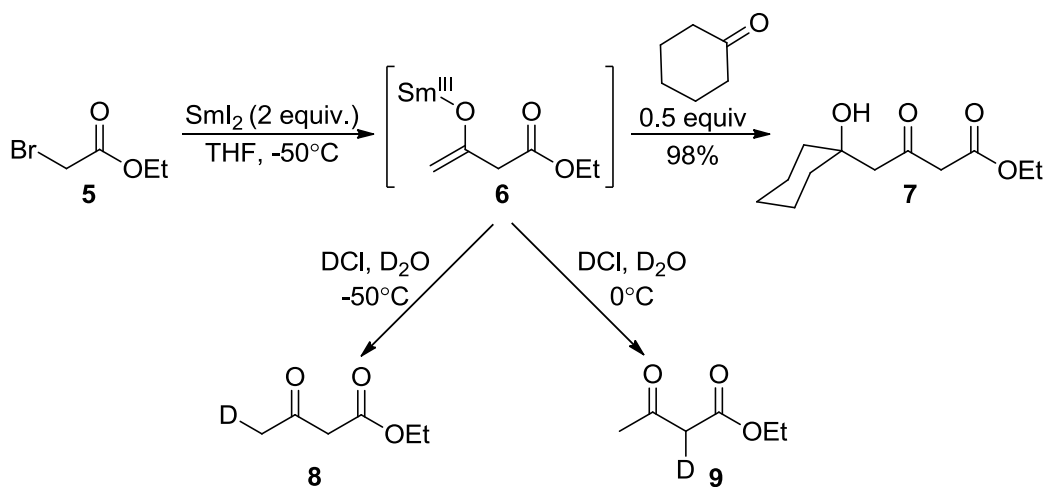
Intermolecular Reformatsky reactions can also proceed with control over the stereochemistry.⁷⁹ Coordination of the incoming carbonyl species with the Sm-enolate positions the electrophile in a manner that the addition takes place in one orientation, producing a single diastereomer (Scheme 1.30). High diastereoisomeric excess is difficult to achieve with other aldol reactions, once again highlighting the impact of Sm-reactions on synthetic chemistry.



Scheme 1.30 Sm(II) chelation in the Reformatsky reaction

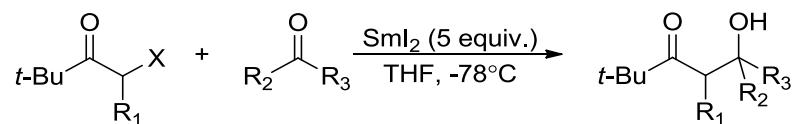
While there is still a lot to be learned about the reactivity of Sm-enolates, their ability to direct the Reformatsky reaction is apparent, and the results of these reactions have provided some useful insight. Utimoto and Matsubara were able to produce Sm-enolates (Scheme 1.31, **6**) from α -bromo esters, which could successfully couple with cyclohexanone in high yields (Scheme 1.31, **7**).⁸⁰ When the enolate formed *in situ* was quenched with D₂O at the reaction temperature (-50°C), the expected deuterated species

was isolated (Scheme 1.31, **8**); however, when the temperature was raised to 0°C after reduction, followed by quenching with D₂O, a rearranged product was obtained (Scheme 1.31, **9**). This experiment identified that the intermediate enolate is stable at low temperatures (-50 °C), but goes through a thermal isomerization when the temperature is raised. Furthermore, the isomerized enolate could not couple with aldehydes or ketones to produce a Reformatsky product.



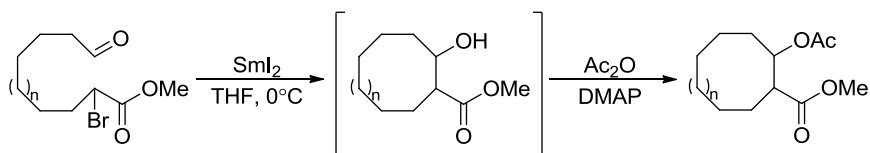
Scheme 1.31 Sm-enolates in Reformatsky reactions

Jamison explored a range of intermolecular Reformatsky reactions⁸¹ and found that primary and secondary α -bromo and α -chloroketones can be used to form the enolates. The enolates can also react with simple and hindered aldehydes and ketones (Table 1.7).

Table 1.7 Variety of haloketones and carbonyl substrates in the Reformatsky reaction

Entry	X	R ₁	R ₂	R ₃	Yield (%)
1	Br	H	H	Cy	94
2	Br	Me	H	Cy	80
3	Cl	H	H	Cy	>99
4	Cl	Me	H	Cy	94
5	Br	H	t-Bu	Me	98
6	Cl	H	t-Bu	Me	93

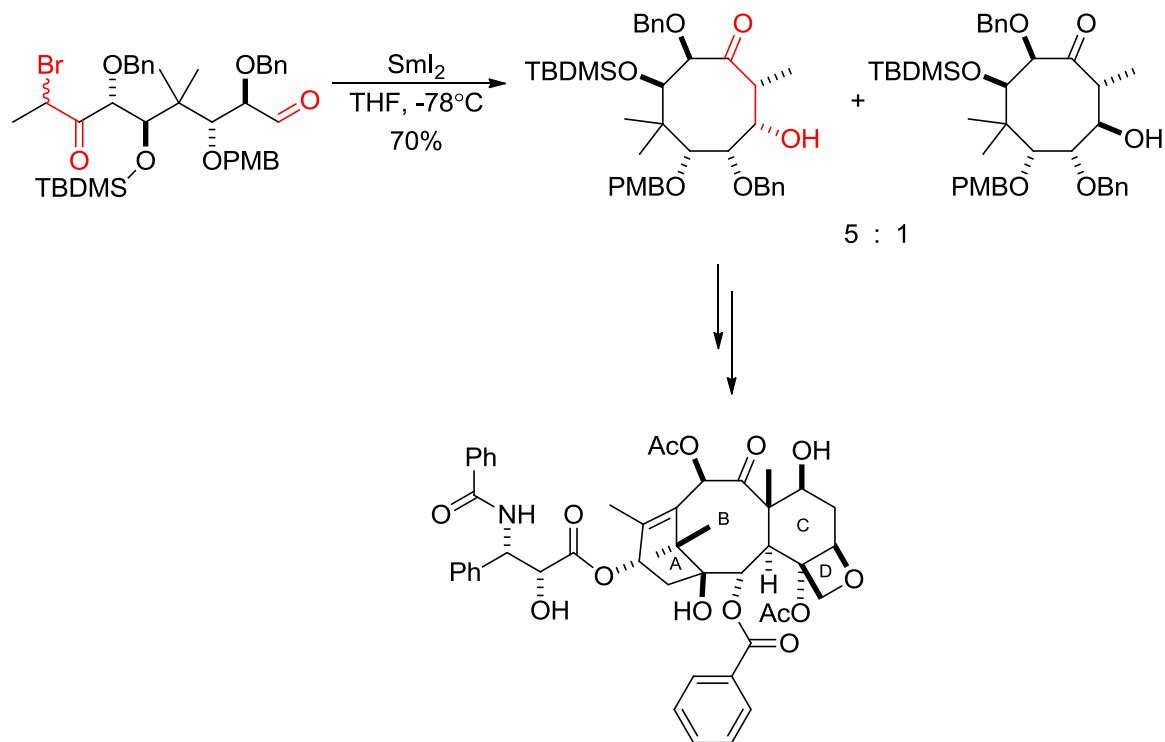
Inanaga used an intramolecular Reformatsky reaction to produce large carbocycles,⁸² a moiety common in many natural products. These large ring structures are often difficult to construct, but the SmI₂-mediated method proceeded with a simple, mild procedure obtaining high yields (Table 1.8).

Table 1.8 Large carbocycles from Sm- Reformatsky reaction

Entry	n	Final ring size	Yield (%)
1	1	8	68
2	2	9	70
3	4	11	74
4	7	14	82
5	8	15	82

In 1999, Mukaiyama published a total synthesis of the natural product paclitaxel, an anti-cancer drug marketed as Taxol®.⁸³ The Sm-mediated Reformatsky reaction was used to construct the highly functionalized 8-membered ring, which becomes the interior

ring B in the final product (Scheme 1.32). The Reformatsky reaction allowed the cyclization to proceed with high diastereoselectivity and a 70% isolated yield.

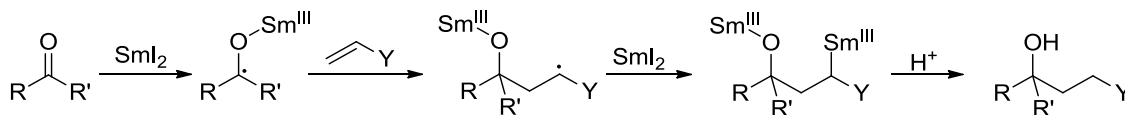


Scheme 1.32 Reformatsky reaction in the synthesis of Taxol®

1.3.4 Ketyl-Olefin Coupling

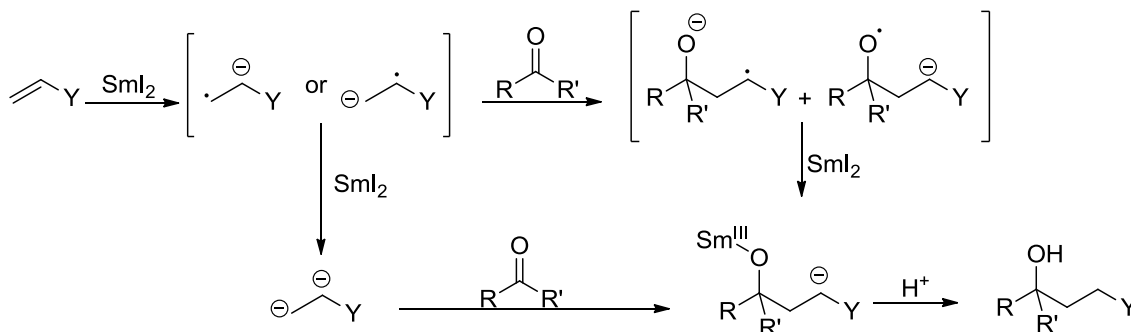
The single electron reduction of a carbonyl species followed by an inter- or intramolecular radical addition to an alkene is fundamentally one of the most important bond-forming reactions in organic synthesis. Intramolecular reactions lead to the formation of a variety of carbo- and heterocyclic ring systems of various sizes. Traditionally the mechanism for the carbonyl-alkene coupling is thought to proceed through a “carbonyl first” order (Scheme 1.33), in which the carbonyl is reduced to form

a ketyl radical anion, which adds to an olefin.⁸⁴ Further reduction by SmI₂ forms an organosamarium intermediate, which can be protonated upon acidic work up, or by a proton source in solution.



Scheme 1.33 Ketyl-olefin coupling—ketyl radical formed first

Procter also suggested that when electron-deficient alkenes are involved, an “alkene-first” mechanism could occur (Scheme 1.34). Within this scheme, SmI₂ preferentially reduces the alkene, followed by anionic (or radical) addition to the carbonyl functionality.⁸⁴

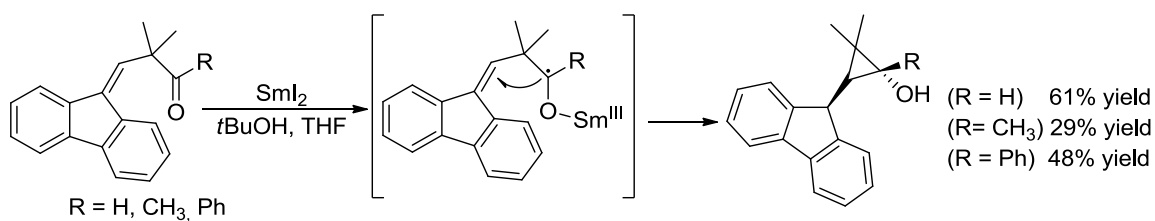


Scheme 1.34 “Alkene-first” mechanism in ketyl-olefin couplings

Procter has carried out a series of studies to differentiate between these two mechanisms, and the reaction conditions and cosolvents play a role in which pathway the reaction proceeds. Within these reactions, the outcome of intramolecular ketyl-olefin

cyclizations could be altered depending on the carbonyl substrate, stereochemistry of the alkene, as well as the proton source involved in the reaction.

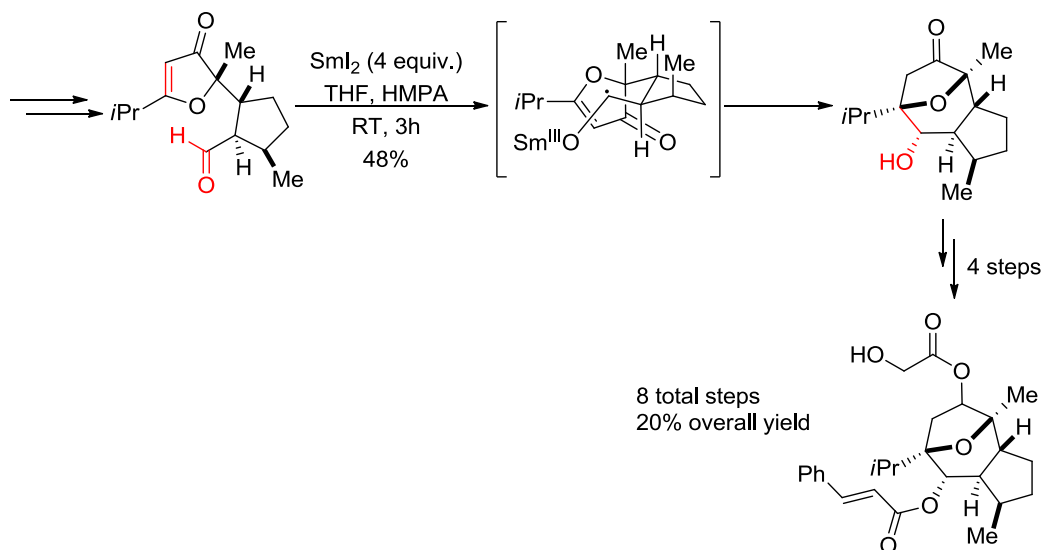
3-*Exo-trig* cyclizations of β,γ -unsaturated carbonyl compounds were carried out to produce cyclopropanols (Scheme 1.35).^{85,86} Although various cyclizations have been carried out using the Sm-mediated ketyl-olefin method, this was the first report in which a 3-membered ring was formed with aldehydes and ketones without the aid of ester-activated alkenes.



Scheme 1.36 3-*Exo-trig* cyclizations of β,γ -unsaturated carbonyl compounds

SmI₂-mediated ketyl-olefin cyclization cascade reactions often proceed with excellent control of structure and stereochemistry. This property is eloquently demonstrated when reductive cascades are used in integral carbon-carbon bond forming reactions which close large skeletons of natural products. An excellent example is the use of SmI₂ in the synthesis of englerin A, a guaiane sesquiterpene natural product. Englerin A has only recently been isolated,^{87,88} and has already exhibited a range of biological activities, including selective growth inhibition against six renal cancer cell lines, which is 2-3 –fold more potent than current pharmaceutical treatments with exceptionally low toxicity in mouse models. These unique properties suggest this compound has a high medicinal potential and is a hot target for synthetic chemists. The structure of Englerin A

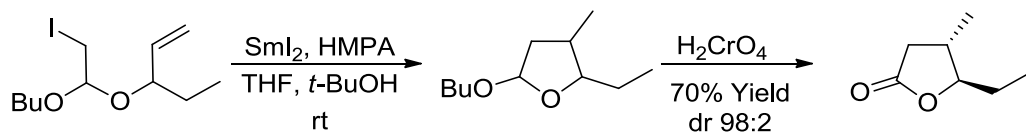
contains a highly functionalized 5-6-5 oxatricyclic framework and two ester-bearing stereogenic centers (Scheme 1.37). Chain and coworkers⁸⁹ established a short synthesis of this complex natural product using SmI₂ in a key carbon-carbon bond forming step to produce the strained cyclic interior, while maintaining the absolute stereochemistry of the natural product. The second synthetic step calls for a Michael addition, in which a diastereomeric mixture of aldehydes (2:1 *dr* desired: Σ others) cannot be avoided. Even with this caveat, Sm/HMPA-mediated ketyl-radical cyclization onto an alkene forms the desired structure in 43% yield, with the correct stereochemistry and oxidation level needed to perform the subsequent reactions (Scheme 1.37). This critical carbon-carbon bond forming reaction was not successful using any other single electron reductant, such as titanium(III), vanadium(I) or lithium naphthalenide. The use of HMPA was necessary to achieve the desired chemical transformation. This synthetic approach produces a 20% overall yield in an 8-step synthesis of the natural product Englerin A.



Scheme 1.37 Ketyl-olefin cyclization in the synthesis of englerin A

1.3.5 Halide-Olefin Coupling

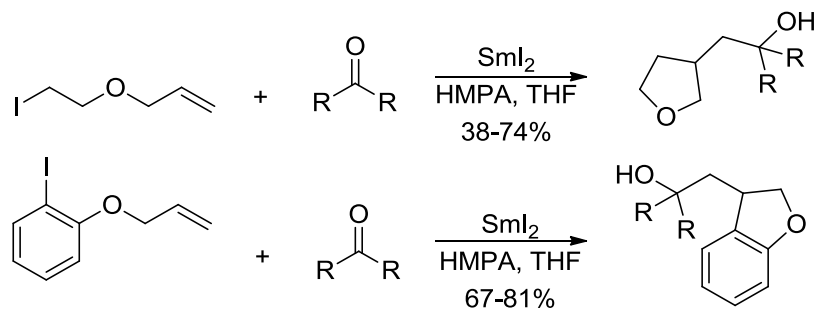
Another method of carbon-centered radicals adding or cyclizing onto unsaturated regions arise from radicals formed through halide reduction. Prior to the use of SmI_2 , halide reductions were commonly initiated by tributyltin hydride. While this reagent can successfully promote radical formation and successive cyclization, the experimental procedure for the removal of the tin-containing byproducts after the reaction is extensive. Also, the radicals produced are often quenched through hydrogen atom transfer by the tin hydride in solution, leading to a diminished amount of desired cyclized product. Utilizing SmI_2 has greatly improved the conditions and scope of these reactions. The most successful and most commonly reported halide-olefin reactions are intramolecular. Fukuzawa used an intramolecular cyclization with SmI_2/HMPA to form a substituted lactone in a simple two-step procedure (Scheme 1.38).⁹⁰



Scheme 1.38 Halide-olefin cyclization

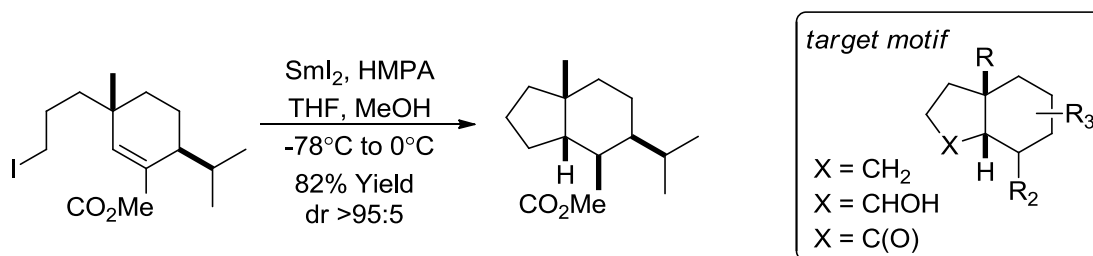
Molander has shown that SmI_2 -mediated halide-olefin couplings can proceed through tandem intramolecular cyclization followed by intermolecular coupling (Scheme 1.39).⁹¹ Within this process, Molander concluded that the alkyl halide was reduced to a radical followed by radical cyclization onto the pendant olefin forming a terminal carbon radical. An intermediate organosamarium is produced through a second single-electron

transfer to the radical, which then adds to the carbonyl electrophile. It is important to note that the radical cyclization is faster than the reduction of the radical intermediate, which would lead to β -elimination of one of the two alkoxy groups.



Scheme 1.39 Halide-olefin cyclization followed by tandem Barbier reaction

The Sm-mediated halide-olefin cyclization provided a stereoselective route to compounds with *cis*-hydrindane cores.⁹² The desired bicyclic product was obtained in high yield and a single diastereomer was isolated (Scheme 1.40).

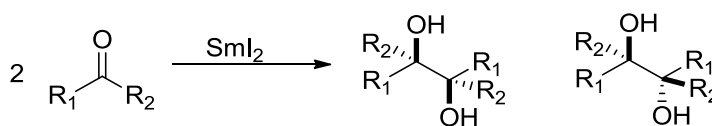


Scheme 1.40 Stereoselective syntheses of *cis*-hydrindane cores

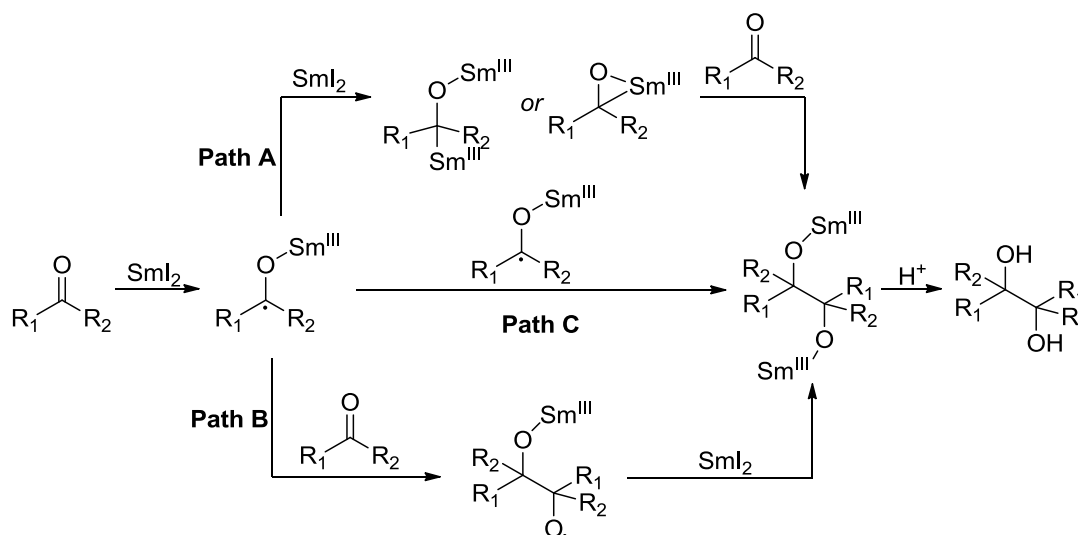
1.3.6 Pinacol coupling

Traditional pinacol reactions are the reductive coupling of carbonyl groups to form 1,2-diols (Scheme 1.41). SmI₂ provides a straightforward, mild method for

synthesizing this important moiety with high yield. The path the reaction follows depends on the carbonyl functionality being reduced (aldehyde, ketone, or conjugated carbonyl). After the initial electron transfer to reduce the carbonyl, the radical anion produced could proceed through three different pathways (Scheme 1.42). In Path A, the ketyl radical is reduced by a second electron transfer forming a dianionic or metallaoxirane species, which can add to another carbonyl, forming the coupled product. Path B assumes after the initial electron transfer to form the ketyl radical, a radical-radical coupling occurs. In Path C, the radical formed from the reduction couples with an unreacted carbonyl compound.

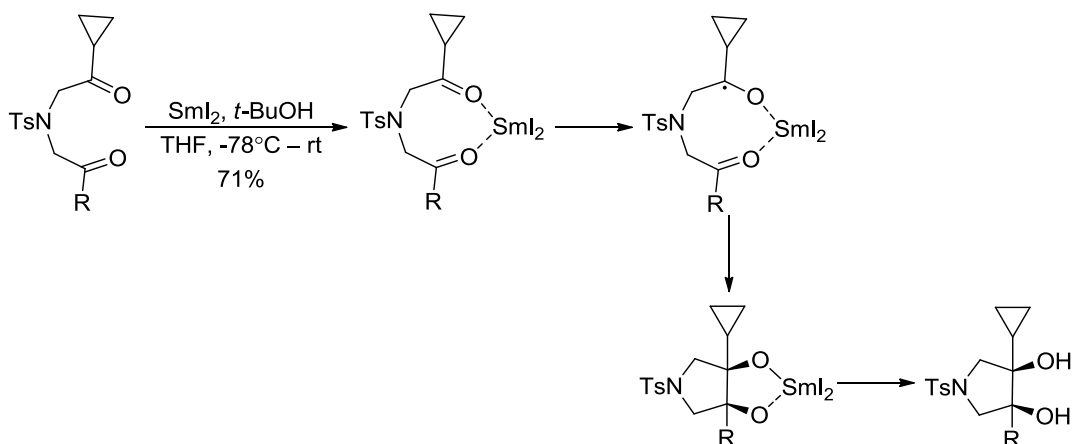


Scheme 1.41 Pinacol coupling with two aldehydes or ketones



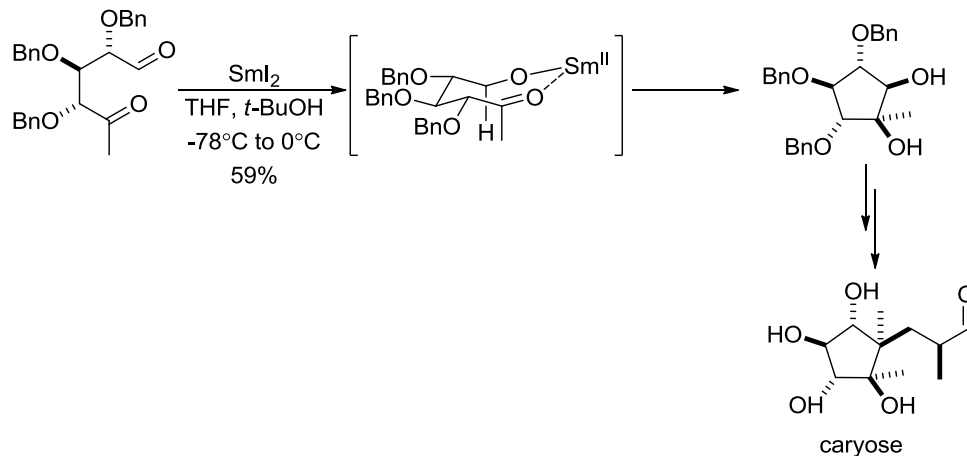
Scheme 1.42 Potential pathways for Sm-mediated pinacol coupling

With an intramolecular pinacol reaction there is strong evidence⁹³ that the mechanism follows through a pathway similar to Path C (Scheme 1.42), where an oxophilic Sm(II) is coordinated to both of the carbonyl oxygens (Scheme 1.43). The bridged structure stabilizes the ketyl intermediate and facilitates inner-sphere single-electron transfer, promoting bond formation.



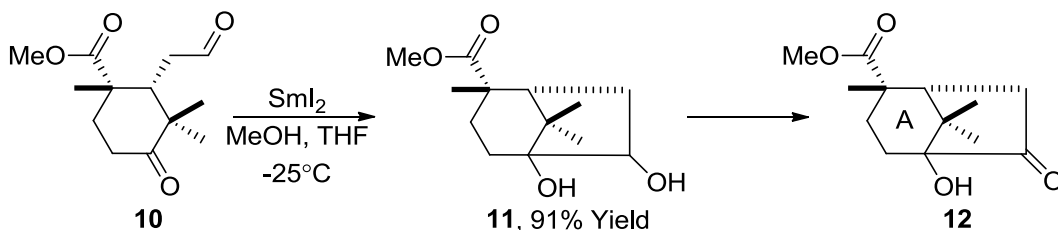
Scheme 1.43 Intramolecular pinacol reductive coupling

As compared to intermolecular pinacol reactions, intramolecular cyclizations tend to have a greater degree of diastereoselectivity. In the synthesis of the monosaccharide, caryose, a Sm-mediated pinacol coupling was used to construct *cis*-1,2-diols from 1,5- and 1,6-dicarbonyl precursors.⁹⁴ The cyclization produced the *cis* stereoisomer almost exclusively. The selectivity stems from the polar substituent group α to the reacting carbonyl, which orients *anti* to the newly formed *cis*-1,2-diol (Scheme 1.44).



Scheme 1.44 Ketyl-radical cyclization to form caryose

Intramolecular pinacolization is used for the synthesis of the bicyclic ring system of Taxol®. Intramolecular reductive coupling of the aldehyde and ketone by SmI_2/MeOH in THF provides bicyclic diol **11** in a 91% yield. Subsequent Swern oxidation provides key intermediate **12** in an 85% yield (Scheme 1.45).⁹⁵



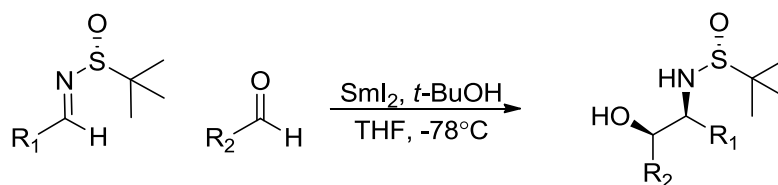
Scheme 1.45 Intramolecular pinacolization for the bicyclic ring system of Taxol®

Coupling of a carbonyl species with imine derivatives (such as oximes and hydrazones) is commonly referred to as a hetero-pinacolization, and has found utility in the formation of heterocycles and both vicinal and β -amino alcohols. It has been

proposed that the reaction proceeds through formation of a ketyl radical which adds to the C=N bond.⁸⁴

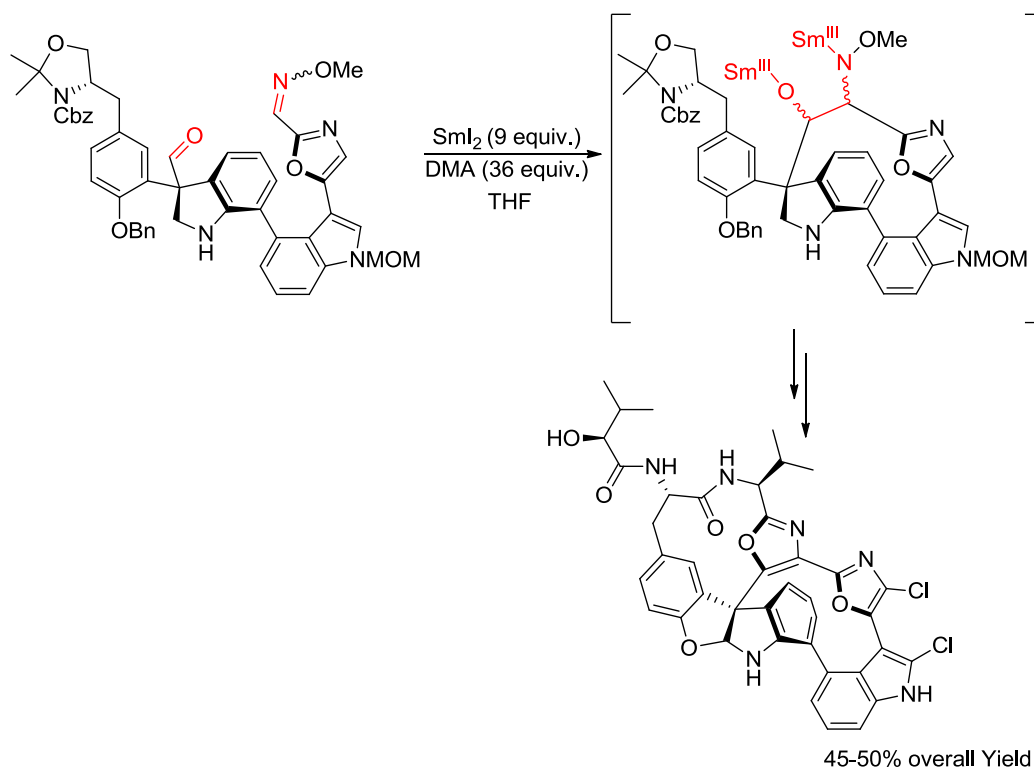
While hetero-pinacolization is the most direct route for constructing β -amino alcohols, achieving control over the stereoselectivity has been an issue in the reactions reported. Xu and Lin devised a system which couples N-sulfinyl imine with an aldehyde to obtain the desired β -amino alcohol with high yields and excellent control over the stereo- and chemoselectivity (Table 1.9).⁹⁶ The diastereoselectivity is achieved through a chelation controlled pathway where the final stereochemistry was directed by the N-sulfinyl group and the steric bulk of the aldehyde.

Table 1.9 Coupling of N-sulfinyl imine with aldehydes to form β -amino alcohols



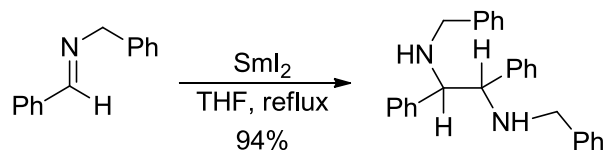
Entry	R ₁	R ₂	Yield (%)	dr	ee
1	4-CH ₃ C ₆ H ₄	<i>i</i> -Pr	92	>99:1	98
2	4-CH ₃ C ₆ H ₄	C ₆ H ₁₁	90	99:1	>99
3	4-CH ₃ C ₆ H ₄	PhC ₂ H ₄	95	88:12	95
4	Ph	<i>i</i> -Pr	86	99:1	97
5	BnOCH ₂	<i>i</i> -Pr	82	>99:1	97

An excellent example of the use of hetero-pinacolization is the formation of the macrocycle of diazonamide A.^{97,98} The aldehyde-oxime pinacol reaction closed a 14-membered ring (Scheme 1.46), the largest ring reported through this mechanism, and was the first to trap the intermediate organosamarium with a reagent other than a simple acylating agent (step not shown).



Scheme 1.46 Pinacol coupling to form 14-membered ring of diazonamine A

Pinacol-type reactions also describe homocoupling reactions of imines to form diamines or asymmetric coupling of imines with nitrones or other imine derivatives. One of the first reports of SmI_2 -mediated imine coupling was done by Enholm⁹⁹ (Scheme 1.47), and the mechanism was assumed to proceed through a similar radical coupling or radical attack as for pinacol homocoupling (Scheme 1.42). The vicinal diamines formed were achieved with high yields, but an undetermined mixture of meso- and d,l,-diastereomers was obtained.



Scheme 1.47 Pinacol homocoupling of imines

1.4 Project Goals

This dissertation focuses on studying the mechanistic impacts that the inclusion of different additives have on the Sm(II)-mediated reactions. Additives can be used to further tune the rate and selectivity of SmI₂ reduction, which is a dominant factor in the success of many of the reactions. The studies carried out focus on obtaining mechanistic information on the systems through detailed kinetic and spectroscopic studies to determine the role of the additives. The knowledge of the mechanism of the systems and of the impact that the additives have will assist synthetic chemists in choosing suitable SmI₂-additive systems for their desired transformations. The areas that were studied include (a) relative rates of reduction with SmI₂, (b) SmI₂-HMPA in the samarium Barbier reaction, (c) SmI₂-Ni(II) in the samarium Barbier Reaction, (d) SmI₂-H₂O in the reductive ring-opening of lactones and (e) SmI₂-H₂O-amine in the reduction of esters.

Chapter 2. SmI₂ Reduction of an Aldehyde vs. α,β -Unsaturated Ester

2.1 Background and Significance

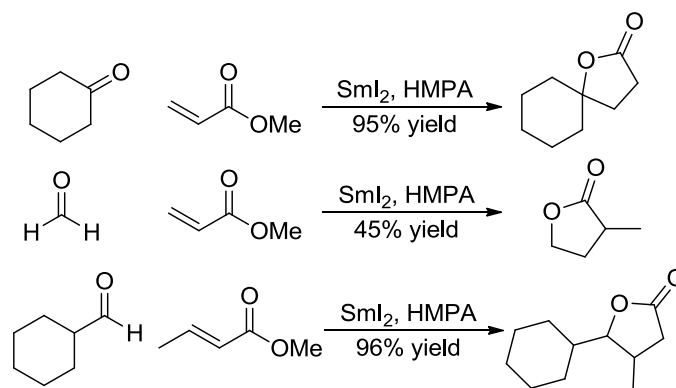
2.1.1 SmI₂ Reduction of Various Functional Groups

A powerful trait of SmI₂ single-electron reductions is the ability of the reagent to reduce different substrates at varying rates. As a consequence, SmI₂ can be used for sequential selective functional group reduction and follow-up bond-forming reactions in complex substrates or bimolecular coupling. This variation of reduction rate is the driving force behind many of the carbon-carbon bond forming reactions carried out by SmI₂, such as the Barbier and Reformatsky reactions, as well as ketyl-olefin and halide-olefin couplings.

The difference in the rate of reduction of various functional groups was first observed by Kagan in his initial experiments with SmI₂.¹ The reductive coupling of benzyl bromide to form 1,2-diphenylethane was completed within 20 min with an 82% yield, while the same reaction with benzyl chloride required 1.5 h to achieve a 67% conversion. Additionally, he reported complete reduction of halides within a few hours (SmI₂ with no additives), while the reactions of carbonyl containing substrates (aldehydes and ketones) were carried out for a day. Reduction of a 1:1 mixture of *n*-octanal and 2-octanone led to selective reduction of the aldehyde, suggesting a difference in rates with the reduction of different carbonyls.¹ Based on these principles of varying rates of reduction with SmI₂, Kagan carried out the Barbier reaction, a carbon-carbon bond

forming reaction in which both substrates are added to the reductant simultaneously. These systems produced the coupled tertiary alcohol product in high yield and minimal side product formation.¹

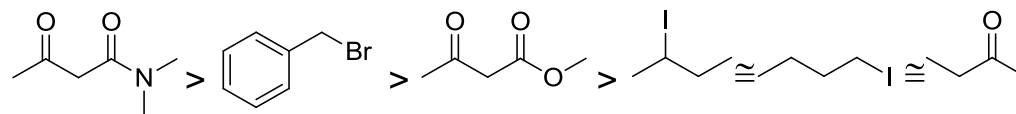
Inanaga used SmI₂ to carry out a cross-coupling of aldehydes or ketones with α,β -unsaturated esters to form lactone frameworks.⁴⁹ This type of coupling was previously accessible only through electrolytic methods or reduction with Zn metal.^{100,101} Using SmI₂ provided a mild, straightforward approach with minimal effort and very short reaction times (3-4 h with SmI₂, 1 min with SmI₂-HMPA). While the mechanism of the reaction was not discussed by Inanaga, it seems likely that the high degree of selectivity was achieved through the reaction proceeding through a ketyl-olefin coupling pathway. Previous reports had shown that α,β -unsaturated esters are only reduced at the point of unsaturation, and that the carbonyl remains unreacted in the presence of SmI₂.¹ Based on those findings it was believed that the aldehyde or ketone is preferentially reduced to its radical anion by SmI₂, followed by radical attack onto the olefin of the α,β -unsaturated ester, and subsequent radical cyclization to form the final lactone. More current results suggest that the α,β -unsaturated ester is reduced, followed by radical attack into the carbonyl of the aldehyde or ketone (*vide infra*).



Scheme 2.1 Ketyl-olefin radical cyclization to form lactones

These early results set the stage for exploration of the rates of reactivity of SmI_2 with individual functional groups, typically investigated through competition studies or kinetic experiments. Rate constants for the reduction of different substrates by SmI_2 have unveiled some general trends in reactivity (Scheme 2.2).

In the absence of any additives, SmI_2 reduces alkyl halides and ketones at similar rates ($10^{-4} \text{ M}^{-1}\text{s}^{-1}$).¹³ The rate of reduction of a carbonyl in a β -ketoester or amide is drastically increased (10^{-1} and $10^2 \text{ M}^{-1}\text{s}^{-1}$ respectively). Flowers *et al.* suggested that this increase in rate is due to the dicarbonyl providing a region for Sm-chelation, stabilizing the transition state and facilitating the electron transfer.^{13,68} A slight increase in rate of alkyl halides reduction occurred when a secondary radical is produced from the reduction (Scheme 2.2). Additionally, reduction of a benzyl halide yielded an order of magnitude increase in rate.⁵⁵ These relative rates of reduction provide some insight into the expected reactivity in a bimolecular heterocoupling reaction or reduction of multifunctional compounds containing these functional groups.

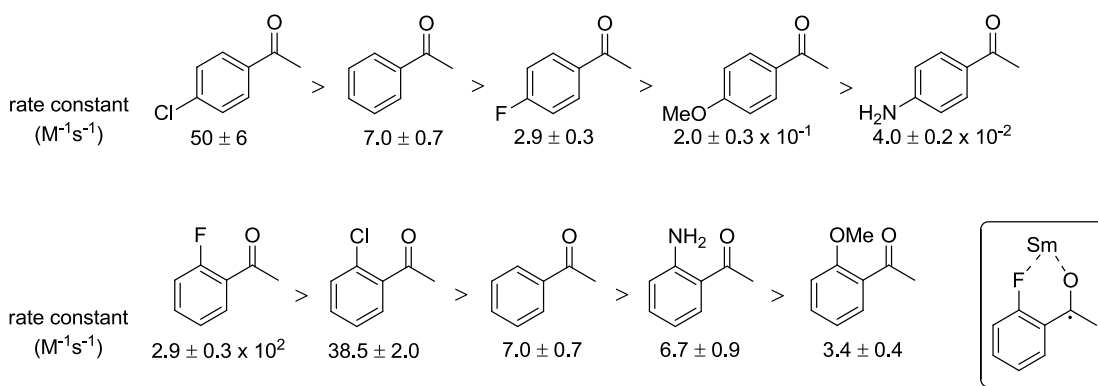


Scheme 2.2 Relative rates of reduction by SmI_2 .

While studying the rate of reduction of ketones, Flowers *et al.* found that the presence of a fluorine, methoxy, or amino substituent at the 4'-position of acetophenone decreased the rate of reduction. (Scheme 2.3).⁶⁸ The substituents tested increase the electron density to the ketone, making it more difficult to reduce. The chlorine substitution increased the rate of reduction as compared to the unsubstituted acetophenone. This change possibly occurs through the ability of chlorine to act as a deactivating ortho/para director. Additional activation parameter studies on the system indicated a highly ordered transition state for the reductions, suggesting coordination between the oxygen of the carbonyl and Sm, a trait commonly seen with ketone reductions by SmI_2 .

The trends for the reduction of acetophenone with a 2'-substitution revealed some major differences as compared to the 4'-substituted substrates. The rate constants observed for the amino and methoxy substitutions are an order of magnitude or more greater as compared to the substitutions placed at the 2'-position on the aryl ring (Figure 2.3).⁶⁸ An increase in the rate of reduction was also observed with the halide substitutions, in which both fluoride and chloride at the 2'-position caused the rates to be faster than acetophenone by one and two orders of magnitude, respectively. The increase in rate is most likely a result of Sm-chelation between the oxygen of the carbonyl and the

substituent at the 2'-position. Activation parameters also indicate a highly ordered transition state, again providing support for the chelated intermediate. The greatest rate enhancement was observed with the 2'-fluorine substitution. Based on the thermodynamic properties observed, samarium may be fluorophilic, thus increasing the interaction and stability of the transition state through Sm-chelation between the oxygen and fluorine (Scheme 2.3). This interaction and increase in rate will have a large impact on reactions requiring the reduction of β -substituted fluoroketones. Methods directed towards asymmetric synthesis of chiral organofluorine compounds are of interest within the pharmaceutical industry, and these results suggest that SmI_2 may exhibit selectivity to form ketyl radicals in positions where fluorine chelation can occur.



Scheme 2.3 Rate constants for the reduction by SmI_2

Kinetic work in the Flowers group has also highlighted how the inclusion of additives and cosolvents drastically affects the rate in which SmI_2 reduces various functional groups.^{14,19,24-26,52,55,57,102-104} In addition, as shown above, the position of the substitutions and formation of Sm-bound intermediates greatly affects the rate and

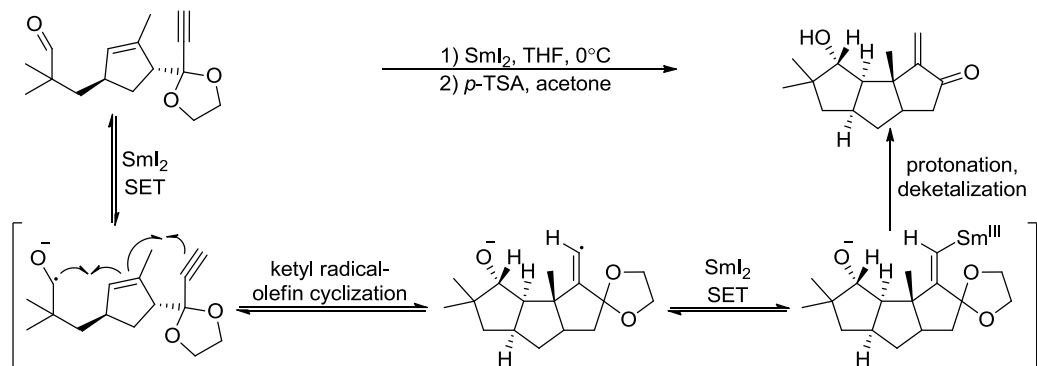
success of many reactions.¹⁰⁵⁻¹⁰⁷ Based on all of these parameters it has been difficult putting together a database of rate constants for a large range of functional groups; however, this information is vital for synthetic chemists as they develop and design new Sm-mediated reactions for complex molecules.

2.1.2 SmI₂ in Cascade Syntheses

Cascade or sequential reactions carry out a sequence of multiple bond-forming transformations in one-pot, without isolation or purification of any intermediate products. As the reaction progresses, the product from an initial transformation participates in a subsequent reaction for additional bond formation. This series of transformations allows for the formation of complex multifunctional and polycyclic compounds. However, for sequential reactions to be useful they must be extremely efficient and chemoselective to proceed with high yields and minimize unwanted side product formation. In Sm-mediated cascade reactions the different rates of reduction of various functional groups is exploited, and pathways are designed in a way that the sequential reductions and radical reactions take place in an order which properly assembles the complex molecule desired.

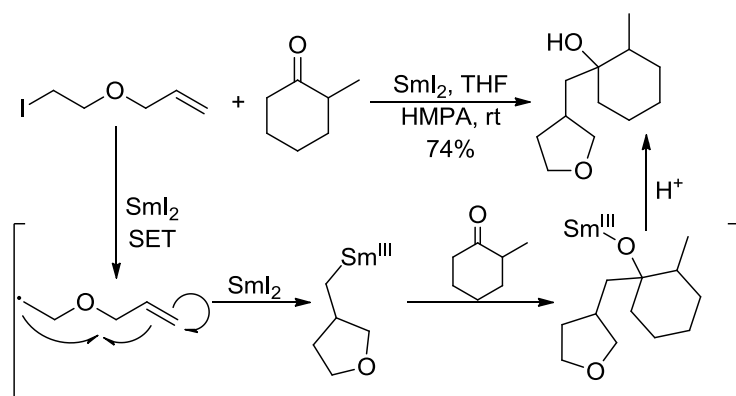
A *radical-radical cyclization* facilitated a critical step in the synthesis of (±)-hypnophilin, a pharmaceutical target (Scheme 2.4).¹⁰⁸ A ketyl radical forms through reduction by SmI₂, which goes through a tandem *5-exo-trig* cyclization of the radical onto the alkene followed by a *5-endo-dig* cyclization of the newly formed tertiary radical onto the alkyne to form the radical-bearing tricyclic system. The final product is obtained following a second SET from SmI₂ and proton abstraction. Radical-radical sequential

reactions are favored for stable radicals that are relatively inert to reduction by SmI_2 to the corresponding anion (e.g. tertiary, aryl and allylic radicals).



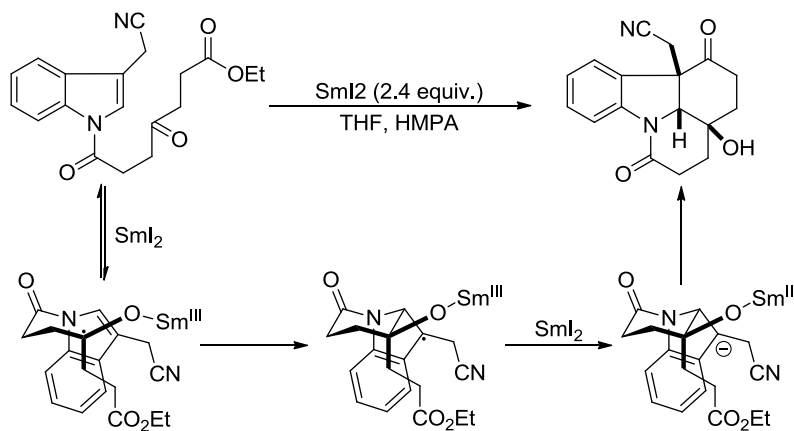
Scheme 2.4 Sm-mediated cascade for the synthesis of (±)-hypnophilin

Sm -mediated *radical-anion cascade* reactions are the most commonly employed examples of SmI_2 -cascade reactions. These systems usually proceed through an initial radical-alkene cyclization, as shown below (Scheme 2.5).¹⁰⁹ The initial single-electron transfer to the carbon-iodide forms a primary radical, which readily proceeds through an intramolecular *5-exo-trig* cyclization to form a cyclopentane containing a pendant primary radical. The radical can be reduced to an organosamarium after a second electron transfer. The organosamarium then proceeds through an intermolecular Sm -Barbier reaction, which upon protonation forms the final coupled alcohol in a 74% yield.



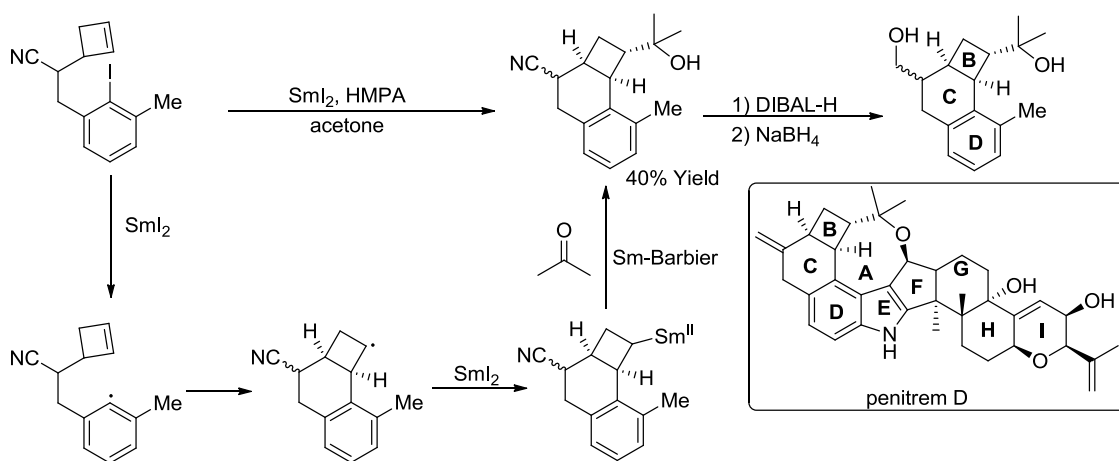
Scheme 2.5 Tandem intramolecular radical cyclization, Sm-Barbier coupling

A radical-anionic cascade reaction was utilized in the synthesis of strychnine, a *Strychnos* alkaloid,¹¹⁰ forming three stereogenic centers in the polycyclic system (Scheme 2.6). The mechanism proposed for the reaction initiates with the reduction of the internal ketone forming a tertiary radical, which adds to the unsaturation on the pentane ring. After a second electron transfer by SmI_2 , addition into the carbonyl completes the transformation.



Scheme 2.6 Synthesis of a *Strychnos* alkaloid

For the synthesis of the BCD ring structure of penitrem D, a radical-alkene cyclization followed by a Barbier coupling was carried out (Scheme 2.7).¹¹¹ The starting material was designed to promote radical-alkene cyclization to form a stable six-membered ring upon reduction with SmI_2 . The pendant radical was then reduced to an organosamarium, which is followed up with an intermolecular Barbier reaction with acetone. The product of the cascade is reacted to reduce the nitrile to a primary alcohol—an intermediate construct for the synthesis of penitrem D.

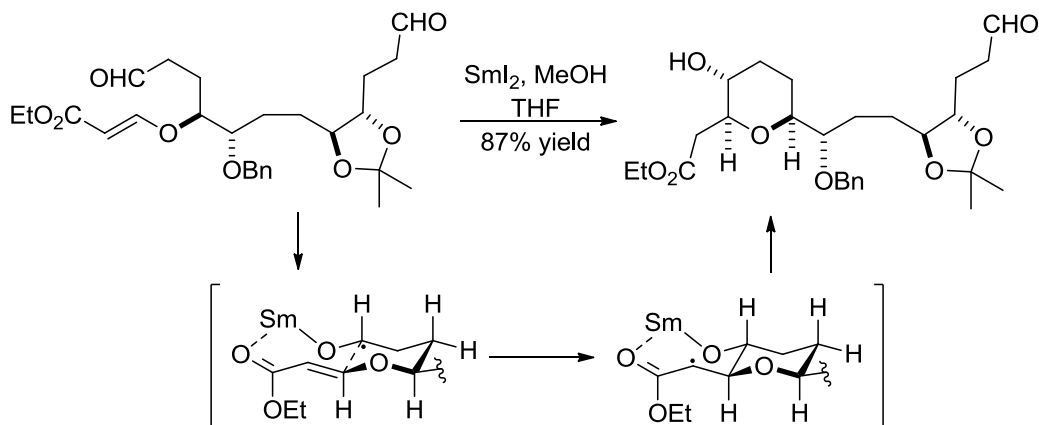


Scheme 2.7 Radical-anionic cascade for the synthesis of the BCD ring structure of penitrem D

These systems highlight just a few of the many examples of SmI_2 in cascade reactions. As stated previously, the key to their success is the difference in the rate at which SmI_2 reduces the susceptible functional groups. These rate differences can lead to selective reactivity of one functional group on complex multifunctional starting materials.

2.1.3 Selective Cyclization of Functionalized Dialdehyde Compounds by SmI₂

When cascade reactions are performed with substrates containing multiple reductive functionalities, it is often difficult to determine the pathway through which the cascade proceeds. Nakata utilized SmI₂ in a key ring-closing step in the stereoselective synthesis of Mucocin, an antitumor agent.¹¹² They observed the selective reduction of one aldehyde, while another pendant aldehyde remained unreacted on the molecule. They proposed the selectivity arose from a Sm-chelated intermediate, with the ketyl radical anion and the carbonyl from the α,β -unsaturated ester within close proximity on the molecule (Scheme 2.8). This chelation also facilitated the subsequent radical addition onto the olefin to close the six-membered ring.



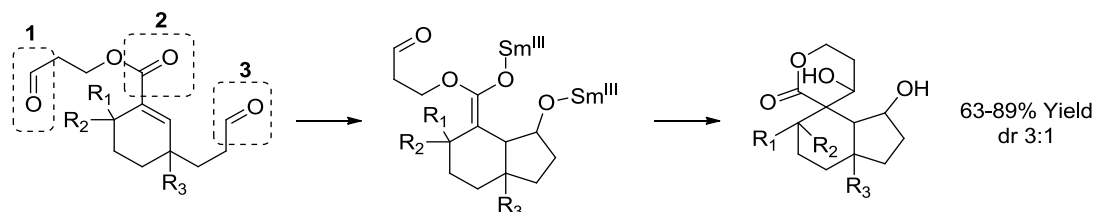
Scheme 2.8 Sm-mediated ring closure in the total synthesis of Mucocin.

A similar dialdehyde cyclization cascade was developed by Procter, forming a tricyclic system with 4 stereocenters and high diastereoselectivity (Scheme 2.9).¹¹³ The proposed driving force behind the desired cyclization is Sm-mediated selective reduction

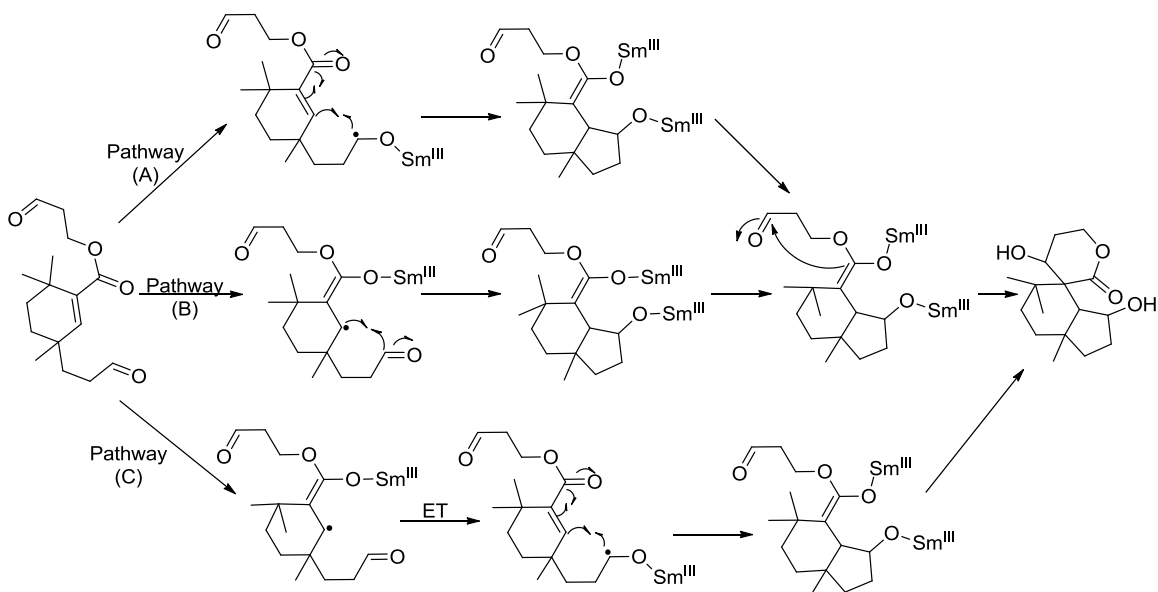
of the aldehyde carbonyls “one at a time” as it proceeds through the cascade.¹¹³ The proposal of one pendant aldehyde being selectively reduced over another is surprising since they are in nearly identical environments, and based on thermodynamic properties it is unclear why one would be reduced at a rate different than the other. In the starting molecule, there are three accessible carbonyl groups available for reduction by SmI₂, two pendant aldehydes (Scheme 2.9, carbonyls **1** and **3**), and an internal α , β -unsaturated ester (Scheme 2.9, carbonyl **2**). Rate constants for the reduction of these individual functional groups by SmI₂ have not been determined, so it is uncertain which functionality would be preferentially reduced. However, due to the selective nature of the reaction, the mechanism most likely follows a discrete pathway.

Based on the isolated product, a few mechanistic pathways could be envisioned (Scheme 2.10). Pathway A assumes the reduction and subsequent cyclization of aldehyde **3** occurs at a rate faster than a similar reduction and cyclization can take place at aldehyde **1**, causing the initial step to predominate through the radical cyclization onto the neighboring olefin. In both pathways B and C, the α , β -unsaturated ester is reduced preferentially over the aldehydes, forming a Sm-enolate. In pathway B, the radical proceeds through radical addition to aldehyde **2**, followed by cyclization of the enolate into aldehyde **1**. Finally, another pathway can be envisioned with initial SmI₂ reduction of the α , β -unsaturated ester, in which following reduction, the electron is transferred to the aldehyde within close proximity, reforming the ester. The ketyl radical then proceeds through radical addition onto the olefin.^{26,114} Without additional kinetic information it is

difficult to elucidate which pathway it proceeds through. Even without knowledge of the mechanism, the information at hand conveys that the reaction maintains control over the diastereoselectivity, which could be attributed to the strong chelation of Sm(III) and oxygen, possibly through a bridging intermediate. By determining the rates in which SmI₂ reduces both aldehydes and α,β -unsaturated esters insight into the potential pathway of the cyclization will be gained, allowing this Sm-mediated cyclization to be applied more efficiently to other syntheses.



Scheme 2.9 Proposed intermediate for cyclization



Scheme 2.10 Possible mechanistic pathways for cyclization

2.2 Experimental

2.2.1 Materials

THF was purified after purging with argon gas and passing over a column of activated alumina by a Solvent Purification System (Innovative Technology Inc.; MA). Dried solvents and reagents were stored in an Innovative Technology, Inc. drybox containing an argon atmosphere and a platinum catalyst for drying. Octanal and tertiary butanol (*t*BuOH) were purchased from Acros and distilled under vacuum (octanal from CaO) before use. Lithium diisopropyl amine (2 M in THF) and resublimed iodine crystals were purchased from Aldrich. *n*-Butyl acrylate, trifluoroethanol (TFE), copper(II) iodide, Comin's reagent (N-(5-chloro-2-pyridyl)bis(trifluoromethane sulfonamide), Pd(II) acetate, *n*-butyl lithium and triphenylphosphine were purchased from Alfa Aesar and used with no further purification. 3-methyl-2-cyclohexen-1-one and iodomethane were purchased from Acros, and CO(g) from Airgas, all used with no further purification. 3-butyl-3,6,6-trimethylcyclohex-1-ene methylcarboxylate was synthesized via the method described below (2.2.3.1). SmI₂ was prepared by stirring Sm metal and iodine in THF until the characteristic blue color of Sm(II) appeared. The concentration of SmI₂ (0.10 M in THF) was determined by iodometric titration.

2.2.2 Instrumentation

Proton and carbon NMR were recorded on Bruker 500 MHz spectrometer. GC-MS analysis was performed with HP 5890 Series Gas Chromatograph with an HP Mass

Selector Detector. Kinetic studies in THF were performed using a computer-controlled SX-20 MV stopped-flow reaction spectrophotometer (Applied Photophysics Ltd., Surrey, UK). Column chromatography was performed on CombiFlash Rf 200 series (Teledyne ISCO).

2.2.3 Methods

2.2.3.1 Synthesis of 3-butyl-3,6,6-trimethylcyclohex-1-ene methylcarboxylate

The procedure for the synthesis of 3-butyl-3,6,6-trimethylcyclohex-1-ene methylcarboxylate was carried out through a modified protocol outlined by D.J. Procter (*Org. Biomol. Chem.* **2011**, 9, 2433).

3-Methyl-2-cyclohexen-1-one (623 μ L, 5.5 mmol) in 5 mL THF was added to a stirring solution of lithium diisopropyl amide (LDA) (20 mL, 2 M in THF), cooled to -78°C . The reaction mixture was warmed to room temperature and stirred for 30 min. Upon cooling to -78°C the reaction was treated with MeI (9.0 mL, 27.6 mmol), dropwise, and stirred at room temperature for 12 h. The reaction was quenched with H_2O (50 mL) and extracted with EtOAc. The organic layer was dried with MgSO_4 and concentrated with rotary evaporation. The crude reaction mixture was identified as 3,6-dimethylcyclohex-2-enone by GCMS, as well as remaining starting material as the remaining balance of the reaction.

The crude product of 3,6-dimethylcyclohex-2-enone was subjected to the second methylation by repeating the procedure described above. After work up of the reaction,

the crude product was purified by silica gel chromatography (1% EtOAc in petroleum ether) to yield 3,6,6-trimethylcyclohex-2-enone (77% yield, two steps).

*n*BuLi in THF (3.6 mL, 2.6M in THF, 9.4 mmol) was added dropwise to a stirring solution of CuI (0.9 g, 4.7 mmol) in THF (30 mL) at -20°C. The solution was stirred at 0°C for 30 min before being cooled to -20°C and treated dropwise with 3,6,6-trimethylcyclohex-2-enone (0.3 g, 2.3 mmol) in THF (20 mL). The reaction mixture was stirred at room temperature for 3 h, then cooled to 0°C. Comin's reagent (1.85 g, 4.7 mmol) in THF (20 mL) was added and stirred for 5 h at room temperature. The reaction was quenched with aq. sat NH₄Cl and extracted with ethyl ether. The crude reaction mixture was purified by silica gel chromatography (1% EtOAc in petroleum ether) to yield 3-butyl-3,6,6-trimethylcyclohex-1-ene methylcarboxylate (60% yield).

In the glovebox, the triflate product in dried DMF (7.5 mL) was added to Pd(OAc)₂ (0.05 g, 0.23 mmol) and Ph₃P (0.13 g, 0.50 mmol). The resulting reaction mixture was treated with Et₃N (675 μL, 4.8 mmol) followed by dried MeOH (4.9 mL, 4.87 mmol). The reaction was removed from with the box, and degassed with CO for 30 min. The resulting red solution was stirred at 40°C for 12 h under a CO balloon. The reaction was quenched with H₂O and extracted with ethyl ether. The product was purified via column chromatography, eluted with 5% EtOAc in petroleum ether, followed by a second column, eluted with 1% EtOAc in petroleum ether. An overall yield of 1.65% of the purified product was obtained at the end of the four step synthesis.

2.2.3.2 General Procedure for SmI₂ Reduction

Reactions were carried out in a drybox with degassed reagents. SmI₂ was prepared as described above. Substrate (8.0×10^{-4} mol) was added to SmI₂ (20 mL, 0.1 M) with either *t*BuOH (5.1 mL, 0.054 mol) or TFE (4.07 mL, 0.054 mol). The reactions of substrate, proton donor and SmI₂ were stirred for 12 hours to ensure complete conversion. The reaction was quenched by exposing to air. The reaction mixture was then washed with 1 M aq. HCl and extracted twice with ether. The organic layer was washed individually with H₂O, Na₂S₂O₃ and brine, dried over MgSO₄ and then concentrated to obtain the reduced product(s).

2.2.3.3 General Procedure for Stopped-Flow Studies

The SmI₂-proton donor solution and substrate were taken separately in airtight Hamilton syringes from a drybox and injected into the stopped-flow system. The cell box and the drive syringes of the stopped-flow reaction analyzer were flushed a minimum of three times with degassed solvents to make the system oxygen-free. The concentration of SmI₂ used for the study was 5 mM. Under pseudo-first order conditions, the concentrations of the substrates (20-80 mM) and proton sources (125 mM) were kept high relative to SmI₂. Observed reaction rate constants were determined from exponential fitting of the decays of SmI₂ at 555 nm. The decay of the SmI₂ displayed first-order behavior over >3 half-lives for SmI₂.substrate combinations.

Using the initial rates method of kinetic analysis the concentration of the substrates were held at only a slight excess (4-9 mM), while the concentration of the proton sources remained high (125 mM). Linear decays within the first 5% of the reaction were fit to determine observed reaction rates.

Rate orders for octanal, *n*-butyl acrylate, TFE, *t*BuOH and 3-butyl-3,6,6-trimethylcyclohex-1-ene methylcarboxylate were derived from the plots of $\ln k_{\text{obs}}$ vs. $\ln[\text{substrate}]$. The rate order for SmI_2 was determined by two methods: (a) fractional times method from the decay traces of SmI_2 (under pseudo first order conditions), and (b) plots of $\ln k_{\text{obs}}$ vs. $\ln[\text{SmI}_2]$ using initial rates method. The rate plots were generated from the absorption decay traces obtained from a stopped-flow spectrophotometer.

2.3 Results

2.3.1 Kinetic Data

To obtain a greater understanding of how the different functional groups will be reduced by SmI_2 , kinetic experiments were carried out to determine the rate constants of both an α,β -unsaturated ester and an aldehyde. By obtaining the rate of reduction for both substrates a direct comparison could be made to determine if one functional group is reduced significantly faster over another. This understanding of the relative rates of reduction by SmI_2 can then be applied to SmI_2 -mediated cascade reactions, and aid in their design and efficiency.

2.3.1.1 Pseudo-First Order Rates

Octanal was chosen as the model aldehyde, and *n*-butyl acrylate was chosen as the α,β -unsaturated ester. The rate orders and rate constants determined from these kinetic experiments can be found in Table 2.1. In all cases, the proton source was found to be zero order, and does not play a role in the rate of the reaction.

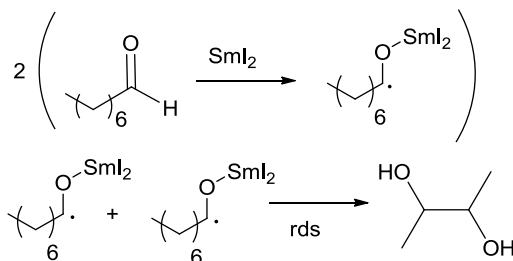
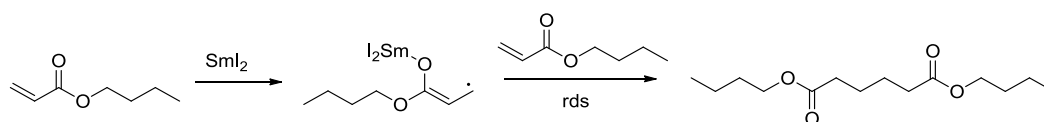
For the reduction of octanal, a second order for both SmI_2 and substrate were observed. These rate orders imply a reaction pathway in which two molecules of octanal are reduced by SmI_2 , followed by radical-radical homocoupling to form a pinacol product in the rate determining step (Scheme 2.11). These kinetic observations are supported by the synthetic results, in which the coupled pinacol predominates in addition to octanol formation.

For the reduction of *n*-butyl acrylate, a second order in substrate and first order in SmI_2 were determined. These rates suggested a mechanism in which SmI_2 reduces the acrylate to a radical anion, followed by radical addition to the olefin of a second unreacted acrylate (Scheme 2.12). A second order in substrate implies that the radical anion attack onto a second molecule of acrylate is the rate determining step, meaning that the rate constant obtained does not represent the initial reduction of the substrate by SmI_2 .

Table 2.1 Pseudo-first order rates for SmI₂ reduction of octanal and *n*-butyl acrylate

Substrate	Proton Source	Order of Substrate ^{a,b}	Order of SmI ₂ ^c	Order of Proton Source ^d	Rate Constant (M ⁻¹ s ⁻¹) ^{a,b}
Octanal	<i>t</i> -BuOH	2.2 ± 0.1	1.7 ± 0.1	0	0.04 ± 0.01
Octanal	TFE	1.8 ± 0.1	2.0 ± 0.1	0	0.03 ± 0.01
<i>n</i> -butyl acrylate	<i>t</i> -BuOH	2.0 ± 0.1	1.0 ± 0.1	0	0.10 ± 0.01
<i>n</i> -butyl acrylate	TFE	2.2 ± 0.1	1.0 ± 0.1	0	0.12 ± 0.01

^a[SmI₂] = 5 mM, [proton source] = 125 mM, [octanal] = 350-500 mM. ^b[SmI₂] = 5 mM, [proton source] = 125 mM, [*n*-butyl acrylate] = 350-450 mM. ^c initial rates method. ^d[SmI₂] = 5 mM, [substrate] = 400 mM, [proton source] = 50-200 mM.

**Scheme 2.11** Homocoupling of octanal**Scheme 2.12** Reductive coupling SmI₂ reduction of *n*-butyl acrylate

Based on the results of the pseudo-first order rates, in both cases the rate determining step of the reaction was a post-electron transfer radical coupling. Since the objective of these kinetic studies was to determine the rate constant of single-electron transfer by SmI₂, the rate constants found cannot be compared to determine the difference in rate in which SmI₂ reduces the two functional groups.

We recognized that under the conditions used in the above pseudo-first order rates, the concentration of the substrate far exceeded the concentration of the proton source ($[\text{substrate}] = 350\text{-}500\text{ mM}$, $[\text{proton source}] = 125\text{ mM}$). Since the radical anion produced from the reduction of *n*-butyl acrylate attacks an unreacted acrylate molecule, the large excess of substrate will easily outcompete the proton source and promote coupling. Pseudo-first order rates were attempted at lower concentrations of *n*-butyl acrylate (75-125 mM). Again, the reaction displayed a second order in substrate (Figure 2.1), indicating that even in a system where the concentration of the proton source is greater than the substrate concentration radical addition to the olefin is still rate limiting.

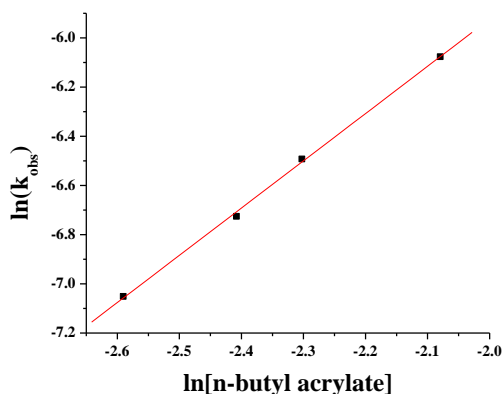
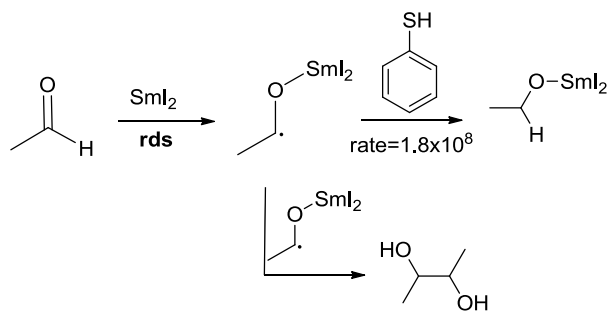


Figure 2.1 Rate order of *n*-butyl acrylate under pseudo-first order conditions. $[\text{SmI}_2] = 5\text{mM}$, $[\text{TFE}] = 125\text{mM}$, $[\text{n-butyl acrylate}] = 75\text{-}125\text{mM}$. Rate Order 1.92 ± 0.04 .

2.3.1.2 Radical Traps

To intercept the product radicals before the subsequent coupling occurs, radical traps were used. Radical trapping agents typically have a labile hydrogen atom, or contain a stable radical. As a product radical is produced through SmI_2 reduction, the

radical intermediate will react with the trap faster than a dimerization pathway. As a result, the initial reduction would become rate determining, allowing the electron transfer to be monitored (Scheme 2.13).



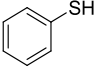
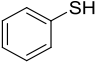
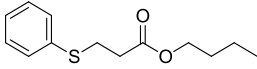
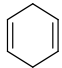
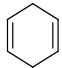
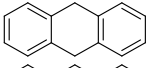
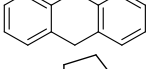
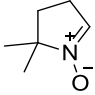
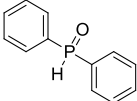
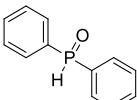
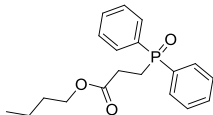
Scheme 2.13 Thiophenol as radical trap in SmI_2 reduction of an aldehyde.

Molander¹¹⁵ and others,^{116,117} have used thiophenol as a radical scavenger in Sm -mediated syntheses, and rates for hydrogen abstraction from thiophenol are faster¹¹⁸ than the coupling rates observed in the pseudo first order experiments. When thiophenol was added to the reduction of octanal with SmI_2 , the desired alcohol product was obtained. With *n*-butyl acrylate, nucleophilic addition of thiol onto the olefin occurred. We then carried out kinetic experiments to determine if the presence of the radical scavenger allowed observation of the initial electron transfer from SmI_2 ; however, interference in the UV spectra in the region of SmI_2 decay prevented observation of the rates.

Next, we attempted additional radical scavengers with the two substrates (Table 2.2). Tributyl tin hydride can be used to donate a hydrogen atom to radicals (entries 3 and 4); however, a complex mixture of tin-coordinated products formed, with none of the desired protonated products observed. Triethylsilane (entries 5 and 6) and 9, 10

dihydroanthracene (entries 9 and 10) did not alter the outcomes for either of the substrates. DMPO radical spin trap and diphenylphosphine oxide (entries 11 and 12) reacted with SmI_2 , and starting substrates were isolated. Additionally, diphenylphosphine oxide reacted with *n*-butyl acrylate through nucleophilic addition into the olefin in addition to the side reaction with SmI_2 (entry 13). In all cases, the radical scavengers attempted did not trap the intermediate radical.

Table 2.2 Radical scavengers included in reduction of octanal and *n*-butyl acrylate.

Entry	Substrate	Radical Scavenger	Product(s)
1	octanal		octanol
2	<i>n</i> -butyl acrylate		
3	octanal	Bu_3SnH	Sn Products
4	<i>n</i> -butyl acrylate	Bu_3SnH	Sn Products
5	octanal	Et_3SiH	pinacol
6	<i>n</i> -butyl acrylate	Et_3SiH	coupled
7	octanal		pinacol
8	<i>n</i> -butyl acrylate		coupled
9	octanal		pinacol
10	<i>n</i> -butyl acrylate		coupled
11	<i>n</i> -butyl acrylate		<i>n</i> -butyl acrylate
12	octanal		octanal
13	<i>n</i> -butyl acrylate		

In all cases, the substrate and radical trap were combined in approx. 4 mL THF and SmI_2 was added slowly dropwise. After reacting overnight the reactions were worked up, and products identified by GCMS analysis.

2.3.1.3 Initial Rates

In another attempt to observe the initial electron transfer from SmI₂ to an aldehyde and α,β -unsaturated ester, the initial rates method was employed. The initial rates method utilizes lower concentrations of substrate, close to synthetic conditions. An initial linear region of the decay within the first 5% of the reaction provides the initial observed rate (s⁻¹).

Reduction of octanal by SmI₂ in the presence of TFE yields first order in substrate and SmI₂ (Table 2.3). These rate orders indicate the initial electron transfer from SmI₂ to the aldehyde is observed, with a rate constant of $4.0 \times 10^{-3} \text{ M}^{-1}\text{s}^{-1}$ corresponding to the rate of reduction. Likewise, a rate order of nearly one for *n*-butyl acrylate and one for SmI₂ indicates the electron transfer from SmI₂ to the α,β -unsaturated ester is observed at a rate of $2.0 \times 10^{-3} \text{ M}^{-1}\text{s}^{-1}$.

Table 2.3 Initial rates for the reduction of octanal and *n*-butyl acrylate by SmI₂.

Substrate	Order of Substrate ^a	Order of SmI ₂ ^b	Rate Constant (M ⁻¹ s ⁻¹) ^a
octanal	0.94 ± 0.04	1.1 ± 0.03	4.0 ± 0.1 × 10 ⁻³
<i>n</i> -butyl acrylate	0.83 ± 0.05	0.91 ± 0.05	2.0 ± 0.1 × 10 ⁻³
cyclic α,β -unsat ester	0.99 ± 0.03	0.94 ± 0.03	6.5 ± 0.2 × 10 ⁻²

^a[SmI₂] = 5 mM, [TFE] = 125 mM, [substrate] = 4-9 mM. ^b[substrate] = 5 mM, [TFE] = 125 mM, [SmI₂] = 4-9 mM.

While the rate order of 0.83 for *n*-butyl acrylate can be viewed as first order, it is a less than unity, fractional order. A rate order of 0.5 often indicates dimer formation. In this case, it is possible the fractional order for acrylate may indicate a monomer-dimer

equilibrium, through coordination of the carbonyl of *n*-butyl acrylate to the oxophilic samarium metal center (Figure 2.2).

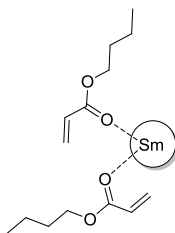


Figure 2.2 α,β -Unsaturated ester substrate “dimer” tethered to Sm metal.

Comparison of the rates of the two substrates shows that octanal is reduced faster than *n*-butyl acrylate by a factor of two. However, previous work with SmI_2 reductions indicates an order of magnitude difference in rate is necessary before selective reduction of one functional group over another occurs, inconsistent with the selectivity observed in the reductive cyclization of the multifunctional dialdehyde used by Proctor (Scheme 2.9).

Taking a closer look at the starting material of this reaction, the cyclic form of the α,β -unsaturated ester may be a better model substrate to study and compare to the rate of reduction of an aldehyde. With the cyclic α,β -unsaturated ester, a secondary radical will form from the reduction. As compared to the primary radical from the linear α,β -unsaturated ester, the enhanced stability of a secondary radical will most likely provide a faster rate. A change in rate between substrates which form primary or secondary radicals is observed with the reduction of alkyl halides.¹³

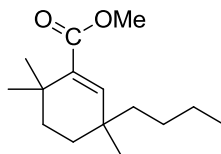


Figure 2.3 Cyclic α,β -unsat. ester: 3-butyl-3,6,6-trimethylcyclohex-1-ene methylcarboxylate

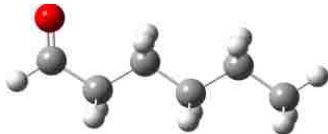



3-butyl-3,6,6-trimethylcyclohex-1-ene methylcarboxylate (cyclic α,β -unsat. ester) was synthesized for kinetic analysis (Figure 2.3). Through initial rates, a rate order of one for substrate and SmI_2 , and a rate constant of $6.5 \pm 0.2 \times 10^{-2}$ were observed (Table 2.3). This rate is an order of magnitude faster than the reduction of octanal by SmI_2 . These rates provide evidence that for the reductive cyclization of Procter's dialdehyde substrate, the interior α,β -unsaturated ester is preferentially reduced by SmI_2 in the presence of the two pendant aldehydes.

2.3.2 Computational Data

To provide more insight into stability of the intermediate radical anions formed through the reduction by SmI_2 , computational calculations were carried out on an aldehyde and α,β -unsaturated esters. Calculations were carried out using Gaussian 09. All structures were fully optimized at B3LYP/6-31G(d,p) level. Frequency calculations verified the identity of each stationary point as a minimum with zero imaginary frequency. Zero-point vibrational energy (ZPVE) corrections were added to the energies and were not scaled.

Energies were determined for the starting materials as well as their corresponding radical anions. The differences in energy between the two states of the substrate indicate the thermodynamic ease of reduction to form the radical anion. The data contained in Table 2.4 identifies the energy difference between the starting aldehyde and its radical anion is greater than the α,β -unsaturated esters by greater than 10 kcal/mol. Therefore, the electron transfer to form the radical anion requires less energy with α,β -unsaturated ester substrates as compared to aldehydes. In contrast to the experimental data, there is little difference between the linear and cyclic forms of the α,β -unsaturated esters. Overall, these results support the kinetic data which found the reduction of cyclic α,β -unsaturated ester by SmI_2 is more facile than reduction of aldehydes.

Table 2.4 Energy calculations for starting substrates and their corresponding radical anions

entry	Substrate	$\Delta E + \text{ZPVE}$ (kcal/mol)
1	 hexanal	14.68
2	 acrylate	-1.96
3	 Z-methyl-butenoate	-2.74
4	 E-methyl-butenoate	2.22

5

methyl 3,3,6,6-
tetramethylcyclohex-1-
enecarboxylate (2)-0.05

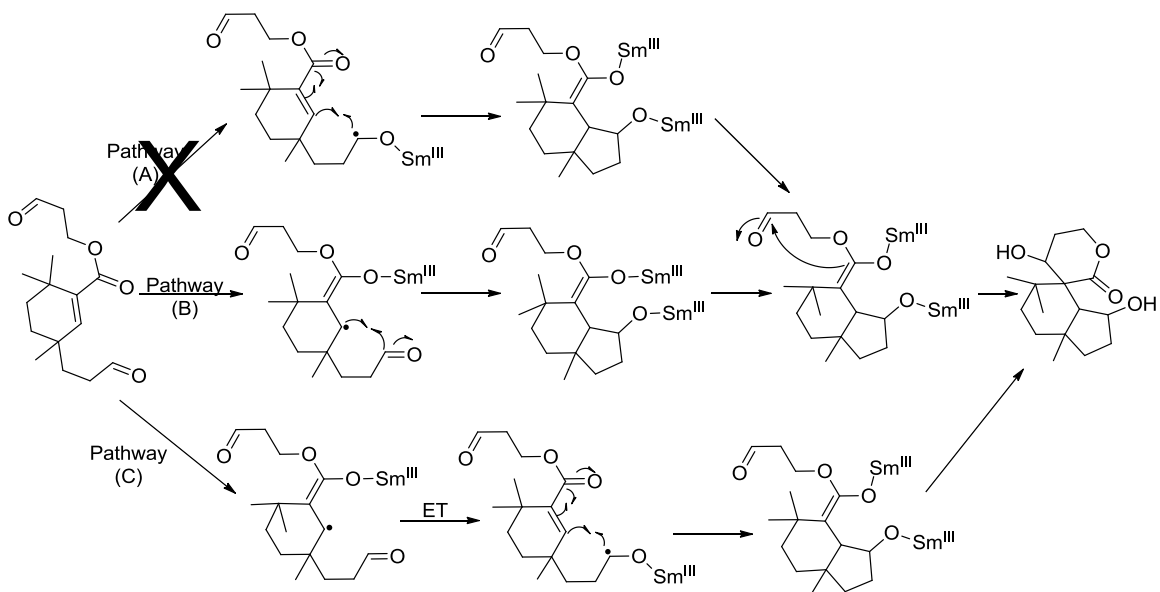
2.4 Conclusions

SmI_2 is a remarkably useful single-electron reductant since it has the ability to reduce many different functional groups. Furthermore, the reductions are carried out at different rates, allowing SmI_2 to be a valuable reagent in reductive couplings or cascade reactions where multiple functional groups are present on a molecule. Many examples of SmI_2 -mediated cascade reactions can be seen in the literature, but without the knowledge of the different rates by which SmI_2 reacts with the different functionalities, it can be difficult to predict the pathway the cascades proceed through, and therefore difficult to rationally design new cascade systems.

The issues of radical coupling that were encountered while carrying out the kinetic experiments highlight the difficulty in trying to determine the facile electron transfer rates with SmI_2 . Even in systems where only one substrate/functional group is reduced by SmI_2 and a proton source is added, intermolecular coupling through radical addition can be a prominent pathway. While the propensity for radical addition may be problematic for kinetic experiments, the active radical intermediate is one of the reasons Sm -mediated cascade reactions can be such a powerful tool. Overcoming these issues in

the kinetic studies not only provided the valuable information of individual rate constants, but also provided insight of how strongly favored the radical reactions are. The observations of homocoupling through radical addition onto the olefin for α,β -unsaturated esters and the high likelihood for pinacol formation of aldehydes are reactions which need to be taken into consideration when designing new complex syntheses.

From kinetic experiments it was observed that SmI_2 reduces cyclic α,β -unsaturated esters an order of magnitude faster than it reduces an aldehyde. Additionally, the radical anion intermediate of an α,β -unsaturated ester is more than 10 kcal/mol more stable than an aldehyde radical anion, providing further evidence that in the case of the SmI_2 -mediated reduction, the α,β -unsaturated ester is reduced more readily than an aldehyde. This insight allows us to predict that, in the case of the functionalized dialdehyde cyclization, the α,β -unsaturated ester moiety is selectively reduced in the presence of an aldehyde, eliminating one of the possible mechanistic pathways (Scheme 2.14, pathway A). Pathway B seems the most likely mechanism for the reaction, since previous mechanistic studies support radical addition from an α,β -unsaturated ester to a carbonyl (pathway B, Scheme 2.14).¹⁰⁵ This information provides insight which will be vital as SmI_2 -cascade reactions are designed in which both an aldehyde and α,β -unsaturated ester functional groups are present in the reaction.



Scheme 2.14 Possible mechanistic pathways for the reductive cyclization

Chapter 3. Impact of HMPA on the Samarium Barbier Reaction

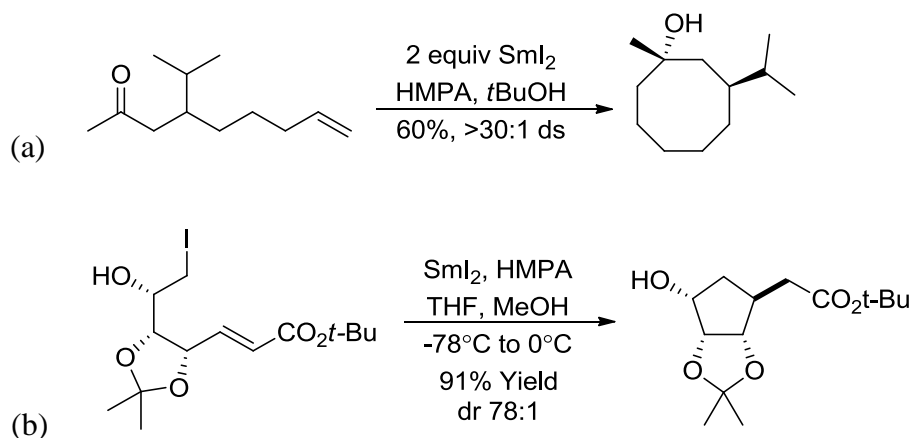
3.1 Background and Significance

3.1.1 SmI₂ and HMPA in Organic Reactions

Despite its suspected toxicity, HMPA is still a commonly used additive in SmI₂ reactions. The reason for its persistent use in synthesis is that no other additive displays the same increased rate and stereoselectivity that can be achieved with Sm-HMPA. The ability of HMPA to coordinate to Sm, producing a more powerful ground state reductant was discussed in Chapter 1. In addition to this effect, several groups have studied reactions initiated by SmI₂-HMPA and have uncovered complex mechanistic roles for the additive. Depending on the substrates involved, HMPA can act in a variety of ways in addition producing a more powerful reductant. Studies have shown that in various reactions HMPA also acts in the precipitation of Sm(III), coordinates in the transition state with intermediate Sm-complexes, and interacts with substrate.

Inanaga first identified the impact of HMPA on SmI₂-reactions as he observed a drastic increase in rates of reduction of alkyl and aryl halides.⁶ Reactions which typically took hours with SmI₂ were complete within a few minutes with SmI₂-HMPA. The increased rate of reduction increased the efficiency of many SmI₂-mediated coupling reactions and reducing side product formation²⁴ Molander found HMPA was required to achieve the formation of an 8-membered ring through a ketyl-olefin cyclization (Scheme 1.40, a).¹¹⁹ Bennett used a Sm-mediated cyclization to form functionalized cyclopentanes

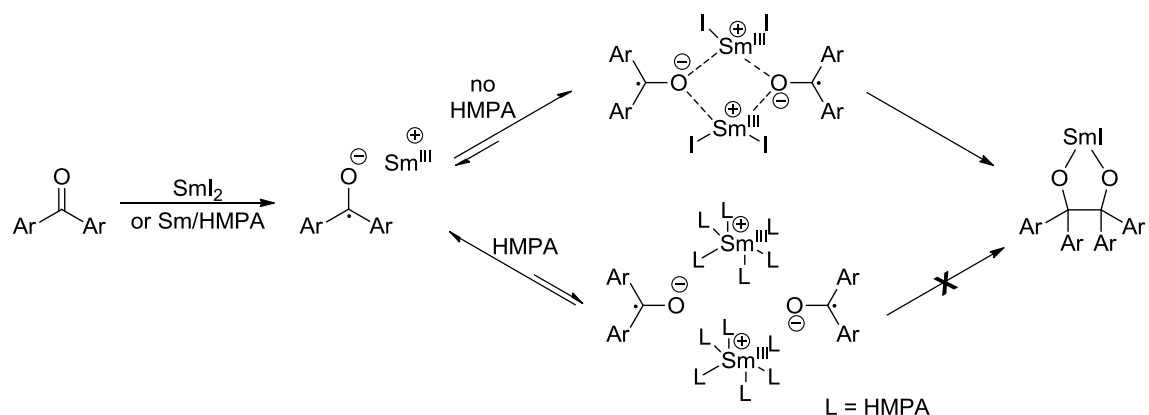
from sugar-derived substrates.^{119,120} The cyclization proceeded with a high degree of diastereoselectivity and high yields (Scheme 1.40, b). The addition of HMPA as well as a proton source was required to avoid competing 1,4-reductions of the α,β -unsaturated ester and cleavage of the allylic C-O bond.



Scheme 3.1 (a) key-olefin and (b) halide-olefin cyclizations promoted with SmI_2 -HMPA

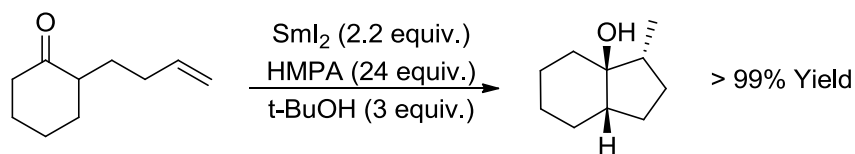
While examining the effect of HMPA on pinacol coupling, it was found that HMPA actually retards the rate of bimolecular coupling of biaryl ketyl radicals by complexing and sequestering Sm(III) .¹²¹ As HMPA was added in increasing amounts (3-20 equiv) to the pinacolization of *p,p'*-dichlorobenzophenone (Scheme 3.1), the rate of the coupling steadily decreased. HMPA complexes very tightly to Sm, and has the ability to displace other ligands such as THF and alcohols.^{26,28,53,122} Sm(II) and Sm(III) , in the absence of HMPA, bridge the colligating radical anions, facilitating the coupling reaction. However, when HMPA is included it preferentially binds to Sm(III) , and competes for

Sm-coordinated ketyl after the reduction, obstructing the lanthanide from fulfilling the needed post-electron transfer bridging role (Scheme 3.2).¹²¹



Scheme 3.2 HMPA post-electron transfer role in pinacol coupling

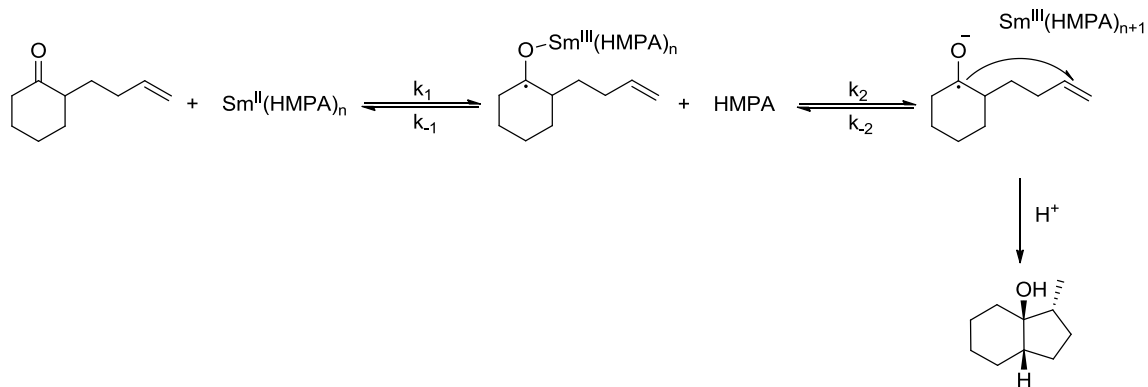
Conversely, HMPA has been shown to accelerate SmI_2 -initiated ketyl-olefin cyclizations through a critical interaction with the intermediate Sm(III) -ketyl radical. Molander studied a series of ketyl-olefin cyclization reactions containing increasing amounts of HMPA, and proposed that the sterically encumbered SmI_2 -HMPA complex was responsible for the observed products and diastereoselectivities of 5- and 6-*exo*-ketyl-olefin cyclizations (Scheme 3.3).³⁵ He credited the success of the reaction to protection of the intermediate ketyl radical formed after initial electron transfer being shielded from solvent by proximal coordinated Sm(III) -HMPA.



Scheme 3.3 Sm-HMPA in ketyl-olefin cyclization

Recent kinetic studies have shown that the addition of HMPA in the Sm-mediated coupling of carbonyls and alkenes plays an important post electron-transfer mechanistic role beyond what was proposed by Molander.³⁵ The rate of the intramolecular carbonyl-olefin cyclization was monitored over a range of HMPA concentrations, and if HMPA was not included in the reaction, the desired cyclization did not occur.

Due to its oxophilic nature, Sm(III)-HMPA coordinates and stabilizes the ketyl intermediate. However, the sterically encumbered Sm-HMPA-ketyl complex hinders radical addition to the pendent olefin. When excess HMPA is present in solution (>10 equiv), the cosolvent can coordinate to the Sm-metal in the transition state, releasing it from the ketyl intermediate (Scheme 3.4). The loss of Sm(III) from the anion intermediate produces a solvent-separated ion pair, which is now free to undergo the 5-*exo-trig* cyclization.¹⁰⁴ This mechanistic insight into the role of HMPA was unexpected, and could not have been predicted through observations of product formation alone. This example highlights the significant information that can be gained through detailed kinetic and mechanistic studies, especially in reference to the complex role of additives in Sm-mediated reactions.



Scheme 3.4 Post-electron transfer role of HMPA in ketyl-olefin cyclization

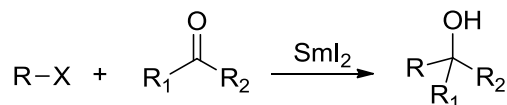
Although these studies have provided critical mechanistic insight into important bond-forming reactions that occur through initial reduction of a carbonyl, these examples also highlight the diverse roles HMPA can play in various reaction systems. In addition, there are still numerous gaps in our understanding of the mechanistic role of HMPA in the reduction of alkyl halides and reductive coupling of alkyl halides with carbonyls. HMPA plays numerous roles in Sm-mediated reactions aside from producing a more powerful reductant, and for this reason investigation of specific reactions is imperative for a complete understanding of the cosolvent within SmI_2 reactions.

3.1.2 Samarium-Barbier Reaction

The Barbier reaction is similar to the traditional Grignard reaction, in which an alkyl halide and carbonyl containing substrate are coupled to form a substituted alcohol product (Scheme 3.5). Procedurally, the Grignard reaction is a two-step reaction. Activated magnesium is treated with the alkyl halide, forming the intermediate organomagnesium Grignard reagent (RMgX) *in situ*. The carbonyl substrate is added,

which couples to form the desired substituted alcohol. The Barbier reaction is an identical coupling reaction; however, the components are added to the reaction concurrently.

The organomagnesium produced in the traditional Grignard reaction is similar to the organosamarium intermediate which is formed in Sm(II)-mediated reactions (see Chapter 1), and for this reason the Barbier and Grignard reactions were among some of the first carbon-carbon bond-forming approaches attempted with SmI₂.¹ In both the Grignard and Barbier procedure, the desired alcohol product is formed in high yields using SmI₂.^{1,24}

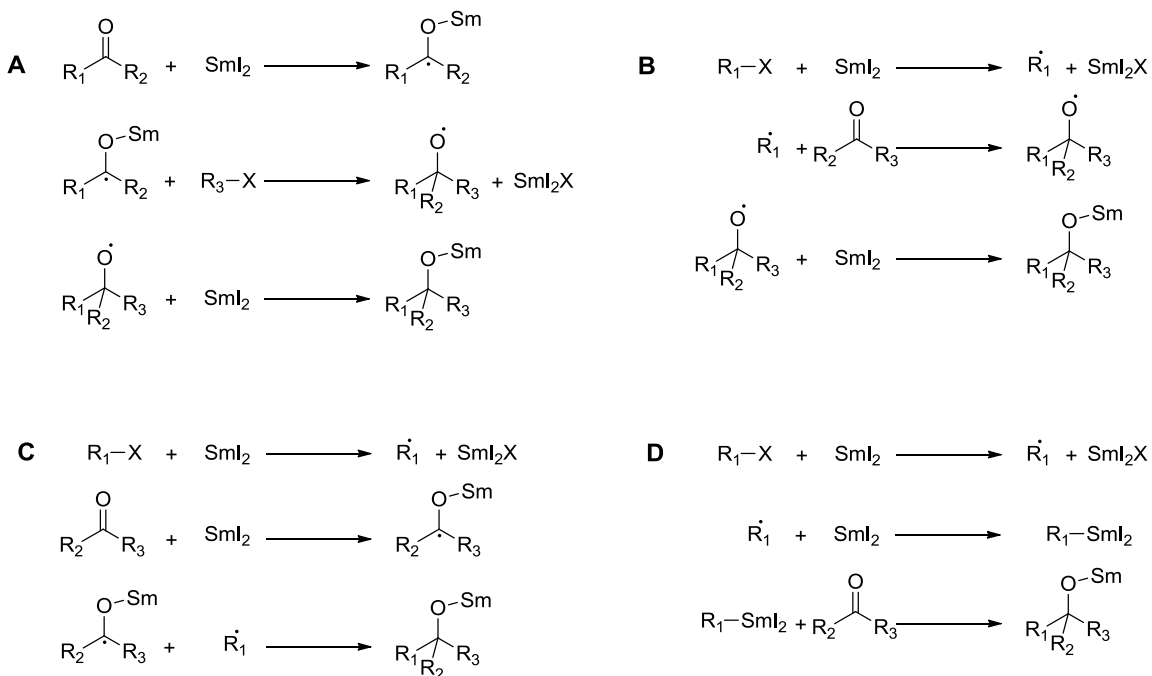


Scheme 3.5 Samarium Barbier reaction

Due to the order of addition for the Grignard procedure, the mechanism is straightforward: SmI₂ reduces the alkyl halide to a radical, and through a second, facile, electron-transfer an organosamarium is formed.^{2,123} The carbonyl substrate is then added to the reaction mixture, allowing the organosamarium to nucleophilically add to the carbonyl, and upon workup the alcohol product is formed. In the Barbier procedure, both substrates are reacted with SmI₂ at the same time, and for this reason a variety of possible mechanisms could be envisioned.

Kagan and Curran have proposed various possible mechanisms for the samarium Barbier reaction (Figure 3.6).^{2,124 50} In one pathway, SmI₂ initially reduces the ketone

substrate to produce a ketyl radical. The radical is then attacked by the alkyl halide through an S_N2-type mechanism to form the new carbon-carbon bond and alkoxy radical, which can be reduced by another SmI₂ (Scheme 3.6, A). This possibility was dismissed by Kagan when he found no evidence of S_N2-type inversion when optically active halides were employed.² With the observation of racimized products, Kagan also proposed that the reduction of the alkyl halide is a key step, and is most likely the substrate initially reduced by SmI₂.



Scheme 3.6 Possible mechanisms of the samarium Barbier reaction. (a) S_N2 substitution (b) Radical addition (c) Ketyl-radical coupling (d) Organometallic addition

If the alkyl halide proceeds through the single-electron transfer with SmI₂ first, the radical could then add to the carbonyl to form an alkoxy radical which proceeds through a second single-electron transfer to form the organosamarium intermediate

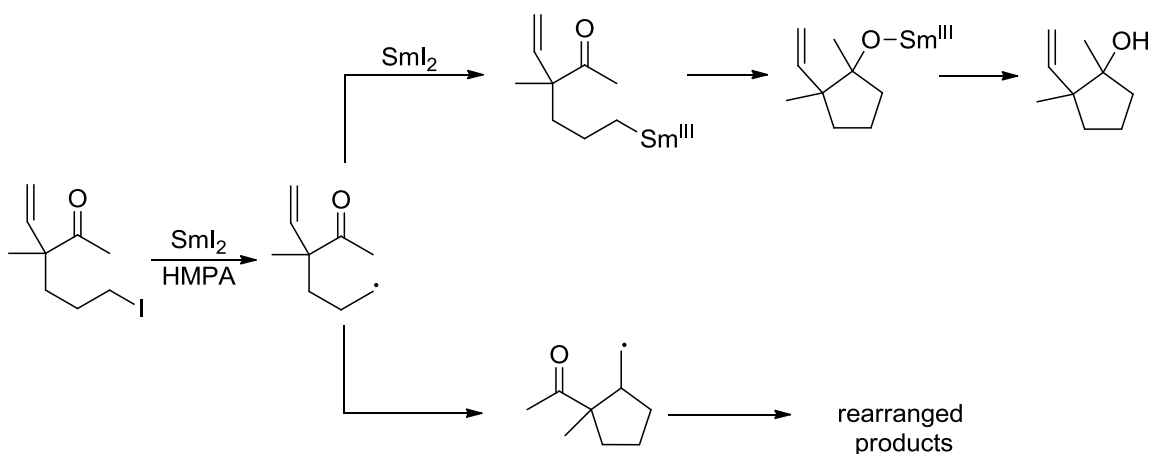
(Scheme 3.6, B). Curran proposed that this mechanism is unlikely for bimolecular samarium Barbier reactions due to the slow radical addition step. He also notes that if the intermediate alkoxy radicals proposed for mechanisms A and B are present, products obtained from side reactions and fragmentation should be observed. However, formation of such side products was not observed.⁵⁰

Pathways C and D are very likely for the reaction, and hard to distinguish between. Both ketones and alkyl halides are susceptible to reduction by SmI₂, and ketyl-radical coupling could be expected if the accumulation of both radicals is produced at a similar rate. In fact, rate studies done by Flowers have shown that the rate constant for reduction of 2-butanone and 1-iodobutane were found to be nearly identical at $(7 \pm 3) \times 10^{-4}$ and $(8 \pm 2) \times 10^{-4} \text{ M}^{-1}\text{s}^{-1}$ respectively.¹³ Pathway C of Scheme 3.6 portrays the reduction of both substrates to a primary and ketyl radical, which then undergo radical-radical coupling to form the product organosamarium. The last possibility is categorized as an organometallic addition (Scheme 3.6, D), in which an organosamarium is formed through two successive reductions of the alkyl halide. The organosamarium reagent then goes through a nucleophilic addition with the carbonyl to produce the product.

In the presence of HMPA, the selectivity of the reaction is dramatically increased, and the Barbier product is obtained in nearly quantitative yields. Furthermore, upon the addition of HMPA, the rates of reduction for alkyl iodides increased nearly 4 orders of magnitude ($2.6 \pm 0.1 \text{ M}^{-1}\text{s}^{-1}$ with 6 equiv. HMPA) whereas the increase in rate of dialkyl ketone reduction was significantly less pronounced ($(8 \pm 1) \times 10^{-4} \text{ M}^{-1}\text{s}^{-1}$ with 6 equiv.

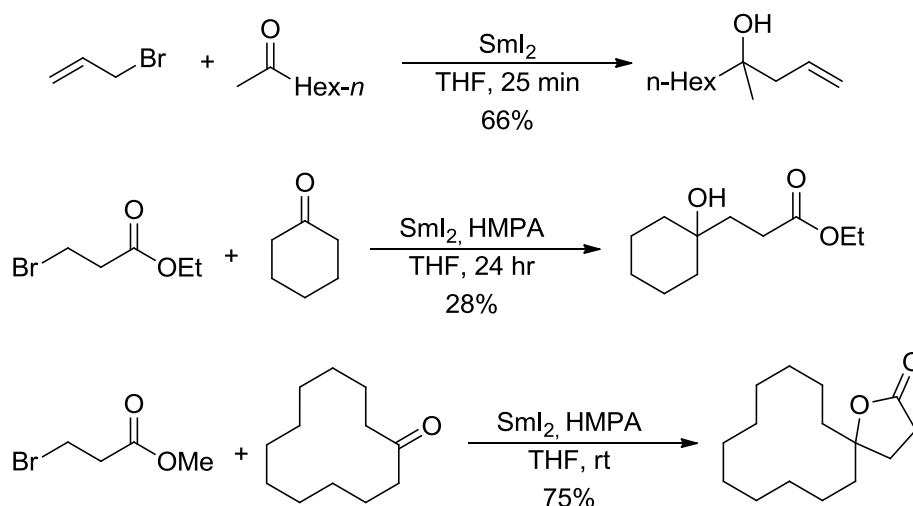
HMPA).¹³ These kinetic results suggest that pathway D, in which the alkyl halide is selectively reduced by SmI_2 , is likely occurring when in the presence of HMPA, but the basis of this effect is unknown.

Curran used a “radical clock” to gain information about the formation of an organosamarium intermediate as compared to a radical within an intramolecular Barbier cyclization reaction (Scheme 3.7).¹²⁵ Based on known rates for the cyclization of a radical onto the alkene,^{126,127} it was suspected that some radical cyclization products would be obtained along with the alcohol product from the anionic pathway. Surprisingly, when the radical clock was subjected to SmI_2 reduction, the tertiary alcohol was obtained as the sole product. This result indicated that within the *intramolecular* Sm-Barbier reaction, the sequential single-electron transfers to form the organosamarium intermediate are faster than radical cyclization onto the olefin.



Scheme 3.7 Radical vs. organosamarium pathways

Intermolecular Barbier reactions have been completed with allylic, benzylic, and propargylic halides, which successfully couple with ketones (Scheme 3.8).¹ In the absence of either substrate, homocoupling occurs, demonstrating the ability of Sm(II) to independently reduce both substrates.



Scheme 3.8 Intermolecular examples of Sm-Barbier reaction

One of the intriguing features of the samarium Barbier reaction is the selective reduction of alkyl halides over carbonyls by SmI₂ in the presence of HMPA. In the absence of HMPA, reactions are inefficient, providing mixtures of coupled and reduced products along with unreacted starting material.²⁴ Conversely, reactions containing 8 or more equivalents of HMPA (based on [SmI₂]) provide Barbier products exclusively.²⁴ While a great deal of mechanistic insight on the Barbier and Grignard procedure has been gained through the research of Kagan, Curran, Flowers, and others, an overall general mechanism for the Barbier reaction has not been indisputably established. In this study, the samarium Barbier reaction, with the inclusion of HMPA, was investigated to gain

insight on the impact the additive has on the mechanism and determine the role of HMPA within the reaction system.

The role that HMPA is playing within the Samarium Barbier reaction was initially explored through the coupling of primary alkyl halides, 1-iodododecane and 1-bromodecane, to 3-pentanone. The study was then extended to observe how secondary and tertiary alkyl halides proceeded in the coupling reaction, and if the role of HMPA changed with the substituted substrates.

3.2 Experimental

3.2.1 Materials

THF was purified after purging with argon gas and passing over a column of activated alumina by a Solvent Purification System (Innovative Technology Inc.; MA). Dried solvents and reagents were stored in an Innovative Technology, Inc. drybox containing an argon atmosphere and a platinum catalyst for drying. 3-pentanone (**3**) and HMPA were purchased from Acros and distilled under vacuum from CaO before use. Iodododecane (**1**), bromodecane (**2**), 2-iodobutane (**6**), 2-iodo-2-methylpropane (**7**), 2-bromopropane (**8**), 2-bromo-2-methylpropane (**9**), iodoethane, bromoethane and samarium metal were purchased from Acros and used with no further purification. Resublimed iodine crystals were purchased from Aldrich and used with no further purification. SmI_2 was prepared by stirring Sm metal and iodine in THF until the

characteristic blue color of Sm(II) appeared. The concentration of the Sm complex (0.10 M in THF) was determined by iodometric titration.

3.2.2 Instrumentation

Proton and carbon NMR were recorded on Bruker 500 MHz spectrometer. GC-MS analysis was performed with HP 5890 Series Gas Chromatograph with an HP Mass Selector Detector. HR-MS was performed at the Mass Spectrometry Facility at Notre Dame University. Kinetic studies in THF were performed using a computer-controlled SX-20 MV stopped-flow reaction spectrophotometer (Applied Photophysics Ltd., Surrey, UK).

3.2.3 Methods

3.2.3.1 General Procedure for the Samarium Barbier Reaction

The reaction was carried out in a drybox with degassed reagents. SmI₂ was prepared as described above. HMPA (730 μ L, 0.042 mol) was added to SmI₂ (8.4 mL, 0.1 M) and the characteristic blue color of SmI₂ turned to a deep purple. Separately, alkyl halide (**1**, **2**, **6**, **7**, **8**, or **9**) (0.4 mmol) and 3-pentanone (**3**) (42.37 μ L, 0.4 mmol) were combined in 5mL THF. The substrate solution was added dropwise to SmI₂-HMPA. After stirring for 10 minutes the purple color subsided to a muted gray. The reaction was quenched by exposing to air. The reaction mixture was then washed with NH₄Cl and extracted twice with ether. The organic layer was washed individually with H₂O,

Na₂S₂O₃ and brine, dried over MgSO₄ and then concentrated to obtain the pure Barbier product (**4** pale yellow oil, 0.0758 g, 83%; **5** pale yellow oil, 0.0761 g, 82.5%).

3.2.3.2 General Procedure for Stopped-Flow Studies

The SmI₂-HMPA combination and substrates were taken separately in airtight Hamilton syringes from a drybox and injected into the stopped-flow system. The cell box and the drive syringes of the stopped-flow reaction analyzer were flushed a minimum of three times with degassed solvents to make the system oxygen-free. The concentration of SmI₂ used for the study was 5 mM. To determine rate constants, the concentrations of the substrates were kept high relative to SmI₂-HMPA combination (125 mM) to maintain pseudo first-order conditions. Observed reaction rate constants were determined from exponential fitting of the decays of SmI₂-HMPA complex at 550 nm. The decay of the SmI₂-HMPA combination displayed first-order behavior over >3 half-lives for SmI₂-HMPA-substrate combinations.

Rate orders for HMPA, 3-pentanone (**3**), iodododecane (**1**), bromodecane (**2**), 2-iodobutane (**6**), 2-iodo-2-methylpropane (**7**), 2-bromopropane (**8**), and 2-bromo-2-methylpropane (**9**) were derived from the plots of $\ln k_{\text{obs}}$ vs. $\ln[\text{substrate}]$. The rate order for SmI₂ was determined from fractional times method from the decay traces of SmI₂. The rate plots were generated from the absorption decay traces obtained from a stopped-flow spectrophotometer.

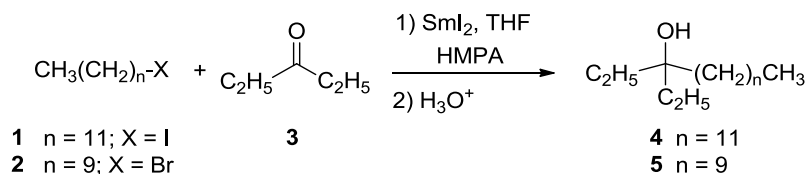
3.2.3.2 General Procedure for NMR Experiments

NMR experiments were carried out on Bruker 500 MHz instrument. Samples were prepared of alkyl halide (0.084 mmol) and 1 and 2 equivalents of HMPA (0.084 mmol and 0.168 mmol) in d8-THF. ^1H and ^{13}C NMR experiments were performed at 0 °C due to the low boiling point of bromoethane (38 °C).

3.3 Results

3.3.1 Kinetic Analysis of Samarium Barbier Reagents

A series of rate studies was performed with Barbier reactions of 1-iodododecane (**1**) and 1-bromodecane (**2**) with 3-pentanone (**3**) to determine the rate orders of the individual components in the samarium Barbier reaction, shown in Scheme 3.9. Rate constants for reduction and rate orders for all components are shown in Table 3.1.



Scheme 3.9 Samarium Barbier reaction with primary alkyl halides

Rate orders of one for SmI_2 and alkyl halide and zero for **3** are consistent with previous studies of the Barbier reaction, in which the reaction initiates by single electron transfer to the alkyl halide to form a radical (in the rate determining step), followed by a

second single electron transfer to from an organosamarium.^{13,24,50,65} Surprisingly, the rate order of HMPA was first order (1.0 ± 0.1) for the reaction of **1** and **3** and nearly first order (0.8 ± 0.1) for the coupling of alkyl bromide substrate **2** and **3**. The first order dependence of HMPA indicates that HMPA is playing a role in the mechanism before or during the initial electron transfer.

Table 3.1 Rate orders for alkyl halide, 3-pentanone, SmI₂ and HMPA

Alkyl halide	Rate Order				k (M ⁻² s ⁻¹)
	RX ^a	3 ^b	SmI ₂ ^c	HMPA ^d	
1	1.1 ± 0.1	0	1.0 ± 0.1	1.0 ± 0.1	4.3 ± 0.2
2	0.96 ± 0.01	0	1.0 ± 0.1	0.8 ± 0.1	0.15 ± 0.01

^a[SmI₂] = 5 mM; [HMPA] = 50 mM; [**1**] = 45-260 mM; [**2**] = 50-300 mM. ^b[SmI₂] = 5 mM; [**1**] = 110 mM; [**2**] = 125mM; [HMPA] = 50 mM; [**3**] = 50-300 mM. ^cFractional time method (see Appendix). ^d[SmI₂] = 5 mM; [HMPA] = 10-160 mM; [**1**] = 110 mM; [**2**] = 125 mM; [**3**] = 125 mM.

To further explore the effect of HMPA, the rates of reduction of **1** and **2** in the presence and absence of **3** were monitored with increasing concentrations of HMPA from 0-300 equiv with respect to SmI₂ (Figure 3.1). The results of this experiment show two important characteristics: (1) the impact of HMPA on the rate of reduction of **1** and **2** increases linearly up to 32 equiv and saturates only at very high concentrations of the additive, and (2) the presence of the ketone does not affect the rate of reaction in the presence of [HMPA]. The zero order for ketone further solidifies the supposition that in the presence of HMPA, alkyl halides are reduced preferentially to the carbonyl substrate in solution.

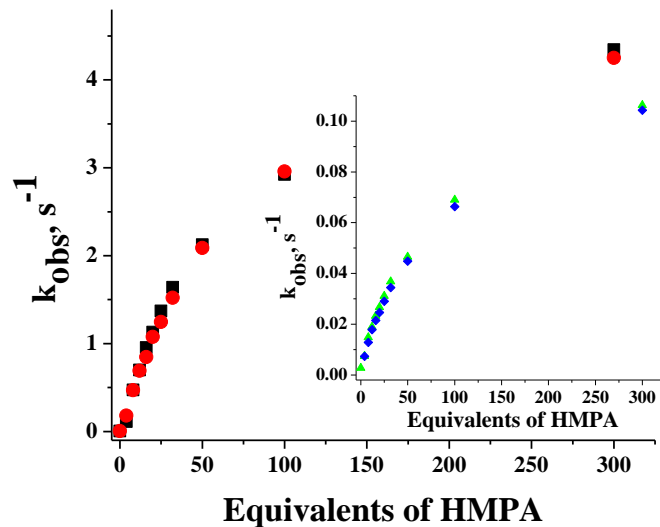


Figure 3.1 Equivalents of HMPA versus k_{obs} for the reduction of **1** in the presence (■) and absence (●) of **3**. The inset shows equivalents of HMPA versus k_{obs} for the reduction of **2** in the presence (◆) and absence (▲) of **3**. $[\text{SmI}_2] = 5 \text{ mM}$; $[\mathbf{1}] = 110 \text{ mM}$; $[\mathbf{2}] = 125 \text{ mM}$; $[\mathbf{3}] = 125 \text{ mM}$.

Previous studies have shown that the addition of 10 equiv of HMPA to SmI_2 produces $[\text{Sm}(\text{HMPA})_6]\text{I}_2$,²⁷⁻²⁹ which is a more powerful reductant when compared to SmI_2 alone.^{31,32} If the only role of HMPA in the Barbier reaction is to increase the reducing power of SmI_2 through coordination, then the rate enhancements shown in Figure 3.3 would be expected to reach a plateau at concentrations closer to 10 equiv. However, the first order behavior of HMPA is observed up to 32 equiv, indicating the additive is playing an additional role in the reaction.

The first order rates for SmI_2 and the alkyl halide indicate that the dissociative electron transfer from SmI_2 to RX is rate limiting. It is also well established that the likely second single electron transfer to form an organosamarium is very facile.^{13,29} Given

these observations, it is difficult to envision a post-electron transfer role for HMPA occurring *before* the organosamarium is formed.

Lewis base activation provides a useful method for accelerating reactions, through dative bond interaction between electron rich and electron poor reagents.¹²⁸ Although Lewis base activation of alkyl halide bonds has not been explored in detail, this approach has been applied to several important processes and is best exemplified by the elegant work of Denmark and coworkers.¹²⁹ In the late 1960's, Wigfield proposed that the ratios of C vs. O alkylation of the anion of ethylacetoacetate was a result of the interaction between solvent (HMPA or DMSO) and alkyl halides.¹³⁰ He proposed an S_N2-type complex, involving the interaction of the nucleophilic oxygen of solvent with the halogen bearing carbon of the alkyl halide (Figure 3.2).

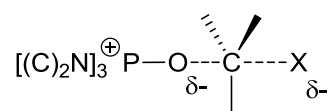


Figure 3.2 HMPA-alkyl halide complex proposed by Wigfield.

The formation of the complex was rationalized on the basis of changes in the P=O (or S=O) bond stretching frequency to lower wave numbers in the presence of a range of alkyl halides. Although the hypothesis of Wigfield is reasonable, it is also possible that the shifts in P=O (or S=O) stretching frequencies could result from a generalized solvent dielectric effect. However, given these findings, could the kinetic behavior of HMPA in the Sm-Barbier reaction possibly result from interaction through Lewis base activation with the alkyl halide?

3.3.2 DFT Calculations

To explore the degree of interaction between HMPA and an alkyl halide, DFT calculations were carried out using Gaussian03.¹³¹ Bromoethane was chosen as a model substrate for ease of computation. Optimization of all structures were performed under tight optimization conditions employing a B3LYP¹³² hybrid functional with 6-311+G(d,p) basis set.¹³³ To model solvent effects, single-point energy calculations were performed on the gas phase optimized geometries using the Onsager^{134,135} model with THF as the solvent ($\epsilon=7.58$). A complex between bromoethane and HMPA was identified on the potential energy surface that was more stable than the individual components by 3.2 kcal/mol (after the addition of ZPVE corrections, see Appendix 8.2.4) as shown in Figure 3.3.

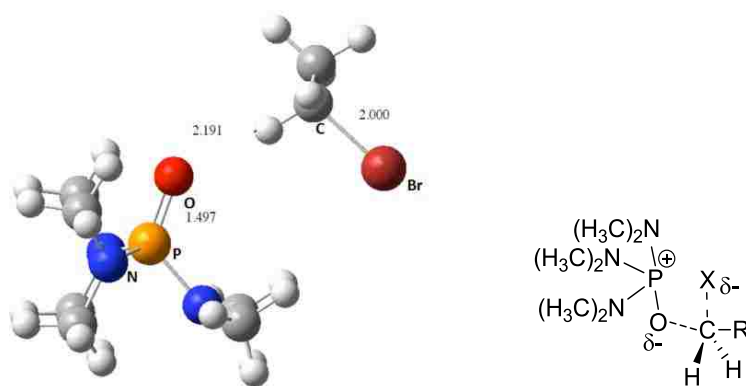


Figure 3.3 Calculated gas phase complex between HMPA and bromoethane. Colors indicate Grey-C, Blue-N, Red-O, Dark Red-Br, Orange-P and White-H. The distances marked are in angstrom units.

Elongation of the C-Br bond of bromoethane from 1.987 to 2.000 Å as well as the P=O bond from 1.492 to 1.497 Å of HMPA was observed for the complex, indicating

significant interaction between the two reactants. Furthermore, Mulliken charges calculated for the complex shows significant polarization of C-X bond of bromoethane as well as the P=O bond of HMPA in the complex. (see Appendix 8.2.4.1). The Mulliken charges on the methylene bearing the bromide change from -0.262 to -0.254 in the complex. Polarization of the carbon halide bond increases the reactivity of the substrate, thus facilitating its reduction by [SmI₂-HMPA].

3.3.3 NMR Titration Experiments

To further investigate the degree of interaction between HMPA and alkyl halides in THF, a series of ¹H and ¹³C NMR titration experiments were carried out through successive addition of HMPA to either iodoethane or bromoethane in d₈-THF. If the hypothesis that the alkyl halide and HMPA are interacting to form a complex is correct, the proposed interaction and effect of the bond elongation on neighboring atoms should be observed by NMR.

Upon addition of 1 equiv of HMPA to iodoethane, the ¹H chemical shift of the methylene bearing the halide shifted downfield by 0.008 ppm. Addition of a second equiv of HMPA led to a further downfield shift of 0.014 ppm (Figure 3.4(a)). In ¹³C NMR experiments on the same substrate, the chemical shift values for the addition of 1 and 2 equiv of HMPA shifted downfield by 0.087 and 0.174 ppm respectively (Figure 3.5(a)). These experiments observed the methylene protons shifting significantly, while the hydrogens on the methyl experienced only a slight or negligible shift in the presence of HMPA (Figures 3.4(b) and 3.5(b)). This observation suggests that the change in the

alkyl halide that occurs upon the addition of HMPA is not an overall solvent effect on the substrate, but a result of interaction with the carbon attached to the halide to the greatest extent. These deshielding effects observed in the ^{13}C NMR experiments are consistent with the computational data which identified an interaction between the oxygen of HMPA and the methylene carbon. Similar downfield shifts were seen with bromoethane and HMPA (Table 3.2). While the change in ^1H ppm as was nearly identical between iodoethane and bromoethane with HMPA, there is a slightly less pronounced effect observed in the carbon NMR spectra with bromoethane. This slightly smaller shift of the methylene carbon could be indicating less of an interaction, and lower polarization of the C-Br bond as HMPA is added. If the first order role that HMPA is playing in the reaction is to interact and elongate the carbon-halide bond, this slightly decreased interaction could explain why a less than unity order of HMPA was observed in the kinetic experiments, as compared to the alkyl iodide substrate.

Table 3.2 NMR shifts of primary alkyl halides in the presence of HMPA

	^1H NMR			^{13}C NMR		
	ΔCH_2 (ppm)	ΔCH_3 (ppm)	ΔHMPA (ppm)	ΔCH_2 (ppm)	ΔCH_3 (ppm)	ΔHMPA (ppm)
Iodoethane + 1 equiv HMPA	0.008	0.003	0.002	0.087	0.017	0.010
Iodoethane + 2 equiv HMPA	0.014	0.003	0.000	0.174	0.036	0.017
Bromoethane + 1 equiv HMPA	0.008	0.001	0.003	0.076	0.022	0.007
Bromoethane + 2 equiv HMPA	0.014	0.002	0.006	0.132	0.035	0.007

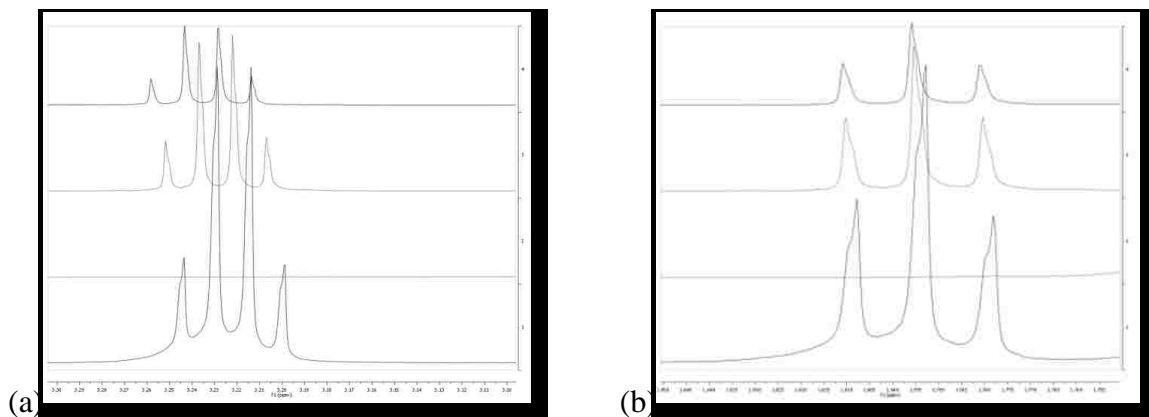


Figure 3.4 Iodoethane ^1H NMR shifts (a) $-\text{CH}_2\text{-I}$ (b) $-\text{CH}_3$

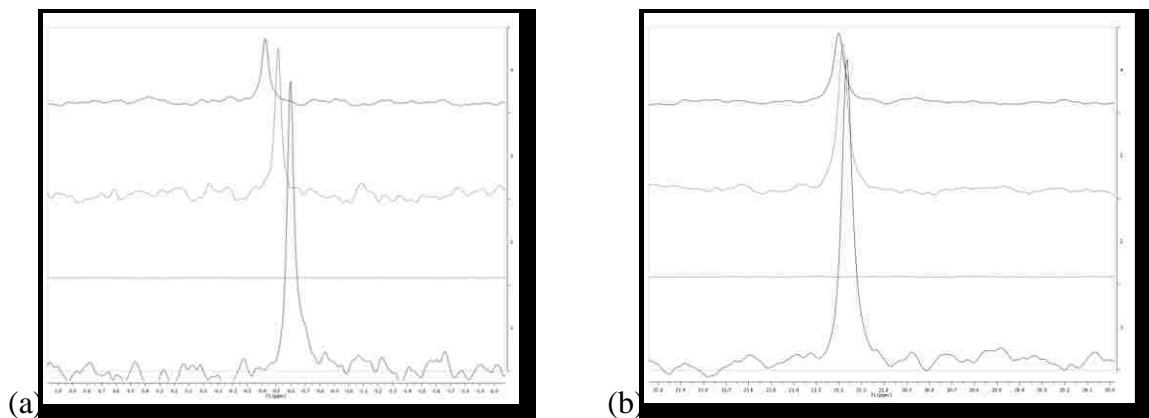


Figure 3.5 Iodoethane ^{13}C NMR shifts (a) $-\text{CH}_2\text{-I}$ (b) $-\text{CH}_3$

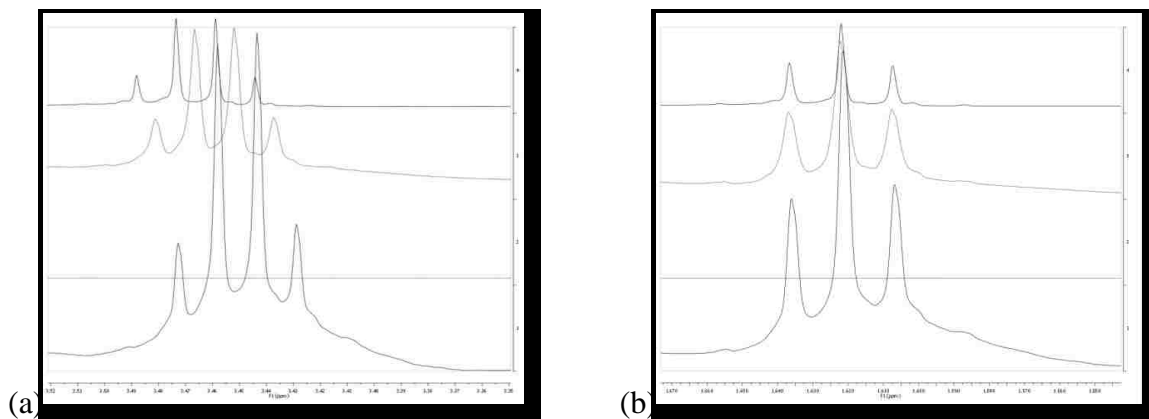


Figure 3.6 Bromoethane ^1H NMR shifts (a) $-\text{CH}_2\text{-I}$ (b) $-\text{CH}_3$

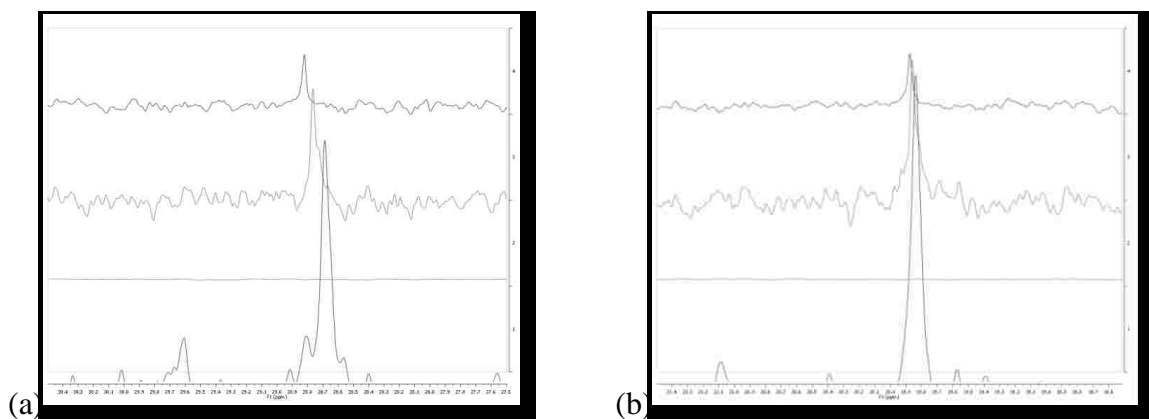


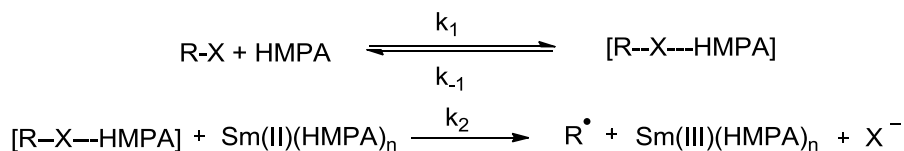
Figure 3.7 Bromoethane ^{13}C NMR shifts (a) $-\text{CH}_2\text{-I}$ (b) $-\text{CH}_3$

The spectroscopic, kinetic, and computational data provide the following details about the samarium Barbier reaction: (1) The rate of reaction is zero order in ketone and first order in alkyl halide, SmI_2 , and HMPA. (2) At high concentrations, HMPA displays saturation behavior. (3) Interaction of HMPA with an alkyl halide leads to elongation of the carbon-halide bond making the substrate more susceptible to reduction.

3.3.4 Proposed Mechanism of the Samarium Barbier Reaction with HMPA

3.3.4.1 Derivation of Rate Expression

Scheme 3.10 shows the initial activation of the carbon-halide bond by HMPA and the subsequent reduction of the RX-HMPA complex proposed for the samarium Barbier reaction with HMPA.



Scheme 3.10 Rate limiting step of the samarium Barbier reaction with HMPA

Assuming that k_2 is the rate determining step, the overall rate expression for the reaction is given as:

$$\frac{d[SmI_2]}{dt} = k_2[HMPA - R - X][Sm(HMPA)] \quad (3.1)$$

Steady state approximation is applied to intermediate [HMPA-R-X] to give:

$$\frac{d[HMPA-R-X]}{dt} =$$

$$k_1[RX][HMPA] - k_{-1}[HMPA - R - X] - k_2[Sm(HMPA)][HMPA - R - X] = 0 \quad (3.2)$$

$$k_1[RX][HMPA] = k_{-1}[HMPA - R - X] + k_2[Sm(HMPA)][HMPA - R - X] \quad (3.3)$$

Because RX exists in two states, both uncomplexed and complexed with HMPA, a mass balance is required to account for both of the species, where $[RX]_T$ is the total concentration of the alkyl halide as the equilibrium shifts between free RX and RX-HMPA complex.

$$[RX]_T = [RX] + [HMPA - R - X] \quad (3.4)$$

$$[RX] = [RX]_T - [HMPA - R - X] \quad (3.5)$$

Introducing this term in equation 3.3 produces the expression:

$$k_1([RX]_T - [HMPA - R - X])[HMPA] = k_{-1}[HMPA - R - X] + k_2[Sm(HMPA)][HMPA - R - X] \quad (3.6)$$

$$k_1[RX]_T[HMPA] - k_1[HMPA - R - X][HMPA] = k_{-1}[HMPA - R - X] + k_2[Sm(HMPA)][HMPA - R - X] \quad (3.7)$$

Both sides are divided by k_1 and solved for $[HMPA-R-X]$ giving:

$$[HMPA - R - X] = \frac{[RX]_T[HMPA]}{\frac{k_{-1} + k_2[Sm(HMPA)]}{k_1} + [HMPA]} \quad (3.8)$$

Substituting $[HMPA-R-X]$ into the overall rate expression of the reaction (eq 3.1) gives:

$$\frac{d[SmI_2]}{dt} = \frac{k_2[Sm(HMPA)][RX]_T[HMPA]}{\frac{k_{-1} + k_2[Sm(HMPA)]}{k_1} + [HMPA]} \quad (3.9)$$

Assuming ($k_2 \ll k_{-1}$) since the reduction is rate limiting, and that $K_d = k_{-1}/k_1$, the expression simplifies to:

$$\frac{d[SmI_2]}{dt} = \frac{k_2[Sm(HMPA)][RX]_T[HMPA]}{K_d + [HMPA]} \quad (3.10)$$

which expresses first order behavior for $Sm(HMPA)$, RX , and $HMPA$, as well as the saturation behavior observe for $HMPA$ (*vide supra*), where K_d is the dissociation constant of $[HMPA-R-X]$.

3.3.4.2 Derived Equation Fit to Saturation Plots

Classic Michaelis-Menten (M-M) saturation kinetics follow the rate, $v = \frac{V_{max}[S]}{K_m + [S]}$,

in which V_{max} is the maximum rate reached by the reaction at saturation, K_m is the M-M

constant which represents the concentration of the substrate at $\frac{1}{2} V_{\max}$ and the substrate is first order in the reaction (Figure 3.8).

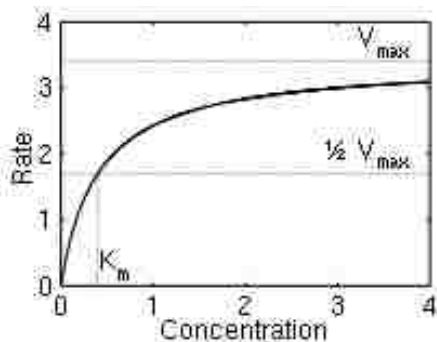


Figure 3.8 Michaelis-Menten saturation plot

The derived rate expression for the reaction (eq 3.10) can directly be used as a fit for the saturation plots observed for the samarium Barbier reaction (Figure 3.1), in which [HMPA] is the substrate, V_{\max} is the maximum rate reached at saturation ($k_2[\text{Sm}(\text{HMPA})][\text{RX}]_T$) and K_d is the dissociation constant for the formation of the alkyl halide- HMPA complex (Figure 3.9). In the M-M equation the substrate is assumed to be first order since it is the only reactant. Since the samarium Barbier reaction is more complex, $[\text{S}]^n$ is used in order to determine the order of the substrate, HMPA.

$$-\frac{d \text{SmI}_2}{dt} = \frac{\overbrace{k_2[\text{Sm}(\text{HMPA})][\text{RX}]_T}^{V_{\max}} \overbrace{[\text{HMPA}]^n}^{[\text{S}]^n}}{K_d + \underbrace{[\text{HMPA}]^n}_{K_m}}$$

Figure 3.9. Relationship between rate expression 3.10 and Michaelis-Menten saturation kinetics.

Based on the expression depicted in Figure 3.9, equation 3.11 was fit to the saturation curves obtained as the [HMPA] increased in the samarium Barbier reaction (Figure 3.10 and 3.11)

$$y = \frac{(V_{max})(X^n)}{K_d + X^n} \quad (3.11)$$

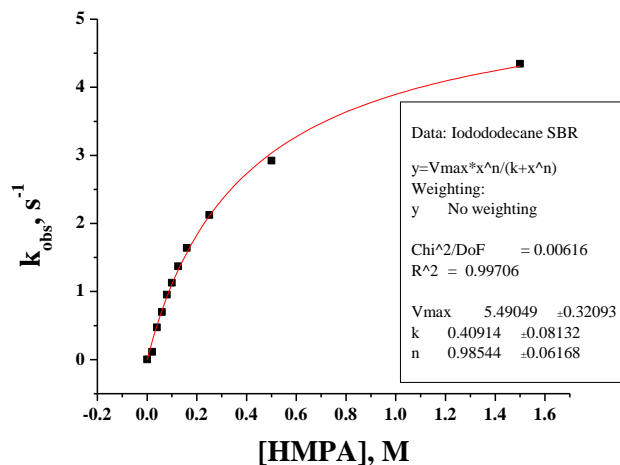


Figure 3.10 Fit of saturation plot of iodododecane (1). [HMPA] versus k_{obs} for the samarium Barbier reaction with **1**. $[SmI_2] = 5 \text{ mM}$; **[1]** = 22 equiv.; **[3]** = 25 equiv.; [HMPA] = 0-300 equiv. $V_{max} = 5.49 \pm 0.32$, $K_d = 0.41 \pm 0.08 \text{ M}$, $n = 0.99 \pm 0.06$.

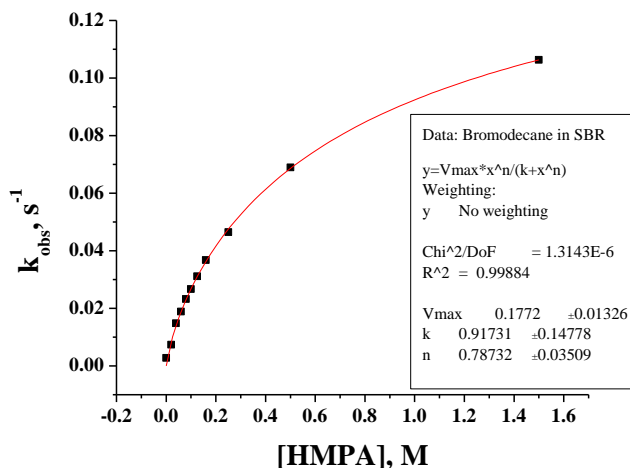


Figure 3.11. Fit of saturation plot of bromodecane (2). [HMPA] versus k_{obs} for the samarium Barbier reaction with **2**. $[SmI_2] = 5 \text{ mM}$; **[2]** = 25 equiv.; **[3]** = 25 equiv.; [HMPA] = 0-300 equiv. $V_{max} = 0.18 \pm 0.01$, $K_d = 0.92 \pm 0.15 \text{ M}$, $n = 0.79 \pm 0.04$.

Table 3.3 Fit of experimental data to equation 3.11, shown in Figures 3.12 and 3.13.^a

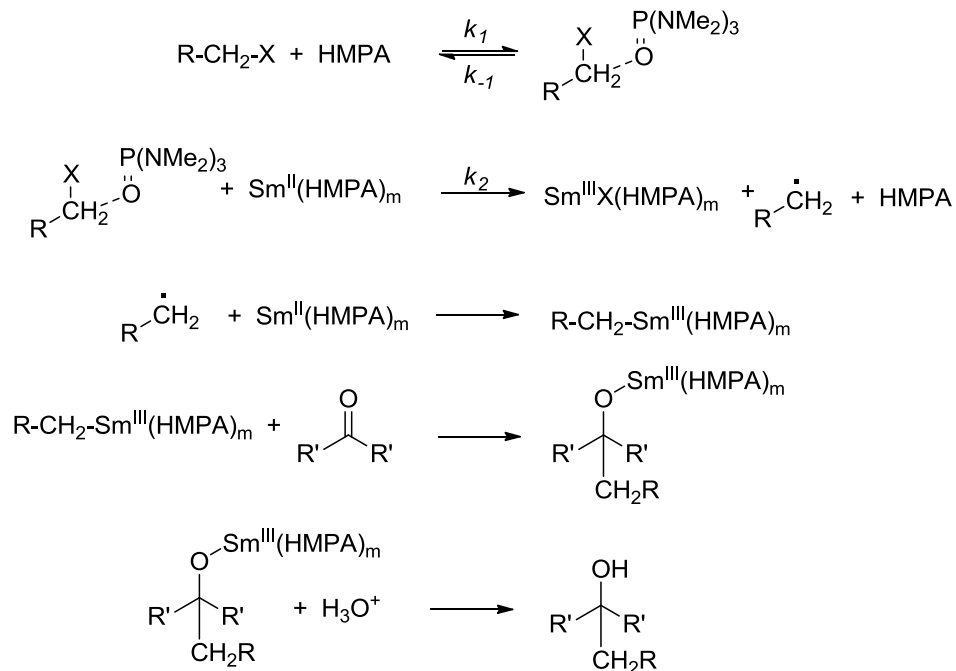
Alkyl halide	V_{\max} (s^{-1})	K_d (M)	n
1	5.5 ± 0.3	0.41 ± 0.08	0.99 ± 0.06
2	0.18 ± 0.01	0.9 ± 0.2	0.79 ± 0.04

^aThe fit for each system to eq 3.11 provided an $r^2 > 0.997$.

The rate order for HMPA obtained from eq 3.11 is the same as that acquired from $\ln[\text{HMPA}]$ vs. $\ln k_{\text{obs}}$ plot of the linear region of the data contained in Figure 3.1 (Table 3.1). Of particular importance is the K_d of the complex of HMPA and alkyl halides **1** and **2** (0.41 ± 0.08 M and 0.92 ± 0.15 M, respectively). These data show that HMPA has a higher affinity for alkyl iodides than alkyl bromides, consistent with previous studies of Wigfield.¹³⁰

3.3.4.3 Proposed Mechanism

On the basis of our kinetic and computational studies as well as previous work contained in the literature on the samarium Barbier reaction, we propose the detailed mechanism shown in Scheme 3.11. Coordination of HMPA to SmI_2 produces $\text{Sm}(\text{HMPA})_m$. In an initial equilibrium step, excess HMPA interacts with the alkyl halide producing a polarized intermediate with an elongated C-X bond which is reduced by the $\text{Sm}(\text{HMPA})_m$ complex in the rate-limiting step of the reaction (k_2). Reduction of the resultant radical produces an organosamarium intermediate, which attacks the electrophilic carbon of the ketone.^{50,65} Subsequent acidic workup produces the final alcohol product.



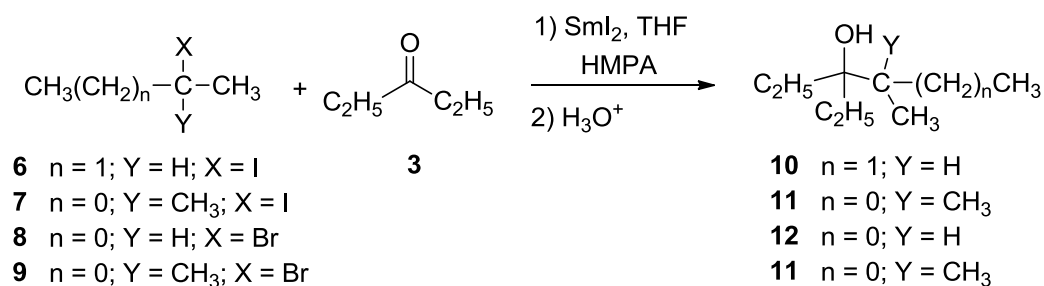
Scheme 3.11 Proposed mechanism of the Sm-Barbier reaction with HMPA

3.3.5 Samarium Barbier Reaction with Secondary and Tertiary Alkyl Halides

Following the conclusions of HMPA in the samarium-Barbier reaction with primary alkyl halides, the potential complex formation of the HMPA with secondary and tertiary alkyl halides was explored. It was suspected that a complex would be less stable with the more sterically hindered alkyl halide. Previous publications have investigated the efficiency of secondary and tertiary alkyl halides within the samarium Barbier reaction, but none which also included HMPA as a cosolvent.⁶⁵ With SmI₂ alone, the tertiary alkyl halides have been unsuccessful in coupling reactions.

3.3.5.1 Kinetic Analysis of Samarium Barbier Reagents

Pseudo first-order rate studies were performed with stopped-flow spectroscopy to determine the order of each of the reagents involved in the samarium Barbier reaction with a range of substituted alkyl iodide and alkyl bromide substrates: 2-iodobutane (**6**), 2-iodo-2-methylpropane (**7**), 2-bromopropane (**8**) and 2-bromo-2-methylpropane (**9**) (Scheme 3.12).



Scheme 3.12 Samarium Barbier reaction with secondary and tertiary alkyl halides

As expected, the rate constant increased substantially from the primary to the tertiary alkyl halide (Table 3.4). This rate increase is due to a more stable radical formation in which $1^\circ < 2^\circ < 3^\circ$. SmI_2 and all of the alkyl halides exhibited first order behavior, and the ketone still remained zero order; however, the order of HMPA varied slightly with the increase in alkyl halide substitution.

Focusing first on the alkyl iodides, the order of HMPA decreased from 1.0 ± 0.1 for the primary RX, to 0.83 ± 0.05 for the tertiary halide substrate. The first order behavior of HMPA observed with the primary alkyl halide is a result of the activation of the C-X bond with HMPA in a 1:1 complex. A lesser order of HMPA with the secondary

and tertiary alkyl halides implies a weaker interaction, resulting from steric hindrance by the substituted groups. An identical trend is observed with the rate orders of the alkyl bromides, which display an overall lesser order of HMPA due to the less stable complex formation when compared to the alkyl iodides.

Table 3.4 Rate orders of the reagents in the samarium Barbier reaction.

Alkyl Halide	Rate Order ^a				k (M ⁻² s ⁻¹)
	RX ^c	3 ^d	SmI ₂ ^e	HMPA ^f	
1 ^b	1.1 ± 0.1	0	1.0 ± 0.1	1.0 ± 0.1	4.3 ± 0.2
6	0.96 ± 0.02	0	1.0 ± 0.1	0.92 ± 0.04	14.6 ± 0.4
7	1.05 ± 0.01	0	1.0 ± 0.1	0.83 ± 0.05	125.2 ± 1.3
2 ^b	0.96 ± 0.01	0	1.0 ± 0.1	0.8 ± 0.1	0.15 ± 0.01
8	1.01 ± 0.02	0	1.0 ± 0.1	0.71 ± 0.1	0.75 ± 0.01
9	1.04 ± 0.01	0	1.0 ± 0.1	0.64 ± 0.02	3.8 ± 0.02

^aAll kinetic runs were repeated at least two times. ^bResults from table 3.2. ^c[SmI₂] = 5 mM; [HMPA] = 50 mM; [RX] = 50-300mM; [3-pentanone] = . ^d[SmI₂] = 5 mM; [RX] = 125mM; [HMPA] = 50 mM; [3-pentanone] = 50-300 mM. ^eFractional times method (see Appendix 8.2.2.27). ^f[SmI₂] = 5 mM; [HMPA] = 10-160 mM; [RX] = 125 mM; [3-pentanone] = 125 mM.

Saturation plots with increasing amounts of HMPA (4-300 equiv) in the samarium Barbier reactions were fit to equation 3.11. Dissociation constants for the HMPA-alkyl halide complexes were determined from these data (Table 3.5, saturation plots Appendix 8.2.2.10, 14, 19, 23. Plot fits 8.2.3.1, 2, 3, 4). For the alkyl iodides, the dissociation constants are consistent with the kinetic data which implied the interaction with HMPA decreases from primary to tertiary halide substrates. The alkyl bromide substrates do not show as clear of a trend. V_{\max} and n (order of HMPA) values obtained from the saturation fit also align with the experimental kinetic data.

Table 3.5 Fit of experimental data to equation 3.11.^a

Alkyl Halide	V _{max}	K _d	n ^b
1^c	5.49 ± 0.32	0.41 ± 0.08	0.99 ± 0.06
6	20.57 ± 1.3	0.56 ± 0.1	0.94 ± 0.05
7	147 ± 16	0.73 ± 0.2	0.84 ± 0.07
2^c	0.18 ± 0.01	0.92 ± 0.15	0.79 ± 0.04
8	0.73 ± 0.04	0.60 ± 0.08	0.86 ± 0.04
9	3.85 ± 0.18	0.62 ± 0.08	0.79 ± 0.03

^aThe fit for each system to eq 2 provided an $r^2 > 0.997$. ^border of HMPA. ^cData from Table 3.3.

The nearly first order rate of HMPA with all of the substituted alkyl halide substrates is indication that the role of polarizing the carbon-halide bond is still present with the sterically hindered alkyl halides. As described from the saturation data above, as the steric hindrance around the halide increases ($3^\circ > 2^\circ > 1^\circ$), the order and first order role of HMPA starts to decrease. We suspect this is occurring due to a weaker interaction between the two reagents. We also believe that the complex between HMPA and these different substrates differ slightly from the dipole-dipole type complex identified for the primary alkyl halides.

Based on the orientation that was observed with the primary alkyl halide and HMPA presented previously (section 3.3.2), we hypothesize that the increase in steric bulk around the alpha carbon may disrupt the dipole-dipole interaction, and could force the complex to resemble the S_N2 configuration originally proposed by Wigfield (Figure 3.4). This shift in the orientation will still allow for the polarization in the C-X bond to occur, evident by the kinetic data presented above, but due to the loss of the stabilizing interaction of the dipoles the equilibrium will slightly shift to disfavor the complex.

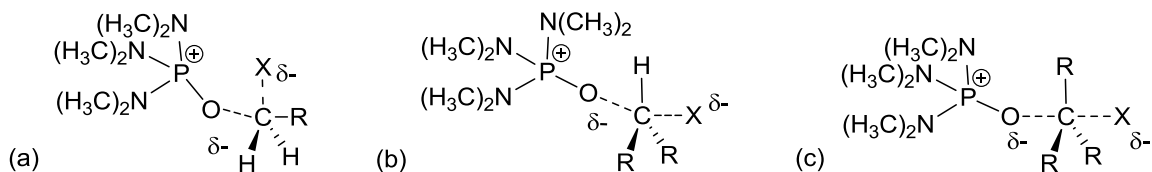


Figure 3.12 Proposed complexes with HMPA and (a) primary alkyl halides, (b) secondary alkyl halides and (c) tertiary alkyl halides.

3.3.5.2 NMR Titration Experiments

Low temperature NMR studies were again performed with the substituted alkyl halide substrates in d8-THF to examine the complex formation observed from the computational data. As expected, significant shifts of the signals alpha to the halide were seen across the iodo and bromo series (see appendix Table 8.2.5.1.7). The ^1H methylene and methylene shifts were consistently greater than the methyl proton shifts and carbon shifts, further indicating an interaction at the position alpha to the halide. The shifts between the 1° , 2° and 3° substrates were similar, suggesting the HMPA-RX interaction remains intact even with the substitutions on the alkyl halide.

Synthetically, few examples have been shown to couple secondary and tertiary alkyl halides in the samarium Barbier reaction. With 2-iodobutane and 2-bromopropane in the Sm-Barbier reaction with HMPA the desired tertiary alcohol Barbier product was formed selectively, however less than 20% of an isolated yield was obtained. With 2-iodo-methylpropane, and 2-bromo-3-methylpropane, a pinacol product was predominantly formed with a 40% yield. It is possible that the alkyl halide substrates

were reduced to their corresponding low molecular weight alkanes. Efforts to isolate side products were not made.

3.4 Conclusion

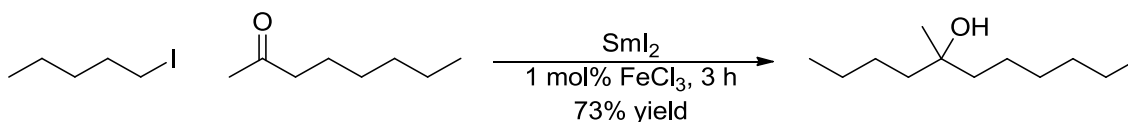
The presence of HMPA is critical for the selective coupling of alkyl halides and ketones by SmI_2 . Although previous rate studies have shown that HMPA dramatically accelerates the reduction of alkyl halides over ketones, the mechanistic basis for this rate acceleration was unknown. We demonstrated that the selectivity observed in the samarium Barbier reaction is in part a result of activation of the alkyl halide bond by HMPA. This interaction of HMPA with alkyl halides leads to elongation of the carbon-halide bond making it more susceptible to reduction, thus providing the basis for the selective reduction responsible for success of the samarium Barbier reaction. A complex is formed not only with a primary alkyl halide, but secondary and tertiary substrates as well. Although the bond activation did not produce quantitative yields for the Barbier reaction with the more substituted alkyl halide substrates, this knowledge of HMPA-RX interaction can be used to promote other reactions which require an activated secondary or tertiary alkyl halide, and may have an important impact for activation of bonds in other electron transfer processes.

Chapter 4. Catalytic Ni(II) in SmI₂ Reactions: Sm(II) or Ni(0) Chemistry?

4.1 Background and Significance

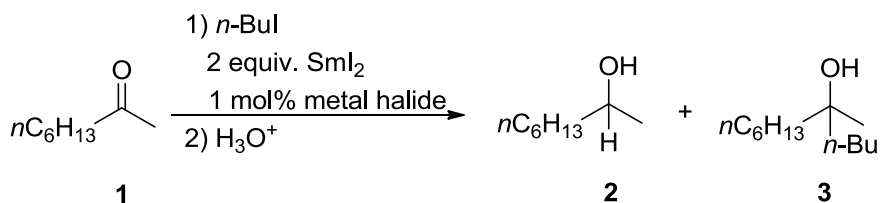
4.1.1 Transition Metal Salts in SmI₂ Reactions

Transition metal salts and complexes are important components of many reactions involving samarium diiodide (SmI₂).^{17,84,136-139} Within the seminal paper of Kagan, he described the use of catalytic amounts of ferric chloride with SmI₂ to accelerate several coupling reactions between alkyl iodides and ketones.¹



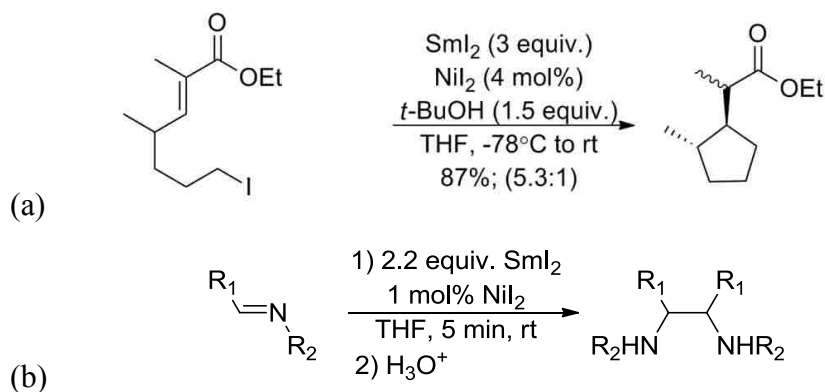
Scheme 4.1 Samarium Barbier reaction with catalytic amount of FeCl₃

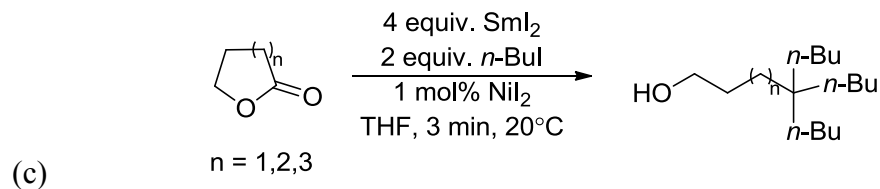
In 1996, Namy and Kagan described the use of catalytic amounts of various transition metal salts to improve the reaction time and product yield of the samarium Barbier reaction.⁶⁰ With the addition of these salts (FeCl₃, CuCl₂, NiI₂, AgBr, among others) the reaction was complete within 10 minutes, with above average yields. In this report NiI₂ provided the greatest improvement.

Table 4.1 Various transition metal salts in the samarium Barbier reaction

Entry	Transition metal halide	1 (%)	2 (%)	3 (%)
1	None	80	traces	20
2	FeCl_3	21	traces	79
3	CuI	48	traces	52
4	NiI_2	10	traces	90

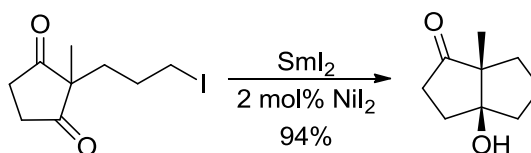
In the following years, several other reactions were most efficient with the inclusion of a catalytic amount of transition metal salts or complexes. In an intramolecular halide-olefin cyclization, Molander observed an increase in rate of reaction when NiI_2 was used in a catalytic amount (Scheme 4.2a).¹⁴³ In addition, Namy found the highest yield and rate in the homo pinacol coupling of imines,^{61a} (Scheme 4.3b) and ring opening of lactones (Scheme 4.2c)^{61b} when utilizing catalytic NiI_2 .



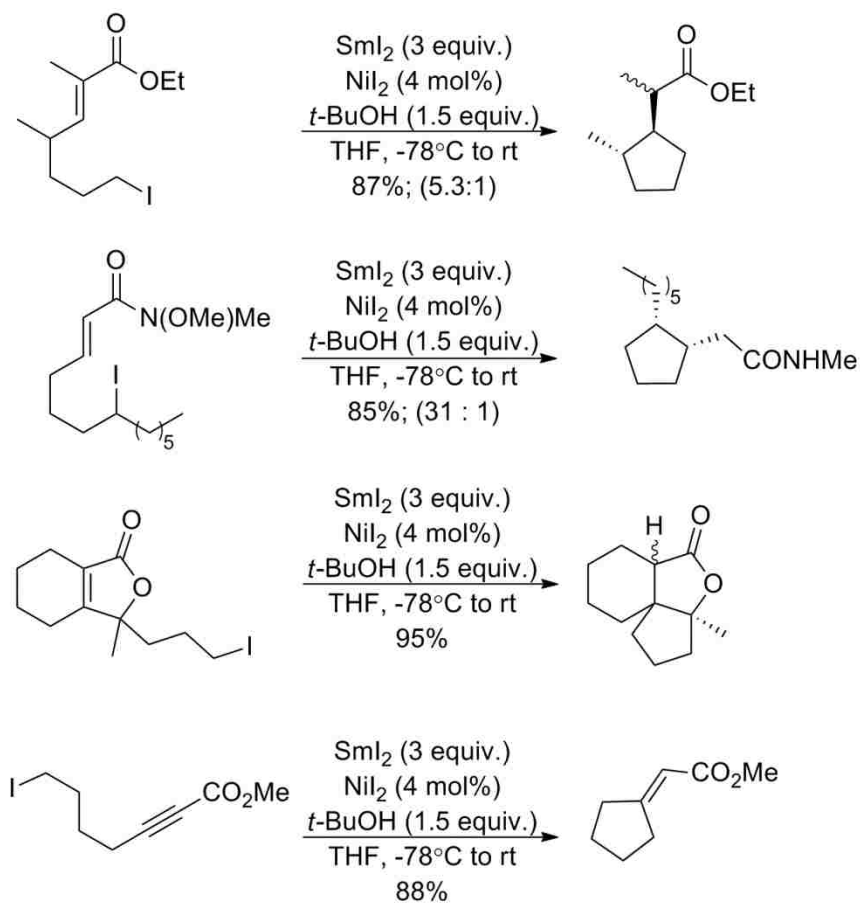


Scheme 4.2 Catalytic amount of NiI_2 used in SmI_2 reactions

Molander included catalytic NiI_2 in intramolecular Barbier reactions¹⁴⁰ to form bicyclic hydroxyl ketones (Scheme 4.3). When NiI_2 was not added, undesired side products were obtained. He also found that the addition of NiI_2 in catalytic amounts is critical for the intramolecular cyclization of halides onto activated olefins (Scheme 4.4).^{143,144} The cyclizations were successful with primary and secondary halides with α,β -unsaturated esters and amides, and was later expanded to cyclization with α,β -unsaturated lactones to form bicyclic products.



Scheme 4.3 Intramolecular Barbier reaction with catalytic NiI_2



Scheme 4.4 Halide-olefin cyclization with NiI_2

While it is unmistakable that the transition metal catalyst enhanced these reactions, as well as others, it was unclear what role Ni(II) was playing within the mechanism of the reaction. A few reports have suggested that Ni(II) salts could be reduced to Ni(0) by SmI_2 ,^{141,142} however, no detailed studies on these suppositions have been initiated.

Nickel complexes in both the (0) and (II) oxidation states are extremely useful in a range of synthetically important carbon-carbon bond forming reactions.¹⁴⁵ Activation of

catalytic systems employing Ni(0) can be initiated by the *in situ* reduction of Ni(II) to Ni(0) with a stoichiometric reductant.¹⁴⁶ In fact, examination of methods employed to produce Ni nanoparticles show that they are typically formed through reductions of Ni(II) starting materials.¹⁴⁷⁻¹⁵¹ Evaluation of the E° values of Sm(III)/Sm(II) and Ni(II)/Ni(0) redox couples clearly demonstrate that SmI₂ has the capacity to readily reduce Ni(II) to Ni(0) (Sm(III)/Sm(II) = -1.33 V; Ni(II)/Ni = -0.25 V).¹⁵² Recent work by Ogoshi and Kurosawa has demonstrated that facile reduction of Ni(II) by SmI₂ in the presence of *trans, trans, trans*-1,5,9-cyclododecatriene (CDT) provides good yields of the Ni(0) complex, Ni(CDT).¹⁵³

Based on these examples in the literature, could Ni(0) and Ni(II) intermediates be responsible for the unique chemistry initiated by the addition of catalytic amounts of NiI₂ to SmI₂-mediated reactions? Furthermore, is the process driven by homogeneous chemistry, or colloidal Ni(0)? Herein we show that SmI₂ does in fact reduce the Ni(II) catalyst to Ni(0), and that Ni(0) is then responsible for carrying out the subsequent chemical reaction.

4.2 Experimental

4.2.1 Materials

THF was purified after purging with argon gas and passing over a column of activated alumina by a Solvent Purification System (Innovative Technology Inc.; MA).

Dried solvents and reagents were stored in an Innovative Technology, Inc. drybox containing an argon atmosphere and a platinum catalyst for drying. SmI_2 was prepared by stirring Sm metal and iodine in THF until the characteristic blue color of Sm(II) appeared. The concentration of the Sm complex (0.10 M in THF) was determined by iodometric titration. 3-pentanone (**5**) was purchased from Aldrich and distilled under vacuum from CaO before use. Iodododecane (**4**), Sm metal and $\text{Ni}(\text{acac})_2$ were purchased from Acros and used with no further purification. NiI_2 and $\text{Ni}(\text{DPPE})_2\text{Cl}_2$ were purchased from Aldrich and used with no further purification. Ni nanoparticles (aps 20 nm) were purchased from Sunano.

4.2.2 Instrumentation

Proton and carbon NMR were recorded on Bruker 500 MHz spectrometer. GC-MS analysis was performed with HP 5890 Series Gas Chromatograph with an HP Mass Selector Detector. HR-MS was performed at the Mass Spectrometry Facility at Notre Dame University. Kinetic studies in THF were performed using a computer-controlled SX-20 MV stopped-flow reaction spectrophotometer (Applied Photophysics Ltd., Surrey, UK). UV/vis spectroscopy experiments were performed on a Shimadzu UV-1601 UV-Visible Spectrophotometer controlled by UV Probe (version 1.11) software. TEM images were taken with JOEL JEM-2000FX transmission electron microscope. This is a standard research TEM operating at up to 200 kV; with a lanthanum hexa-boride filament for high resolution work, is equipped with XEDS for point analysis and has two digital cameras.

4.2.3 Methods

4.2.3.1 General Procedure for the Samarium Barbier Reaction with Ni(II)

The Barbier reaction was carried out in a drybox with degassed reagents. Ni(II) salts (0.004 mmol) were added to 2 mL THF and stirred to dissolve. SmI₂ (4.0 mL, 0.1 M) was added drop wise to the Ni(II) solution, and with slow addition the solution turned brown. Separately, **4** (49.3 μL, 0.2 mmol) and **5** (21.2 μL, 0.2 mmol) were added to 5 mL THF. The substrate solution was added drop wise to the SmI₂-Ni solution. This reaction was left to stir for 5-15 min (depending on the Ni(II) additive) and the progress of the reaction was monitored by GC-MS. The reaction was quenched by exposing to air and adding 0.1M HCl. The reaction mixture was then washed with water and extracted twice with ether. The organic layer was washed individually with H₂O, saturated aqueous Na₂S₂O₃, and brine, dried over MgSO₄ and then concentrated on a rotary evaporator to obtain the pure Barbier product (**6**).

4.2.3.2 General Procedure for Stopped-Flow Studies

Kinetic experiments in THF were performed with a computer-controlled SX.20 MV stopped-flow spectrophotometer (Applied Photophysics Ltd. Surrey, UK). The SmI₂ and substrates with Ni(II) were taken separately in airtight Hamilton syringes from a drybox and injected into the stopped-flow system. The cell block and the drive syringes of the stopped flow reaction analyzer were flushed a minimum of three times with dry, degassed THF to make the system anaerobic. When using reaction progress kinetic

analysis (RPKA), the concentration of SmI_2 used for the study was 20 mM. The concentrations of the substrates were kept at synthetically relevant conditions with only slight excess with respect to SmI_2 (as indicated in text). When using pseudo-first-order conditions the $[\text{SmI}_2]$ was 5 mM and the concentration of the substrates was kept high relative to $[\text{SmI}_2]$ (125 mM). In all cases the mol% of Ni(II) species were determined with respect to $[\text{SmI}_2]$ (1-5 mol%). The reaction rates were determined from the decay of SmI_2 absorbance at 555 nm. Under reaction progress kinetic analysis conditions, rate was determined from the decay of the SmI_2 absorbance at 555 nm. Rate = $(\Delta[\text{SmI}_2]/\Delta\text{time, s})$. The pseudo-first-order rate constants were determined using standard methods.¹⁵⁴ The decay of the SmI_2 displayed first order behavior over > 3 half-lives.

4.2.3.3 General Procedure for the Preparation of TEM Samples

SmI_2 (5 mM) was added dropwise to a stirring solution of $\text{Ni}(\text{acac})_2$ (2.5 mM) and triphenylphosphine (TPP) (1.0 mM) in THF. The reaction was left to stir for 10 min to ensure complete reduction of the Ni(II) species. The solution was then centrifuged on a DuPont Sorvall SS-3 Automatic Centrifuge for 5 min at 5000 rpm. The supernatant was decanted off and the pellet was resuspended in THF. The resuspended solution was then introduced to a TEM slide and solvent evaporated off.

4.3 Results

4.3.1 UV-Vis Identification of Ni(0)

Careful examination of the experimental procedures utilizing Ni(II) in SmI₂ reactions revealed that in most cases, the Ni(II) salt and SmI₂ are premixed before addition of substrates.^{60,140,143,144,155,156-158} To initially study the SmI₂-Ni(II) system, SmI₂ in THF was slowly titrated into solutions of NiI₂, Ni(II) acetylacetonate (Ni(acac)₂), and 1,2-bis(diphenylphosphino)ethane Ni(II) chloride (Ni(DPPE)₂Cl₂). In each case the blue color of the SmI₂ dissipated immediately, producing a brown solution. Over time, a precipitate gradually formed from the solution. The UV-Vis spectra of a series of solutions of SmI₂ containing increasing amounts of NiI₂ were observed as shown in Figure 4.1. As the concentration of NiI₂ increased, the UV-Vis bands corresponding to SmI₂ decreased, and a broad absorbance from 350-500 nm, consistent with the plasmon resonance of colloidal Ni(0) began to emerge.¹⁵⁹ Similar behavior was observed across the range of Ni(II) salts examined.

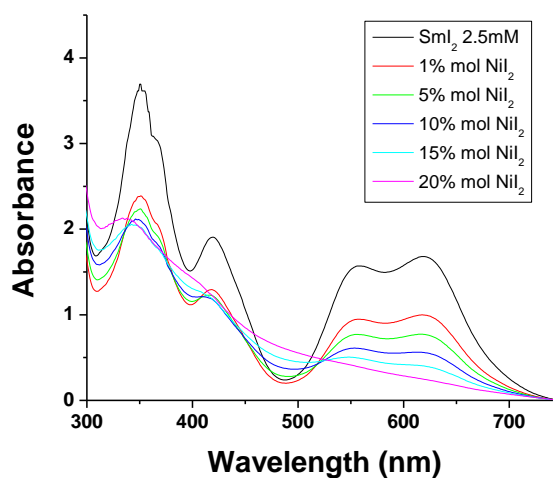


Figure 4.1 UV-Vis spectra of SmI₂ in THF (2.5 mM) containing increasing amounts of NiI₂.

4.3.2 TEM Images of Ni Nanoparticles

To gain more insight into the reaction between SmI_2 and Ni(II) , transmission electron microscopy (TEM) was used to characterize the solid precipitate obtained from a freshly prepared solution. Figure 4.2 contains a TEM image of the solid obtained from the addition of SmI_2 to Ni(acac)_2 in THF. The TEM images display nanoparticles in the 5-10 nm range. The particles showed evidence of aggregation over the time period in which precipitation was observed in the earlier UV-vis experiment.

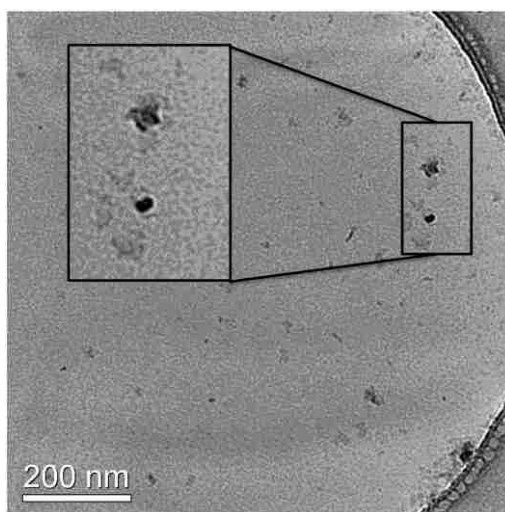


Figure 4.2 TEM image of nanoparticles produced upon the addition of 1.5 mL of SmI_2 (5 mM) to 1.5 mL of Ni(acac)_2 (2.5 mM) and TPP (1.0 mM).

4.3.3 Kinetic Data: Reaction Progress Kinetic Analysis

With the knowledge that colloidal Ni(0) is being formed, the rate of reduction of Ni(II) by SmI_2 was examined via stopped-flow spectrophotometry using the initial rates method. Since NiI_2 has limited solubility under the conditions required for rate studies,

Ni(DPPE)₂Cl₂ was used as the Ni(II) salt. The reaction was monitored at 486 nm to observe the growth of the plasmon resonance as colloidal Ni(0) is formed, while SmI₂ exhibits minimal absorbance at this wavelength, as shown in Figure 4.3. The rate of growth of the plasmon resonance was determined using the linear region of the absorbance growth from 0.2-0.5 s. A plot of initial rate for the reduction of Ni(DPPE)₂Cl₂ versus concentration of SmI₂ is shown in Figure 4.4. The rate constant determined from this approach is $11.20 \pm 0.01 \text{ M}^{-1}\text{s}^{-1}$. This experiment demonstrates that in the absence of organic substrates, Ni(0) nanoparticle formation is a facile process. The question remains, is colloidal Ni(0) responsible for the reactivity observed for reactions of SmI₂ containing catalytic amounts of Ni(II) salts?

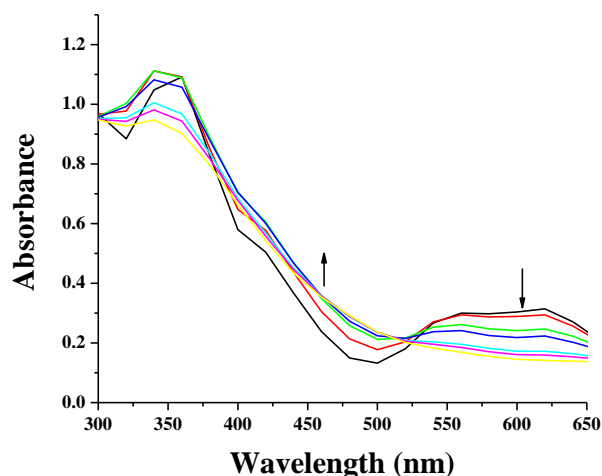


Figure 4.3 Time-resolved UV-vis spectrum of the reduction of Ni(DPPE)₂Cl₂ by SmI₂. [SmI₂] = 5 mM; [Ni(DPPE)₂Cl₂] = 1.0 mM; [4] = 15 mM; [5] = 15 mM

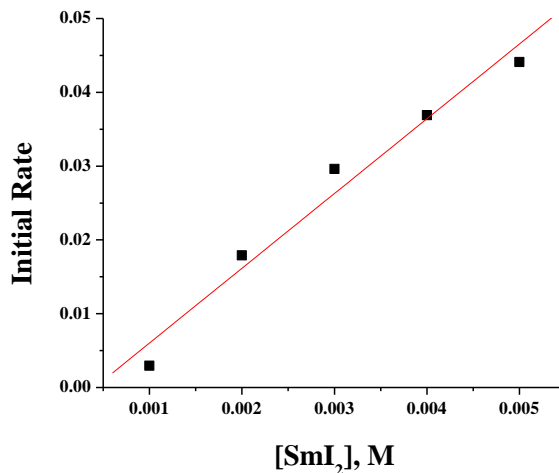
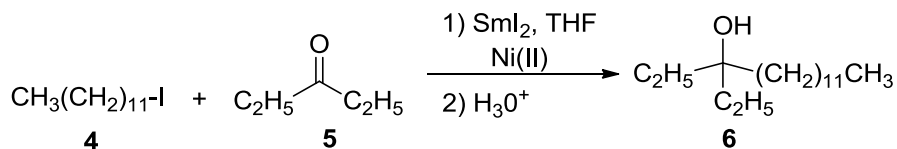


Figure 4.4 Plot of initial rates vs. $[\text{SmI}_2]$ for the reduction of $\text{Ni}(\text{DPPE})_2\text{Cl}_2$ by SmI_2 . $[\text{SmI}_2] = 1\text{-}5 \text{ mM}$; $[\text{Ni}(\text{DPPE})_2\text{Cl}_2] = 1.0 \text{ mM}$. Rate constant = $10 \pm 1 \text{ M}^{-1}\text{s}^{-1}$.

To further explore the system, the coupling of iodododecane (**4**) and 3-pentanone (**5**) in a samarium Barbier reaction was chosen as a model reaction (Scheme 4.5) to study the impact of Ni(II) salts on SmI_2 reactions since the rates of reduction of both substrates by SmI_2 are well-established.¹⁰⁷ For both substrates, the rate constant for reduction by SmI_2 is five orders of magnitude slower than the rate constant for Ni(II) reduction by SmI_2 , determined above. (Rate constants for 2-butanone and 1-iodobutane were found to be nearly identical at $(7 \pm 3) \times 10^{-4}$ and $(8 \pm 2) \times 10^{-4} \text{ M}^{-1}\text{s}^{-1}$ respectively).¹⁰⁷



Scheme 4.5 Ni(II) catalyzed samarium Barbier reaction.

The study began by using 1 mol% Ni(II) within the Barbier reaction as described by Kagan.⁶⁰ The results of these experiments are shown in Table 4.2. In the absence of Ni(II), the reaction is sluggish, resulting in a 69% yield of product after 72 hours, with the remainder of the reaction mixture consisting of unreacted starting material (Table 4.2, entry 1). The use of 1 mol% NiI₂, Ni(acac)₂, or Ni(DPPE)₂Cl₂ led to nearly quantitative yields of product in 5-15 minutes (Table 4.2, entries 2-4).

Table 4.2 Reaction of **4** and **5** with SmI₂ and/or various Ni additives.^a

entry	Ni additive	Reaction Time	Yield ^b
1	none	72 h	69% ^c
2	NiI ₂ (1mol%)	5 m	98%
3	Ni(acac) ₂ (1 mol%)	15 m	93%
4	Ni(DPPE)Cl ₂ (1 mol%)	10 m	95%
5	Ni nanoparticles ^d	15 h	NR
6	SmI ₂ -NiI ₂ Centrifuged- Solid ^e	15 h	NR
7	SmI ₂ -NiI ₂ Centrifuged-Supernant ^f	5 m	96%

^aNi(II) additive. ^bYields based on NMR ratio between Barbier product and reduced dodecane. No starting material remained. ^cIsolated yield of Barbier product. ^dCommercial Ni(0) 20 nm powder. ^eSmI₂ (0.96 mmol) was added to a solution of NiI₂ (0.48 mmol) dropwise to form brown solution. After 5 minutes of stirring the solution was centrifuged for 5 minutes at 5000 rpm. The solid obtained in the reaction was separated and washed with THF before being subjected to the substrates (0.4 mmol). ^fSupernatant obtained from procedure (e) was isolated and reacted with the substrates. NR = no reaction.

To test whether Ni nanoparticles are capable of initiating the reaction, commercially available Ni nanoparticles (20 nm average particle size) were reacted with **4** and **5** in THF (Table 4.2, entry 5). No reaction occurred over a range of [Ni(0)] added. Since the nanoparticles formed *in situ* from the reduction of Ni(II) by SmI₂ were smaller in diameter (as determined by TEM), another experiment was initiated in which SmI₂ and NiI₂ were pre-mixed, the solution centrifuged, and precipitate obtained. These particles

were then washed with THF in an inert atmosphere and mixed with **4** and **5**. No reaction occurred, which provides evidence that although Ni nanoparticles are formed during the course of the reaction, they do not initiate the Barbier reaction. This result raises the question: is it possible that soluble Ni(0) is capable of initiating the reaction? To test this hypothesis, SmI₂ was mixed with a stoichiometric amount of Ni(II). The colloidal suspension was filtered and **4** and **5** were added to the supernatant. Nearly a quantitative yield of **6** was obtained after 5 minutes (Table 4.2, entry 7).

Based on the information obtained thus far, it is clear that Ni(II) salts are acting as catalysts in the samarium Barbier reaction. To investigate the mechanism by which the catalyst functions, reaction progress kinetic analysis (RPKA) experiments were employed.¹⁶⁰⁻¹⁶² This method allows kinetic analyses to be performed on a system under synthetically relevant conditions. The “same excess” experiment of RPKA probes catalyst stability and determines if it is being deactivated during the course of the reaction. In order to run same excess experiments, the rates of two reactions are monitored: one run set at initial conditions, and the second run (50% run) set at one half of the initial reaction concentrations, with every other reagent maintaining the same excess as Run 1, as shown in Table 4.3.

The Barbier reaction was monitored using the RPKA method with a catalytic amount of Ni(DPPE)₂Cl₂, by stopped-flow spectrophotometry, in which the decay of SmI₂ was monitored at 555 nm. Run 1 was performed with a 0.03 M excess of the substrates (with respect to SmI₂ at 0.02 M) and the catalyst set at 1 mol% (2.0 x 10⁻⁴ M)

with respect to SmI_2 (Table 4.3, Run 1). In Run 2, $[\text{SmI}_2]$ was 0.01 M; one half of the SmI_2 concentration in Run 1. The reagent concentrations were decreased in an equivalent amount with respect to $[\text{SmI}_2]$ in order to maintain the same excess concentrations (See Appendix 8.3.2.2). Identical to Run 1, the $[\text{Ni(II)}]$ was maintained at 2.0×10^{-4} M (Table 4.3, Run 2). Under these conditions, Run 2 possesses the reaction concentrations that would be present at the midpoint of Run 1.

Ideally in a catalytic reaction system, the concentration of catalyst remains constant through the course of the reaction. As a result, if the catalyst is active and constant, the concentration of Ni should be the same half way through the reaction as it was at the beginning. If the catalyst is *not* being deactivated during the course of the reaction, the plots of Runs 1 and 2 will overlay. If catalyst *is* deactivated through decreasing $[\text{Ni(DPPE)}_2\text{Cl}_2]$, then the plots of the two runs will not overlay. Runs 1 and 2 were plotted as rate as a function of concentration and no overlay was observed (Figure 4.5). This observation indicates that the catalyst is being deactivated, by the $[\text{Ni}]$ decreasing over the course of the reaction.

Table 4.3 Same excess RPKA reaction conditions

Run	SmI_2 (M)	4 (M)	4 excess (M)	5 (M)	5 excess (M)	Ni(II) (M)
1	0.02	0.040	0.030	0.040	0.030	2.0×10^{-4}
2	0.01	0.035	0.030	0.035	0.030	2.0×10^{-4}

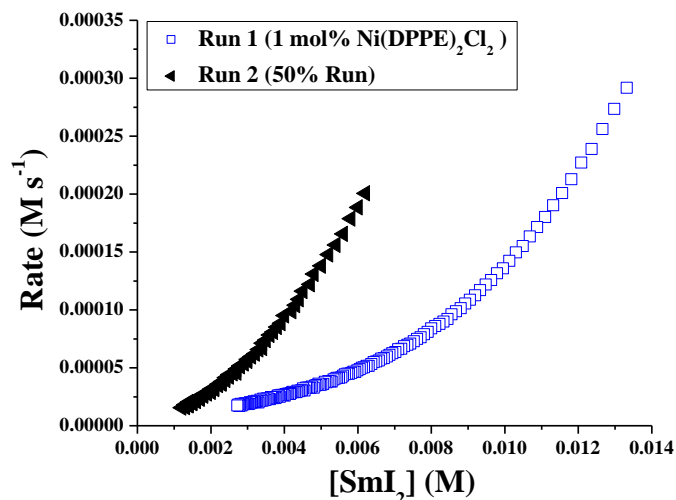


Figure 4.5 Rate vs $[\text{SmI}_2]$ for same excess experiments. (\square) Run 1 and (\blacktriangleleft) Run 2. Reaction conditions listed in Table 4.3.

As described from the experiments in Table 4.2, both the purchased Ni(0) nanoparticles (Table 4.2, entry 5), as well as the solid Ni(0) obtained from the $\text{SmI}_2/\text{NiI}_2$ mixture (Table 4.2, entry 6) did not initiate the Barbier reaction. However, when the substrates were reacted with the supernatant (Table 4.2, entry 7) the reaction proceeded. This information, together with the observation that the catalyst is being deactivated with 1 mol% Ni(II), suggest that the deactivation pathway of the catalyst is the formation of aggregated colloidal Ni(0). As Ni(II) is rapidly reduced to Ni(0) by SmI_2 , some Ni(0) aggregates and precipitates out of solution, while some concentration of Ni(0) remains soluble. The remaining soluble Ni(0) is then responsible for catalyzing the reaction.

Even though the Barbier reaction proceeds to completion with 1 mol% Ni(II), deactivation of the catalyst occurs. To determine if an optimal conditions for the reaction could be created, thereby enhancing the efficiency of the samarium Barbier reaction, the

[Ni(II)] was increased. Figure 4.6 displays data resulting from the new concentrations of Ni(DPPE)₂Cl₂ added to the system: 3 mol% (Table 4.4, Runs 3 and 4), and 5 mol% (Table 4.4, Runs 5 and 6). As indicated by less deviation in the runs of the same excess experiments, deactivation is decreased but not prevented with the addition of higher concentrations of Ni(II). From these results, 3 mol% catalyst loading was deemed most ideal to employ in further experiments since the least amount of deactivation was observed at this concentration.

Table 4.4 Same excess RPKA conditions.

Run	SmI ₂ (M)	4 (M)	4 excess (M)	5 (M)	5 excess (M)	Ni(II) (M)
3	0.02	0.040	0.030	0.040	0.030	6.0 x 10 ⁻⁴
4	0.01	0.035	0.030	0.035	0.030	6.0 x 10 ⁻⁴
5	0.02	0.040	0.030	0.040	0.030	0.001
6	0.01	0.035	0.030	0.035	0.030	0.001

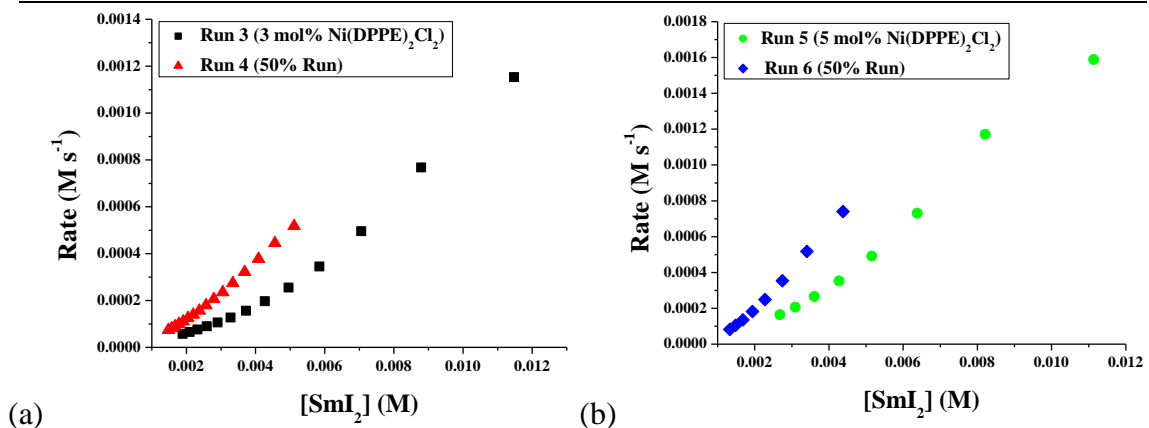


Figure 4.6 Rate vs [SmI₂] for same excess experiments. (a) (■) Run 3 and (▲) Run 4 (Table 4.4) (b) (●) Run 5 and (◆) Run 6 (Table 4.4).

RKPA “different excess” experiments describe changing the concentration of one reagent and observing the impact it has on the rate. To determine the rate orders of **4** and

5, the excess concentrations were doubled in turn and the reaction profiles of each were examined. Table 4.5 displays the concentrations of each reaction component. When the decays of Runs 7 and 8 were plotted, overlay was observed (Figure 4.7), indicating that an increase in [4] does not change the reaction rate, a finding consistent with a zero-order dependence of 4. Similar overlay is observed when Runs 7 and 9 are plotted (Figure 4.8), also indicating a zero-order for 5. These orders were also observed under pseudo-first order conditions (see Appendix 8.3.2.3 and 8.3.2.4).

Table 4.5 Conditions for “different excess” experiments to determine reaction orders of the substrates 4 and 5.

Run	SmI ₂ (M)	4 (M)	4 excess (M)	5 (M)	5 excess (M)	Ni(II) (M)
7	0.02	0.04	0.03	0.04	0.03	2.0 x 10 ⁻⁴
8	0.02	0.07	0.06	0.04	0.03	2.0 x 10 ⁻⁴
9	0.02	0.04	0.03	0.07	0.06	2.0 x 10 ⁻⁴

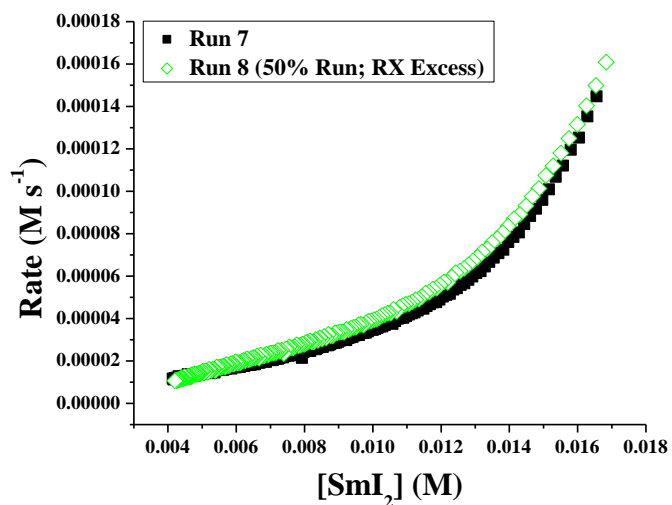


Figure 4.7 Plot of rate vs [SmI₂] for different excess experiment. (■) Run 7 and (◇) Run 8 to determine 4 reaction order. Reaction conditions listed in Table 4.5. Overlay indicates that the reaction is zero order in 4.

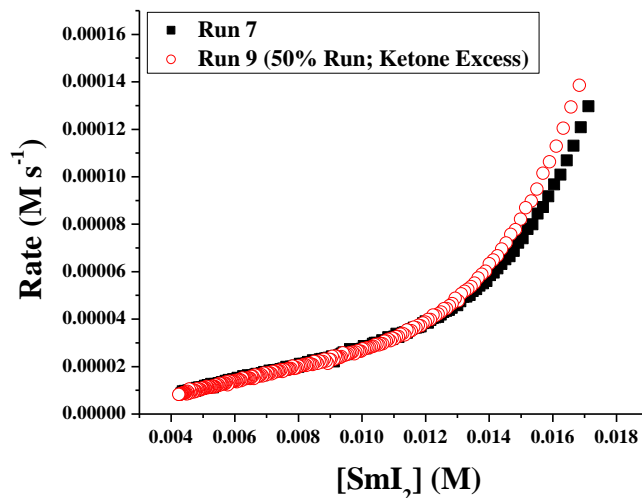


Figure 4.8 Plot of rate vs $[\text{SmI}_2]$ for different excess experiment. (■) Run 7 and (○) Run 9 to determine **5** reaction order. Reaction conditions listed in Table 4.5. Overlay indicates the reaction is zero order in **5**.

Moreover, using “different excess” experiments with respect to $[\text{Ni}]$, the order of Ni can be determined. Using the reaction profiles obtained in Figures 4.6, the reaction profiles obtained when the $[\text{Ni}]$ was increased were plotted. When an overlay was not observed, it indicated the concentration of $\text{Ni}(\text{DPPE})_2\text{Cl}_2$ has an effect on the rate determining step of the reaction. The plots were normalized with respect to $[\text{Ni}]$ by dividing the rate by the concentration of the Ni catalyst (6.0×10^{-4} M, 8.0×10^{-4} M and 0.001 M respectively). Overlay of the plots indicate that the reaction is first order in Ni catalyst (Figure 4.9).

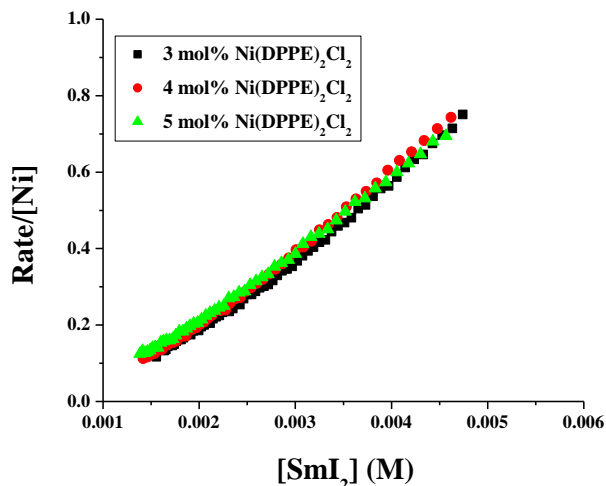


Figure 4.9 Turn-over frequency of Ni(II) in the samarium Barbier reaction. $[\text{SmI}_2] = 0.01\text{M}$; $[\mathbf{4}] = 0.035\text{M}$; $[\mathbf{5}] = 0.035\text{M}$; $[\text{Ni}(\text{DPPE})_2\text{Cl}_2] = (\blacksquare) 6.0 \times 10^{-4}\text{M}$; $(\bullet) 8.0 \times 10^{-4}\text{M}$, $(\blacktriangle) 1.0 \times 10^{-3}\text{M}$.

Further, the order of SmI_2 in the reaction was determined using traditional pseudo-first order kinetic methods. $[\text{Ni}(\text{DPPE})_2]$ was kept consistent at 3 mol% with respect to SmI_2 , while both $\mathbf{4}$ and $\mathbf{5}$ were set at a 10 equivalent excess. A first order dependence of SmI_2 was found in the reaction (Figure 4.10).

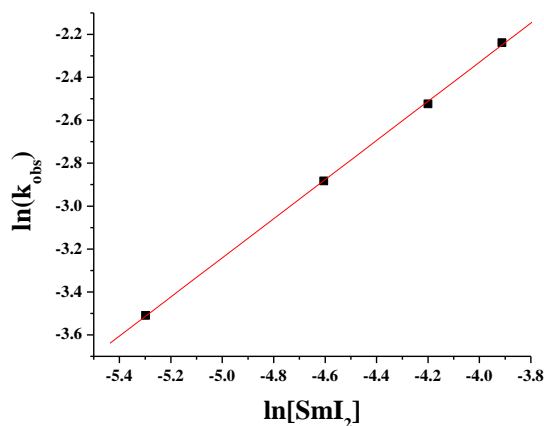


Figure 4.10 Rate order of SmI_2 in the Ni(II)-catalyzed samarium Barbier reaction. $[\text{SmI}_2] = 5\text{-}20 \text{ mM}$; $[\text{Ni}(\text{DPPE})_2\text{Cl}_2] = 0.15\text{-}0.60 \text{ mM}$ (3 mol% with respect to $[\text{SmI}_2]$); $[\mathbf{4}] = 0.2 \text{ M}$; $[\mathbf{5}] = 0.2 \text{ M}$. Rate order = 0.91 ± 0.01 .

Finally, the rate constant of the Barbier reaction with Ni(II)-catalyst was examined using the initial rates method, with increasing concentration of Ni(DPPE)₂Cl₂ added to the system. A rate constant of $16.6 \pm 1.5 \text{ M}^{-1}\text{s}^{-1}$ was obtained from these data (Figure 4.11). This value is in good agreement with the rate constant found for the reduction of Ni(DPPE)₂Cl₂ by SmI₂ in the absence of substrates (Figure 4.4), further indicating that the rate-determining step in the cycle is the initial reduction of Ni(II).

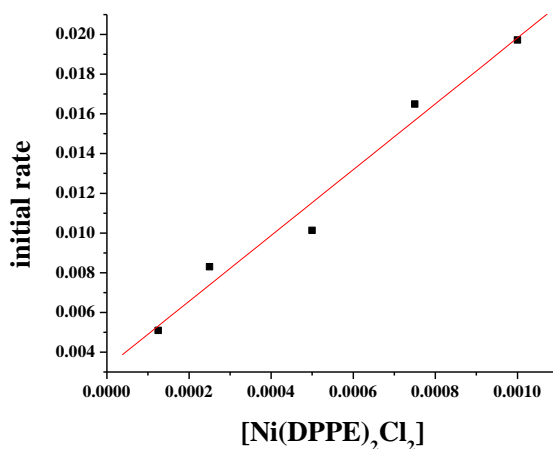


Figure 4.11 Rate constant of Ni(DPPE)₂Cl₂ in the samarium Barbier reaction. [SmI₂] = 5 mM; [Ni(DPPE)₂Cl₂] = 0.5-4 mol%; [**4**] = 50 mM; [**5**] = 50 mM. Rate constant = $16 \pm 2 \text{ M}^{-1}\text{s}^{-1}$.

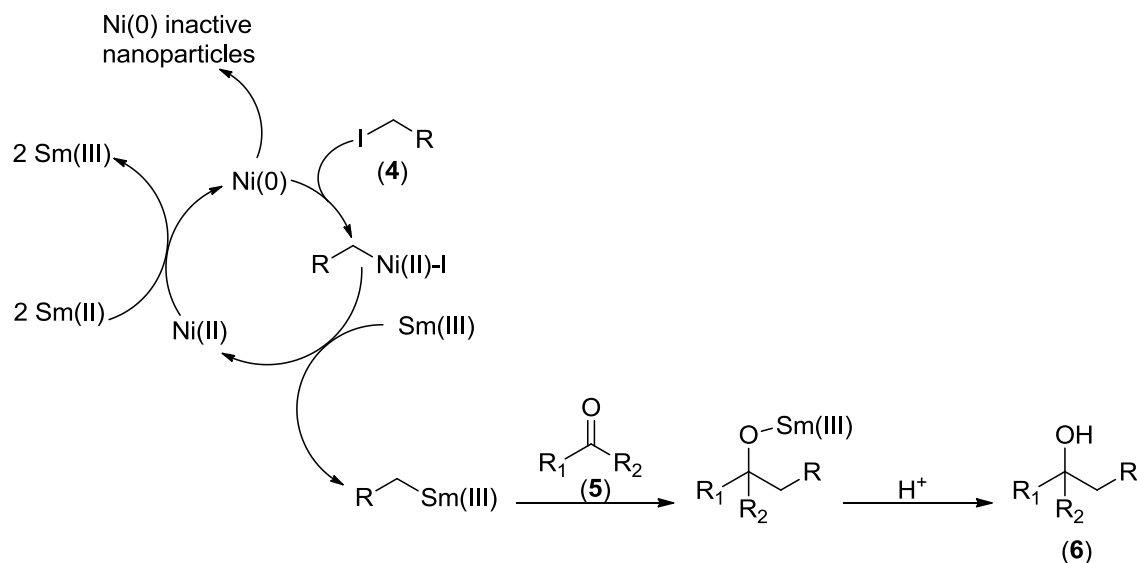
The experimentally determined rate orders for each of the components of the Barbier reaction are included in Table 4.6. Rate orders of zero are observed for both **4** and **5**, while Ni(II) and SmI₂ are first order. These data suggest the initial reduction of Ni(II) by SmI₂ is the rate determining step in the reaction.

Table 4.6 Reaction orders for the reagents in the Ni(II)-catalyzed Barbier reaction.

SmI ₂	Ni(DPPE) ₂ Cl ₂	4	5
0.91 ± 0.01	1.0 ± 0.1	0	0

4.3.4 Proposed Mechanism

The data compiled on the $\text{SmI}_2/\text{Ni(II)}$ -initiated Barbier reaction show the following: (1) SmI_2 reduces Ni(II) salts; (2) Ni(0) nanoparticles are formed upon reduction; (3) Ni(II) salts catalyze the reaction; however, (4) colloidal Ni(0) does not initiate the Barbier reaction; (5) Ni(II) salts are reduced significantly faster than alkyl iodides or dialkyl ketones by SmI_2 ; and (6) the reaction is zero order in alkyl halide and ketone and first order in SmI_2 and Ni(II) . Given these findings, we propose the mechanism described in Scheme 4.6. Ni(II) is initially reduced to Ni(0) through two single electron transfers from two equivalents of SmI_2 . Ni(0) either inserts into the alkyl halide bond through a facile oxidative addition, or aggregates to form colloidal Ni(0) , a pathway which deactivates the catalyst. After oxidative addition, transmetallation occurs in which Sm(III) releases Ni(II) , and a more stable organosamarium intermediate forms.¹⁶³ The organosamarium then adds to the ketone and final protonation of the Sm(III) alkoxide provides the final carbinol product. It is important to note that transmetallation may occur at an alternative stage. For instance, after oxidative addition, the organonickel species may directly add to the ketone forming a nickel alkoxide. Due to the high oxophilicity of Sm , transmetallation would release Ni(II) , forming Sm-alkoxide , followed by protonation in the work-up.



Scheme 4.6 Catalytic cycle of Ni(0)-mediated Barbier coupling.

4.4 Conclusions

Catalytic amounts of Ni(II) salts are routinely used in a variety of SmI₂ reductions, improving the reaction time or product ratio, without a clear understanding of the mechanistic role of the Ni(II) catalyst. This mechanistic study is the first instance identifying that the reaction thought to be driven by the unique features of SmI₂ is in fact a result of known Ni(0) chemistry.^{164,165} Given the use of Ni(II) and other transition metal salts in many reactions initiated by SmI₂, it is likely that this facet of the reaction chemistry and mechanism is more prevalent than recognized. With this greater understanding of the system, SmI₂ could be adapted to other systems which require a mild method for *in situ* Ni(0) formation.

Chapter 5. Addition of H₂O to SmI₂ Reactions: Reduction of Lactones

5.1 Background and Significance

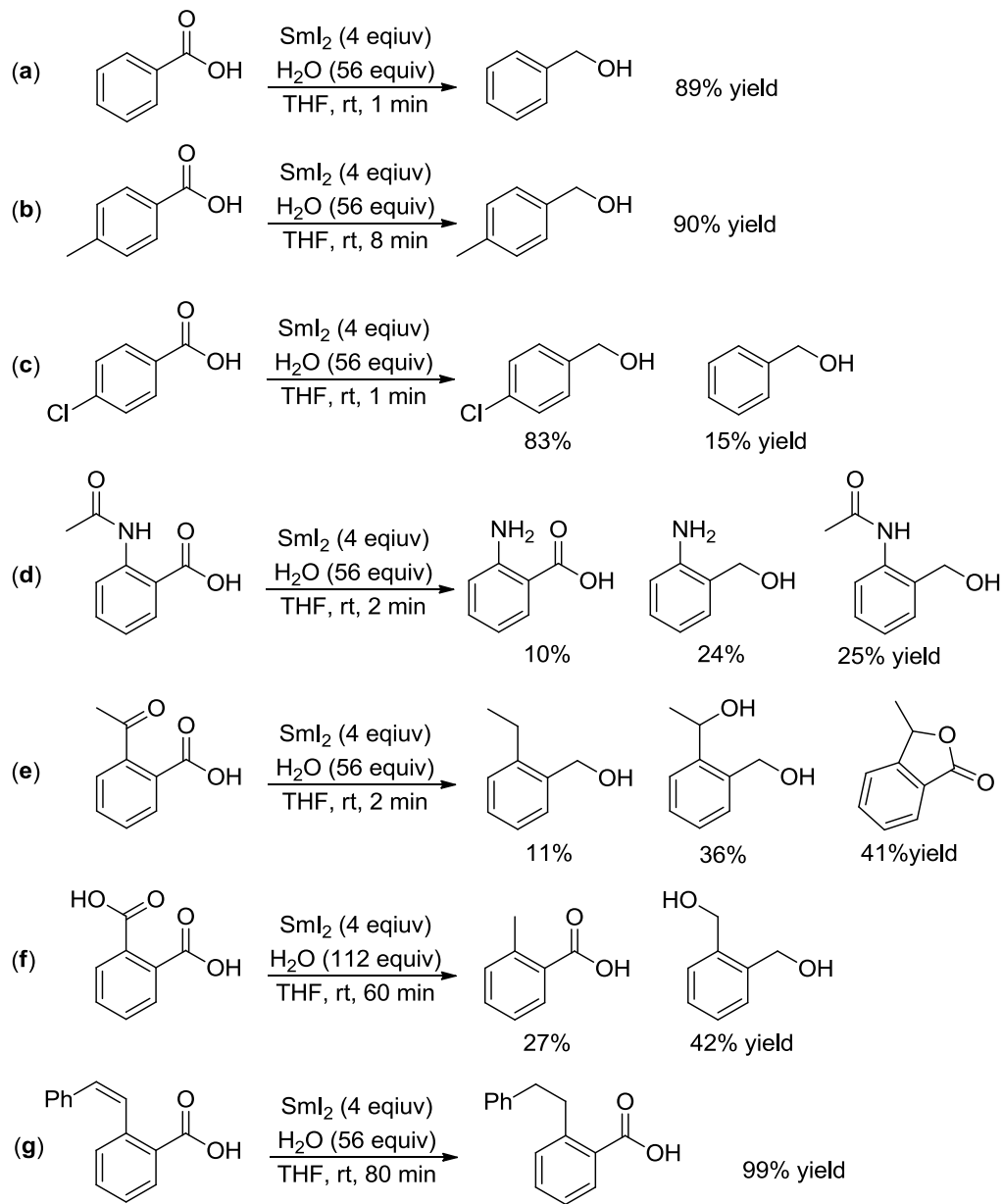
Due to the sensitivity of SmI₂ to air and moisture, the presence of H₂O in SmI₂ reactions was initially regarded as detrimental to the reagent; however, Kagan found that H₂O could be used as a proton source in the reduction of 2-octanone to 2-octanol.¹ In the following years, examples in the literature suggested that H₂O was not only participating in the reaction as a proton source, but that H₂O was also functioning as a ligand to SmI₂, enhancing the reducing ability. While it was speculated, it was not until the work by Curran³⁶ followed by the detailed spectroscopic studies by Flowers⁵² that these suppositions were answered (see Chapter 1, section 1.2.2.2).

Observing the effect of H₂O on SmI₂-mediated reactions through synthetic yields and competition studies provides necessary information on the reactivity of the Sm-H₂O system; however, also including kinetic studies in the analysis provides rates of reduction which can be used to explicitly compare the effect of different substitutions or directing groups included on the substrate. The SmI₂-H₂O reductive ring-opening of lactones was studied to determine the impact of directing groups on the rate of reduction. These data provided information to gain understanding on the roles H₂O plays in the SmI₂-mediated reaction, and the rate at which the electron transfer occurs

5.1.1 SmI₂-H₂O Reduction Systems

Substrates, such as carboxylic acids, esters, amides, and nitriles are stable in the presence of SmI₂,^{1,2} however, Kamochi observed high reactivity using SmI₂ with high concentrations of H₂O.¹⁶⁶ Aromatic carboxylic acids were reduced to their corresponding alcohols with 56 equiv H₂O (Scheme 5.2, a). Additionally, alteration of the amount of H₂O to lower concentrations *decreased* the yield and reaction rate. These observations suggest that H₂O plays an active role within the rate determining step of the reaction, and it is critical for product formation.

As substitutions were placed on the benzyl ring of the carboxylic acid, non-selective reduction of the side chains was observed. Halides were reduced, and a mixture of benzyl alcohol and *p*-chloro benzyl alcohol was obtained (Scheme 5.1, c). Additionally, carbamoyl and carbonyl functionalities were reduced by the SmI₂-H₂O system (Scheme 5.1, d and e), and dicarboxylic acids were partially reduced to a methyl group (Scheme 5.1, f). The olefin of cinnamic acid was selectively reduced over the carboxyl group by SmI₂-H₂O (Scheme 5.1, g).



Scheme 5.1 SmI₂-H₂O reduction of aromatic carboxylic acids

Detailed studies on the effect of proton donors on SmI₂ reactions uncovered that in many cases H₂O acted differently than typical proton sources. Conversion of β-hydroxyketones to 1,3-diols by SmI₂ led to high diastereoselectivities with low H₂O

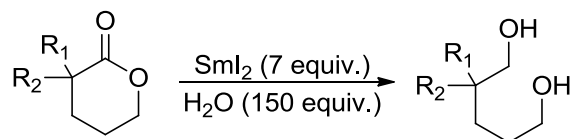
concentrations, while at higher concentrations the selectivity was lost. When the same reduction was carried out with a broad concentration range of MeOH as the proton source the high diastereoselectivities were maintained.⁴³ These reports, along with others, indicated that perhaps Curran's assumption that H₂O coordinated to the Sm-metal was correct.

The Flowers group examined how SmI₂ and H₂O interacted, and how aqueous solutions of SmI₂ impacted the coordination sphere and electronic properties of the single-electron reductant. As described in the introduction of this dissertation (section 1.2.2.2), based on a combination of UV-Vis, CV, conductance, VPO and kinetic experiments it was deduced that H₂O can coordinate to the samarium metal center.^{52,55} At concentrations of 20-50 equiv, the coordination of H₂O displaces the iodide ions to the outer sphere and solvent begins to be displaced. Additionally, CV studies identified the oxidation potential increased negatively to -1.6 ± 0.1 V vs. a saturated Ag/AgNO₃ reference electrode as H₂O is added (60 equiv). At higher concentrations of H₂O (500 equiv) it is increased further to -1.9 ± 0.1 V. These properties confirmed that H₂O behaves as a coordinating solvent, which impacts the reduction potential of SmI₂ in addition to being a proton source in the reactions.

5.1.2 SmI₂-H₂O Reduction of Lactones

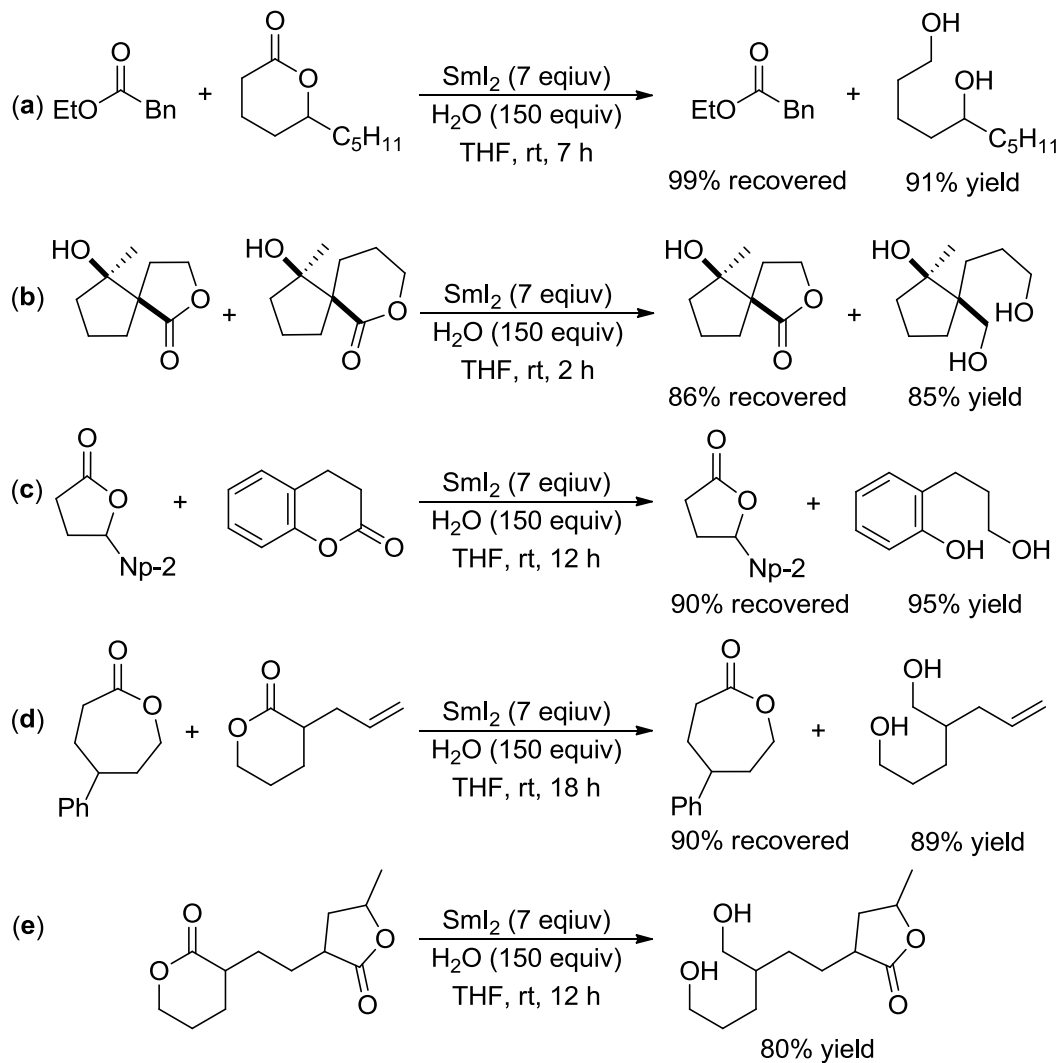
Work by the Procter group found that the addition of H₂O as a cosolvent allows the selective ring-opening reduction of six-membered lactones to form diols (Scheme 5.2). The inclusion of H₂O is critical since SmI₂ itself is not powerful enough to reduce

lactones. However, attempts to use HMPA, DMPU, or LiBr yielded no products. With this observation they began to explore what other aspects of the system H₂O was affecting.¹⁶⁷



Scheme 5.2 Ring-opening reduction of lactones by SmI₂-H₂O

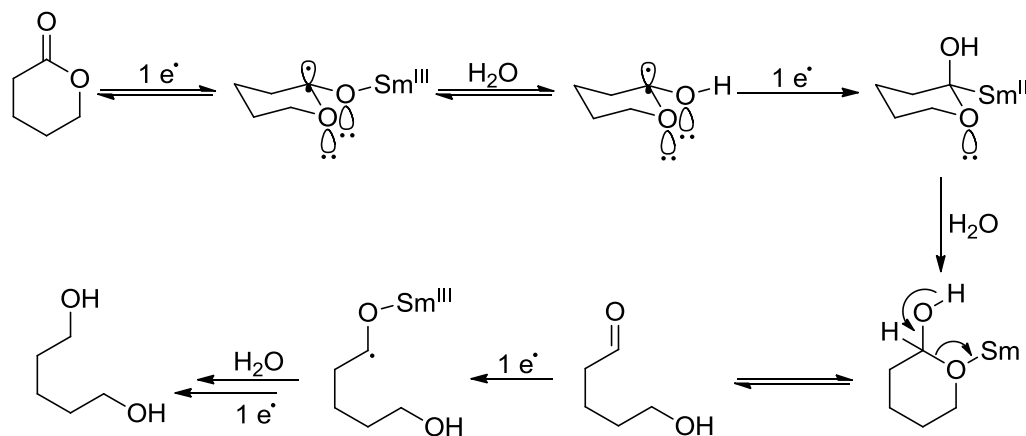
The selectivity that was observed in the initial report was highlighted through competition studies, which indicated that the reduction was specific for the carbonyl contained in the lactone, along with the selective reduction of *six*-membered lactone rings, (Scheme 5.6). Kamochi had previously observed that aromatic esters are efficiently reduced with SmI₂-H₂O,¹⁶⁶ so the nearly quantitative recovery of the unreacted ester and high yield of the ring-opened lactone is indication that either (a) lactones are reduced significantly faster than esters by SmI₂-H₂O or (b) the intermediate radical produced for the reduction of the lactone is more stable than the intermediate ester radical (Scheme 5.3, a). Additional competition experiments illustrate that five- and seven-membered lactone rings do not undergo SmI₂-H₂O reduction, while the six-membered lactone is reduced to its corresponding diol in high yields (Scheme 5.3, b-e).



Scheme 5.3 Competition studies for the reduction of lactones by $\text{SmI}_2\text{-H}_2\text{O}$

Excess SmI_2 is required for these reductions (7 equiv), indicating that more than one electron transfer is taking place. Procter proposed that the ring-opening proceeds through four successive electron transfers and protonations. In this pathway, H_2O (a) coordinates and produces a more powerful reductant, and (b) acts as a proton source, for intermediate anions throughout the course of the reaction. It was proposed that following the initial single-electron transfer to the carbonyl, the radical anion produced is stabilized

by the lone-pairs on both the endocyclic and exocyclic oxygens. The key to the stabilization is the ability of the six-membered ring to adapt a chair conformation and form an axial radical, which is preferred due to the anomeric effect¹⁶⁸⁻¹⁷⁰, and allows the stabilization with the oxygens to occur^c (Figure 5.4). This stability observed in six-membered rings cannot be maintained with labile five-, seven- and eight-membered lactone rings, which were not successful in the Sm-mediated ring opening.¹⁶⁷

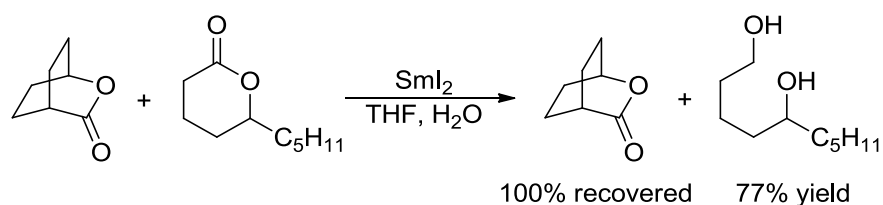


Scheme 5.4 Proposed pathway for the reduction of six-membered lactones by $\text{SmI}_2\text{-H}_2\text{O}$

Further support for the supposition that the driving force for the reduction is due to the stability of the initial radical produced was found in the competition reductions with 2-oxabicyclo[2,2,2]octan-3-one and a six-membered lactone ring (Scheme 5.5).

^c The anomeric effect, proposed by J.T. Edward, describes the tendency of substitutions adjacent to a heteroatom in a cyclohexane ring to prefer the axial orientation, even though the equatorial position would exhibit less steric interactions. It is suspected that the dipoles from the two heteroatoms (or in this case, heteroatom and radical) are aligned in the equatorial conformation, therefore repelling each other, while a more stable, lower energy state is achieved as the substitution sits in the axial position of the chair confirmation.

When reacted with $\text{SmI}_2\text{-H}_2\text{O}$, the bicycle was fully recovered, likely due to the fact that the intermediate radical anion would not be able to adopt the chair conformation, providing support that this structure is necessary for stabilization and subsequent success of the reduction.¹⁰⁶

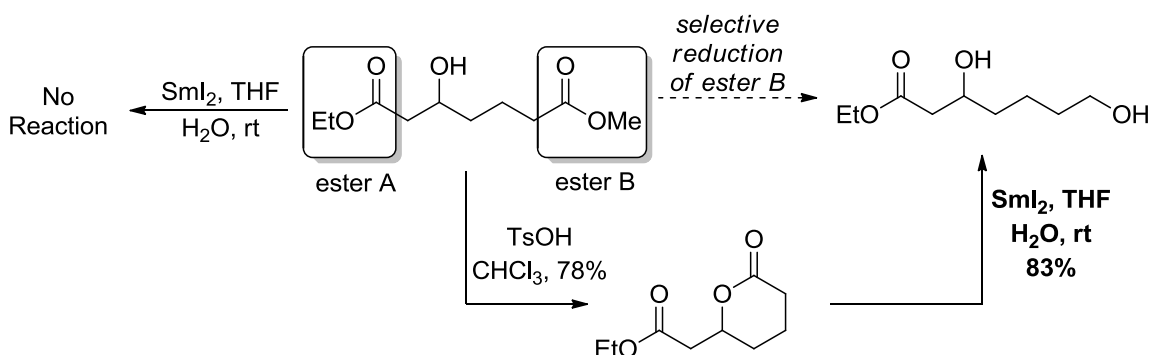


Scheme 5.5 Competition studies with 6-membered lactone and 2-oxabicyclo[2,2,2]octan-3-one

Procter *et al.* have proposed from their studies that the selectivity is directed from the stability of the radical formed from the initial electron transfer. This is based on the observations that (a) products of partially reduced five- or seven-membered lactones were not found, (b) rate studies identified the reaction is first order in $\text{SmI}_2\text{-H}_2\text{O}$ and substrate, making the initial electron transfer rate determining¹⁰⁶ and (c) based on the proposed pathway, it was found that if a five-membered lactol (suspected intermediates in the reduction pathway) is subjected to $\text{SmI}_2\text{-H}_2\text{O}$ the corresponding diols are formed.¹⁶⁷

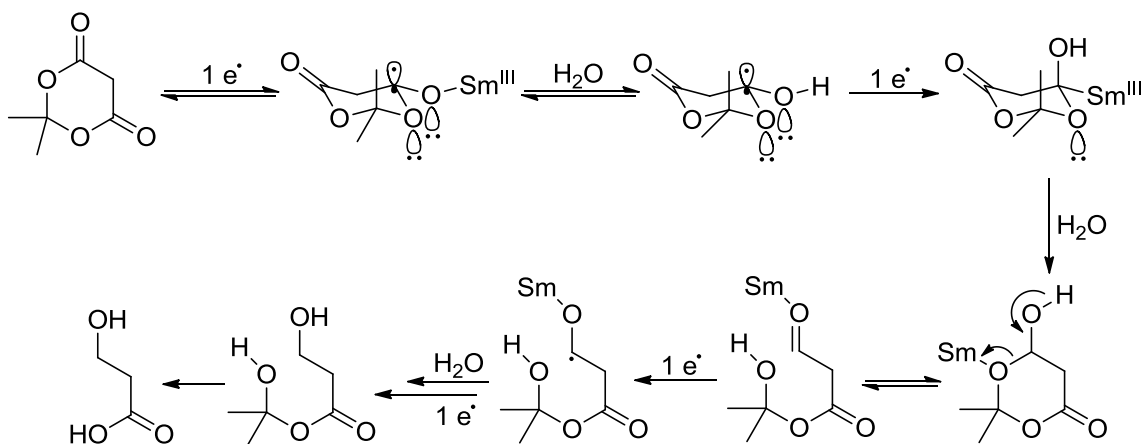
Even though Kamochi reported the ability to reduce activated esters (aryl substituted esters) with $\text{SmI}_2\text{-H}_2\text{O}$, Procter reports difficulty reducing aliphatic esters with the same reductive system.¹⁰⁶ He notes though, while aliphatic esters cannot be reduced, aliphatic diesters with a strategically placed 5-hydroxy group can be cyclized into a 6-membered lactone with an ester substitution in one synthetic step (Scheme 5.9).

Subjecting this lactone to reduction by $\text{SmI}_2\text{-H}_2\text{O}$ forms 1,6-hydroxy ester, a product which mimics the selective reduction of ester B, while ester A remains intact in the final aliphatic product. This could be a powerful tool in synthesis when complex starting materials require site-specific reductions.



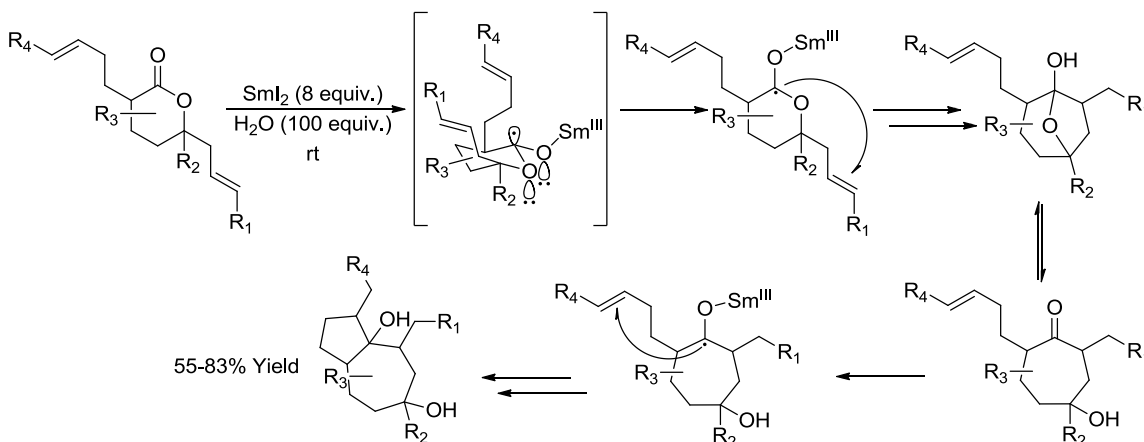
Scheme 5.6 Use of lactone intermediate in the selective reduction of aliphatic diesters

The study of lactones reduced by $\text{SmI}_2\text{-H}_2\text{O}$ was expanded to observe the selectivity of reductions of cyclic 1,3-diester (Meldrum's acid) to 3-hydroxy propanoic acids. Cyclic 1,3-diester are useful building blocks in synthesis, and typically require four steps to form the hydroxyl acid (conversion of Meldrum's acid to the monoacid, activation of the acid as a mixed anhydride, reduction using NaBH_4 , and hydrolysis).¹⁷¹ Reductions with $\text{SmI}_2\text{-H}_2\text{O}$ proceeded cleanly with a variety of α -substituted substrates, and competition studies indicated that the cyclic 1,3-diester were reduced over acyclic 1,3-diester, esters, and in some cases lactones. Similar to the reduction of 6-membered lactone rings, the mechanism was proposed to proceed through the formation of an axial radical-anion intermediate stabilized by the anomeric effect (Scheme 5.7).



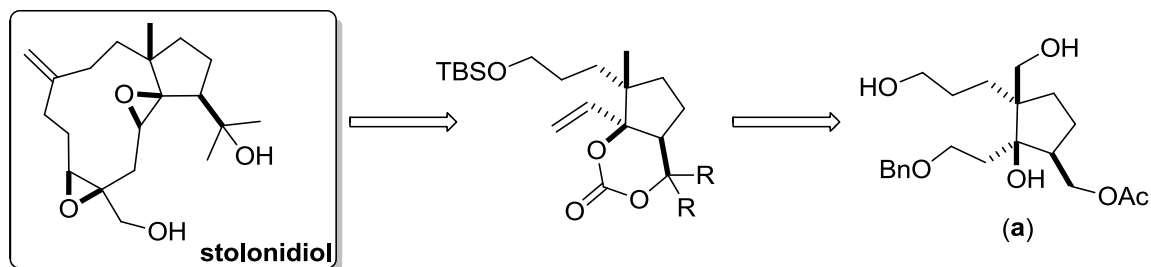
Scheme 5.7 Proposed mechanism for the reduction of 1,3-diester with $\text{SmI}_2\text{-H}_2\text{O}$

The reduction was expanded to radical cascade reactions that proceeded through the radical anion formed after the first electron transfer (Scheme 5.8).¹⁷¹ The radical cyclizes onto the pendant olefin, followed by organosamarium protonation from the excess H_2O in solution. A second electron transfer by SmI_2 produces another radical anion which intramolecularly cyclizes with the remaining olefin to form the final bicyclic product upon protonation.¹⁷²



Scheme 5.8 Radical cyclization cascade initiated through lactone reduction by $\text{SmI}_2\text{-H}_2\text{O}$

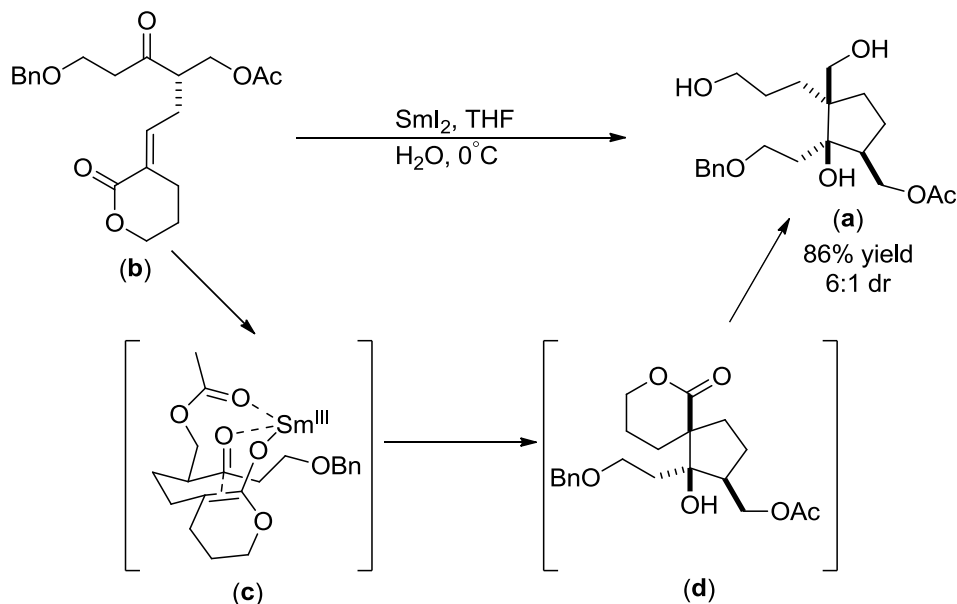
Studies carried out to examine the scope, limitations, and selectivity of the $\text{SmI}_2\text{-H}_2\text{O}$ reduction system with lactones and 1,3-diesters were put to practice in the cyclization cascade towards the synthesis of stolonidiol.¹⁷³ Retrosynthetic analysis identified that triol **(a)** is a synthetic target as an intermediate in the synthesis of the natural product (Scheme 5.9). Additionally, it was envisioned that **a** could be obtained through a radical cyclization with $\text{SmI}_2\text{-H}_2\text{O}$.



Scheme 5.9 Retrosynthesis analysis of stolonidiol through triol **a**

Cyclic substrate **b** (Scheme 5.10) was made through a three-step synthesis, affording the desired substituted lactone in an overall 85% yield and as a single isomer.¹⁷³ Treatment of **b** with $\text{SmI}_2\text{-H}_2\text{O}$ (150 equiv) produced the highly functionalized cyclopentanol **a** in 86% yield, as a 6:1 mixture of diastereomers. Procter proposed that the cascade proceeds through the initial reduction of interior α,β -unsaturated ester within the cyclic lactone, generating a Sm(III) -enolate, which can then undergo diastereoselective aldol cyclization onto the pendant ketone (Scheme 5.10, c). The intermediate spirocyclic cyclopentanol **d** is further reduced to triol **a** in the presence of the primary acetate. The stereochemistry to the major *syn*-isomer is consistent with the

proposed transition state structure in which the carbonyl groups are chelated with the Sm(III) enolate.¹⁷³



Scheme 5.10 Proposed pathway for the cascade cyclization through $\text{SmI}_2\text{-H}_2\text{O}$ reduction

Work highlighting the ability of H_2O to act as both a proton source as well as a chelating additive with SmI_2 expanded the utility of this additive since it is a much safer reagent to use as compared to HMPA. The most recent work done in the Procter lab is allowing lactones to be viewed as important reactive intermediates in large syntheses, intermediates that can allow carbon-carbon and carbon-heteroatom bond formation. These studies were continued to explore how the substitution of an ester functional group on the ring systems impact the reactivity from a synthetic, as well as a kinetic, point of view.

5.2 Experimental

5.2.1 Materials

THF was purified after purging with argon gas and passing over a column of activated alumina by a Solvent Purification System (Innovative Technology Inc.; MA). Dried solvents and reagents were stored in an Innovative Technology, Inc. drybox containing an argon atmosphere and a platinum catalyst for drying. H₂O was degassed with ultra high pure argon for at least 72 h before use in glovebox. Lactone substrates (**1-24**) were synthesized in Procter's research lab at the University of Manchester, Manchester UK. NMR analysis was used to verify the compounds were still pure after shipping. Lactones **25-28** (5-decanolide, δ -valerolactone, γ -butyrolactone, and ϵ -caprolactone) were purchased from Acros, and distilled from CaO before use. Samarium metal was purchased from Acros and used with no further purification. Resublimed iodine crystals were purchased from Aldrich and used with no further purification. SmI₂ was prepared by stirring Sm metal and iodine in THF until the characteristic blue color of Sm(II) appeared. The concentration of the Sm complex (0.10 M in THF) was determined by iodometric titration.

5.2.2 Instrumentation

Proton and carbon NMR were recorded on Bruker 500 MHz spectrometer. GC-MS analysis was performed with HP 5890 Series Gas Chromatograph with an HP Mass

Selector Detector. Kinetic studies were performed using a computer-controlled SX-20 MV stopped-flow reaction spectrophotometer (Applied Photophysics Ltd., Surrey, UK).

5.2.3 Methods

5.2.3.1 General Procedure for Lactone Reduction with Sm-H₂O

(Predominately carried out in Manchester Lab) The reaction was carried out under argon with degassed reagents. SmI₂ was prepared as described above. Lactone (0.36 mmol) in THF (10 mL) was added dropwise to SmI₂ (25 mL, 2.5 mmol), followed by slow addition of degassed H₂O (965 µL, 54 mmol). After stirring for 3-30 h the color subsided to a muted gray. The reaction was quenched by exposing to air. The reaction mixture was then washed with NH₄Cl and extracted twice with ether. The organic layer was washed individually with H₂O, Na₂S₂O₃ and brine, dried over MgSO₄ and then concentrated to obtain the diol product.

5.2.3.2 General Procedure for Stopped-Flow Studies

The SmI₂-H₂O combination and lactones in THF were taken separately in airtight Hamilton syringes from a drybox and injected into the stopped-flow system. The cell box and the drive syringes of the stopped-flow reaction analyzer were flushed a minimum of three times with degassed solvents to make the system oxygen-free. The concentration of SmI₂ used for the study was 10 mM.

To produce a stable SmI₂-H₂O complex with high concentrations of H₂O, extreme caution must be taken. H₂O diluted in 2 mL THF is added dropwise, slowly down the

interior side of the glassware to SmI_2 , also diluted with THF. As the H_2O -THF is being added *slowly*, the SmI_2 must be slightly shaken as to ensure the mixtures are being combined efficiently. The solutions will take on a purple color; however, if the H_2O is added too quickly it will dissipate to a white color within a few minutes. Properly made solutions will remain purple for 15 minutes before they break down.

To determine rate constants, the concentrations of the substrates were kept high relative to SmI_2 -HMPA combination (125 mM) to maintain pseudo first-order conditions. Observed reaction rate constants were determined from exponential fitting of the decays of SmI_2 - H_2O complex at 560 nm.

Rate orders for lactones (**1, 5, 8, 16-28**) were derived from the plots of $\ln k_{\text{obs}}$ vs. $\ln[\text{substrate}]$. The rate order for SmI_2 was determined from fractional times method from the decay traces of SmI_2 , as well as initial rates. The rate plots were generated from the absorption decay traces obtained from a stopped-flow spectrophotometer.

5.3 Results

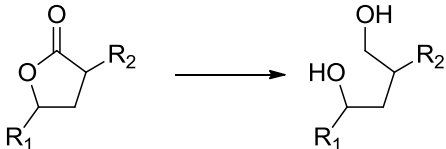
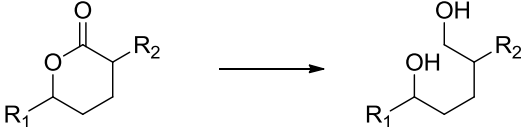
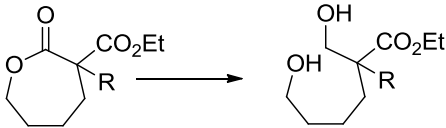
5.3.1 Lactone Reductions

Procter and coworkers have shown the unique ability of SmI_2 - H_2O to reduce lactones; however, these ring-opening reactions were limited to six-membered substrates. Recent work determined that with an ester group placed at the α -position on the lactone ring, reduction of five- and seven-membered lactones is possible (Table 5.1). In all cases, the lactone is selectively reduced to the diol. As substitutions around the lactone ring

were added, no reaction occurred with the side chains and the functional groups were conserved, even with excess of SmI₂ in the system.

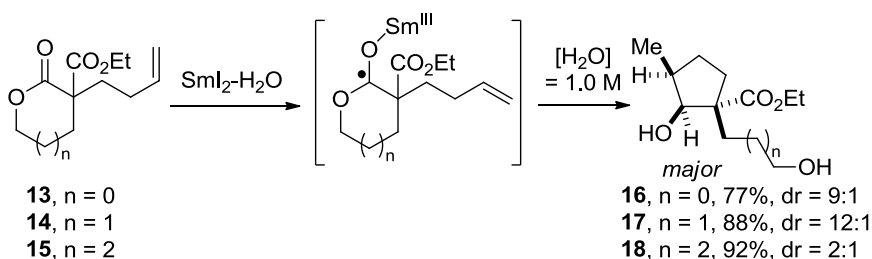
The α -positioned ester seems to be vital for the reduction of the previously stable ring systems, but the impact of the other substitutions acting as directing groups require further investigation. If the rates of reduction are significantly impacted by the directing groups, it could imply that different intermediates are produced, and the mechanistic pathway is altered.

Table 5.1 SmI₂-H₂O-mediated reduction of lactones with directing groups^a

Lactone	Reaction	Yield (%)
		
1	R ₁ = H, R ₂ = CO ₂ Et	83
2	R ₁ = H, R ₂ = CO ₂ tBu	87
3	R ₁ = C ₇ H ₁₅ , R ₂ = C(O)NHCy	94
4	R ₁ = C ₇ H ₁₅ , R ₂ = C(O)NHPh	77
		
5	R ₁ = H, R ₂ = CO ₂ Et	96
6	R ₁ = C ₅ H ₁₁ , R ₂ = CO ₂ Et	72
7	R ₁ = Ph, R ₂ = CO ₂ Et	68
		
8	R = H	87
9	R = Bn	85
10	R = (CH ₂) ₃ CN	92
11	R = (CH ₂) ₄ OAc	95
12	R = (CH ₂) ₄ Ph	99

^a[lactone] = 0.36 mM, [SmI₂] = 7 equiv, [H₂O] = 150 equiv

To further highlight the capacity of the directed reduction of lactones with $\text{SmI}_2\text{-H}_2\text{O}$, reductive cyclizations of lactones bearing tethered olefins as radical traps were carried out. The cyclization of five-, six- and seven-membered lactones proceeded with high yields with increased concentrations of water in the system [1.0 M]. In the case of five- and six-membered rings, exceptional diastereoselectivity was observed, generating five-membered carbocycles with three adjacent stereocenters (one quaternary) (Scheme 5.11). This type of directed reaction represents a significant advance in terms of scope and diastereoselectivity over the previously reported reductive cyclizations of six-membered lactones with pendant olefin chains at the α -position.

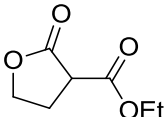
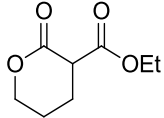
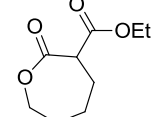
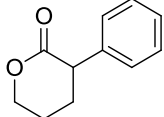
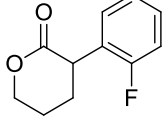
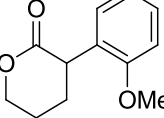
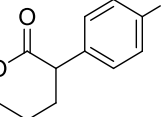
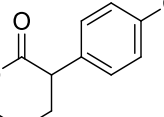
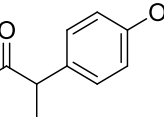
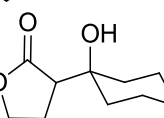


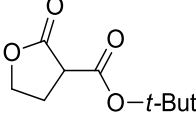
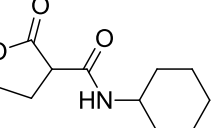
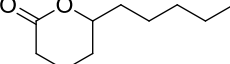
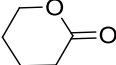
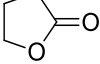
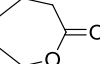
Scheme 5.11 Reductive cyclizations of lactones using $\text{SmI}_2\text{-H}_2\text{O}$ enabled by directing group effect

5.3.2 Kinetic Analysis of $\text{SmI}_2\text{-H}_2\text{O}$ Reduction of Lactones

Kinetic experiments were carried out to elucidate the impact of side chains on the rate of the reaction. The synthetic results suggested that the reductive ring opening of all of the substrates occurred with $\text{SmI}_2\text{-H}_2\text{O}$, except for the reduction of five- and seven-membered lactone rings (**30** and **31**) without any functional group substitutions, as previously reported by Procter (Table 5.2).

Table 5.2 Lactone substrates in kinetic analysis

	Lactone	Rate Constant ($M^{-1}s^{-1}$)	Lactone Order	SmI_2 Order
1		419 ± 45	1.1 ± 0.1	1.0^a
5		610 ± 10	1.0 ± 0.1	1.0^b
8		0.91 ± 0.05	1.3 ± 0.1	1.0^a
19		0.012 ± 0.001	0.9 ± 0.1	1.0^b
20		0.006 ± 0.001	1.0 ± 0.1	1.0^b
21		0.001 ± 0.001	0.8 ± 0.1	1.0^b
22		0.013 ± 0.001	1.3 ± 0.1	1.2^b
23		0.073 ± 0.001	0.95 ± 0.03	1.2^a
24		0.04 ± 0.01	1.05 ± 0.1	1.0^a
25		0.34 ± 0.03	2.2 ± 0.2	1.0^a

26		0.32 ± 0.03	0.97 ± 0.1	1.0^a
27		$> 1.0 \times 10^4$	--	--
28^c		0.0074 ± 0.001	1.1 ± 0.1	1.0^b
29		0.014	0.82 ± 0.03	$1.0^{a,b}$
30		$< 1.0 \times 10^{-5}$	--	--
31		$3.0 \pm 0.2 \times 10^{-4}$	0.16 ± 0.02	1.5^a

^aOrder of SmI₂ determined by initial rates method. ^bOrder of SmI₂ determined by fractional times method. Rate plots for the rate constants and order of the lactones found in the supporting information ^cParmar, D.; Duffy, L.A.; Sadasivam, D.V.; Matsubara, H.; Bradley, P.A.; Flowers, R.A. II; Procter, D.J. *J. Am. Chem. Soc.* **2009**, *131*, 15467–15473,

When the ring size is changed between five-, six-, and seven-membered lactone rings without any substitutions (**29-31**), exclusive selectivity for reduction of the six-membered lactone to form the diol is observed, consistent with the initial work on this system. The selectivity was attributed to the stability of the radical anion due to the anomeric effect in the chair conformation of the six-membered ring, which cannot occur in the five- and seven-membered systems. Since low conversion is observed for reduction of **27**, rates which span over three half-lives could not be obtained, and a rate constant could not be determined. The reduction of the seven-membered ring (**31**) was also very slow; however, and a rate constant of $3.0 \times 10^{-4} \text{ M}^{-1}\text{s}^{-1}$ was observed.

Upon addition of an ester group at the α -position of the lactone rings, reductions of the five- and seven-membered lactones proceed with high yields. The ester functionality on the lactone ring provides a region for Sm(II) or Sm(III) chelation, forming a stable six-membered intermediate (Figure 5.1). This chelation aids in stabilizing the radical formed from the initial electron transfer, providing a new region for anomeric stabilization with the five- and seven-membered lactones.

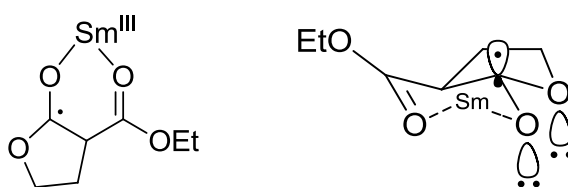


Figure 5.1 SmI₂ chelation through ketyl radical and pendant ester carbonyl

Within the series of the three lactones with only ester substitutions (**1**, **5** and **8**), the six-membered lactone (**5**) reduces with the fastest rate, followed by the five-membered (**1**), and finally, the large seven-membered lactone (**8**). Comparing rates for substrates **5** and **29**, it is clear that the addition of the ester side chain and Sm-chelation greatly enhances the rate of reduction (4 orders of magnitude) as compared to no substitution (**5**) or a simple alkyl chain (**28**). This effect on the rate also adds to the evidence that the chelation is the driving force behind the reduction of the five- and seven-membered lactones.

The rates of reduction of lactones **19-24** were observed to determine if including electron donating or withdrawing groups substituted to the six-membered lactone effected the electron transfer. While there is some variation of rate seen between the different

substitutions and position around the phenyl ring, the difference in rate constants are not significant enough to assume a large effect on the rate of reduction, and are comparable to the unsubstituted six-membered lactone (**5**). These substitutions are most likely too far away from the site of electron transfer to play any significant role.

Lactones **25** and **26** have an oxygen available for the six-member chelation of Sm; however, the rates are two orders of magnitude slower when compared to **1**. It is likely that the bulky cyclohexyl and *t*-butyl groups hinder the formation of the Sm-chelated intermediate to some extent. Decrease in this stabilizing interaction results in a drastic decrease in the rate of reduction. Finally lactone **27**, with an amide substitution, has the fastest rate of all of the lactones studied. So fast in fact that 60% of the reaction was over within the mixing time of the stopped-flow and full decays of the reaction could not be obtained. It is unclear why there is such a drastic difference in rate when compared with the structurally similar **26** and **27**. The presence of the available α -carbonyl for chelation is vital for the ring-opening to occur, and similar steric interaction would be expected between the *t*-butyl and cyclohexyl side chain. While additional electron donation is occurring with the amide substitution, the 4 order of magnitude increase in rate is not likely solely due to the change in heteroatom. Additional rate studies observing six- and seven-membered rings with the amide substitution, as well as change in the alkyl chain coming off of the amide (methyl, *t*-butyl) may provide more insight.

5.4 Conclusions

The collaborative approach to studying the SmI₂-H₂O lactone reduction through kinetic and synthetic analyses allowed us to identify the powerful chelating affect of the carbonyl side chains positioned α - to the lactone. Observations of the effect on the rates of reduction as well as the synthetic outcomes allow us to have a broader view of how SmI₂-H₂O carries out these reductions. Additionally, this insight can allow the reductive system to be applied to more complex syntheses of larger and more functionally diverse synthetic targets.

In order to gain a more in-depth understanding of the potential of these systems, additional mechanistic studies should be carried out to determine the mode of the electron and proton transfers. One possible explanation of the enhanced reactivity the SmI₂-H₂O system is that reduction is facilitated by proton-coupled electron transfer (PCET). In PCET, the concerted action of the proton and electron being transferred at the same time lowers the energy of the transition state, often allowing reductions of uphill energy to take place. To investigate the possibility of this occurring within the reduction of the substituted lactones, kinetic isotope studies need to be carried out to determine the degree to which the protonation is affecting the rate determining step.

In the reduction, H₂O plays two roles within the reaction—it acts as a coordinated ligand, increasing the reduction potential of SmI₂, and provides a proton to the intermediate anions. However, to investigate the impact of H₂O mechanistically, it would be beneficial to determine if these reductions are possible with two different

additives, each having only one role of H₂O. For instance, HMPA could be added to coordinate with SmI₂, and a lower concentration of water (or alcohol) added as the proton source. Observing the effect of these changes on the rate of the reduction could provide insight into whether the assumption of water behaving in both roles is correct.

Chapter 6. SmI₂-H₂O-Amine Reduction System

6.1 Background and Significance

Through the last 30 years of research on SmI₂-mediated reactions, it has become abundantly clear that the inclusion of an additive can not only accelerate the rate of a reaction, but can also drastically alter the mechanism of the system. HMPA is often used due to its ability to coordinate to the Sm-metal center, producing a more powerful reductant, however due to toxicity concerns alternatives are continually being evaluated. Work pioneered by Hilmersson¹⁷⁴ identified a unique additive combination with H₂O and an amine, which drastically increased the rate of Sm-mediated reductions as well as allowed for the reduction of substrates which were not accessible to reduction by SmI₂ alone.

6.1.1 SmI₂-H₂O and SmI₂-Amine Additive Systems

As described in Chapter 1 and in more detail in Chapter 5 of this dissertation, H₂O is a powerful additive for reactions of SmI₂. Spectroscopic evidence indicates that H₂O coordinates to the Sm-metal center at high concentrations, forming a more powerful reductant. Because of the ability of H₂O to act as a ligand as well as a proton donor, this additive facilitated many Sm-cascade reactions.⁵⁶

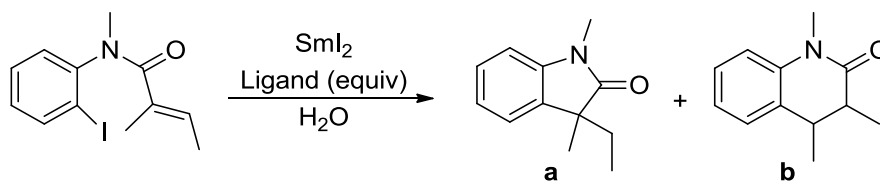
Nitrogen-containing ligands and nitrogen donor solvents have been explored as potential additives to enhance reactions with SmI₂. Evans *et al.* studied the interaction between nitrogen-containing ligands and SmI₂ with X-ray crystallography. The addition

of 2 equiv of $\text{NaN}(\text{SiMe}_3)_2$ to SmI_2 in THF formed $[(\text{Me}_3\text{Si})_2\text{N}]_2\text{Sm}(\text{THF})_2$.¹⁷⁵ Crystal structures confirmed that the ligands coordinated to the Sm metal center through the nitrogen, displacing the majority of the bulk solvent from the coordination sphere. Flowers *et al.* further examined this divalent Sm reagent through spectroscopic, electrochemical, and kinetic analysis.¹⁰⁷ The UV-Vis spectrum of $[(\text{Me}_3\text{Si})_2\text{N}]_2\text{Sm}(\text{THF})_2$ is shifted from the known SmI_2 spectrum. The typical SmI_2 absorbance has four bands at 350, 416, 555 and 615 nm. $[(\text{Me}_3\text{Si})_2\text{N}]_2\text{Sm}(\text{THF})_2$ has two major absorbance bands at 380 and 558 nm, reminiscent of $[\text{Sm}(\text{HMPA})_6]\text{I}_2$ with bands at 382 and 538 nm. CV data showed that the $[(\text{Me}_3\text{Si})_2\text{N}]_2\text{Sm}(\text{THF})_2$ complex is a more powerful reductant than SmI_2 , but not as powerful as $[\text{Sm}(\text{HMPA})_6]\text{I}_2$. Oxidation potentials (vs Ag/AgNO_3) for SmI_2 , $[\text{Sm}(\text{HMPA})_6]\text{I}_2$, and $[(\text{Me}_3\text{Si})_2\text{N}]_2\text{Sm}(\text{THF})_2$ are -1.58 ± 0.04 , -2.35 ± 0.03 and -2.1 ± 0.1 V, respectively. Additionally, the rates of reduction of iodobutane and 2-butanone were increased 5 and 6 orders of magnitude with the amine additive, which is an order of magnitude more pronounced than with HMPA.¹⁰⁷ These results support the conclusion that $(\text{Me}_3\text{Si})_2\text{N}$ is acting as a coordinating ligand to SmI_2 , increasing the oxidation potential and facilitating increased rates of reduction.

$[(\text{Me}_3\text{Si})_2\text{N}]_2\text{Sm}(\text{THF})_2$ (6 equiv) was used in the reduction of nitrobenzene to its corresponding aryl amine, forming a mixture of the desired aniline along with coupled amine, diphenylhydrazine.¹⁷⁶ Previously, it was reported that this reduction required high concentrations of SmI_2 (20 equiv) to complete.^{177,178}

Cabri *et al.* included nitrogen-containing ligands (triethyl amine (Et₃N), 1,8-diazobicyclo[5.4.0]undec-7-ene (DBU), and 1,1,3, 3-tetramethylguanidine (TMG)) in the reduction of aryl iodide trapped through intramolecular addition to an olefin (Table 6.1). The effect these additives had on the cyclization was compared to the efficiency of HMPA.¹⁷⁹

Table 6.1 Effect of nitrogen-containing ligands on reduction and radical cyclization



Entry	Ligand	Time (h) ^a	% Conversion	a/b	% yield (a+b)
1	--	19 ^b	68 ^c	75/25	35
2	HMPA (2 equiv)	4	92	81/19	71
3	DBU (2 equiv)	1	100	73/27	75
4	Et ₃ N (2 equiv)	1	100	70/30	73
5	TMG (2 equiv)	1.5	100	76/24	81
6	TMG (8 equiv)	0.5	100	82/18	85

^aReactions carried out at -18°C. ^bReaction carried out at 0°C. ^cThe produce reduced at the double bond and dehalogenated was 16% of the final mixture.

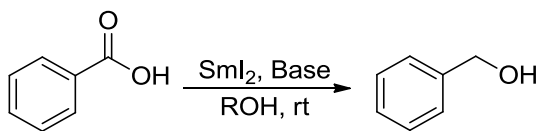
With no additive, the Sm-mediated reaction had a low conversion and yield, leading to reduction in addition to cyclization. The inclusion of amines resulted in a quantitative conversion to the cyclized products, a slight improvement as compared to reactions with HMPA (Table 6.1). In all cases, H₂O was included as a proton source for the system.¹⁷⁹

Since these reports, the most commonly used nitrogen-containing additives in SmI₂ reactions are Et₃N, TMEDA and pyrrolidine *with* H₂O. Compared to work

described in Cabri's report, H₂O is not simply a proton source in these systems, rather the SmI₂-H₂O-amine combination has been found to drastically increase the rate of SmI₂ reduction, and has a more complex reaction mechanism than amine coordination to the Sm-metal.

6.1.2 SmI₂-H₂O-Amine Reduction Systems

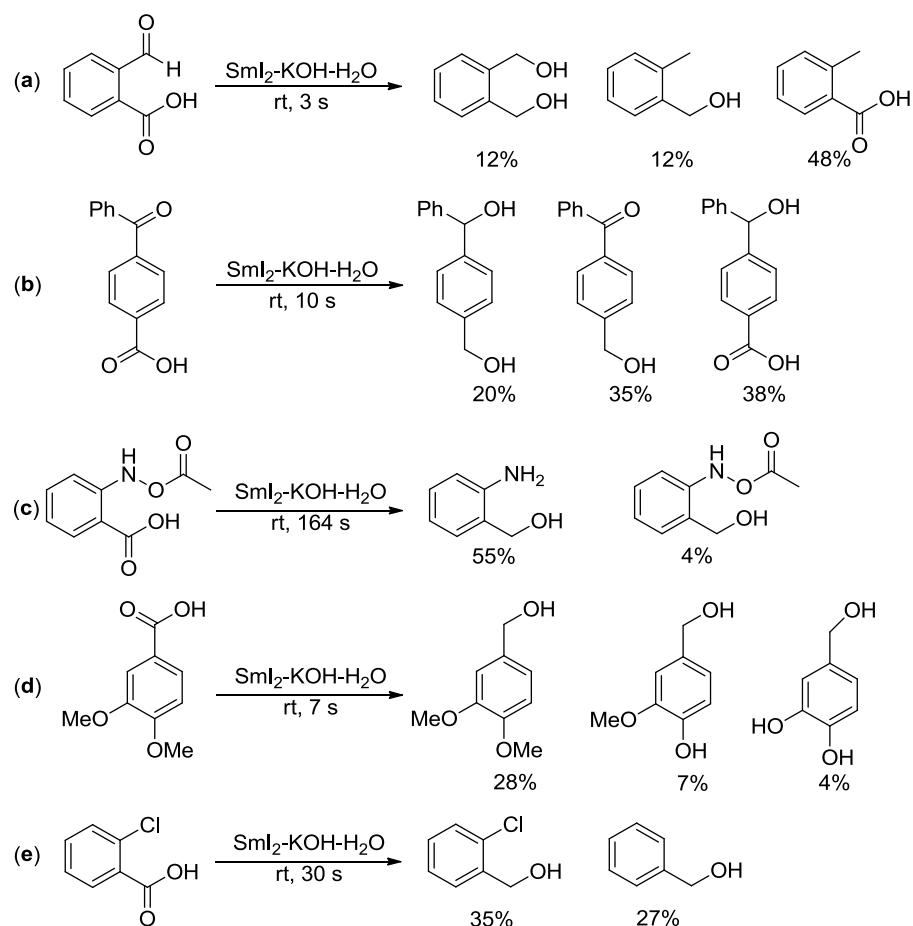
The first reported observation of an increase in the reducing power of SmI₂ with the addition of base and H₂O was performed by Kamochi and Kudo in 1991.¹⁶⁶ The impact of SmI₂ in a basic environment (10% NaOH) led to the extremely facile reduction of benzoic acid, a substrate which Kagan reported could not be reduced by SmI₂ alone. H₂O and methanol were both used as proton sources, and while both additives led to the reduction, longer reaction times and lower yields were observed with MeOH as compared to H₂O (Table 6.2).¹⁸⁰ NaOH, LiNH₂ and NH₃ were also attempted as sources of base in the reaction; however, the highest yield resulted from the combination of NaOH and H₂O, forming 92% of the reduced carboxylic acid within one minute. They noted that the reduction could occur with base only; however, the reaction was slower with lower yields as compared to the SmI₂-H₂O-base combination.

Table 6.2 Reduction of benzoic acid with SmI₂ in a basic environment

Entry	Base	ROH	Time	Yield %
1 ^a	--	--	10 h	0
2 ^b	--	MeOH	10 h	0.6
3 ^c	NaOH	--	4.3h	42
4 ^d	NaOH	MeOH	5 h	52
5 ^e	LiNH ₂	MeOH	5 h	30
6 ^f	NaOH	H ₂ O	60 s	92
7 ^e	LiNH ₂	H ₂ O	60 s	87
8 ^f	NH ₃	H ₂ O	3 s	41

^a[SmI₂] = 0.1 M, 4 mmol; [C₆H₅COOH] = 1 mmol. ^b[SmI₂] = 1 mmol; [C₆H₅COOH] = 0.25 mmol. ^c[SmI₂] = 2 mmol; [C₆H₅COOH] = 1 mmol; [base] = 2 mmol. ^d[SmI₂] = 4 mmol; [C₆H₅COOH] = 1 mmol; [base] = 2 mmol. ^e[SmI₂] = 2 mmol; [C₆H₅COOH] = 0.5 mmol; [base] = 2 mmol. ^f[SmI₂] = 4 mmol; [C₆H₅COOH] = 1 mmol; [base] = 8 mmol.

They expanded the system to reduce aromatic and aliphatic carboxylic acids with Sm-H₂O-NaOH and Sm-H₂O-KOH, and found a general trend in which aliphatic substrates were reduced slower and with lower yields than aromatic carboxylic acids. Substituted benzoic acids bearing aldehyde, halide, or ester functional groups were subjected to the Sm-H₂O-KOH system¹⁸¹ to observe the selective reduction of the carboxylic acids with the other functional groups present. In all cases, some reduction of the side chain was observed in addition to reduction of the carboxylic acid, producing a mixture of products (Scheme 6.1). These results highlight the power of the SmI₂-H₂O-base system to reduce an array of different functional groups in extremely short reaction times; however, little selectivity of the new reducing system was observed.



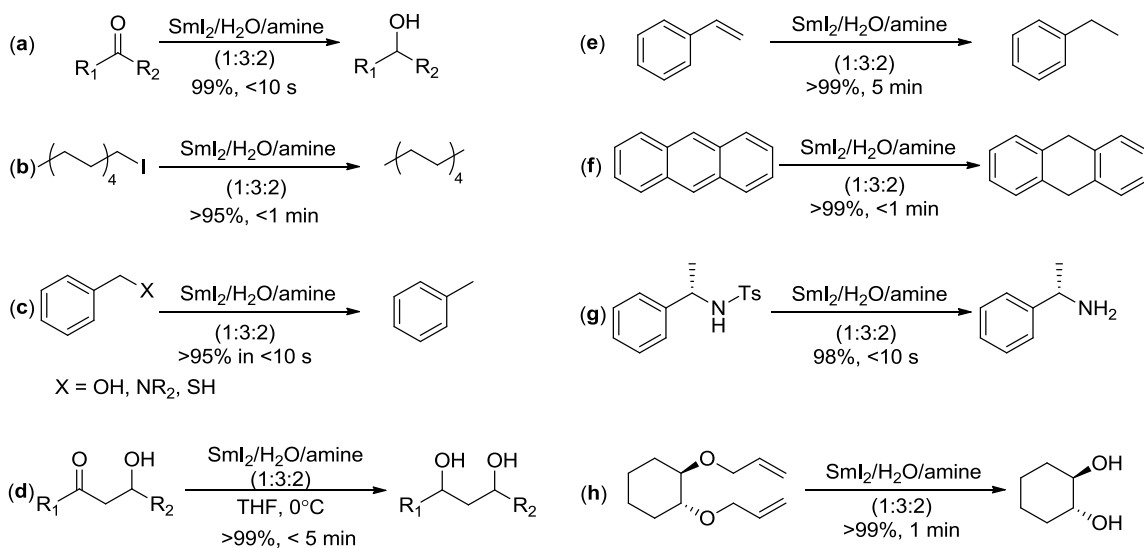
Scheme 6.1 Reduction of substituted benzoic acid with $\text{SmI}_2\text{-H}_2\text{O-KOH}$

In 2002, Hilmersson examined the reduction of ketones to determine the effect of amines (triethyl amine (Et_3N), N,N,N',N' -tetramethylethylenediamine (TMEDA), and N,N,N',N'',N'' -pentamethyldiethylenetriamine (PMDTA)) as additives with a range of proton sources. In this study, he found H_2O provided a far superior effect on the reduction as compared to other proton sources (MeOH and diglycol). Previous reports established that addition of amines³³ or H_2O ⁵² can individually enhance the rate of SmI_2 reduction; however, the combination of H_2O -amine increased the rate greater than what

would be expected from the sum of the individual rate enhancements.¹⁷⁴ The reduction of a ketone by SmI₂ is complete within a few hours, while with SmI₂-H₂O-amine a 99% conversion to the alcohol was observed in less than 10 s. Based on the rates of reduction that he observed, Hilmersson calculated that the SmI₂-H₂O-amine mixture reduced the ketone 700-1000 times faster than SmI₂ without an additive, and 100 times faster than is observed with SmI₂-HMPA.¹⁷⁴

Also in the initial report, the ratio of 1:3:2 SmI₂-H₂O-amine produced the highest conversion. This ratio of the additives is much lower than the large excess of HMPA or DMPU (4-10 equiv) typically used to increase the reduction rate of SmI₂.³³ The low concentrations of H₂O used are significantly smaller than the Sm-H₂O ratio seen in reports where H₂O is acting as the only additive. Typically 150 equiv of H₂O is required to observe rate enhancements.¹⁷²

Initially, Hilmersson explored the impact of the Sm-H₂O-amine system on substrates which can be reduced with SmI₂. Alkyl and aryl ketones^{174,182}, α,β -unsaturated esters¹⁸², imines¹⁸² and alkyl halides¹⁸³ were all reduced within a few minutes or seconds with exceptionally high conversions (Scheme 6.2, a-d). Following the success of these reactions, substrates which cannot be reduced by SmI₂ alone, or SmI₂-HMPA, were examined with SmI₂-H₂O-amine. Reduction of conjugated olefins^{15,184}, deprotection of tosyl amines^{185,186}, and deprotection of allyl ethers¹⁸⁷ all occurred with quantitative conversions (Scheme 6.2, e-h).



Scheme 6.2 Reductions carried out with Sm-H₂O-amine

The initial study by Hilmersson employed Et₃N, TMEDA, and PMDTA as amines, and all reactions were instantaneous.¹⁷⁴ Additionally, as the reaction proceeded, a large amount of precipitate formed. After the reaction was complete, only trace amounts of the amine could be detected in the supernatant, suggesting that a salt of the amine precipitated out of solution as a product of the reaction. IR and ¹H NMR analysis further confirmed the identity of the solid as ammonium halide salts.¹⁸² The rapid formation of a quaternary ammonium salt (R₃N•HI) was proposed to be one of the driving forces of the SmI₂-mediated H₂O and amine reactions.

To further investigate this idea, analogous Lewis bases were used in place of the amine in the reaction. The reduction of 4-phenyl-2-butanone was complete in less than 10 s with nitrogen containing TMEDA in the SmI₂-H₂O-amine system. 1,2-Dimethoxyethane (DME), and 1,2-bis(methylsulfanyl)ethane (MSE), structurally similar

oxygen and sulfur analogs, resulted in only a 40% conversion after 24 hours, even in the presence of excess H₂O (17.5 equiv).¹⁸² The reaction proceeded to completion with 1,2-bis(dimethylphosphino)ethane (DMPE), a phosphorous-containing ligand, in 30 mins; however, excess H₂O was required. These experiments indicated that oxygen- and sulfur-containing additives cannot be used in place of the amine in the SmI₂-H₂O-amine system. The phosphorous-containing ligand yielded product, albeit slower than the amine (Figure 6.1). These results suggest that the ability of the heteroatom on the additive to coordinate to Sm is not the prominent factor for success, or DME would have worked. It was noted that both the DMPE and TMEDA formed insoluble salts in the reaction, again suggesting the formation of precipitate aids in the reaction, through shifting the equilibrium in favor of the products, as suggested by Le Chatelier's principle.¹⁸²

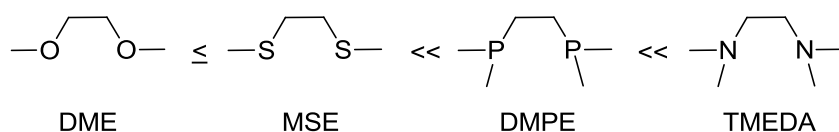
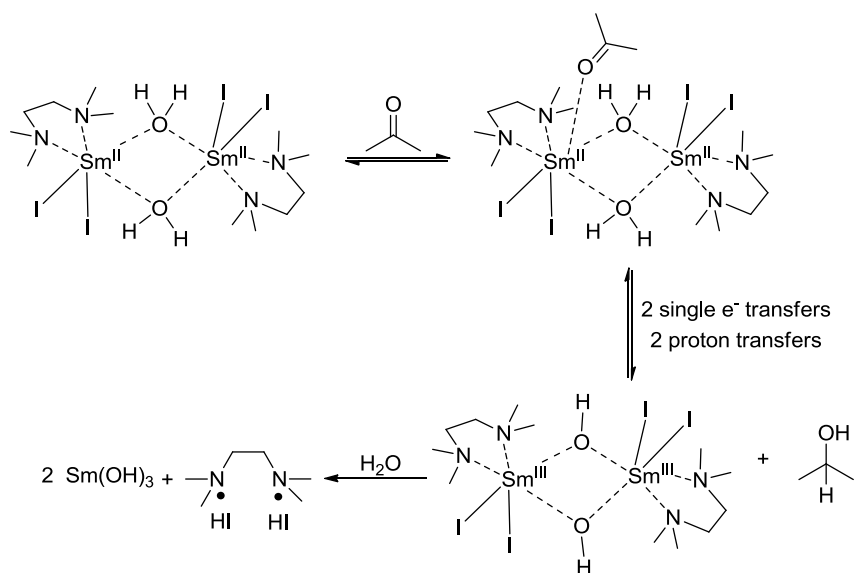


Figure 6.1 Ligands attempted in the reduction of 4-phenyl-2-butanone with SmI₂-H₂O

Further mechanistic studies with various amines in the reduction of 1-chlorodecane¹⁸⁸ provided a general trend. The rate of reduction increased as the basicity of the amine increased. Also, the rate was approximately related to the substitutions on the nitrogen—the fastest rate was observed with secondary amines, and the slowest with tertiary. These results suggest the ability of the amine to act as a more powerful base is a critical part of the mechanism.

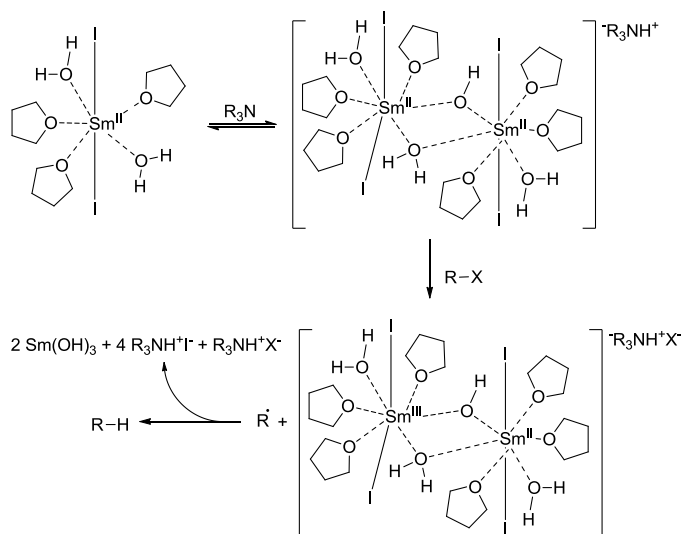
Some inconsistent observations of the SmI₂-H₂O-amine system with the range of different substrates were found, most notably, the kinetic isotope effect. Primary kinetic isotope effects, which indicate that the proton transfer from H₂O is rate-determining, were only observed with the reduction of ketones^{174,182} and benzyl alcohol.¹⁸⁶ The reduction of alkyl halides,^{188,183} conjugated olefins^{15,184} and allyl ethers¹⁸⁷ yielded a $k_H/k_D = 1$. The inconsistent observation of protonation occurring before or during the rate determining step may be a minor difference in the rates of reduction with the different substrates, or it may suggest that the reductions by Sm-H₂O-amine follow discretely different mechanisms based on the substrate being reduced.

In Hilmersson's seminal paper on the reduction of ketones, he proposed that both the amine (bidentate TMEDA) and H₂O coordinate to the Sm-metal center, forming a Sm-dimer through bridging H₂O molecules (Scheme 6.3). This dimer acted as the reductant which carried out the electron transfers and proton transfers to form the alcohol product. This pathway also takes into account the formation of ammonium salts and Sm(III) which precipitate out of solution.¹⁷⁴



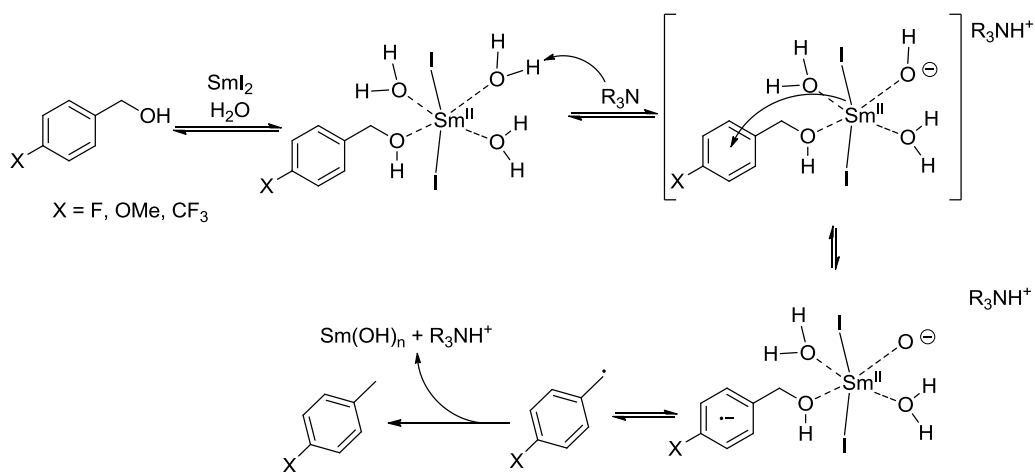
Scheme 6.3 Proposed mechanism for the reduction of ketones by Sm-H₂O-amine

The mechanism was shown to be different for the reduction of alkyl halides. This study was the first which identified that the basicity of the amine altered the reaction rate, suggesting that the role of the amine may not be to act as a coordinating ligand. In this system, Hilmersson proposed that H₂O coordinates to SmI₂, and the amine deprotonates the coordinated H₂O, forming the ammonium salt and a Sm-hydroxide dimer, facilitating the electron transfer to the substrate (Scheme 6.4).¹⁸⁸



Scheme 6.4 Proposed mechanism for the reduction of alkyl halides by Sm-H₂O-amine

In 2009, he proposed a different mechanism for the reduction of benzyl alcohol. In this reaction, H₂O coordinates to the Sm-metal center, followed by amine deprotonation of the coordinated H₂O, producing a Sm-hydroxide as the active reductant (Scheme 6.5). As electron withdrawing and donating groups were added to the aromatic ring, the rate of reduction was affected, suggesting that the electron is transferred to the aromatic ring, forming the radical anion. The anion rearranges to form the benzyl radical intermediate, which is protonated to form toluene.¹⁸⁶



Scheme 6.5 Proposed mechanism for the reduction of benzyl alcohol by Sm-H₂O-amine

In total, Hilmersson's work and proposed mechanisms leave us with very important information that needs to be taken into consideration as we move forward to study the reduction of a new system carried out by SmI₂-H₂O-amine: (a) precipitation of amine salts causes the equilibrium of the reaction to favor the products, and facilitates the facile reduction through Le Chatelier's principle, (b) an overall mechanism of the reductive system has not been generalized across a range of substrates based on differences in KIE and rate orders and (c) in all cases where it was studied, the basicity of the amine impacted the rate, implying its role in the mechanism is likely a deprotonation. These factors were used to shape the kinetic and mechanistic study of esters by SmI₂-H₂O-amine that is described in this chapter.

6.2 Experimental

6.2.1 Materials

THF was purified after purging with argon gas and passing over a column of activated alumina by a Solvent Purification System (Innovative Technology Inc.; MA). Dried solvents and reagents were stored in an Innovative Technology, Inc. drybox containing an argon atmosphere and a platinum catalyst for drying. SmI_2 was prepared by stirring Sm metal and iodine in THF until the characteristic blue color of Sm^{2+} appeared. The concentration of the Sm complex (0.10 M in THF) was determined by iodometric titration. Triethyl amine, morpholine, n-tributyl amine, n-butyl amine and pyrrolidine were purchased from Aldrich and distilled under vacuum from CaO before use. Distilled H_2O was bubbled with purified N_2 for 24 hours, followed by three cycles of freeze-pump-thaw before use.

6.2.2 Instrumentation

Proton and carbon NMR were recorded on Bruker 500 MHz spectrometer. GC-MS analysis was performed with HP 5890 Series Gas Chromatograph with an HP Mass Selector Detector. Kinetic studies in THF were performed using a computer-controlled SX-20 MV stopped-flow reaction spectrophotometer (Applied Photophysics Ltd., Surrey, UK).

6.2.3 Methods

6.2.3.1 General Procedure for Reduction with SmI_2 - H_2O -amine

Reductions were carried out in a drybox with degassed reagents. SmI_2 was prepared as described above. Substrate (0.42 mmol) was added to stirring SmI_2 (25 mL, 0.1 M). Amine (5 mmol) in approx. 2mL THF was added to the stirring reaction, followed by H_2O (7.5 mmol). After the required time, the reaction was exposed to air and stirred until the reaction mixture became a milky white, and the excess SmI_2 was oxidized. The reaction mixture was diluted with EtOAc (20 mL) and HCl (10 mL, 1.0 M). The aqueous layer was extracted with EtOAc (3 x 20 mL), organic layers were combined, washed with saturated aq NaCl (1 x 10 mL), dried over Na_2SO_4 , filtered and concentrated. The crude product was analyzed by GC and NMR.

6.2.3.2 General Procedure for Stopped-Flow Studies

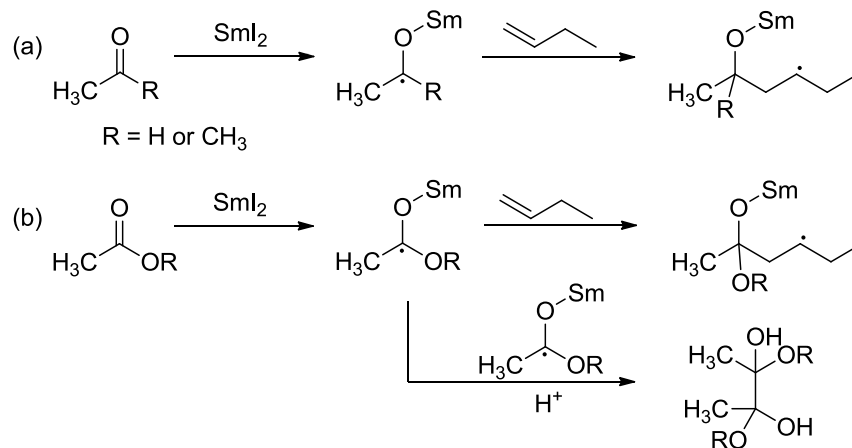
SmI_2 was combined with the methyl ester substrate in an airtight Hamilton syringe, H_2O and the amine were combined in the other syringe, taken from a drybox and injected into the stopped-flow system. The cell box and the drive syringes of the stopped-flow reaction analyzer were flushed a minimum of three times with degassed solvents to make the system oxygen-free. Due to the precipitation that was formed from the reaction, the sample handling unit was washed with dilute nitric acid (0.01M), distilled water (2X), THF (3X) and finally degassed THF (3X) between each sample put on the stopped-flow. The concentration of SmI_2 used for the study was 10 mM. The concentrations of the substrates were kept high relative to SmI_2 (500 mM) to maintain pseudo first-order conditions. Observed reaction rate constants were determined from

exponential fitting of the decays of SmI₂-HMPA complex at 550 nm. The decay of the SmI₂ displayed double exponential decays over >3 half-lives.

Rate orders for SmI₂, H₂O, amine and methyl ester were derived from the plots of $\ln k_{\text{obs}}$ vs. $\ln[\text{substrate}]$. The rate order for SmI₂ was also determined from fractional times method from the decay traces of SmI₂. The rate plots were generated from the absorption decay traces obtained from a stopped-flow spectrophotometer.

6.3 Results

Sm-mediated reduction of aldehydes or ketones form intermediate ketyl radical anions. These radical anions are integral to many Sm-mediated carbon-carbon bond forming reactions as they undergo radical-radical coupling or cyclization onto an olefin (Scheme 6.6, a). Esters and amines are carbonyl substrates which are not reduced under the mild conditions of SmI₂, even with HMPA. Esters are typically reduced to an alcohol through a two-electron reduction under harsh conditions with LiAlH₄, sodium borohydride with metal salts, or with sodium metal in absolute ethanol.^{189,190} Harnessing a Sm-system which has the ability to carry out a single-electron reduction of esters would provide access to the functionalized radical anion, which would drastically expand the type of reactions that could be carried out with SmI₂ (Scheme 6.6).



Scheme 6.6 (a) ketyl radicals formed through SmI_2 reduction of aldehydes or ketones (b) radical anion from ester single-electron reduction

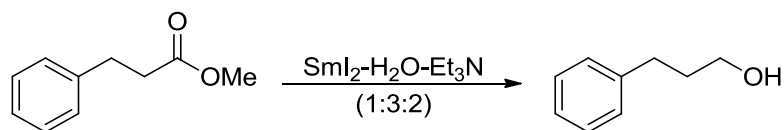
6.3.1 Synthetic Results

In an initial study by Procter *et al.*, hydrocinnamic acid methyl ester was reduced to its corresponding alcohol in a 95% yield in less than 5 minutes with SmI_2 with H_2O and Et_3N as additives.¹⁹¹ Both additives were required for the reduction to occur (Table 6.3, entries 1-4, and 13), and a $\text{Sm-H}_2\text{O-Et}_3\text{N}$ ratio of 1:3:2 was optimized for the reduction. Surprisingly, the use of $\text{SmI}_2\text{-H}_2\text{O}$ (800 equiv H_2O), which facilitated lactone ring-opening reductions in the Procter lab, was unsuccessful with the reduction of the ester (Table 6.3, entry 2).^{171,191}

MeOH , $t\text{BuOH}$ and ethylene glycol were also used as proton sources in the system; however, lower conversions and longer reaction times were required to obtain any of the reduced alcohol (Table 6.3, entries 5-7). These results are consistent with Hilmersson's findings that H_2O provides superior rate enhancement compared to other

proton sources with SmI₂ and amines.¹⁷⁴ A variety of amines were tested in the reaction (Table 6.3, entries 8-12), all of which carried out the reduction at different rates; details on the impact of the amines will be discussed further following kinetic studies in section 6.3.2.

Table 6.3 Reaction conditions for the reduction of hydrocinnamic acid methyl ester by SmI₂-H₂O-amine



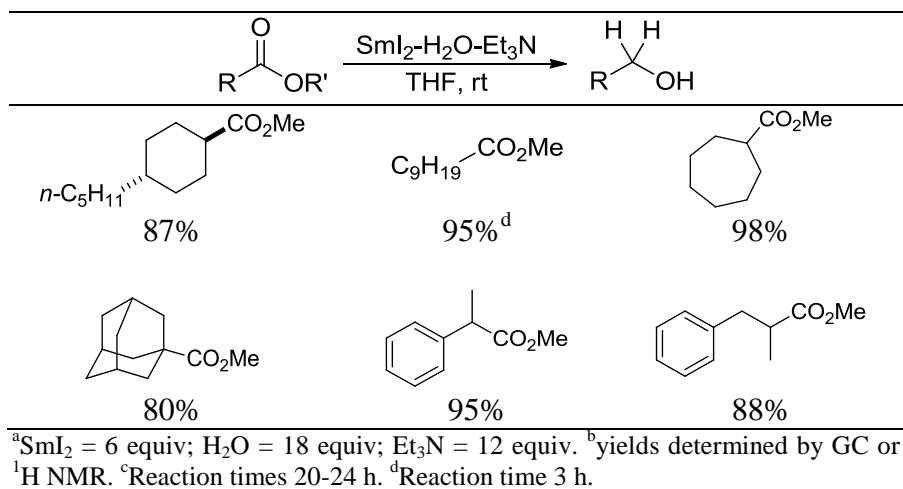
	Amine	Proton source	equiv. (amine)	equiv. (proton source)	% Conversion			
					60 s	300 s	1 h	24 h
1	-	H ₂ O	-	12	nd	nd	nd	<2
2	-	H ₂ O	-	800	nd	nd	nd	<2
3	Et ₃ N	-	12	-	nd	nd	nd	5-7
4	Et ₃ N	H ₂ O	12	18	89	96	nd	nd
5	Et ₃ N	MeOH	12	18	nd	0	0.8	9
6	Et ₃ N	<i>t</i> BuOH	12	18	0	0	0	0
7	Et ₃ N	(HOCH ₂) ₂	12	9	12	27	64	95
8	<i>i</i> -Pr ₂ NH	H ₂ O	12	18	75	85.6	nd	nd
9	<i>n</i> -BuNH ₂	H ₂ O	12	18	95	98.5	nd	nd
10	Pyrrolidine	H ₂ O	12	18	94	99.5	nd	nd
11	Piperidine	H ₂ O	12	18	74	94	99	nd
12	Morpholine	H ₂ O	12	18	74	90	nd	nd
13	Pyrrolidine	-	12	-	nd	nd	0	<2

All reactions carried out with strict exclusion of oxygen, using standard benchtop techniques for handling air-sensitive reagents. ^aQuenched by bubbling air through reaction mixtures until decolorization occurred. ^bConversion determined by GC or ¹H NMR.

Procter has shown SmI₂-H₂O-Et₃N can readily reduce a range of unactivated primary, secondary, and tertiary alkyl esters to their corresponding alcohols in high yields (Table 6.4).¹⁹¹ Interestingly, to achieve high yields, a specific order of addition must be

carried out for the reductions. The substrate is initially added to solutions of SmI_2 , followed by addition of the amine, swiftly followed by the addition of H_2O to the solution. As soon as the H_2O is added, the formation of a large amount of white precipitate is observed. If SmI_2 is premixed with the H_2O and amine before the substrate is added, decreased yields over longer reaction times are observed.

Table 6.4 Esters reduced to alcohols by $\text{SmI}_2\text{-H}_2\text{O-Et}_3\text{N}^{\text{a,b,c}}$



6.3.2 Kinetic Results

6.3.2.1 Pseudo-First Order Rates

To elucidate details of the mechanism of the $\text{SmI}_2\text{-H}_2\text{O}$ -amine system, pseudo-first order rates were examined using stopped-flow spectroscopy. Rate orders of one were found for all components of the reaction: hydrocinnamic acid methyl ester, SmI_2 , Et_3N , and H_2O (Table 6.5, see appendix for all plots), with a rate constant of 1.3 ± 0.1

$M^{-1}s^{-1}$ (Figure 6.2). These orders indicate that all components participate in the reaction before or at the rate determining step.

Table 6.5 Results from Pseudo-first order rate experiments

Rate Orders				Rate Constant ^a
MeEster ^a	SmI ₂ ^b	Et ₃ N ^c	H ₂ O ^d	
1.01 ± 0.07	0.88 ± 0.08	1.19 ± 0.012	1.00 ± 0.10	$1.3 \pm 0.1 M^{-3}s^{-1}$

^aSmI₂ = 10 mM, H₂O = 100 mM, Et₃N = 100 mM, methylester = 400-700 mM. ^bSmI₂ = 10-20 mM, H₂O = 100 mM, Et₃N = 100 mM, methylester = 500 mM. ^cSmI₂ = 10 mM, H₂O = 100 mM, methylester = 500 mM, Et₃N = 50-200 mM. ^dSmI₂ = 10 mM, Et₃N = 100 mM, methylester = 500 mM, H₂O = 50-150 mM.

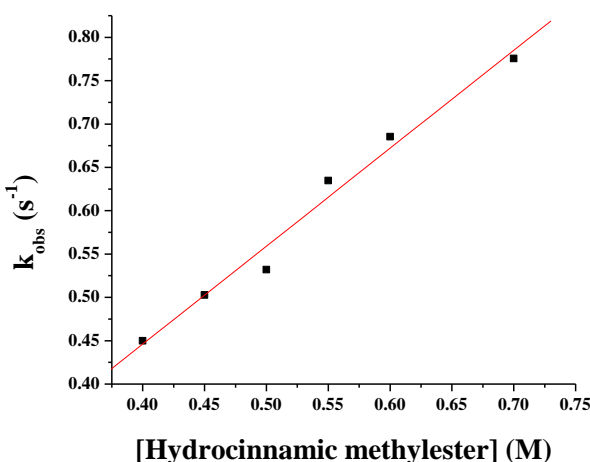


Figure 6.2. Plot of k_{obs} vs [hydrocinnamic methylester]. SmI₂ = 10 mM, H₂O = 100 mM, Et₃N = 100 mM, methylester = 400-700 mM. T = 25.0 ± 0.1 °C. Rate Constant = 1.3 ± 0.1 M⁻³s⁻¹.

It is interesting to note that the order of addition required for the synthesis to achieve the highest yields needed to be mimicked in the kinetic studies in order to obtain reproducible kinetic decays. SmI₂ and methyl ester were premixed and then combined with a mixture of H₂O and amine. Since SmI₂ does not interact with the ester substrate without H₂O and amine, no loss in [SmI₂] was observed with premixing SmI₂ and

substrate. Additionally, as described below, if the amine does not interact with SmI₂ the amine can be premixed with SmI₂-MeEster in the kinetic experiments, but H₂O must be separated from SmI₂. These conditions allowed for reproducible experiments, as well as provide further information to the final mechanism (*vide infra*).

6.3.2.2.6 Impact of H₂O

H₂O has a delicate concentration balance in the SmI₂-H₂O-amine reduction system. Hilmersson and Procter have both optimized the SmI₂-H₂O-amine system to maintain low concentrations of both additives in a 1:3:2 equiv ratio.^{174,191} Previously reported Sm-H₂O systems require high concentrations of H₂O (150 equiv.) to achieve increased rates; however, high concentrations of H₂O in the Sm-H₂O-amine system prevent the reduction from occurring, and starting material is recovered. The effect of increasing the concentration of H₂O was observed through kinetic experiments. As shown previously, as the concentration of H₂O increased, the rate increased linearly, indicating first order in the reagent, with up to 15 equiv of the additive. Saturation kinetics were observed at concentrations of H₂O over 25 equiv (Figure 6.3, a), and as the concentration of H₂O increased further, the additive became detrimental to the reaction, sharply decreasing the rate (Figure 6.3, b). It was determined that these high concentrations did not allow the reduced product to be formed.

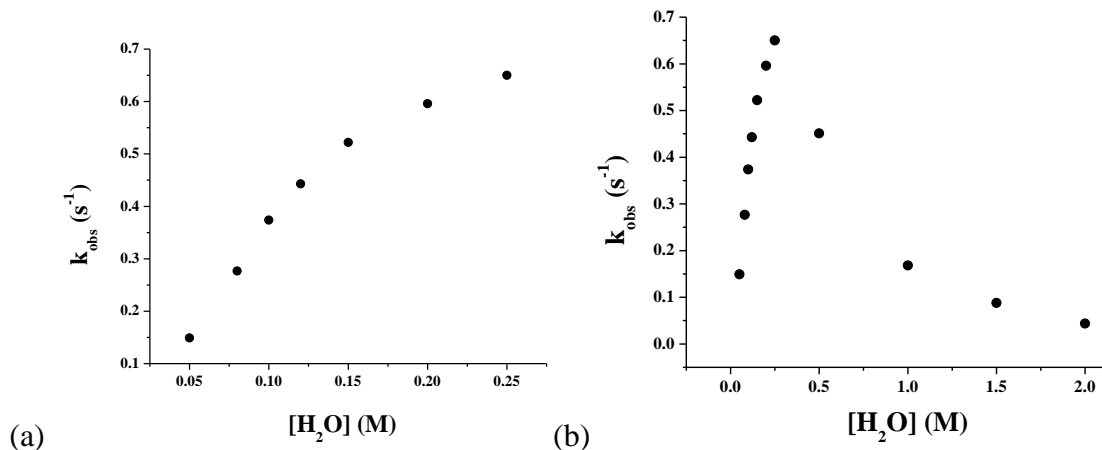


Figure 6.3 Plot of k_{obs} vs $[H_2O]$. (a) $SmI_2 = 10$ mM, $Et_3N = 100$ mM, methylester = 500 mM, $H_2O = 50$ mM- 250 mM. (b) (a) $SmI_2 = 10$ mM, $Et_3N = 100$ mM, methylester = 500 mM, $H_2O = 50$ -2 M. $T = 25.0 \pm 0.1$ °C.

Previous investigations of the interaction between SmI_2 and H_2O have shown that due to the oxophilic nature of Sm, H_2O coordinates to the Sm-metal center (see Chapter 1). At concentrations above 50 equiv H_2O (with respect to SmI_2), the UV spectra of SmI_2 in THF starts to converge and shift, indicating a disruption and change in the coordination sphere.⁵² CV studies have also shown that the oxidation potential of SmI_2 is increased, and a more powerful reductant is produced after the addition of 60 equiv. H_2O .⁵² Finally, conductance studies have identified that 20 equiv of H_2O or more are needed to observe conductance corresponding to the displacement of iodide ions from SmI_2 .⁵⁷

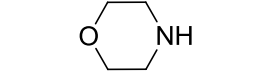
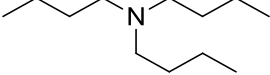
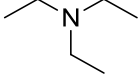
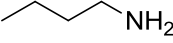

These results indicate that H_2O can coordinate to SmI_2 ; however, to observe this interaction spectroscopically in the ground state, high concentrations of H_2O are needed, concentrations much higher than are used in the SmI_2 - H_2O -amine system. It is important

to note, even though these spectroscopic techniques do not detect an interaction at low concentrations, that does not mean that H₂O is not coordinated in the *transition state*. Based on all of the known interaction of the highly oxophilic samarium, even at low concentrations of H₂O, some amount will coordinate.

6.3.2.3 Impact of Basicity of Amines

Based on results observed by Hilmersson,¹⁸⁸ we explored how the rate of the reduction was affected by the basicity of the amine used. As expected, the rates obtained at 0°C increased as the basicity of the amine increased (Table 6.6). The effect on the rate implies that the first order role the amine plays within the reaction is dependent on the additive's ability to act as a base. These rates also reflect the yields obtained in the initial set of experiments in Table 6.3, with *n*-butyl amine and pyrrolidine producing over 90% yield of the alcohol after the first 300 s sample.

Table 6.6 Rate of reduction with different amines in the reduction of hydrocinnamic methyl ester.^a

Amine	$pK_{BH^+}^b$	Rate ($M^{-3}s^{-1}$) at 0°C	
	morpholine	9.0 ± 0.2	0.16 ± 0.02
	n-tributyl amine	10.0 ± 0.5	1.12 ± 0.09
	triethyl amine	10.6 ± 0.3	4.7 ± 0.2
	n-butyl amine	10.7 ± 0.1	114 ± 6
	pyrrolidine	11.3 ± 0.2	591 ± 12

^aSmI₂ = 10 mM, H₂O = 100 mM, methylester = 500 mM, Et₃N = 50-200 mM. T = 0.0 ± 0.1 °C.

^bDetermined from ACD lab prediction algorithm¹⁸⁸

To determine if there is any degree of interaction between SmI_2 and the additives in the ground state, UV spectra of SmI_2 with 2 and 10 equiv of the amine were examined. Of the amines listed above, only pyrrolidine and morpholine affected the UV spectrum. The addition of low concentrations (2 equiv) of pyrrolidine and morpholine reduced the absorbance bands of SmI_2 , but did not shift them (pyrrolidine, Figure 6.4. See appendix 8.5.3.1- 8.5.3.5 for UV-spectra of all amines in Table 6.6).

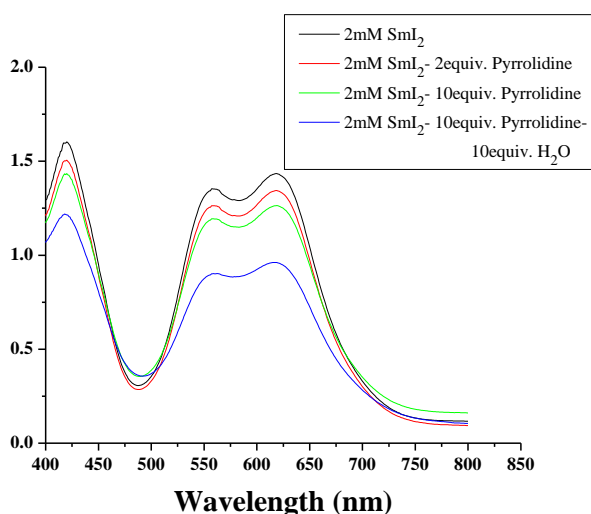


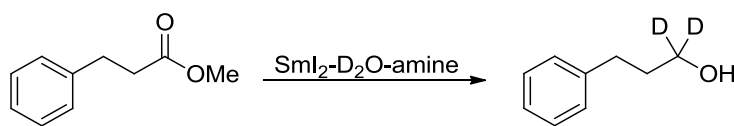
Figure 6.4 UV-Vis of SmI_2 with pyrrolidine and pyrrolidine- H_2O . $[\text{SmI}_2] = 2 \text{ mM}$, $[\text{pyrrolidine}] = 4 \text{ mM}$ and 20 mM , $[\text{H}_2\text{O}] = 20 \text{ mM}$.

6.3.2.4 Kinetic Isotope Effects

To determine the role of Sm-bound water deprotonation, kinetic isotope effects (KIE) were observed. Under the conditions of the kinetic experiments, a $k_{\text{H}}/k_{\text{D}}$ of 1.05 was observed with Et_3N and 1.2 with pyrrolidine in the system (Table 6.7). Primary kinetic isotope effects ($k_{\text{H}}/k_{\text{D}} > 2$), indicate a bond breaking event at the R-H/R-D bond,

while a k_H/k_D of 1.0 defines that the rate was not impacted with the change from H to D. In the case of the $\text{SmI}_2\text{-H}_2\text{O-amine}$ system a very small KIE was observed in both cases with the addition of D_2O (Table 6.7). Hilmersson previously reported a similar low KIE with reductions with $\text{SmI}_2\text{-H}_2\text{O-amine}$.¹⁸⁸ Further insight into how the low KIE impacts the proposed mechanism is described in section 6.3.3.

Table 6.7 Kinetic isotope effects with Et_3N and pyrrolidine



	k_H/k_D
$\text{SmI}_2/\text{H}_2\text{O}/\text{Et}_3\text{N}$	1.05 ± 0.01
$\text{SmI}_2/\text{H}_2\text{O}/\text{pyrrolidine}$	1.2 ± 0.1

[SmI_2] = 10 mM; [X_2O] = 10 equiv; [amine] = 10 equiv

6.3.2.5 Activation Parameters

Activation parameters were determined by observing the effect of temperature on the rate of the reaction. The data was fit to the linear form of the Eyring equation (equation 6.1), where, k_{obs} is the observed decay rate constant, h is Planck's constant, k_B is the Boltzmann constant, R is the universal gas constant, T is temperature in Kelvin, ΔH^\ddagger is the enthalpy of activation and ΔS^\ddagger is the entropy of activation. Gibb's free energy of activation is calculated from $\Delta G^\ddagger = \Delta H^\ddagger - T \Delta S^\ddagger$, and activation energy from $E_a = \Delta H^\ddagger + RT$.

$$\ln\left(\frac{k_{\text{obs}} h}{k_B T}\right) = -\frac{\Delta H^\ddagger}{RT} + \frac{\Delta S^\ddagger}{R} \quad (6.1)$$

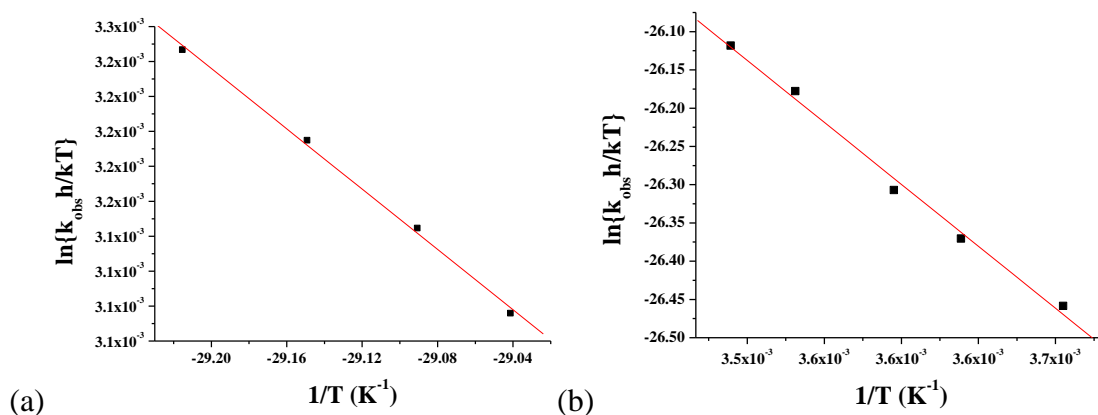


Figure 6.5 Eyring plot from the reduction of hydrocinnamic acid methyl ester with (a) $\text{SmI}_2\text{-H}_2\text{O-Et}_3\text{N}$ and (b) $\text{SmI}_2\text{-H}_2\text{O-pyrrolidine}$.

Table 6.8 Activation parameters with $\text{SmI}_2\text{-H}_2\text{O-amine}$ ^a

	ΔH^\ddagger (kcal/mol)	ΔS^\ddagger (cal/mol K)	ΔG^\ddagger (kcal/mol) ^b	E_a (kcal/mol) ^c
Et_3N	2.2 ± 0.1	-50.6 ± 0.3	17.5 ± 0.2	2.8 ± 0.7
pyrrolidine	5.4 ± 0.3	-32.9 ± 0.9	14.4 ± 0.6	6.0 ± 0.3

^aEyring activation parameters were obtained from $\ln(k_{\text{obs}}h/kT) = \Delta\text{H}^\ddagger/RT + \Delta\text{S}^\ddagger/R$. ^bCalculated from $\Delta\text{G}^\ddagger = \Delta\text{H}^\ddagger - T \Delta\text{S}^\ddagger$. ^cCalculated from, $\text{E}_a = \Delta\text{H}^\ddagger + RT$.

The activation parameters of this system with Et_3N and pyrrolidine provide invaluable information on the transition state of the reaction. With both amines, a large, negative entropy (ΔS^\ddagger) indicates a *highly* ordered system, which is consistent with a transition state in which SmI_2 is coordinated with one or both of the additives. The relatively low values for the change in enthalpy indicate that within the rate determining step of the reaction there is a small change in the bond reorganization energy (ΔH^\ddagger), and therefore very little bond forming or breaking occurs, consistent with an early transition state.

6.3.3 Proposed Mechanism

First order rates for SmI_2 , methyl ester, H_2O , and amine were observed, indicating all components are involved in or before the rate determining step. We propose a transition state in which H_2O coordinates to the Sm center and is deprotonated by the amine. While the kinetic isotope effects appear to contradict this, the low KIE for both Et_3N and pyrrolidine is consistent with an early transition state in which the hydrogen bond-breaking is not fully complete in the transition state.¹⁹² Wigfield and Dauben described an “early transition state” as the position of the transition state along the reaction coordinate which is reactant-like.^{193,194} With this definition in mind, an early transition state in the $\text{SmI}_2\text{-H}_2\text{O}$ -amine would resemble the configuration of the components coming together, and the hydrogen bond being elongated, but not yet broken.

Further insight and evidence for this action can be found in the difference in activation parameters with Et_3N or pyrrolidine in the reaction. The $\text{SmI}_2\text{-H}_2\text{O}$ -amine system exhibits a highly ordered transition state through the large negative ΔS^\ddagger with both Et_3N and pyrrolidine; however Et_3N , is more negative by 17 cal/mol K (Table 6.8). Moreover, assuming the bond being cleaved in the rate determining step is the hydrogen-oxygen bond of coordinated H_2O , the greatest impact on the ΔH^\ddagger would correspond to the extent in which the hydrogen bond is broken in the transition state. Based on the Hammond postulate, the low ΔH^\ddagger with both amines reflects a system which has an early transition state.¹⁹⁵ The more basic pyrrolidine deprotonates the coordinated H_2O more rapidly than Et_3N . While the hydrogen bond is not fully broken in an early transition

state, the O-H bond is elongated and the N-H bond begins to form in the transition state (Figure 6.6, c), decreasing the order in the system (higher ΔS). Moreover, the extent at which the hydrogen bond is broken is reflected in both amines in the change in enthalpy. A larger ΔH^\ddagger for the system with pyrrolidine agrees with the hydrogen bond being more elongated and greater change in the bond reorganization energy as compared to the slower proton transfer with the less basic amine.

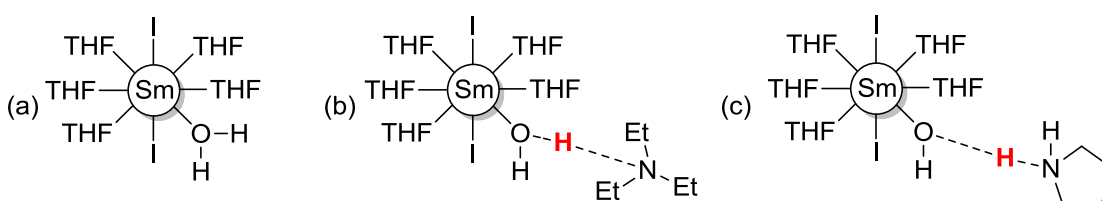
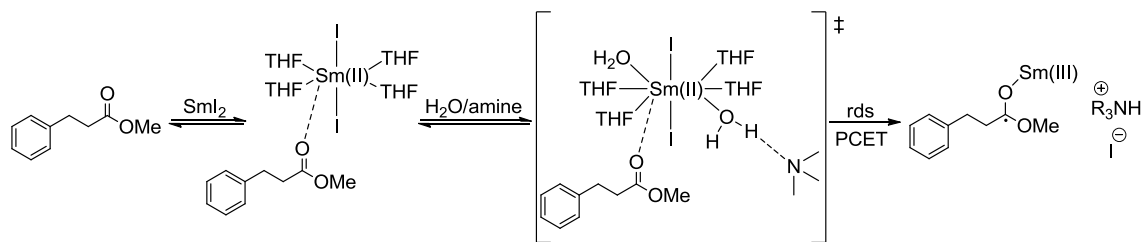


Figure 6.6 Transition state images of (a) highly ordered H₂O coordinated to SmI₂ in THF (b) hydrogen bond elongation as Et₃N deprotonates coordinated H₂O (c) hydrogen bond elongation as pyrrolidine carries out a more facile deprotonation of coordinated H₂O.

Based on all of the data compiled for the SmI₂-H₂O-amine reduction of methyl esters, the following mechanism for the reduction is proposed. Initial combination of SmI₂ and ester provided the best synthetic and kinetic results. Due to the oxophilic nature of SmI₂, the carbonyl of the methyl ester will interact with the coordination sphere of SmI₂, providing an interaction vital for inner-sphere electron transfer.²⁴ As H₂O and amine are added, the components come together in an equilibrium in which H₂O coordinates to SmI₂, and is then deprotonated by the amine, facilitating a proton coupled electron transfer (PCET) in the rate determining step in the reaction (Scheme 6.7).

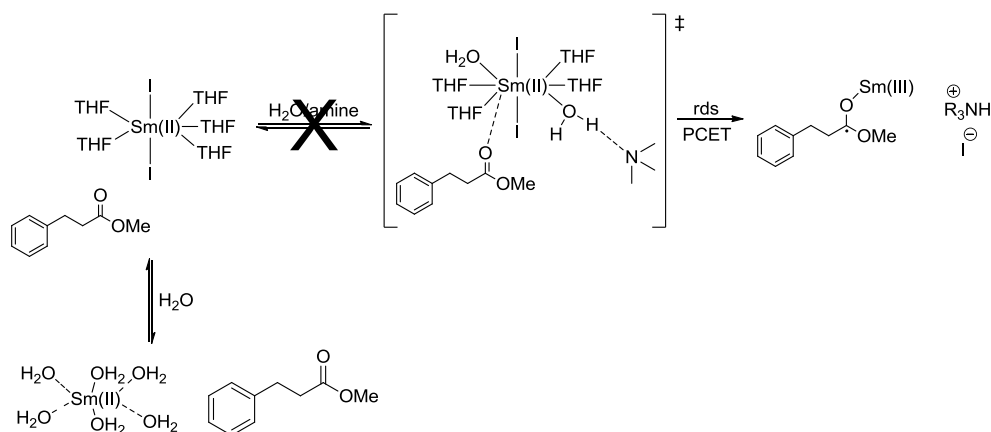


Scheme 6.7 Proposed transition state mechanism of the $\text{SmI}_2\text{-H}_2\text{O}$ -amine system.

PCET is a simultaneous transfer of an electron and proton in a single step. This process is distinctively different from sequential pathways, in which a stable intermediate exists between the two transfers.^{196,197} In PCET reactions, the proton transfer is electronically adiabatic, and the electron responds instantaneously to the proton motion. Circumventing a high energy intermediate allows the coupled proton and electron transfer to be thermodynamically favored, facilitating processes in which the transfer of the proton or the electron separately is energetically unfavorable.¹⁹⁸ The electron and proton may transfer to the same or in different directions, likewise the transfer can be to the same or different species in the reaction.¹⁹⁷

The key component to this mechanism is that the transition state is comprised of all four components of the reaction displaying their first order role in the rate determining step. The highly ordered interaction between them leads to the concerted action of the PCET, allowing this high energy reduction to occur. The formation of the ammonium salt, which is integral to the success of the $\text{SmI}_2\text{-H}_2\text{O}$ -amine reductions,¹⁸² aids in the equilibrium of the transition state by making deprotonation of H_2O by the amine irreversible through precipitation, driving the equilibrium forward as the PCET occurs.

Within this proposed mechanism, it can also be postulated why the addition of high concentrations of H₂O, or pre-mixing SmI₂ and H₂O could be detrimental to the reaction. At high H₂O concentrations, the highly oxophilic Sm will preferentially coordinate H₂O, displacing the THF and iodine.^{52,57} If this occurs, the coordination sphere would be saturated with H₂O, not allowing the substrate to come in close enough proximity for the inner-sphere electron transfer to occur (Figure 6.8), and disrupting the necessary coupled proton and electron transfer. Pre-mixing the substrate with SmI₂ before addition of low concentrations of H₂O also allows the interaction between SmI₂ and the carbonyl to form.

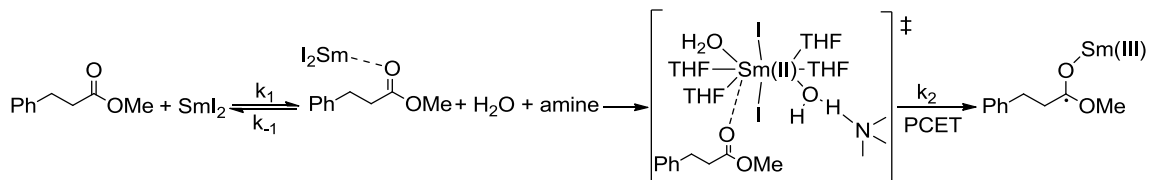


Scheme 6.8 Deleterious effect of high concentrations of H₂O with SmI₂-H₂O-amine

6.3.4 Derived Rate Expression

The rate expression for the reaction was derived by applying the steady state approximation to the formation of the SmI₂-substrate interaction. As the SmI₂ and methyl

ester complex are reacted with H₂O and amine, the reaction readily proceeds through the PCET in the rate determining step of the reaction (Scheme 6.9).



Scheme 6.9 Initial rate determining steps of the reduction of esters by SmI₂-H₂O-amine

Given k_2 is the rate determining step of the reaction (Scheme 6.8), the overall rate expression is:

$$\frac{d[\text{SmI}_2]}{dt} = k_2[\text{Sm-ester}][\text{H}_2\text{O}][\text{amine}] \quad (6.2)$$

Applying the steady state approximation for the formation of SmI₂ and ester complex provides:

$$\frac{d[\text{Sm-ester}]}{dt} = k_1[\text{SmI}_2][\text{ester}] - k_{-1}[\text{Sm-ester}] - k_2[\text{Sm-ester}][\text{H}_2\text{O}][\text{amine}] = 0 \quad (6.3)$$

Solving for [Sm-ester], the expression is:

$$[\text{Sm-ester}] = \frac{k_1[\text{SmI}_2][\text{ester}]}{k_{-1} + k_2[\text{H}_2\text{O}][\text{amine}]} \quad (6.4)$$

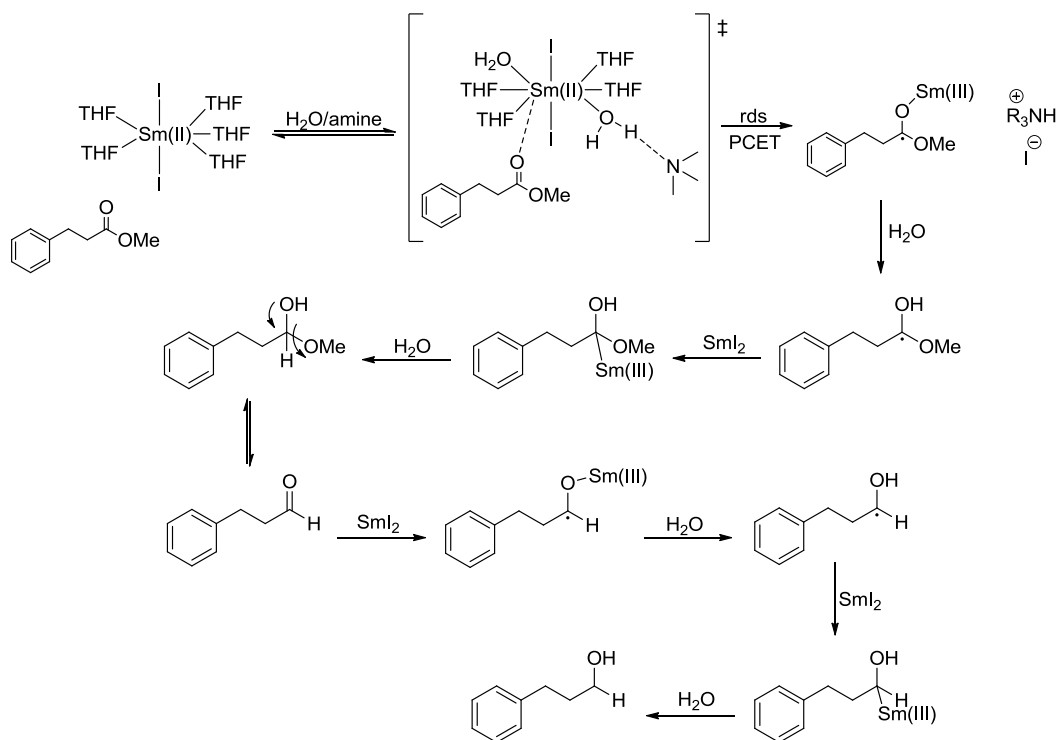
Substituting this factor into the overall rate expression gives:

$$\frac{d[\text{SmI}_2]}{dt} = k_2[\text{H}_2\text{O}][\text{amine}] \left(\frac{k_1[\text{SmI}_2][\text{ester}]}{k_{-1} + k_2[\text{H}_2\text{O}][\text{amine}]} \right) \quad (6.5)$$

Assuming $k_2 \ll k_{-1}$, and defining k_{obs} as $k_1 k_2 / k_{-1}$, the rate expression simplifies to:

$$\frac{d[\text{SmI}_2]}{dt} = k_{\text{obs}}[\text{SmI}_2][\text{ester}][\text{H}_2\text{O}][\text{amine}] \quad (6.6)$$

Following the rate determining step of the reaction, the radical anion is protonated by additional water within the system (Scheme 6.10). Subsequent reduction by SmI_2 leads an organosamarium intermediate, which undergoes loss of the ester leaving group to form an intermediate aldehyde. Since excess SmI_2 was used in the synthesis (6 equiv), the aldehyde is reduced by SmI_2 to intermediate ketyl radical, followed by protonation of the organosamarium to form the final alcohol.



Scheme 6.10 Pathway of ester reduction by $\text{SmI}_2\text{-H}_2\text{O-amine}$

6.3.5 Conclusions

The SmI₂-H₂O-amine system developed by Hilmersson is a mild and effective system for reducing a wide range of functional groups. The rates of reduction are drastically increased, and substrates not previously capable of being reduced by SmI₂ can now be accessed. We set out to understand the mechanism in which SmI₂-H₂O-amine carries out the reduction of esters, a substrate not easily reduced under mild reaction conditions. Rate studies showed that SmI₂, both additives (amine and H₂O), and substrate are all first order in the system. The reaction proceeds through a highly ordered transition state, which facilitates proton coupled electron transfer and carries out the unfavorable reduction. This system is the first instance where proton coupled electron transfer has been suggested for a Sm-mediated reduction. With this knowledge we believe an ester radical anion intermediate exists, and continued studies will determine if this intermediate can be accessed to carry out subsequent carbon-carbon or carbon-heteroatom coupling reactions, with either radical addition onto an olefin, or in an organosamarium nucleophilic addition. These continued studies will further develop the SmI₂-H₂O-amine system and will expand the scope in which SmI₂-mediated processes can be utilized in organic synthesis.

7. Concluding Remarks

As illustrated in the projects carried out, SmI₂ is a mild and efficient single-electron reductant, which is drastically affected by the additives used with it. The additives not only interact and coordinate with SmI₂, but can also carry out diverse roles which alter the mechanisms between the different SmI₂-systems. Understanding the mechanistic pathways of these organic reactions is vital to creating a robust understanding of SmI₂ as a reductant and to design new reductions.

Chapter 2 highlighted the ability of SmI₂ to reduce different functional groups at different rates. By identifying the different rate constants for the reduction, reaction pathways of complex cascade reactions can be better understood or predicted, allowing synthetic chemists to more efficiently design new complex syntheses. Also, the propensity of radical intermediates to interact with each other or other starting materials is equally important to identify so it can also be taken into account in the development of new reactions employing SmI₂. Using initial rates kinetic experiments, we determined that cyclic α,β -unsaturated esters are reduced an order of magnitude faster than aldehydes. This information provided insight into a previously reported SmI₂-cascade reaction in which both functional groups were present.

In chapter 3, HMPA was studied in the samarium Barbier reaction. Previous mechanistic studies have led to the realization that HMPA plays multifaceted roles in SmI₂-reactions. While it has been known that HMPA improves the rate and yield of the samarium Barbier reaction, details on how the reaction proceeded were unclear. Kinetic

and spectroscopic studies identified that HMPA not only coordinates to SmI_2 , but an interaction between HMPA and alkyl halides results in a complex in which the carbon-halide bond is elongated, making it more susceptible to reduction by SmI_2 . This interaction between the alkyl halide and HMPA is the driving force behind the selective reduction of alkyl halides by SmI_2 while in the presence of ketones. These insights not only provide the basis for a mechanistic understanding of SmI_2 -HMPA reductions and the samarium Barbier reaction, but knowledge of the RX -HMPA complex could prove useful in other syntheses needing to activate a carbon-halide bond.

A mechanistic understanding of why catalytic amounts of Ni(II) salts in SmI_2 reactions improved the reactivity was overlooked for nearly 30 years. In chapter 4, a kinetic analysis is reported, which identified that the active reductant interacting with the alkyl halide of the Barbier reaction is not Sm(II) but Ni(0) . SmI_2 readily reduces Ni(II) salts to Ni(0) , which oxidatively inserts into the alkyl halide bond. We also suggest the high efficiency of the Sm-Ni system in the Barbier reaction is due to the transmetallation of Sm(III) , allowing the C-C coupling reaction to proceed through an organosamarium intermediate, while releasing Ni(0) back into the catalytic cycle. This understanding alters the proposed pathways of nearly all of the SmI_2 - NiI_2 systems studied prior to this work. Additionally, an understanding of the fundamental chemistry that is occurring in the reaction will allow SmI_2 - Ni(II) to be applied more appropriately to the development and design of new reactions. Chapters 3 and 4 reported the same samarium Barbier

reaction; however, the change of additive forgoes a complete change in the reaction pathway.

Chapter 5 examined the reduction of lactones by SmI_2 with high concentrations of H_2O . The increased reducing power of SmI_2 with H_2O allowed the selective reduction of six-membered lactones over other ring-sized lactones. The formation of a radical intermediate stabilized by the anomeric effect was proposed to be the driving force for the success of the reaction. As ester functional groups were substituted on the ring alpha to the lactone carbonyl, five- and seven-membered lactones could also be accessed through a Sm-chelated stabilized intermediate. The rate studies carried out on a range of five-, six-, and seven-membered lactones with various substitution patterns identified that the vital feature necessary for reduction stemmed from the ability to form a Sm-coordinated intermediate between the carbonyls of the lactone and ester substitution.

Chapter 6 set out to study the SmI_2 - H_2O -amine reducing system. SmI_2 - H_2O -amine does not have the toxicity concerns which plague SmI_2 -HMPA, and it has been shown to be more powerful than SmI_2 -HMPA in many instances. To further develop this promising system, a greater understanding on the mechanism of action is required. Elegant work by Hilmersson has already provided some answers; however, a large degree of complexity is observed with the system, and differences in the mechanistic pathways are observed with different substrates. Understanding the mechanism in which SmI_2 - H_2O -amine carries out the reduction of esters can (a) provide insight into the SmI_2 - H_2O -amine system which will further the field of carbon-carbon bond forming reactions, and

(b) provide insight into whether an ester radical is being produced as an intermediate, so methods for accessing the reactive intermediate for new reactions and bond forming events can take place. A mechanistic study identified that the integral role of the co-additive system is for the amine to deprotonate Sm-coordinated H₂O, facilitating a vital proton coupled electron transfer through a highly ordered transition state, which allows the normally unfavorable reduction to occur. This is the first instance of proton coupled electron transfer observed in a Sm-mediated reaction. Additionally, the ability to access the reactive intermediate radical anion will greatly expanded the scope of SmI₂ reactions, as this new reduction is adapted to new carbon-carbon bond-forming reactions.

Taken together, these studies describe the complexities observed as additives are included in SmI₂ reactions. By gaining a detailed mechanistic understanding of the reaction pathways, these systems can be utilized to their fullest potential and will allow SmI₂ to be integrated into new areas of synthetic and organometallic chemistry.

References

1. Girard, P.; Namy, J. L.; Kagan, H. B. *J. Am. Chem. Soc.* **1980**, *102*, 2693.
2. Kagan, H. B.; Namy, J. L.; Girard, P. *Tetrahedron* **1981**, *37*, 175-180.
3. Handa, Y.; Inanaga, J.; Yamaguchi, M. *J. Chem. Soc., Chem. Commun.* **1989**, 276.
4. Künzer, H.; Stahnke, M.; Sauer, G.; Weichert, R. *Tetrahedron Lett.* **1991**, *32*, 1949.
5. Molander, G. A.; Hahn, G. *J. Org. Chem.* **1986**, *51*, 1135-1138.
6. Inanaga, J.; Ishikawa, M. *Chem. Lett* **1987**, 1485.
7. Molander, G. A.; Etter, J. B. *J. Org. Chem.* **1986**, *51*, 1778.
8. Ananthanarayan, T. P.; Gallagher, T.; Magnes, P. J. *Chem. Soc., J. Chem. Soc., Chem. Commun.* **1982**, 709.
9. Crombie, L.; Rainbow, L. J. *Tetrahedron Lett.* **1988**, *29*, 6517.
10. Kende, A. S.; Mendoza, J. S. *Tetrahedron Lett.* **1990**, *31*, 7105.
11. Kende, A. S.; Mendoza, J. S. *Tetrahedron Lett.* **1991**, *32*, 1699.
12. Yoneda, R.; Harusawa, S.; Kurihara, T. *J. Org. Chem.* **1991**, *56*, 1827.
13. Prasad, E.; Flowers, R. A. II. *J. Am. Chem. Soc.* **2002**, *124*, 6895-6899.
14. Chopade, P. R.; Prasad, E.; Flowers, R. A. II. *J. Am. Chem. Soc.* **2004**, *126*, 44-45.
15. Dahlén, A.; Nilsson, Å.; Hilmersson, G. *J. Org. Chem.* **2006**, *71*, 1576-1580.
16. Kagan, H. B.; Namy, J. L. *Tetrahedron* **1986**, *42*, 6573-6614.
17. Flowers, R. A., II; Prasad, E. In *Handbook on the Physics and Chemistry of Rare Earths*. Gschneidner, K. A., Jr., Bunzli, J. G. and Pecharsky, V. K. E., Eds.; Elsevier: Amsterdam, 2006; Vol. 36, pp 393-473.
18. Evans, W. J.; Gummersheimer, T. S.; Ziller, J. W. *J. Am. Chem. Soc.* **1995**, *117*, 8999-9002.
19. Shotwell, B. J.; Sealy, J. M.; Flowers, R. A. II. *J. Org. Chem.* **1999**, *64*, 5251-5255.

20. Kuhlman, M. L.; Flowers, R. A. II. *Tetrahedron Lett.* **2000**, *41*, 8049-8052.
21. Hou, Z.; Fujiwara, Y.; Jintoku, T.; Mine, N.; Yokoo, K.; Taniguchi, H. *J. Org. Chem.* **1987**, *52*, 3524-3528.
22. Molander, G. A.; LaBelle, B. E.; Hahn, G. *J. Org. Chem.* **1986**, *51*, 5259.
23. Matsukawa, M.; Tabuchi, T.; Inanaga, J.; Yamaguchi, M. *Chem. Lett* **1987**, 210.
24. Miller, R. S.; Sealy, J. M.; Shabangi, M.; Kuhlman, M. L.; Fuchs, J. R.; Flowers, R. A. II. *J. Am. Chem. Soc.* **2000**, *122*, 7718-7722.
25. Prasad, E.; Knettle, B. W.; Flowers, R. A. II. *J. Am. Chem. Soc.* **2004**, *126*, 6891-6894.
26. Flowers, R. A. II. *Synlett* **2008**, 1427-1439.
27. Hou, Z.; Wakatsuki, Y. *J. Chem. Soc. , Chem. Commun.* **1994**, 1205-1206.
28. Hou, Z.; Zhang, Y.; Wakatsuki, Y. *Bull. Chem. Soc. Jpn.* **1997**, *70*, 149-153.
29. Enehaerke, R. J.; Hertz, T.; Skrydstrup, T.; Daasbjerg, K. *Chem. Eur. J.* **2000**, *6*, 3747-3754.
30. Shabangi, M.; Flowers, R. A. II. *Tetrahedron Lett.* 1997, *38*, 1137-1140.
31. Enemaerke, R. J.; Daasbjerg, K.; Skrydstrup, T. *Chem. Commun.* **1999**, 343.
32. Shabangi, M.; Flowers, R. A. II. *Tetrahedron Lett.* **2007**, *38*, 1137-1140.
33. Shabangi, M.; Sealy, J. M.; Fuchs, J. R.; Flowers, R. A. II. *Tetrahedron Lett.* **1998**, *39*, 4429-4432.
34. Nishiura, M.; Katagiri, K.; Imamoto, T. *Bull. Chem. Soc. Jpn.* **2001**, *74*, 1417-1424.
35. Molander, G. A.; McKie, J. A. *J. Org. Chem.* **1992**, *57*, 3132-3139.
36. Hasegawa, E.; Curran, D. P. *J. Org. Chem.* **1993**, *18*, 5008-5010.
37. Hojo, M.; Aihara, H.; Hosomi, A. *J. Am. Chem. Soc.* **1996**, *118*, 3533-3534.
38. Sen, A.; Chebolu, V. *Inorg. Chem.* **1987**, *26*, 1821-1823.

39. Hakansson, M.; Vestergren, M.; Gustafsson, B.; Hilmersson, G. *Angew. Chem. Int. Ed.* **1999**, *38*, 2199-2201.
40. Teprovich, J. A.; Balili, M. N.; Pintauer, T.; Flowers, R. A. II. *Angew. Chem. Int. Ed.* **2007**, *46*, 8160-8163.
41. Dahlen, A.; Hilmersson, G. *Tetrahedron Lett.* **2001**, *24*, 5565-5569.
42. Yoshida, A.; Manamoto, T.; Inanaga, J.; Mikami, K. *Tetrahedron Lett.* **1998**, *39*, 1777-1780.
43. Keck, G. E.; Wager, C. A.; Sell, T.; Wager, T. T. *J. Org. Chem.* **1999**, *64*, 2172-2173.
44. Molander, G. A.; Kenny, C. *J. Am. Chem. Soc.* **1989**, *111*, 8236-8246.
45. Yacovan, A.; Hoz, S. *J. Am. Chem. Soc.* **1996**, *118*, 261-262.
46. Johnston, D.; McCusker, C. F.; Muir, K.; Procter, D. J. *J. Chem. Soc., Perkin Trans. 1.* **2000**, 681-695.
47. Hutton, T. K.; Muir, K.; Procter, D. J. *Org. Lett.* **2002**, *4*, 2347.
48. Hutton, T. K.; Muir, K.; Procter, D. J. *Org. Lett.* **2003**, *5*, 4811-4814.
49. Otsubo, K.; Inanaga, J.; Yamaguchi, M. *Tetrahedron Lett.* **1986**, *27*, 5763-5764.
50. Curran, D. P.; Feving, T. L.; Jasperse, C. P.; Tottleben, M. J. *Synlett* **1992**, 943-961.
51. Namy, J. L.; Souppe, J.; Kagan, H. B. *Tetrahedron Lett.* **1983**, *24*, 765.
52. Prasad, E.; Flowers, R. A. I. *J. Am. Chem. Soc.* **2005**, *127*, 18093.
53. Evans, W. J.; Gummersheimer, T. S.; Ziller, J. W. *J. Am. Chem. Soc.* **1995**, *117*, 8999.
54. Evans, W. J.; DeCoster, D. M.; Greaves, J. *Macromolecules* **1995**, *28*, 7929.
55. Maisano, T.; Tempest, K. E.; Sadasivam, D. V.; Flowers, R. A. I. *Org. Biomol. Chem.* **2011**, *9*, 1714-1716.
56. Sautier, B.; Procter, D. J. *Chimia* **2012**, *66*, 399-403.

57. Sadasivam, D. V.; Teprovich, J. A. J.; Procter, D. J.; Flowers, R. A. II. *Org. Lett.* **2010**, *12*, 4140-4143.
58. Fuchs, J. R.; Mitchell, M. L.; Shabangi, M.; Flowers, R. A.,II. *Tetrahedron Lett.* **1997**, *38*, 8157-8158.
59. Kamochi, Y.; Kudo, T. *Tetrahedron Lett.* **1991**, *32*, 3511-3514.
60. Machrouhi, F.; Hamann, B.; Namy, J.L.; Kagan, K. B. *Synlett* **1996**, *7*, 633-634.
61. (a) Machrouchi, F.; Namy, J. L. *Tetrahedron Lett.* **1999**, *40*, 1315-1318. (b) Namy, J.L. *Tetrahedron Lett.* **2002**, *43*, 8007-8010.
62. Ito, Y.; Takahashi, K.; Nagase, H.; Honda, T. *Org. Lett.* **2011**, *13*, 4640-4643.
63. Maity, S.; Ghash, S. *Tetrahedron Lett.* **2007**, *48*, 3355-3358.
64. Molander, G. A.; McKie, J. A. *J. Org. Chem.* **1991**, *56*, 4112-4120.
65. Curran, D. P.; Totleben, M. J. *J. Am. Chem. Soc.* **1992**, *114*, 6050-6058.
66. Fukuzawa, S.; Mutoh, K.; Tsuchimoto, T.; Hiyama, T. *J. Org. Chem.* **1996**, *61*, 5400-5405.
67. Fukuzawa, S. -.; Yahara, Y.; Kamiyama, A.; Hara, M.; Kikuchi, S. *Org. Lett.* **2005**, *7*, 5809-5812.
68. Prasad, E.; Flowers, R. A. I. *J. Am. Chem. Soc.* **2002**, *124*, 6357-6361.
69. Skrydstrup, T.; Jarreton, O.; Mazéas, D.; Urban, D.; Beau, J. M. *Chem. Eur. J.* **1998**, *4*, 655-671.
70. Wipf, P.; Venkatraman, S. *J. Org. Chem.* **1993**, *58*, 3455-3459.
71. Totleben, M. J.; Curran, D. P.; Wipf, P. *J. Org. Chem.* **1992**, *57*, 1740-1744.
72. Molander, G. A.; Harris, C. R. *J. Am. Chem. Soc.* **1995**, *117*, 3705-3716.
73. Nishikawa, K.; Nakahara, H.; Shirokura, Y.; Nogata, Y.; Yoshimura, E.; Umezawa, T.; Okino, T.; Matsuda, F. *Org. Lett.* **2010**, *5*, 904-907.
74. Lowe, J. T.; Panek, J. S. *Org. Lett.* **2008**, *17*, 3813-3816.

75. Bode, H. B.; Zeeck, A. *J. Chem. Soc., Perkin Trans. 1.* **2000**, 323-328.
76. Bode, H. B.; Zeeck, A. *J. Chem. Soc., Perkin Trans. 1.* **2000**, 2665-2670.
77. Molander, G. A.; Quirnbach, M. S.; Silva, L. F. J.; Spencer, K. C.; Balsells, J. *Org. Lett.* **2001**, 3, 2257-2260.
78. Molander, G. A.; Etter, J. B. *J. Am. Chem. Soc.* **1986**, 109, 6556-6558.
79. Fukuzawa, S. -.; Matsuzawa, H.; Yoshimitsu, S. *J. Org. Chem.* **2000**, 65, 1702.
80. Utimoto, K.; Matsui, T.; Takai, T.; Matsubara, S. *Chem. Lett.* **1995**, 24, 197-198.
81. Sparling, B. A.; Moslin, R. M.; Jamison, T. F. *Org. Lett.* **2008**, 10, 1291-1294.
82. Inanaga, J.; Yokoyama, Y.; Handa, Y.; Yamaguchi, M. *Tetrahedron Lett.* **1991**, 32, 6371-6374.
83. Mukaiyama, T.; Shiina, I.; Iwadare, H.; Saitoh, M.; Nishimura, T.; Ohkawa, N.; Sakoh, H.; Nishimura, K.; Tani, Y.; Hasegawa, M.; Yamada, K.; Saitoh, K. *Chem. Eur. J.* **1999**, 5, 121-161.
84. Procter, D. J.; Flowers, R. A. I.; Skrydstrup, T. *Organic Synthesis Using Samarium Diiodide: A Practical Guide*; Royal Society of Chemistry Publishing: UK, 2010.
85. Armesto, D.; Ortiz, M. J.; Agarrabeitia, A. R.; Martin-Fontecha, M. *Org. Lett.* **2004**, 6, 2261-2264.
86. Martin-Fontecha, M.; Agarrabeitia, A. R.; Ortiz, M. J.; Armesto, D. *Org. Lett.* **2010**, 12, 4082-4085.
87. Ratnayake, R.; Covell, D.; Ransom, T. T.; Gustafson, K. R.; Beutler, J. A. *Org. Lett.* **2009**, 11, 57-60.
88. Beutler, J. A.; Ratnayake, R.; Covell, D.; Johnston, T. R. WO 2009/088854, 2009.
89. Li, Z.; Nakashige, M.; Chain, W. J. *J. Am. Chem. Soc.* **2011**, 133, 6553-6556.
90. Fukuzawa, S.; Tsuchimoto, T. *Synlett* **1993**, 803-804.
91. Molander, G. A.; Harnig, L. S. *J. Org. Chem.* **1990**, 55, 6171-6176.

92. Findley, T. J. K.; Sucunza, D.; Miller, L. C.; Davies, D. T.; Procter, D. J. *Chem. Eur. J.* **2008**, *14*, 6862-6865.
93. Foster, S. L.; Handa, S.; Krafft, M.; Rowling, D. *Chem. Commun.* **2007**, 4791-4793.
94. Adinolfi, M.; Barone, G.; Iadonisi, A.; Mangoni, L.; Manna, R. *Tetrahedron* **1997**, *53*, 11767-11780.
95. Arseyiadis, S.; Yashunsky, D. V.; Pereira de Freitas, R.; Munoz, M.; Toromanoff, D. E.; Potier, P. *Tetrahedron Lett.* **1993**, *34*, 1137-1140.
96. Zhong, Y.; Dong, Y.; Fang, K.; Izumi, K.; Xu, M.; Lin, G. *J. Am. Chem. Soc.* **2005**, *127*, 11956-11957.
97. Nicolaou, K. C.; Huang, X.; Giuseppone, N.; Rao, P. B.; Bella, M.; Reddy, M. V.; Snyder, S. A. *Angew. Chem. Int. Ed.* **2001**, *40*, 4705.
98. Nicolaou, K. C.; Snyder, S. A.; Giuseppone, N.; Huang, X.; Bella, M.; Reddy, M. V.; Rao, P. B.; Koumbis, A. E.; Giannakakou, P.; O'Brate, A. *J. Am. Chem. Soc.* **2004**, *126*, 10174.
99. Enholm, E. J.; Forbes, D. C.; Holub, D. P. *Synthetic Commun.* **1990**, *20*, 981-987.
100. Shono, T.; Ohmizu, H.; Kawakami, S.; Sugiyama, H. *Tetrahedron Lett.* **1980**, *21*, 5029.
101. Corey, E. J.; Pyne, S. G. *Tetrahedron Lett.* **1983**, *24*, 2821.
102. Choquette, K. A.; Sadasivam, D. V.; Flowers, R. A. II. *J. Am. Chem. Soc.* **2011**, *133*, 10655-10661.
103. Choquette, K. A.; Sadasivam, D. V.; Flowers, R. A. II. *J. Am. Chem. Soc.* **2010**, *132*, 17396-17398.
104. Sadasivam, D. V.; Antharjanam, P. K. S.; Prasad, E.; Flowers, R. A. II. *J. Am. Chem. Soc.* **2008**, *130*, 7728-7729.
105. Hansen, A. M.; Lindsay, K. B.; Antharjanam, P. K. S.; Karaffa, J.; Daasberg, K.; Flowers, R. A. II.; Skrydstrup, T. *J. Am. Chem. Soc.* **2006**, *128*, 9616-9617.
106. Parmar, D.; Duffy, L. A.; Sadasivam, D. V.; Matsubara, H.; Bradley, P. A.; Flowers, R. A. II.; Procter, D. J. *J. Am. Chem. Soc.* **2009**, *131*, 15467-15473.

107. Prasad, E.; Knettle, B. W.; Flowers, R. A. II. *J. Am. Chem. Soc.* **2002**, *124*, 14663-14667.
108. Fevig, T. L.; Elliot, R. L.; Curran, D. P. *J. Am. Chem. Soc.* **1988**, *110*, 5064.
109. Molander, G. A.; Kenny, C. *J. Org. Chem.* **1991**, *62*, 4511.
110. Beemelmans, C.; Reissig, H. U. *Angew. Chem. Int. Ed.* **2010**, *49*, 8021-8025.
111. Rivkin, A.; Gonzalez-Lopez he Turiso, F.; Nagashima, T.; Curran, D. P. *J. Org. Chem.* **2004**, *69*, 3719-3725.
112. Takanhashi, S.; Kubota, A.; Nakata, T. *Angew. Chem. Int. Ed.* **2002**, *41*, 4751-4754.
113. Helm, M. D.; Sucunza, D.; Silva, M. D.; Helliwell, M.; Procter, D. J. *Tetrahedron Lett.* **2009**, *50*, 3224-3226.
114. Molander, G. A.; Etter, J. B.; Zinke, P. W. *J. Am. Chem. Soc.* **1987**, *109*, 453-463.
115. Molander, G. A.; Czako, B.; Rheam, M. *J. Org. Chem.* **2007**, *72*, 1755-1764.
116. Franz, J. A.; Naushadali, K. S.; Alnajjar, M. S. *J. Org. Chem.* **1986**, *51*, 19-25.
117. Banwell, M. G. H.; David, C. R.; McLeod, M. D. *New J. Chem.* **2003**, *27*, 50-59.
118. Franz, J. A.; Naushadali, K. S.; Alnajjar, M. S. *J. Am. Chem. Soc.* **1989**, *111*, 268-275.
119. Bennett, S. M.; Biboutou, R. K.; Zhou, Z. H.; Pion, R. *Tetrahedron* **1998**, *54*, 4761.
120. Salari, B. S. F.; Biboutou, R. K.; Bennett, S. M. *Tetrahedron* **2000**, *56*, 6385.
121. Farran, H.; Hoz, S. *Org. Lett.* **2008**, *10*, 865-867.
122. Shotwell, B. J.; Flowers, R. A., II *Tetrahedron Lett.* **1998**, *39*, 8063.
123. Curran, D. P.; Fevig, T. L.; Totleben, M. J. *Synlett* **1990**, 773-774.
124. Kagan, H. B. *New J. Chem.* **1991**, *14*, 453.
125. Curran, D. P.; Gu., X.; Zhang, W.; Dowd, P. *Tetrahedron* **1997**, *53*, 9023-9042.
126. Chatgialoglu, C.; Ingold, K. U.; Scaiano, J. C. *J. Am. Chem. Soc.* **1981**, *103*, 7739.

127. Lusztyk, J.; Maillard, B.; Deycard, S.; Lindsay, D. A.; Ingold, K. U. *J. Org. Chem.* **1987**, *52*, 3509.
128. Denmark, S. E.; Beutner, G. L. *Angew. Chem. Int. Ed.* **2008**, *47*, 1560-1638.
129. Denmark, S. E.; Eklov, B. M.; Tao, P. J.; Eastgate, M. D. *J. Am. Chem. Soc.* **2009**, *131*, 11770-11787.
130. Wigfield, D. C. *Can. J. Chem.* **1970**, *48*, 2120-2123.
131. Frisch, M. J. *Gaussian 03, revision E.01*; Gaussian, Inc.: Wallingford, CT, 2004; .
132. Becke, A. D. *J. Chem. Phys.* **2009**, *98*, 5648-5652.
133. Hariharan, P. C.; Pople, J. A. *Theor. Chim. Acta* **1973**, *28*, 213-222.
134. Onsager, L. *J. Am. Chem. Soc.* **1936**, *58*, 1486-1493.
135. Wong, M. W.; Frisch, M. J.; Wiberg, K. B. *J. Am. Chem. Soc.* **1991**, *113*, 4776-4782.
136. Edmonds, D. J.; Johnston, D.; Procter, D. J. *Chem. Rev.* **2004**, *104*, 3371-3403.
137. Dahlén, A.; Hilmersson, G. *Eur. J. Org. Chem.* **2004**, 3393-3403.
138. Kagan, H. B. *Tetrahedron* **2003**, *59*, 10351-10372.
139. Molander, G. A. *Chem. Rev.* **1992**, *92*, 29-68.
140. Molander, G. A.; Huérou, V. L.; Brown, G. A. *J. Org. Chem.* **2001**, *66*, 4511-4516.
141. Still, I. W. J.; Toste, D. F. *J. Org. Chem.* **1996**, *61*, 7677-7680.
142. Kagan, H. B. *J. Alloy Compd.* **2006**, 408-412.
143. Molander, G. A.; Harris, C. R. *J. Org. Chem.* **1997**, *62*, 7418-7429.
144. Molander, G. A.; Jean, D. J. S. Jr. *J. Org. Chem.* **2002**, *67*, 3861-3865.
145. Jamison, T. F. *Tetrahedron* **2006**, *62*, 7493-7610.
146. Shukla, P.; Cheng, C. H. *Org. Lett.* **2006**, *8*, 2867-2869.

147. Li, Z.; Deng, Y.; Wu, Y.; Shen, B.; Hu, W. *J. Mater. Sci.* **2007**, *42*, 9243-9238.
148. Li, Z.; Han, C.; Shen, J. *J. Mater. Sci.* **2006**, *41*, 3437-3480.
149. Alonso, F.; Calvino, J. J.; Osante, I.; Yus, M. *Chem. Lett.* **2005**, *34*, 1262-1263.
150. Wu, S. H.; Chen, D. H. *Chem. Lett.* **2004**, *33*, 406-407.
151. Tsuji, M.; Hashimoto, M.; Tsuji, T. *Chem. Lett.* **2002**, *31*, 1232-1233.
152. Harris, D. C. In *Quantitative Chemical Analysis*; Quantitative Chemical Analysis, 6th Edition; W.H. Freeman and Company: New York, **2003**; pp AP23-AP31.
153. Ogoshi, S.; Morita, M.; Inoue, K.; Kurosawa, H. *J. Organomet. Chem.* **2004**, *689*, 662-665.
154. Pedersen, S. U.; Lund, T.; Daasbjerg, K.; Pop, M.; Fussing, I.; Lund, H. Pedersen, S.U.; Lund, T.; Daasbjerg, K.; Pop, M.; Fussing, I.; Lund, H. *Acta. Chem. Scand.* **1998**, *52*, 657.
155. Molander, G. A.; Alonso-Alija, C. *J. Org. Chem.* **1998**, *63*, 4366-4373.
156. Machrouchi, F.; Namy, J. L.; Kagan, H. B. *Tetrahedron Lett.* **1997**, *38*, 7183-7186.
157. Kang, H. Y.; Song, S. E. *Tetrahedron Lett.* **2000**, *41*, 937-939.
158. Molander, G. A.; Wolfe, C. N. *J. Org. Chem.* **1998**, *63*, 9031-9036.
159. Creighton, J. A.; Eadon, D. G. *J. Chem. Soc. Faraday Trans.* **1991**, *87*, 3881-3891.
160. Matthew, J. S.; Klussmann, M.; Iwamura, H.; Valera, F.; Futran, A.; Emanuelsson, A. C. E.; Blackmond, D. G. *J. Org. Chem.* **2006**, *71*, 4711-4722.
161. Blackmond, D. G. *Angew. Chem. Int. Ed.* **2005**, *44*, 4302-4320.
162. Devery, J.; Conrad, J.; MacMillan, D.; Flowers, R. A. II. *Angew. Chem. Int. Ed.* **2010**, *49*, 6106-6110.
163. Sacco, A.; Mastroilli, P. *J. Chem. Soc. Dalton Trans.* **1994**, 2461-2764.
164. Kihara, M.; Ishida, Y.; Kobayashi, S. *J. Chem. Research* **1987**, 236-237.
165. Kihara, M.; Kashimoto, M.; Kobayashi, S. *Tetrahedron* **1992**, *48*, 67-78.

166. Kamochi, Y.; Kudo, T. *Chem. Lett.* **1993**, 1495.
167. Duffy, L. A.; Matsubara, H.; Procter, D. J. *J. Am. Chem. Soc.* **2008**, *130*, 1136-1137.
168. Malatesta, V.; Ingold, K. U. *J. Am. Chem. Soc.* **1981**, *103*, 609.
169. Giese, B.; Dupuis, J. *Tetrahedron Lett.* **1984**, *25*, 1349.
170. Cohen, T.; Bhupathy, M. *Acc. Chem. Res.* **1989**, *22*, 152.
171. Guazzelli, G.; De Grazia, S.; Collins, K. D.; Matsubara, H.; Spain, M.; Procter, D. J. *J. Am. Chem. Soc.* **2009**, *131*, 7214-7215.
172. Parmar, D.; Price, K.; Spain, M.; Matsubara, H.; Bradley, P. A.; Procter, D. J. *J. Am. Chem. Soc.* **2011**, *133*, 2418-2420.
173. Baker, T. M.; Sloan, L. A.; Choudhury, L. H.; Murai, M.; Procter, D. J. *Tetrahedron: Asymmetry* **2010**, *21*, 1246-1261.
174. Dahlén, A.; Hilmersson, G. *Tetrahedron Lett.* **2002**, *43*, 7197-7200.
175. Evans, W. J.; Drummond, D. K.; Zhang, H.; Atwood, J. L. *Inorg. Chem.* **1988**, *27*, 575-579.
176. Brady, E. D.; Clark, D. L.; Keogh, D. W.; Scott, B. L.; Watkin, J. G. *J. Am. Chem. Soc.* **2002**, *124*, 7007-7015.
177. Barlaam, B.; Boivin, J.; Zard, S. Z. *Tetrahedron Lett.* **1993**, *34*, 1023-1026.
178. Wang, L.; Zhou, L. H.; Zhang, Y. M. *Synlett* **1999**, 1065-1066.
179. Cabri, W.; Candiani, I.; Colombo, M.; Franzoi, L.; Bedeschi, A. *Tetrahedron Lett.* **1995**, *36*, 949-952.
180. Kamochi, Y.; Kudo, T. *Chem. Lett.* **1991**, 893-896.
181. Kamochi, Y.; Kudo, T. *Bull. Chem. Soc. Jpn.* **1992**, *65*, 3049-3054.
182. Dahlén, A.; Hilmersson, G. *Chem. Eur. J.* **2003**, *9*, 1123-1128.
183. Dahlén, A.; Hilmersson, G.; Knettle, B. W.; Flowers, R. A. II *J. Org. Chem.* **2003**, *68*, 4870-4875.

184. Dahlén, A.; Hilmersson, G. *Tetrahedron Lett.* **2003**, *44*, 2661-2664.
185. Ankner, T.; Hilmersson, G. *Org. Lett.* 2009, *11*, 503-506. *Org. Lett.* 2009, *11*, 503-506.
186. Ankner, T.; Hilmersson, G. *Tetrahedron* 2009, *65*, 10856-10862. *Tetrahedron* 2009, *65*, 10856-10862.
187. Dahlén, A.; Sundgren, A.; Lahmann, M.; Oscarson, S.; Hilmersson, G. *Org. Lett.* **2003**, *5*, 4085-4088.
188. Dahlén, A.; Hilmersson, G. *J. Am. Chem. Soc.* **2005**, *127*, 8340-8347.
189. Soai, K.; Oyamada, H.; Ookawa, A. *Synthetic Commun.* **1982**, *12*, 463-467.
190. Bianco, A.; Passacantilli, P.; Righi, G. *Synthetic Commun.* **1988**, *18*, 1765-1771.
191. Szostak, M.; Spain, M.; Procter, D. J. *Chem. Commun.* **2011**, *47*, 10254-10256.
192. Holm, T. *J. Am. Chem. Soc.* **1999**, *121*, 515-518.
193. Ashby, E. C.; Boone, J. R. *J. Am. Chem. Soc.* **1976**, *18*, 5524-5531.
194. Wigfield, D. C.; Phelps, D. *Can. J. Chem.* **1972**, *50*, 388-394.
195. Hammond, G. S. *J. Am. Chem. Soc.* **1955**, *77*, 334-338.
196. Hammes-Schiffer, S. *Chem. Rev.* **2010**, *110*, 6937-6938.
197. Hammes-Schiffer, S.; Stuchebrukhov, A. A. *Chem. Rev.* **2010**, *110*, 6939-6960.
198. Warren, J. J.; Tronic, T. A.; Mayer, J. M. *Chem. Rev.* **2010**, *110*, 6961-7001.
199. Keller, D. A.; Marshall, C. E.; Lee, K. P. *Fundam. Appl. Toxicol.* **1997**, *40*, 15-29.
200. European Commission for Employment, Social Affairs and Inclusion Recommendation from the Scientific Committee on Occupational Exposure Limits for hexamethylphosphoramide. *SCOEL/SUM/156* 2010, *SCOEL/SUM/156*.
201. Evans, D. H.; O'Connell, K. M.; Petersen, R. A.; Kelly, M. *J. Chem. Ed.* **1983**, *60*, 290-293.

Chapter 8. Appendix

8.1 SmI₂ Reduction of an Aldehyde vs. α,β -Unsaturated Ester

8.1.1 Compound Identification

8.1.1.1 **3-butyl-3,6,6-trimethylcyclohex-1-ene methylcarboxylate** ¹H NMR (500MHz, CDCl₃) δ (ppm): 0.8734 (3H, t, CH₃); 0.9678 (3H, s, CH₃); 1.1638 (6Hb d, 2 CH₃); 1.2324 (6H, m, 3 CH₂); 1.4972 (4H, m, 2 CH₂); 3.6810 (3H, s, CH₃); 6.4661 (1H, s, CH). ¹³C NMR (125MHz, CDCl₃) δ (ppm):14.0745; 23.4667; 26.2290; 26.4601; 27.5564; 28.0852; 30.1700; 32.9985; 35.7159; 36.9693; 41.8596; 51.1155; 136.5166; 147.6901; 168.1623. GC-MS *m/z* (rel. abundance) 238 (10), 181 (32.5), 121 (100). HRLCMS (ESI) calcd for (+H) C₁₅H₂₇O₂: 239.2024, found: 256.2740.

8.1.2 Kinetic Data: Stopped-Flow Plots

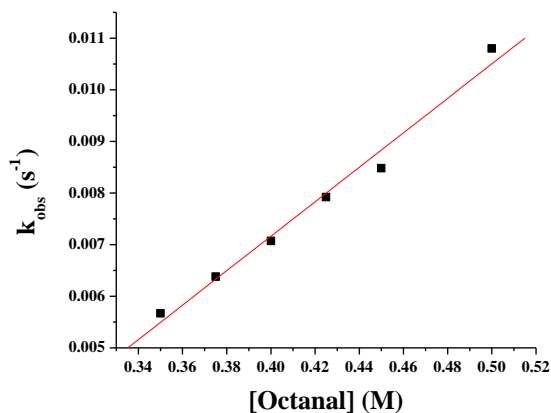


Figure 8.1.2.1. Pseudo-first order rate constant of octanal with TFE. SmI₂ 5 mM, TFE 125 mM, octanal 350-500 mM. Rate constant $0.03 \pm 0.01 \text{ M}^{-1}\text{s}^{-1}$

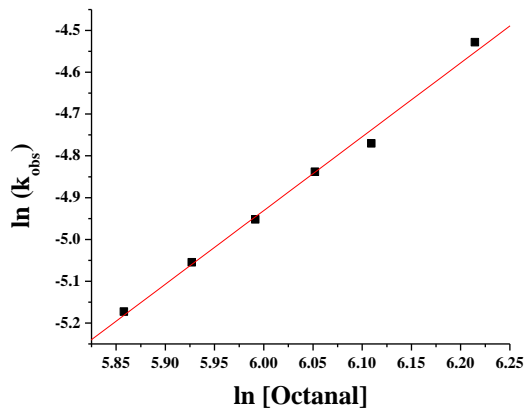


Figure 8.1.2.2. Pseudo-first order rate order of octanal with TFE. SmI_2 5 mM, TFE 125 mM, octanal 350-500 mM. Rate Order 1.8 ± 0.1 .

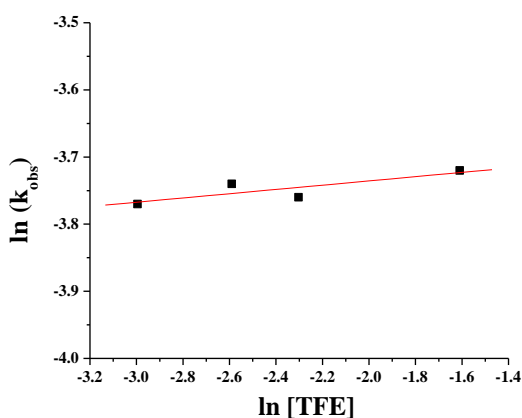


Figure 8.1.2.3. Pseudo-first order rate order of TFE with octanal. SmI_2 5 mM, octanal 40 mM, TFE 50-200 mM,. Rate Order 0.03 ± 0.01 .

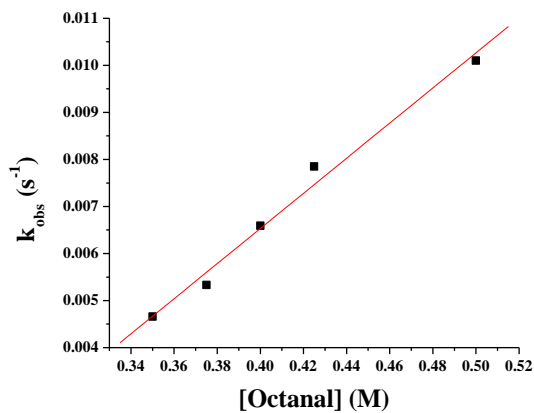


Figure 8.1.2.4. Pseudo-first order rate constant of octanal with tBuOH. SmI_2 5 mM, tBuOH 125 mM, octanal 350-500 mM. Rate constant $0.04 \pm 0.01 \text{ M}^{-1}\text{s}^{-1}$

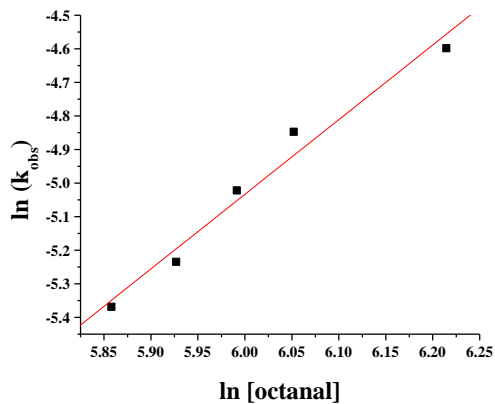


Figure 8.1.2.5. Pseudo-first order rate order of octanal with tBuOH. SmI_2 5 mM, tBuOH 125 mM, octanal 350-500 mM. Rate Order 2.2 ± 0.2 .

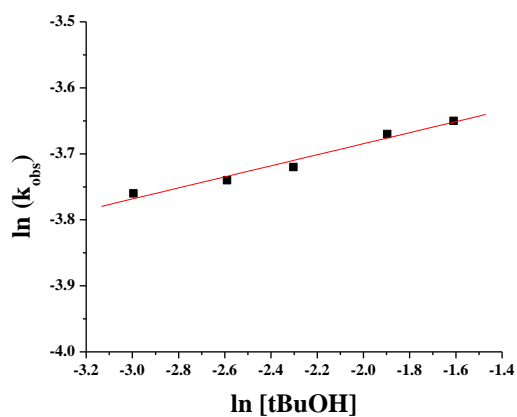


Figure 8.1.2.6. Pseudo-first order rate order of tBuOH with octanal. SmI_2 5 mM, octanal 40 mM, tBuOH 50-200 mM. Rate Order 0.08 ± 0.01 .

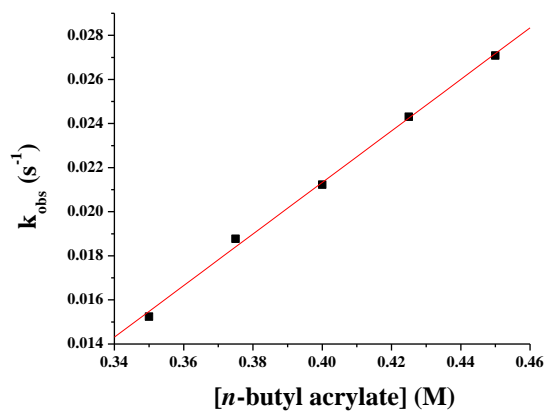


Figure 8.1.2.7. Pseudo-first order rate constant of *n*-butyl acrylate with TFE. SmI_2 5 mM, TFE 125 mM, *n*-butyl acrylate 350-450 mM. Rate constant $0.12 \pm 0.003 \text{ M}^{-1}\text{s}^{-1}$

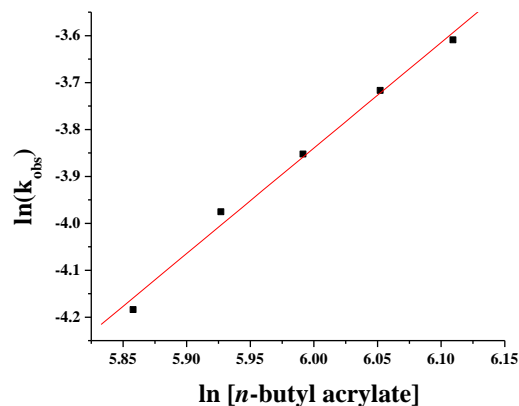


Figure 8.1.2.8. Pseudo-first order rate order of *n*-butyl acrylate with TFE. SmI_2 5 mM, TFE 125 mM, *n*-butyl acrylate 350-450 mM. Rate Order 2.2 ± 0.12 .

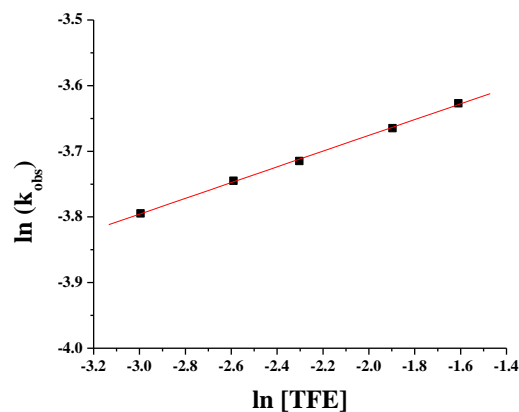


Figure 8.1.2.9. Pseudo-first order rate order of TFE with *n*-butyl acrylate. SmI_2 5 mM, *n*-butyl acrylate 40 mM, TFE 50-200 mM. Rate Order 0.11 ± 0.02

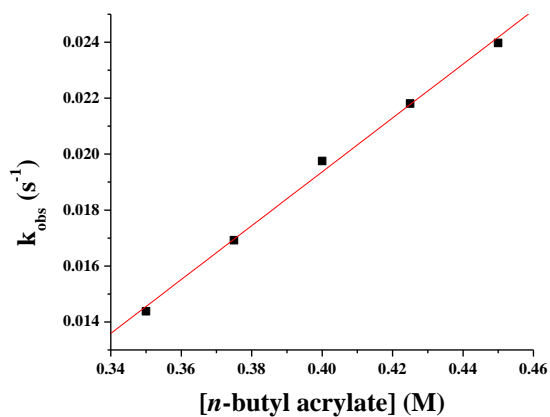


Figure 8.1.2.10. Pseudo-first order rate constant of *n*-butyl acrylate with tBuOH. SmI_2 5 mM, tBuOH 125 mM, *n*-butyl acrylate 350-450 mM. Rate Constant $0.10 \pm 0.01 \text{ M}^{-1}\text{s}^{-1}$.

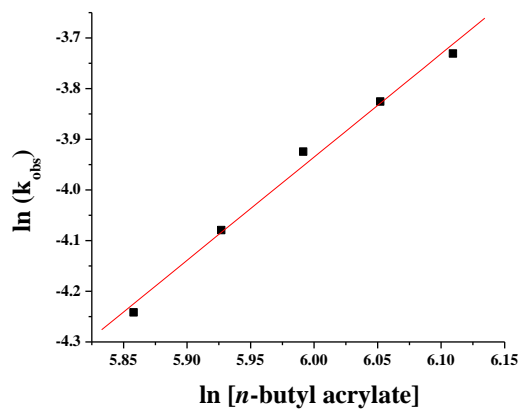


Figure 8.1.2.11. Pseudo-first order rate order of *n*-butyl acrylate with tBuOH. SmI₂ 5 mM, tBuOH 125 mM, *n*-butyl acrylate 350-450 mM. Rate Order 2.04 ± 0.11 .

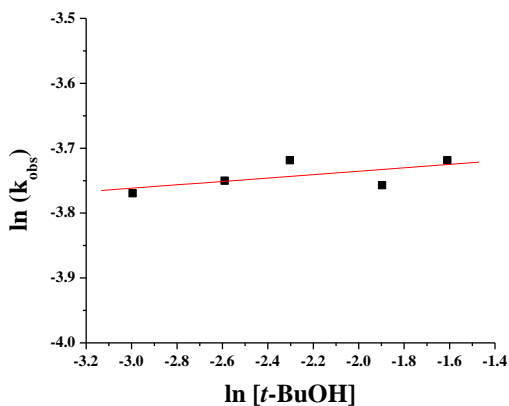


Figure 8.1.2.12. Pseudo first order rate order of tBuOH with *n*-butyl acrylate. SmI₂ 5 mM, *n*-butyl acrylate 40 mM, tBuOH 50-200 mM,. Rate Order 0.03 ± 0.02

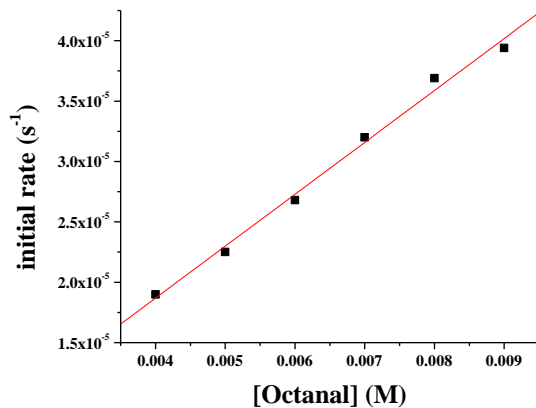


Figure 8.1.2.13. Initial rates rate constant of octanal with TFE. SmI₂ 5 mM, tBuOH 125 mM, octanal 4-9 mM. Linear region 20-150 s. Rate Constant $0.004 \pm 0.001 \text{ M}^{-1}\text{s}^{-1}$.

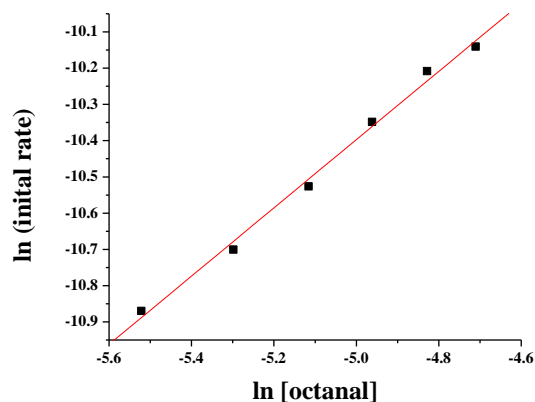


Figure 8.1.2.14. Initial rates rate order of octanal with TFE. SmI_2 5 mM, TFE 125 mM, octanal 4-9 mM. Linear region 20-150 s. Rate order 0.94 ± 0.04 .

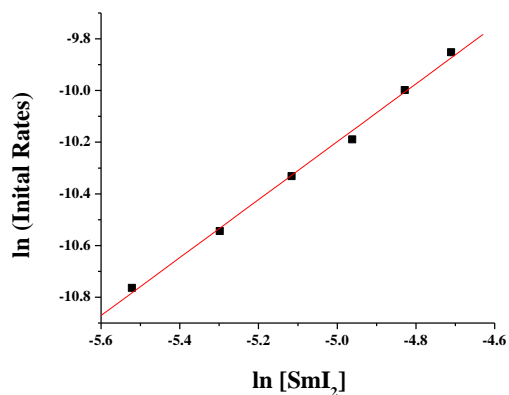


Figure 8.1.2.15. Initial rates rate order of SmI_2 with octanal and TFE. Octanal 5 mM, TFE 125 mM, SmI_2 4-9 mM. Linear region 20-150 s. Rate order 1.1 ± 0.03 .

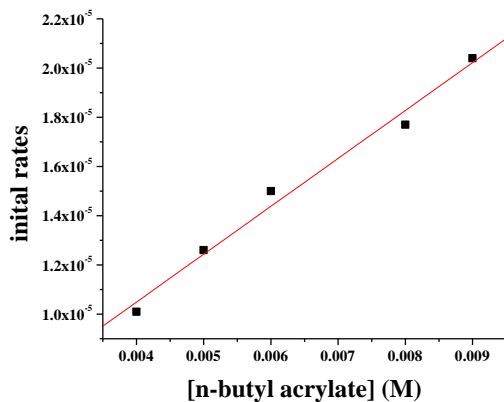


Figure 8.1.2.16. Initial rates rate constant of *n*-butyl acrylate with TFE. SmI_2 5 mM, TFE 125 mM, *n*-butyl acrylate 4-9 mM. Linear region 20-200 s. Rate Constant $0.002 \pm 1.3 \times 10^{-4} \text{ M}^{-1} \text{ s}^{-1}$.

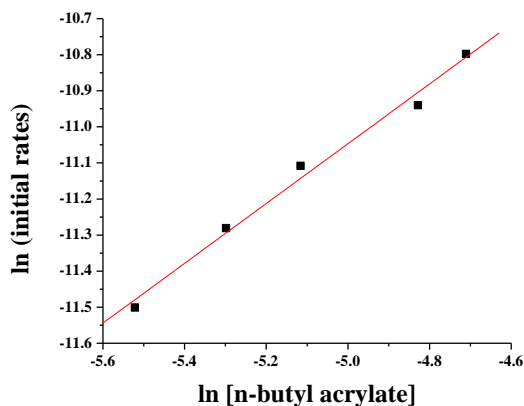


Figure 8.1.2.17. Initial rates rate order of *n*-butyl acrylate with TFE. SmI₂ 5mM, TFE 125 mM, *n*-butyl acrylate 4-9 mM. Linear region 20-200 s. Rate Order 0.83 ± 0.05 .

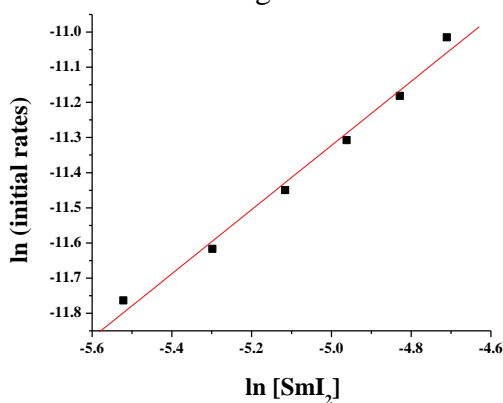


Figure 8.1.18. Initial rates rate order of SmI₂ with *n*-butyl acrylate, TFE. *n*-butyl acrylate 5 mM, TFE 125 mM, SmI₂ 4-9 mM. Linear region 20-250 s. Rate order 0.91 ± 0.05 .

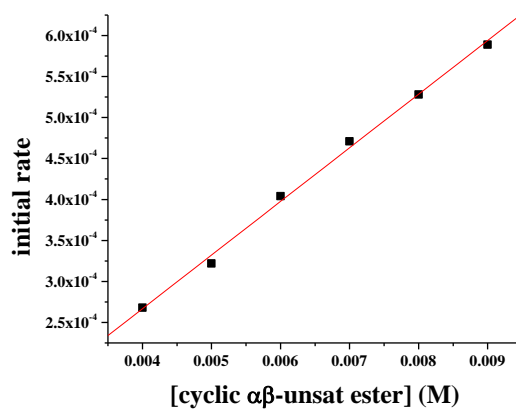


Figure 8.1.19 Initial rates rate constant of cyclic α,β -unsat. ester with TFE. SmI₂ 5 mM, TFE 125 mM, cyclic α,β -unsat. ester 4-9 mM. Linear region 20-80 s. Rate constant $(6.5 \pm 0.03) \times 10^{-2}$.

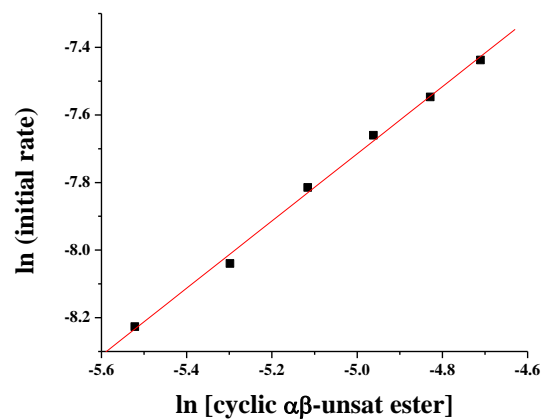


Figure 8.1.20. Initial rates rate order of cyclic α,β -unsat. ester with TFE SmI_2 5 mM, TFE 125 mM, cyclic α,β -unsat. ester 4-9 mM. Linear region 20-80 s. Rate Order 0.99 ± 0.03 .

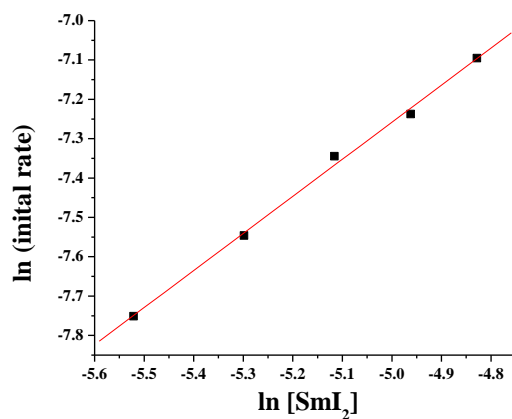
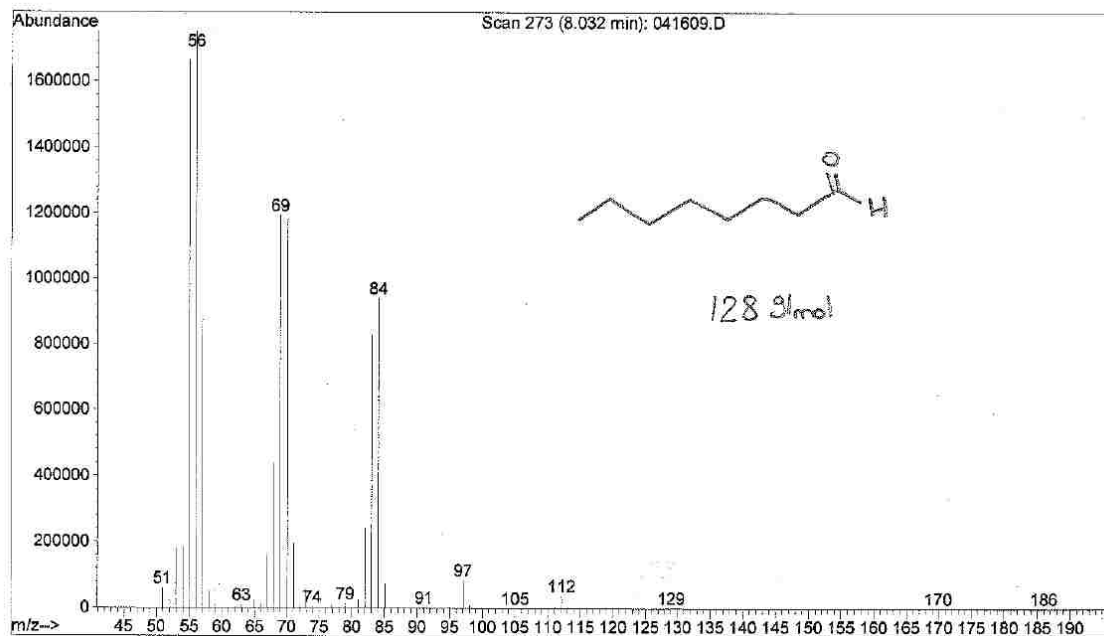
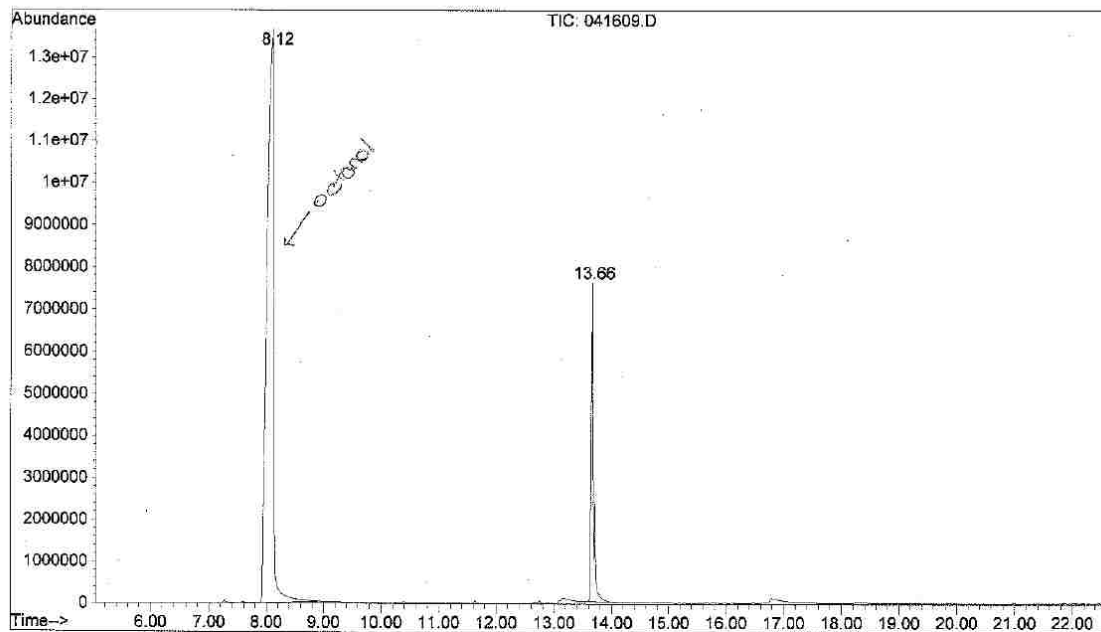


Figure 8.1.21. Initial rates rate order of SmI_2 with α,β -unsat. ester and TFE. α,β -unsat. ester 5 mM, TFE 125 mM, SmI_2 4-9 mM. Linear region 4-25 s. Rate order 0.94 ± 0.03 .

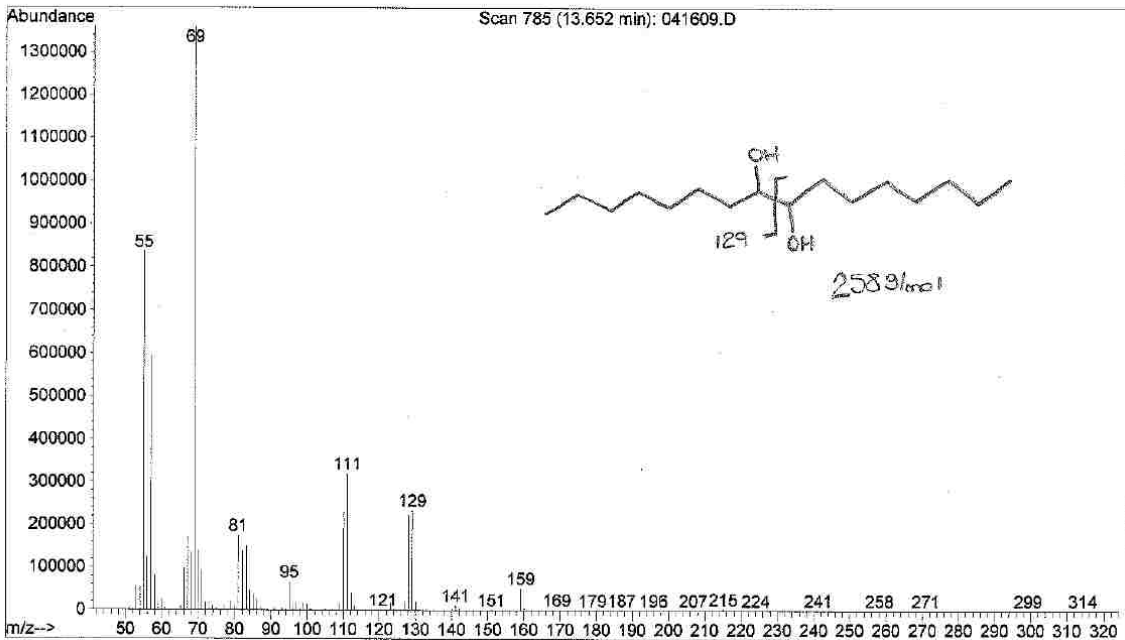
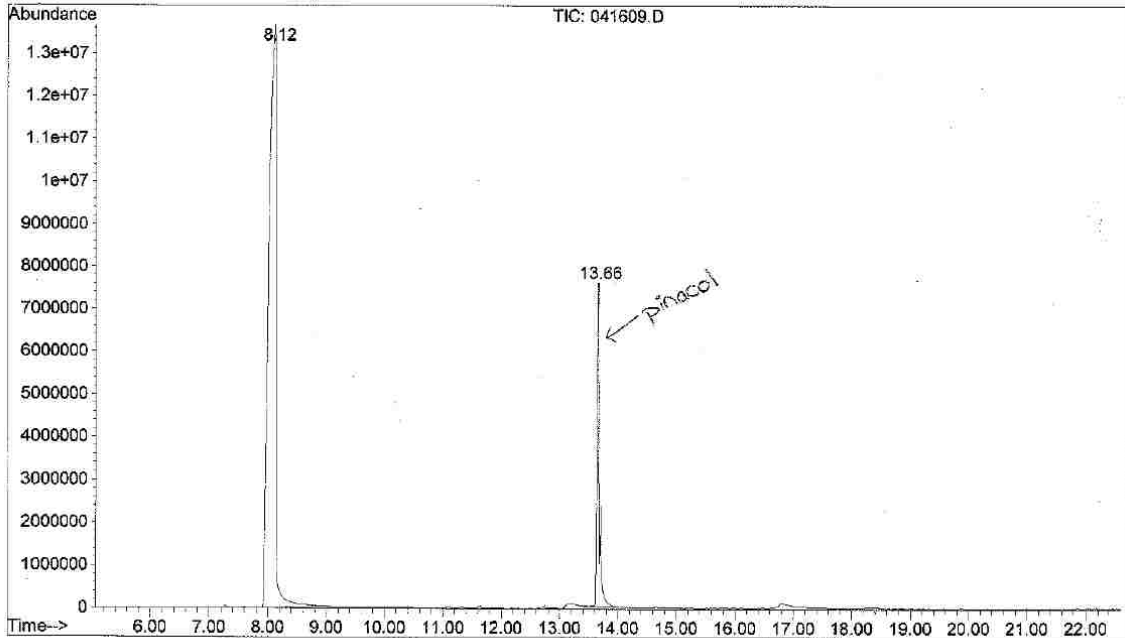
8.1.3 GC-MS Plots: Product Identification

File : C:\HPCHEM\1\DATA\SADA\041609.D
Operator : kim
Acquired : 16 Apr 2009 11:51 using AcqMethod SADA4
Instrument : GC/MS Ins
Sample Name: octanal-tbut-fract10
Misc Info :
Vial Number: 1



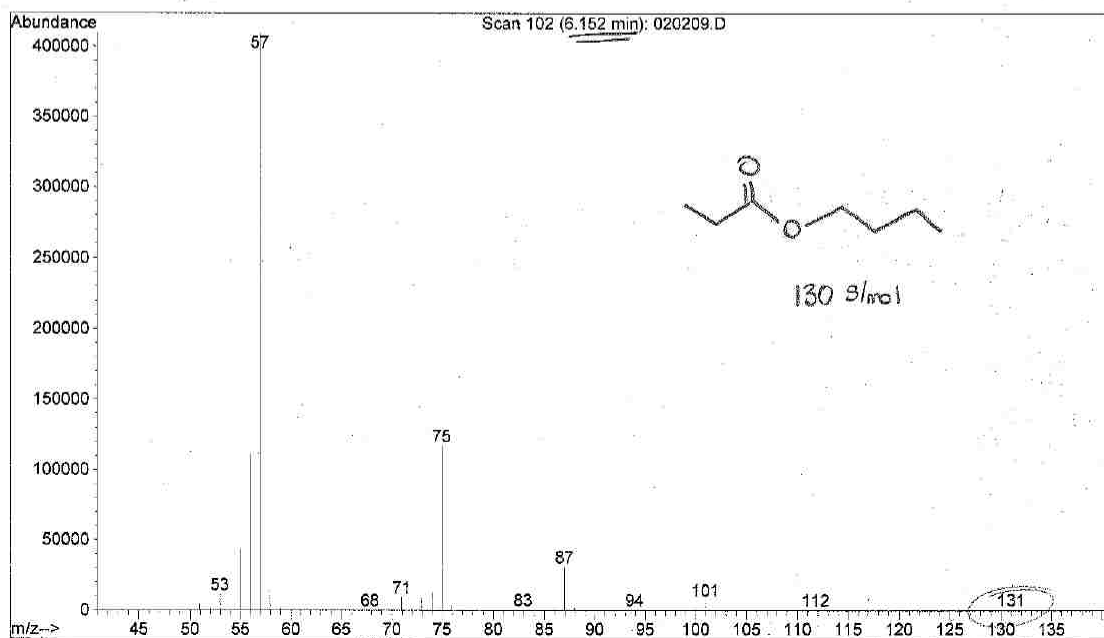
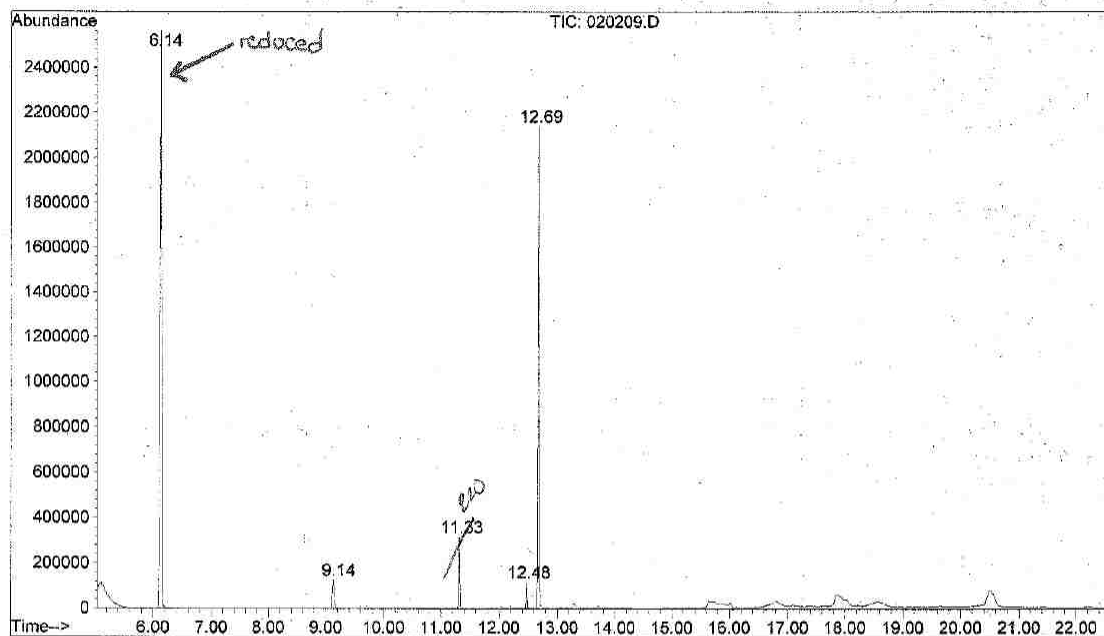
8.1.3.1 Octanal reduction product distribution—octanol GC-MS

File : C:\HPCHEM\1\DATA\SADA\041609.D
 Operator : kim
 Acquired : 16 Apr 2009 11:51 using AcqMethod SADA4
 Instrument : GC/MS Ins
 Sample Name: octanal-tbut-fract10
 Misc Info :
 Vial Number: 1



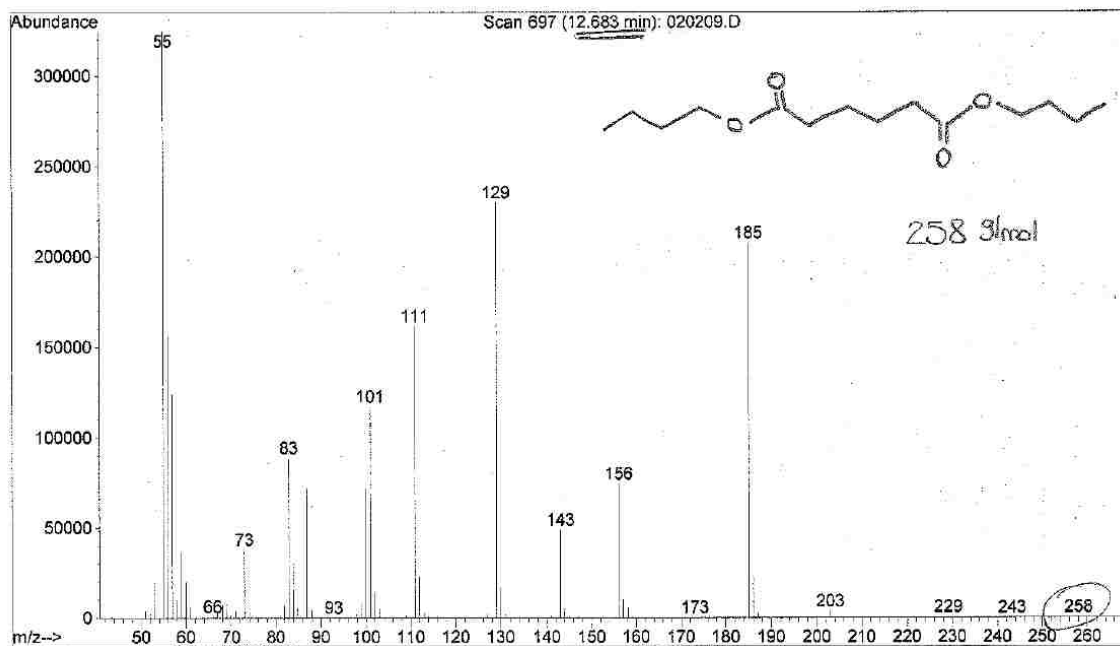
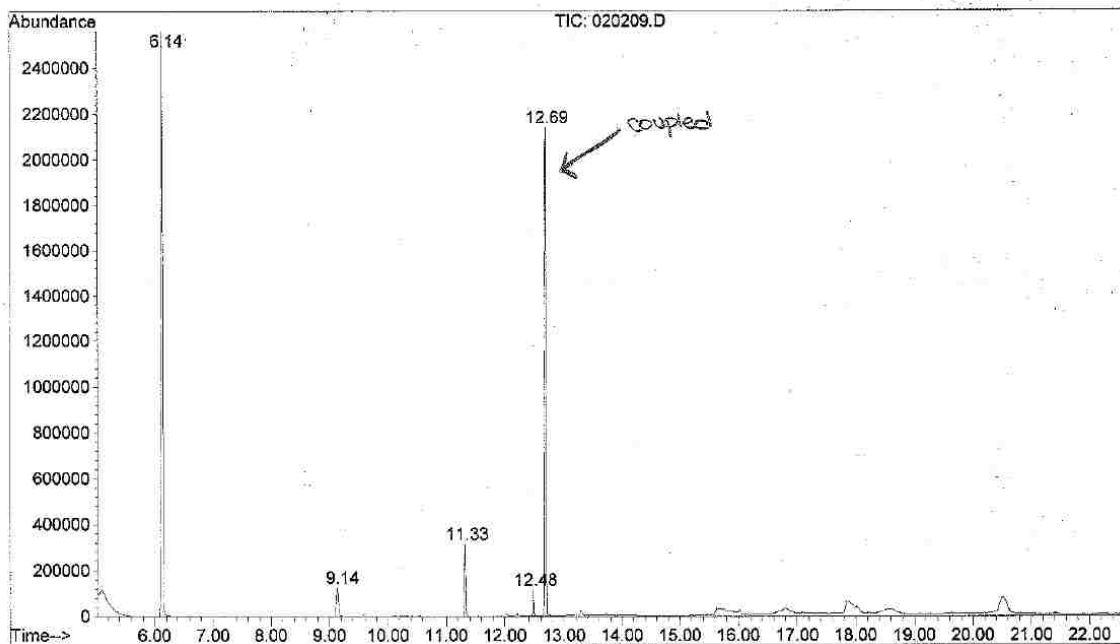
8.1.3.2 Octanal reduction product distribution —pinacol GC-MS

File : C:\HPCHEM\1\DATA\SADA\020209.D
Operator : KIM
Acquired : 2 Feb 2009 18:09 using AcqMethod SADA4
Instrument : GC/MS Ins
Sample Name: NBUTYL ACRYLATE/SMI2
Misc Info :
Vial Number: 1



8.1.3.3 *n*-butyl acrylate reduction product distribution—reduced ester GC-MS

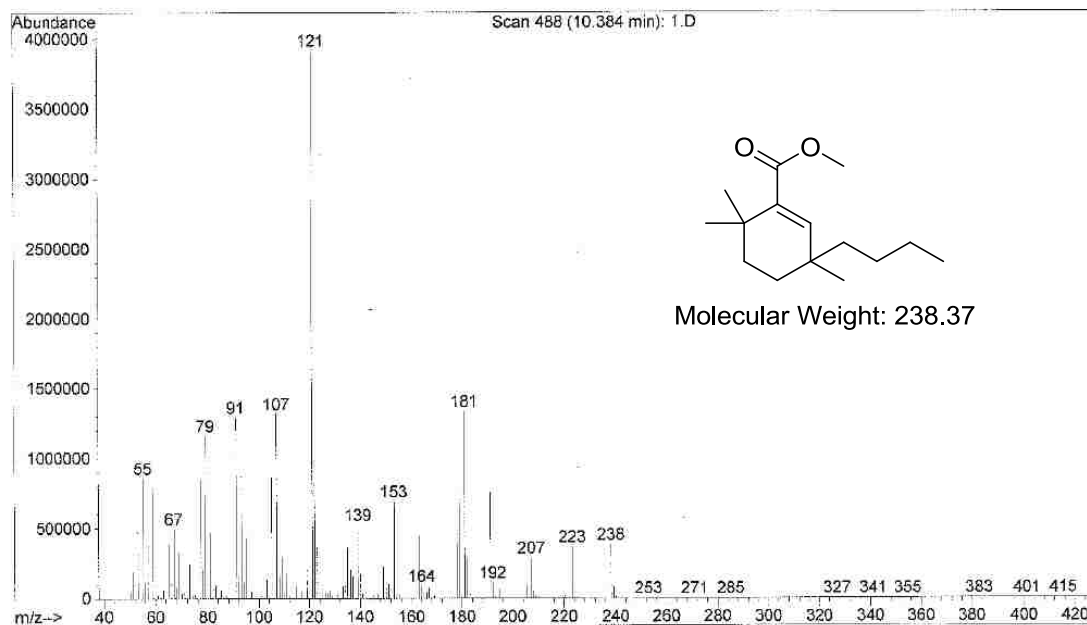
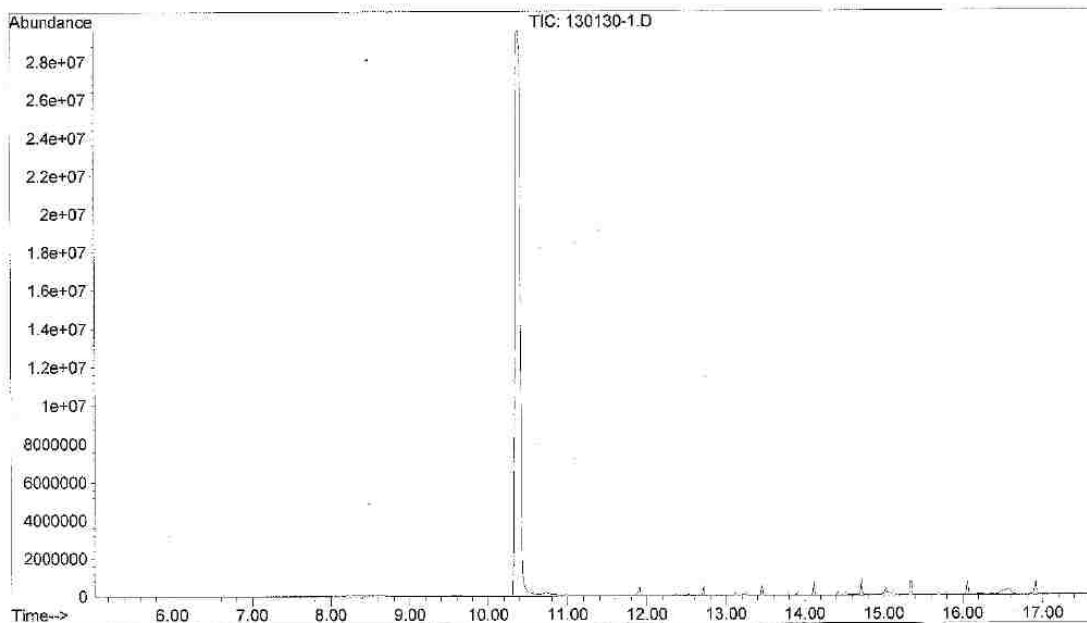
File : C:\HPCHEM\1\DATA\SADA\020209.D
Operator : KIM
Acquired : 2 Feb 2009 18:09 using AcqMethod SADA4
Instrument : GC/MS Ins
Sample Name: NBUTYL ACRYLATE/SMI2
Misc Info :
Vial Number: 1



8.3.1.4 *n*-butyl acrylate reduction product distribution—coupled GC-MS

8.1.4 Starting Material Characterization

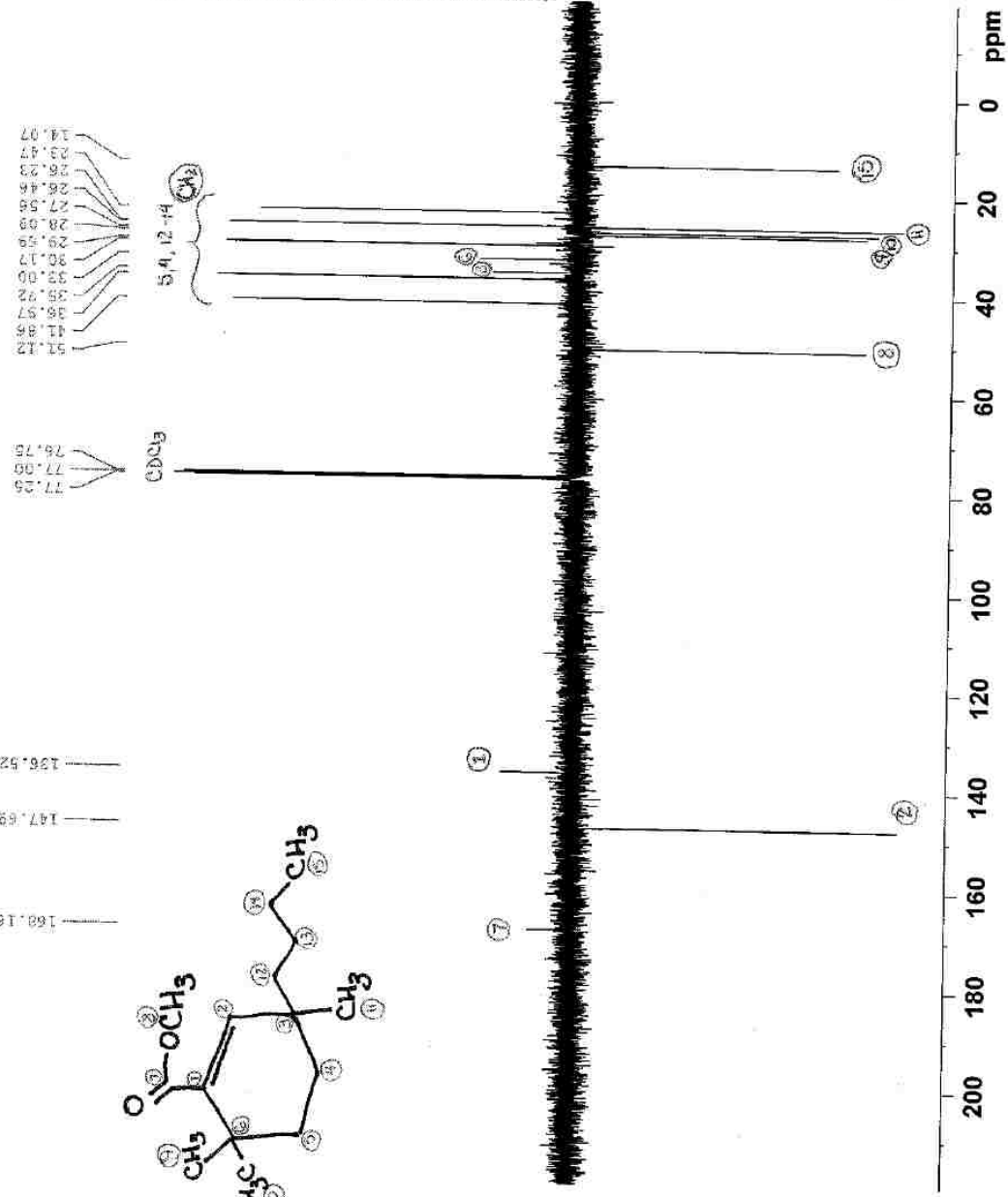
File : C:\HPCHEM\1\DATA\KAT208\130130-1.D
Operator : kim
Acquired : 30 Jan 2013 9:37 using AcqMethod SADA4
Instrument : GC/MS Ins
Sample Name: 3butyl366trimethylcyclohex-1-ene,ethylcarboxy
Misc Info : recovered from kinetics
Vial Number: 1



8.1.4.1 GC-MS 3-butyl-3,6,6-trimethylcyclohex-1-ene methylcarboxylate



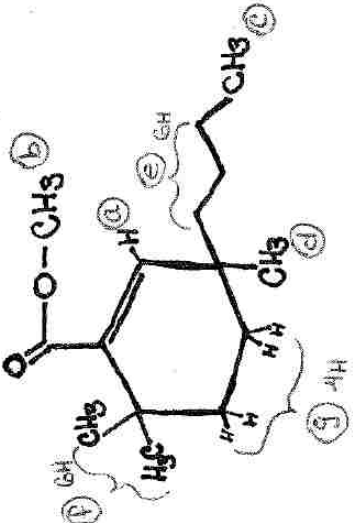
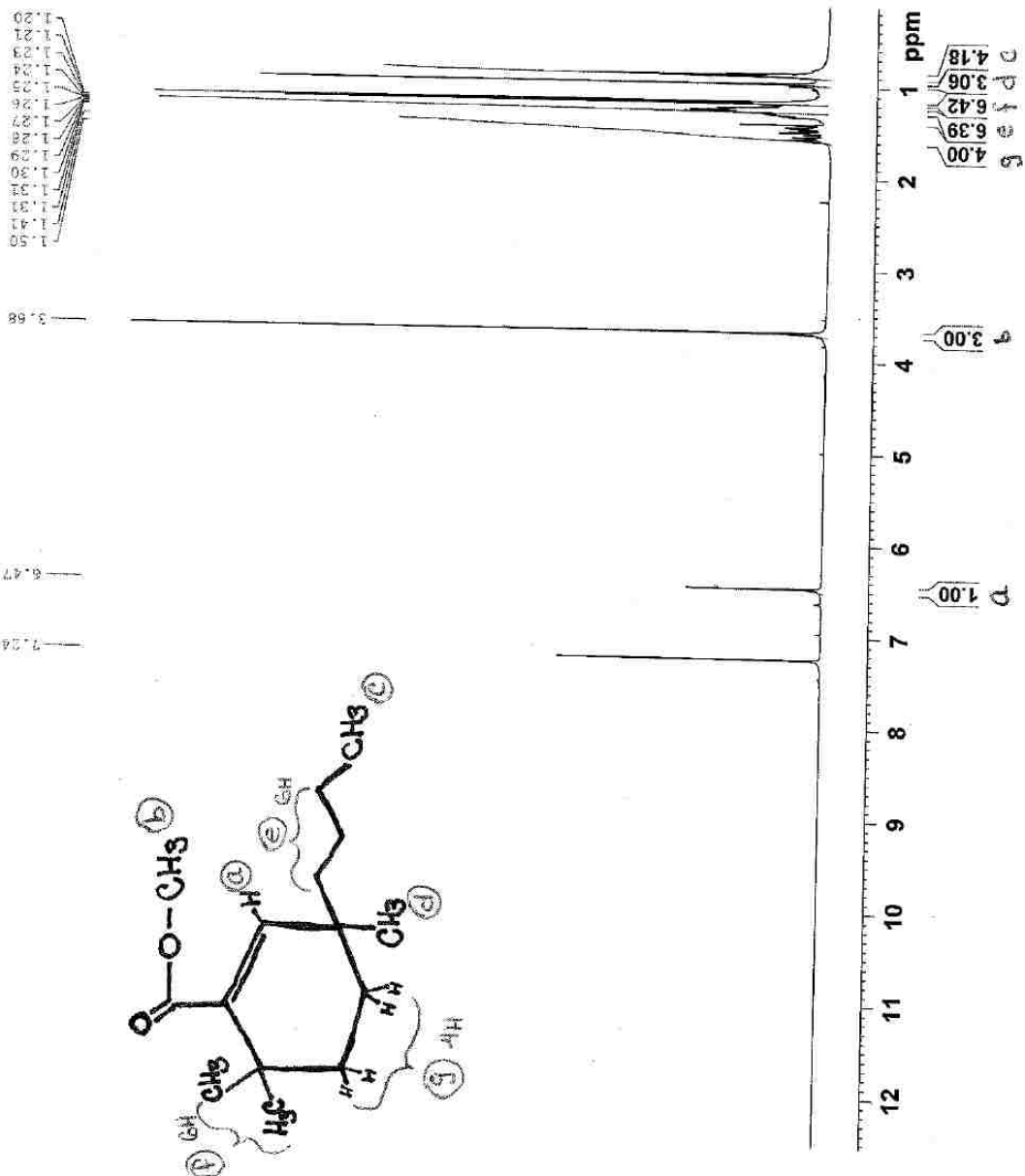
Date: 01/28/2014
 Time: 17:12:53
 Name: 3-butyl-3,6,6-trimethylcyclohex-1-ene methylcarboxylate
 Acq. Mode: 1D
 P1: 12.00
 PC: Acquisition Parameters
 Date_Time: 01/28/2014
 Time: 17:12:53
 Instrument: spect
 Processor: zgpg30
 F2: 125.761
 Aquisition: 300000
 Resolution: 0.3270
 SFO: 500
 AQ: 5.980
 RG: 655
 Data Size: 32768
 Memory Used: 3123
 TD: 65536
 File Name: 3-butyl-3,6,6-trimethylcyclohex-1-ene methylcarboxylate
 Processing: 2
 Scale: 0.00100000
 GB: 1
 PC: Processing parameters
 Date_Time: 01/28/2014
 Time: 17:12:53
 Instrument: spect
 Processor: zgpg30
 F2: 125.761
 Aquisition: 300000
 Resolution: 0.3270
 SFO: 500
 AQ: 5.980
 RG: 655
 Data Size: 32768
 Memory Used: 3123
 TD: 65536
 File Name: 3-butyl-3,6,6-trimethylcyclohex-1-ene methylcarboxylate
 Processing: 2
 Scale: 0.00100000
 GB: 1
 PC: Processing parameters



8.1.4.2 ¹³C NMR 3-butyl-3,6,6-trimethylcyclohex-1-ene methylcarboxylate



Date: 2010-07-26
 Time: 10:00:00
 File: 20100726_001
 F2 - Acquisition Parameters
 Name: 20100726_001
 Date_UTC: 2010-07-26 10:00:00
 Time: 10:00:00
 Date: 2010-07-26
 Time: 10:00:00
 File: 20100726_001
 F2 - Processing parameters
 Name: 20100726_001
 Date_UTC: 2010-07-26 10:00:00
 Time: 10:00:00
 Date: 2010-07-26
 Time: 10:00:00
 File: 20100726_001
 F2 - Processing parameters
 Name: 20100726_001
 Date_UTC: 2010-07-26 10:00:00
 Time: 10:00:00
 Date: 2010-07-26
 Time: 10:00:00
 File: 20100726_001



8.1.4.3 ¹H NMR 3-butyl-3,6,6-trimethylcyclohex-1-ene methylcarboxylate

8.2. Impact of HMPA on the Samarium Barbier Reaction

8.2.1 Product Identification

8.2.1.1 **(4) 3-ethylpentadecan-3-ol** ^1H NMR (500MHz, CDCl_3) δ (ppm): 0.8438 (9H, m, 3 CH_3); 0.9567 (1H s, OH, peak disappears with the addition of D_2O), 1.2370 (20H br s, 10 CH_2); 1.3922 (2H, m, CH_2); 1.4262 (4H, q, $\text{C}(2)\text{H}_2$, $\text{CH}_3\text{CH}_2\text{-C}_{13}\text{H}_{26}\text{-OH}$); OH. ^{13}C NMR (125MHz, CDCl_3) δ (ppm): 7.7941; 14.1343; 22.7060; 23.4124; 29.3702; 29.6622; 29.6814; 30.3263; 31.0478; 31.9376; 38.2339; 74.6412. GC-MS m/z (rel. abundance) 227 (64), 87 (100). HRLCMS (ESI) calcd for $\text{C}_{17}\text{H}_{36}\text{O}$: 256.2761, found: 256.2740.

8.2.1.2 **(5) 3-ethyltridecan-3-ol** ^1H NMR (500MHz, CDCl_3) δ (ppm): 0.8385 (9H, m, 3 CH_3); 1.0981 (1H s, OH, peak disappears with the addition of D_2O), 1.2475 (16H br d, 8 CH_2); 1.4015 (2H, m, CH_2); 1.4319 (4H, q, $\text{C}(2)\text{H}_2$, $\text{CH}_3\text{CH}_2\text{-C}_{13}\text{H}_{26}\text{-OH}$). ^{13}C NMR (125MHz, CDCl_3) δ (ppm): 7.7341; 14.0790; 22.6581; 23.3659; 29.3184; 29.6093; 29.6277; 29.6369; 30.2890; 30.9592; 31.8863; 38.1513, 74.5240. GC-MS m/z (rel. abundance) 199 (34), 87 (100). HRMS (ESI) ($n+\text{Na}$) calcd for $\text{C}_{15}\text{H}_{32}\text{NaO}$: 251.2345, found: 251.2356.

8.2.1.3 **(10) 3-ethyl-4-methylhexan-3-ol** ^1H NMR (500MHz, CDCl_3) δ (ppm): 0.8157-0.9561 (12H, m, 4 CH_3); 1.4097-1.5008 (6H, m, 3 CH_3); 1.5154-1.5903 (1H, m, CH); 2.7926 (1H, s, OH, peak disappears with the addition of D_2O). ^{13}C NMR (125MHz, CDCl_3) δ (ppm): 7.4602; 7.5402; 12.9455; 12.9765; 23.3603; 27.9715; 28.0339; 41.1559; 76.3495. GC-MS m/z (rel. abundance) 115 (54), 87 (100). HRMS (ESI) ($\text{M}+\text{nH}$) calcd for $\text{C}_9\text{H}_{20}\text{O}$: 145.1600, found: 145.1587.

8.2.1.4 **(12) 3-ethyl-2-methylpentan-3-ol** ^1H NMR (500MHz, CDCl_3) δ (ppm): 0.849 (12H, m, 4 CH_3); 0.993 (1H s, OH, peak disappears with the addition of D_2O), 1.435 (2H, m, CH_2); 1.499 (2H, m, CH_2); 1.758 (1H, m, CH). ^{13}C NMR (125MHz, CDCl_3) δ

(ppm):7.593; 16.738; 27.748; 33.496; 75.918. GC-MS m/z (rel. abundance) 101 (94), 87 (100), 57 (83). HRMS (ESI) ($M+nH$) calcd for $C_8H_{18}O$: 131.1430.

8.2.2 Kinetic Data: Stopped-Flow Plots

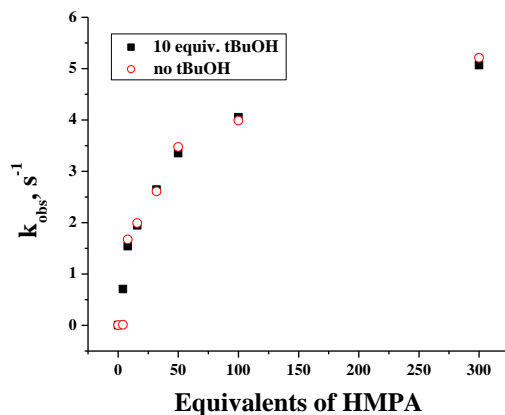


Figure 8.2.2.1 Equivalents of HMPA versus k_{obs} for the reduction of **1**. Comparison of data with and without proton donor source. ■ $SmI_2 = 5$ mM; tBuOH = 10 equiv.; **1** = 22 equiv.; HMPA = 0-300 equiv. ○ $SmI_2 = 5$ mM; **1** = 22 equiv.; HMPA = 0-300 equiv.

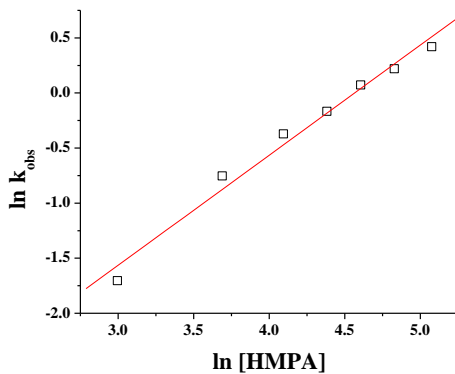


Figure 8.2.2.2 Plot of $\ln[HMPA]$ versus $\ln k_{obs}$ for the reduction of **1**. Rate order of HMPA = 1.0 ± 0.1 . $SmI_2 = 5$ mM; **1** = 22 equiv.; HMPA = 0-32 equiv.

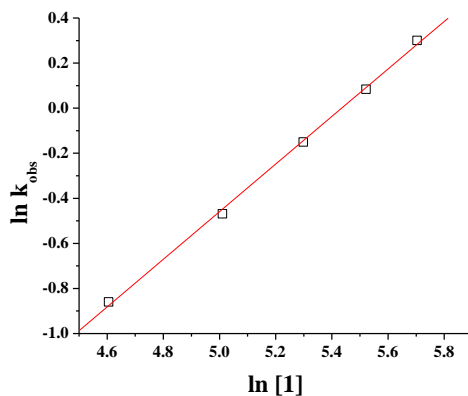


Figure 8.2.2.3 Plot of $\ln[1]$ versus $\ln k_{\text{obs}}$ for the reduction of **1**. Reaction order of **1** = 1.1 ± 0.1 . $\text{SmI}_2 = 5 \text{ mM}$; HMPA = 10 equiv.; **1** = 10-60 equiv.

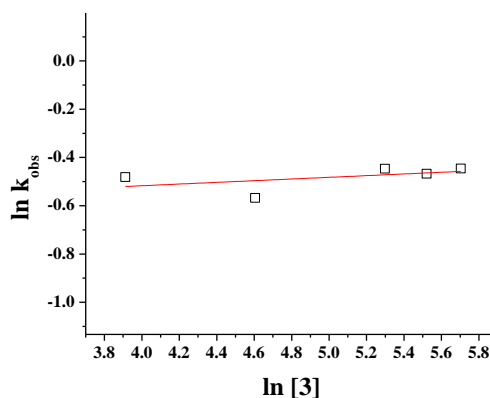


Figure 8.2.2.4 Plot of $\ln[3]$ versus $\ln k_{\text{obs}}$. Rate order of **3**- zero. $\text{SmI}_2 = 5 \text{ mM}$; **1** = 22 equiv.; HMPA = 10 equiv.; **3** = 10-60 equiv.

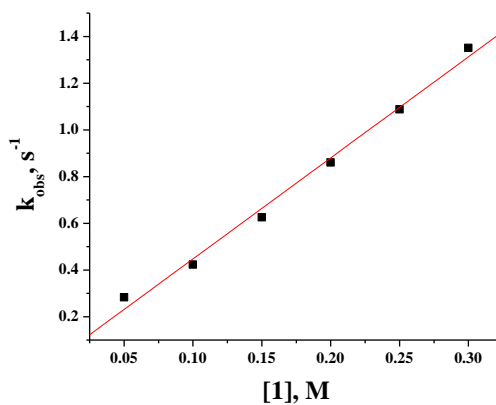


Figure 8.2.2.5 Plot of $[1]$ versus k_{obs} for the reduction of **1**. Rate constant for reduction of **1** = $4.32 \pm 0.20 \text{ M}^{-1}\text{s}^{-1}$. $\text{SmI}_2 = 5 \text{ mM}$; HMPA = 10 equiv.; **1** = 10-60 equiv.

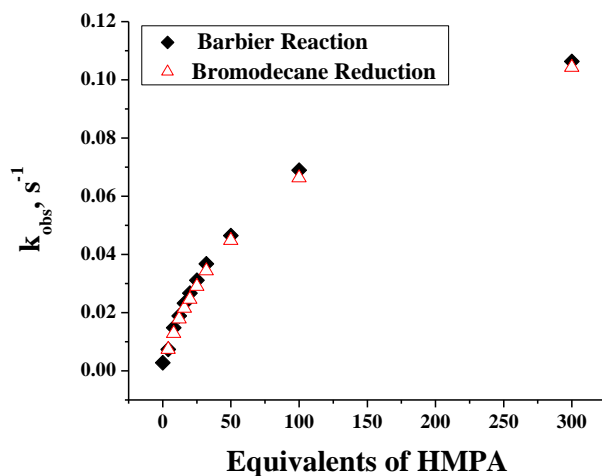


Figure 8.2.2.6 Equivalents of HMPA versus k_{obs} for the reduction of **2** and the samarium barbier reaction with **2**. Comparison of k_{obs} values with and without a ketone present. \blacklozenge $\text{SmI}_2 = 5 \text{ mM}$; **2** = 25 equiv.; **3** = 25 equiv.; HMPA = 0-300 equiv. \triangle $\text{SmI}_2 = 5 \text{ mM}$; **2** = 25 equiv.; HMPA = 0-300 equiv.

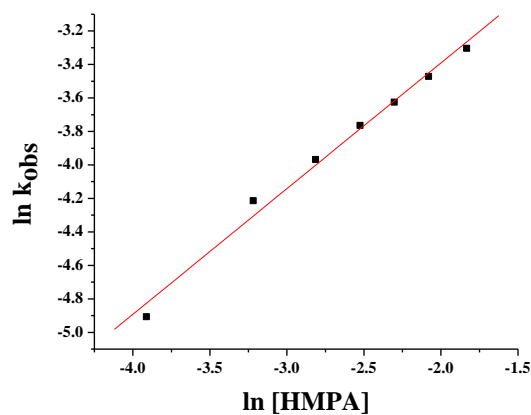


Figure 8.2.2.7 Rate order plot of HMPA with **2** in Samarium Barbier reaction. $\ln[\text{HMPA}]$ versus $\ln k_{\text{obs}}$. $\text{SmI}_2 = 5 \text{ mM}$; **2** = 25 equiv.; **3** = 25 equiv.; HMPA = 0-32 equiv. Rate order = 0.8 ± 0.1 .

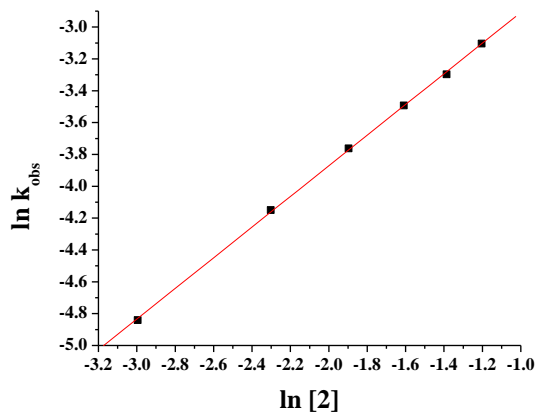


Figure 8.2.2.8 Rate order plot of **2**. $\ln[2]$ versus $\ln k_{\text{obs}}$. $\text{SmI}_2 = 5 \text{ mM}$; **2** = 10-60 equiv.; **3** = 25 equiv.; HMPA = 10 equiv. Rate order = 0.96 ± 0.01 .

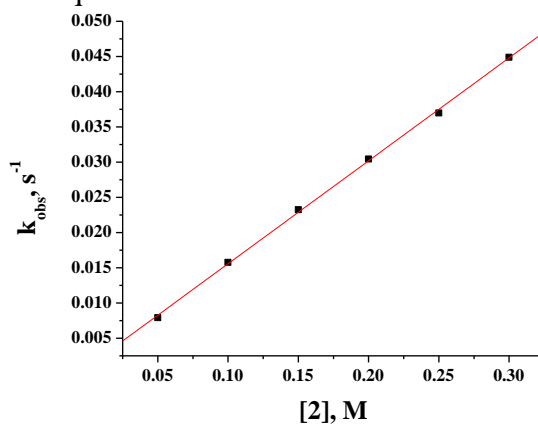


Figure 8.2.2.9 Rate constant plot of **2** in samarium Barbier reaction. $[2]$ versus k_{obs} . $\text{SmI}_2 = 5 \text{ mM}$; **2** = 10-60 equiv.; **3** = 25 equiv.; HMPA = 10 equiv. Rate constant = $0.15 \pm 0.01 \text{ M}^{-1} \text{ s}^{-1}$.

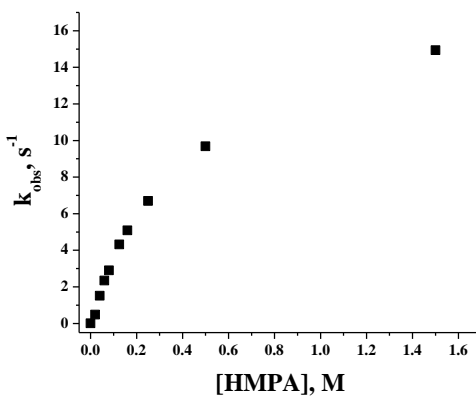


Figure 8.2.2.10 $[\text{HMPA}]$ versus k_{obs} for the SBR with 2-iodobutane. $\text{SmI}_2 = 5 \text{ mM}$; **6** = 25 equiv.; 3-pentanone = 25 equiv.; HMPA = 0-300 equiv.

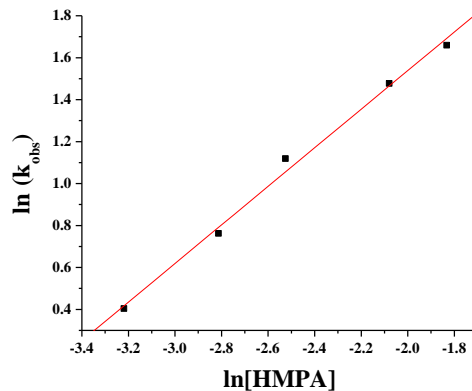


Figure 8.2.2.11 Plot of $\ln[\text{HMPA}]$ versus $\ln k_{\text{obs}}$ for the SBR with 2-iodobutane. Rate order of HMPA = 0.92 ± 0.04 . $\text{SmI}_2 = 5 \text{ mM}$; **6** = 25 equiv.; **3** = 25 equiv.; HMPA = 8-32 equiv.

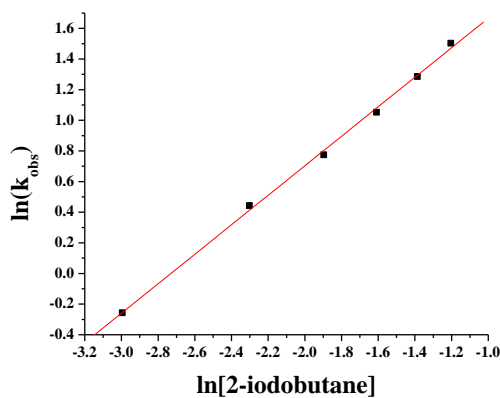


Figure 8.2.2.12 Plot of $\ln[\mathbf{6}]$ versus $\ln k_{\text{obs}}$ for the SBR with 2-iodobutane. Reaction order of **6** = 0.96 ± 0.02 . $\text{SmI}_2 = 5 \text{ mM}$; HMPA = 10 equiv.; **3** = 25 equiv.; **6** = 10-60 equiv.

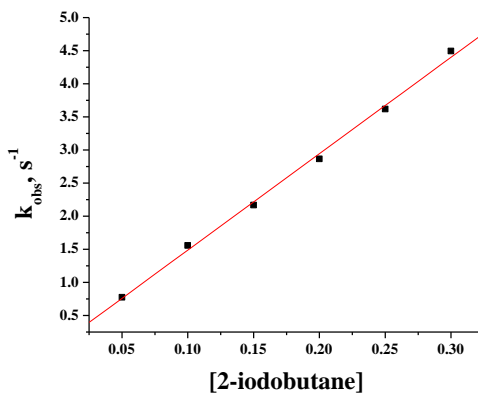


Figure 8.2.2.13 Plot of $[\mathbf{6}]$ versus k_{obs} for the SBR with 2-iodobutane. Rate constant for SBR with **6** = $14.56 \pm 0.40 \text{ M}^{-1}\text{s}^{-1}$. $\text{SmI}_2 = 5 \text{ mM}$; HMPA = 10 equiv.; **3** = 25 equiv.; **6** = 10-60 equiv.

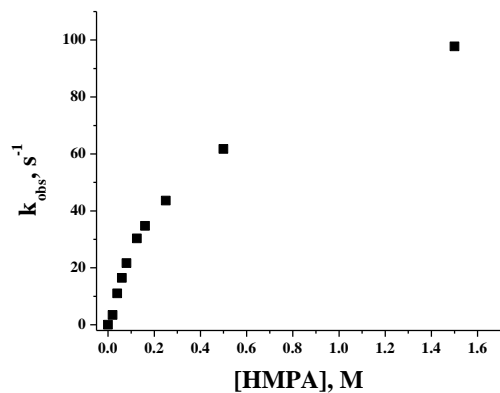


Figure 8.2.2.14 [HMPA] versus k_{obs} for the SBR with **7**. $SmI_2 = 5$ mM; **7** = 25 equiv.; **3** = 25 equiv.; HMPA = 0-300 equiv.

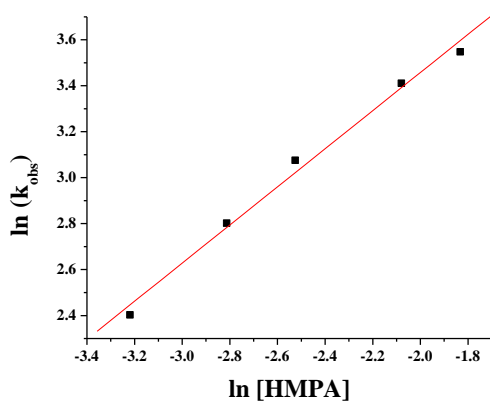


Figure 8.2.2.16 Plot of $\ln[HMPA]$ versus $\ln k_{obs}$ for the SBR with **7**. Rate order of HMPA = 0.83 ± 0.05 . $SmI_2 = 5$ mM; **7** = 25 equiv.; **3** = 25 equiv.; HMPA = 8-32 equiv.

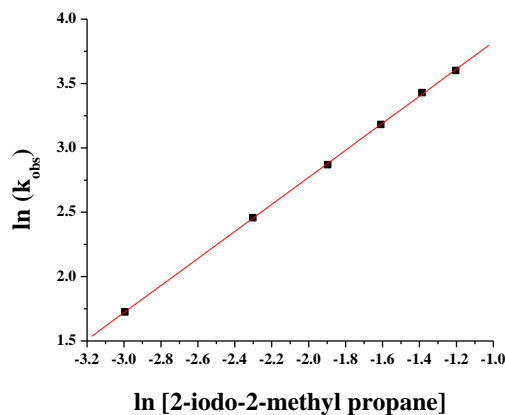


Figure 8.2.2.17 Plot of $\ln[7]$ versus $\ln k_{obs}$ for the SBR with **7**. Reaction order of **7** = 1.05 ± 0.01 . $SmI_2 = 5$ mM; HMPA = 10 equiv.; **3** = 25 equiv.; **7** = 10-60 equiv.

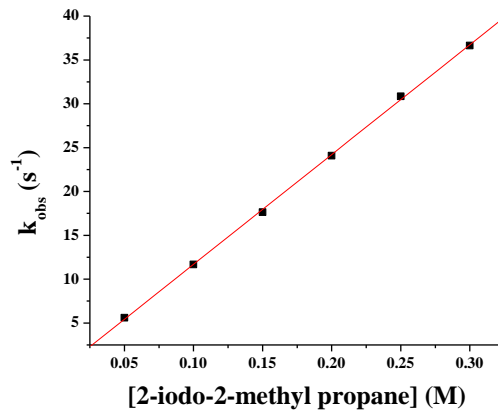


Figure 8.2.2.18 Plot of [7] versus k_{obs} for the SBR with 7. Rate constant for SBR with 7 = $125.2 \pm 1.3 \text{ M}^{-1}\text{s}^{-1}$. $\text{SmI}_2 = 5 \text{ mM}$; HMPA = 10 equiv.; 3 = 25 equiv.; 7 = 10-60 equiv.

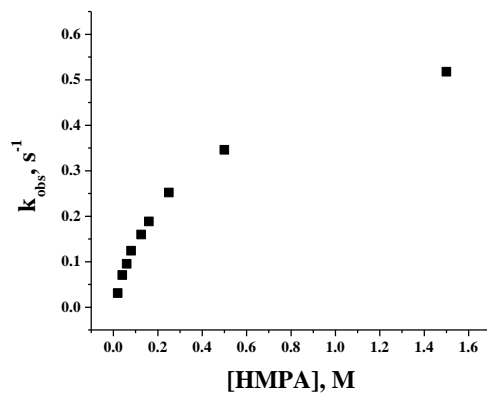


Figure 8.2.2.19 [HMPA] versus k_{obs} for the SBR with 2-bromopropane. $\text{SmI}_2 = 5 \text{ mM}$; 8 = 25 equiv.; 3 = 25 equiv.; HMPA = 0-300 equiv.

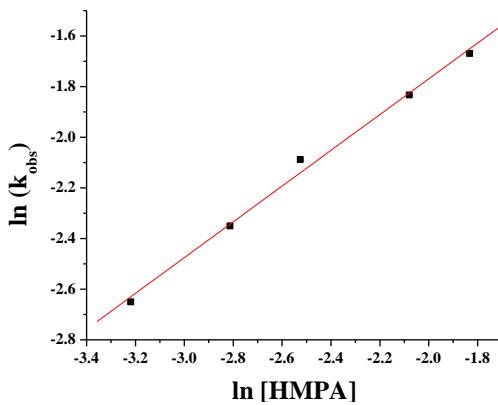


Figure 8.2.2.20 Plot of $\ln[\text{HMPA}]$ versus $\ln k_{obs}$ for the SBR with 8. Rate order of HMPA = 0.71 ± 0.03 . $\text{SmI}_2 = 5 \text{ mM}$; 8 = 25 equiv.; 3 = 25 equiv.; HMPA = 8-32 equiv.

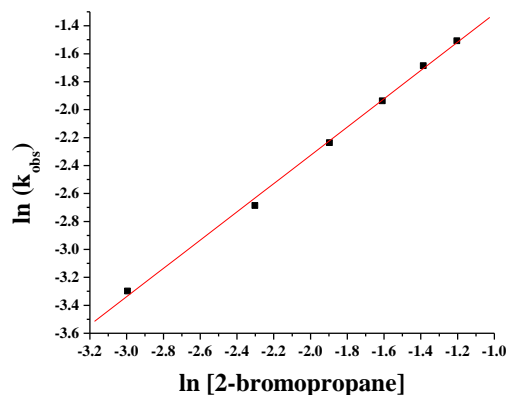


Figure 8.2.2.21 Plot of $\ln[\mathbf{8}]$ versus $\ln k_{\text{obs}}$ for the SBR with $\mathbf{8}$. Reaction order of $\mathbf{8} = 1.0 \pm 0.02$. $\text{SmI}_2 = 5 \text{ mM}$; HMPA = 10 equiv.; $\mathbf{3} = 25 \text{ equiv.}$; $\mathbf{8} = 10\text{-}60 \text{ equiv.}$

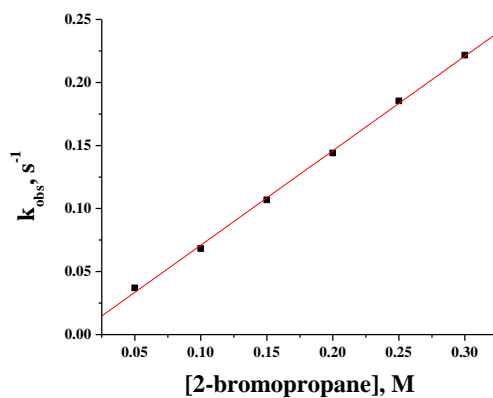


Figure 8.2.2.22 Plot of $[\mathbf{8}]$ versus k_{obs} for the SBR with $\mathbf{8}$. Rate constant for SBR with $\mathbf{8} = 0.75 \pm 0.01 \text{ M}^{-1}\text{s}^{-1}$. $\text{SmI}_2 = 5 \text{ mM}$; HMPA = 10 equiv.; $\mathbf{3} = 25 \text{ equiv.}$; $\mathbf{8} = 10\text{-}60 \text{ equiv.}$

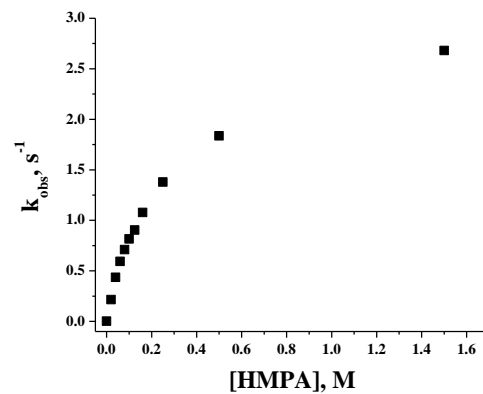


Figure 8.2.2.23 $[\text{HMPA}]$ versus k_{obs} for the SBR with $\mathbf{9}$. $\text{SmI}_2 = 5 \text{ mM}$; $\mathbf{9} = 25 \text{ equiv.}$; $\mathbf{3} = 25 \text{ equiv.}$; HMPA = 0-300 equiv.

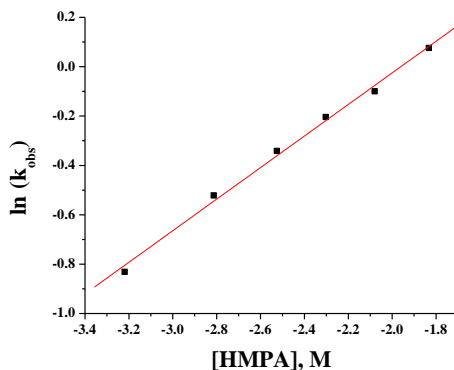


Figure 8.2.2.24 Plot of $\ln[\text{HMPA}]$ versus $\ln k_{\text{obs}}$ for the SBR with **9**. Rate order of HMPA = 0.64 ± 0.02 . $\text{SmI}_2 = 5 \text{ mM}$; **9** = 25 equiv.; **3** = 25 equiv.; HMPA = 8-32 equiv.

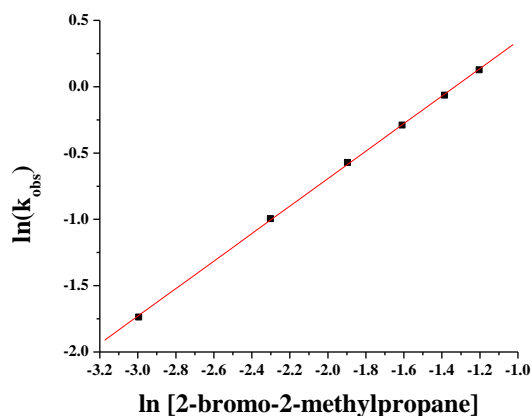


Figure 8.2.2.25 Plot of $\ln[\mathbf{9}]$ versus $\ln k_{\text{obs}}$ for the SBR with **9**. Reaction order of **9** = 1.04 ± 0.01 . $\text{SmI}_2 = 5 \text{ mM}$; HMPA = 10 equiv.; **3** = 25 equiv.; **9** = 10-60 equiv.

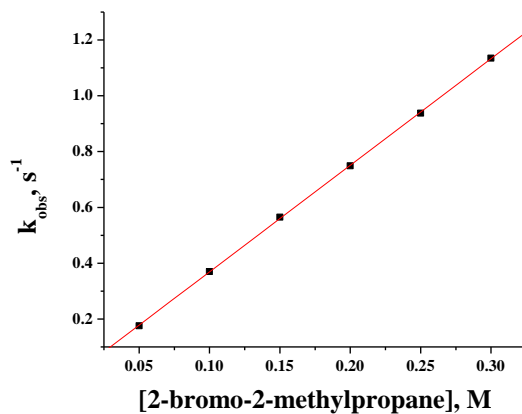


Figure 8.2.2.26 Plot of $[\mathbf{9}]$ versus k_{obs} for the SBR with **9**. Rate constant for SBR with **9** = $3.8 \pm 0.02 \text{ M}^{-1}\text{s}^{-1}$. $\text{SmI}_2 = 5 \text{ mM}$; HMPA = 10 equiv.; **3** = 25 equiv.; **9** = 10-60 equiv.

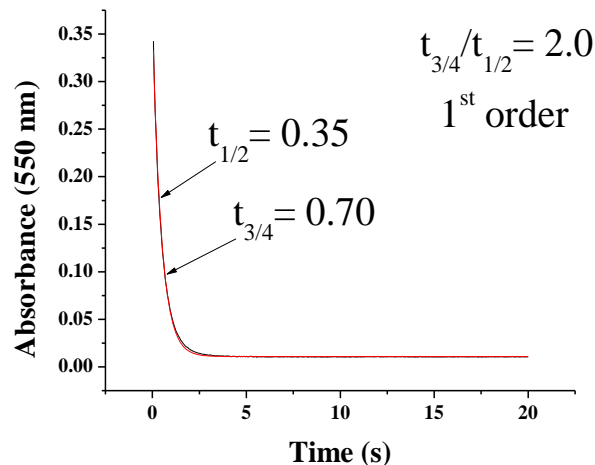


Figure 8.2.2.27 Fractional Times Method. Decay of SmI₂ over time monitored by stopped-flow analysis at absorbance of 550 nm. SmI₂ = 5 mM; HMPA = 50 equiv. (0-300 equiv.); **RX** = 25 equiv.

Table 8.2.2.28 Order of SmI₂ by Fractional Times Method

RX	Average $t_{3/4}/t_{1/2}$	Order
Iodododecane (1)	2.0	1
2-iodobutane (6)	2.3	1
2-iodo-2-methylpropane (7)	2.1	1
Bromodecane (2)	2.0	1
2-bromopropane (8)	2.2	1
2-bromo-2-methylpropane (9)	2.2	1

Table 8.2.2.29 Order of SmI₂. SmI₂ initial concentration doubles, HMPA stays constant at 10 equiv. with respect to SmI₂ and substrate initial concentrations remain the same.

Alkyl halide	[SmI ₂] (mM)	[HMPA] (mM)	[RX] (mM)	[3] (mM)	Rate (k_{obs} , s ⁻¹)
1	2.5	25	125	125	0.3652
	5.0	50	125	125	0.6204
6	5.0	50	125	125	1.55
	10	100	125	125	3.16
7	5.0	50	125	125	13.53
	10	100	125	125	23.70
2	2.5	25	125	125	
	5.0	50	125	125	
8	5.0	50	125	125	0.0736
	10	100	125	125	0.1436
9	5.0	50	125	125	0.4636
	10	100	125	125	0.7544

8.2.3 Derived Equation Fit to Saturation Plots

The derived equation ($y = \frac{(Vmax)(x^n)}{k+x^n}$) (eq 3.11) was fit to the saturation plot of HMPA in the samarium Barbier reaction (SBR).

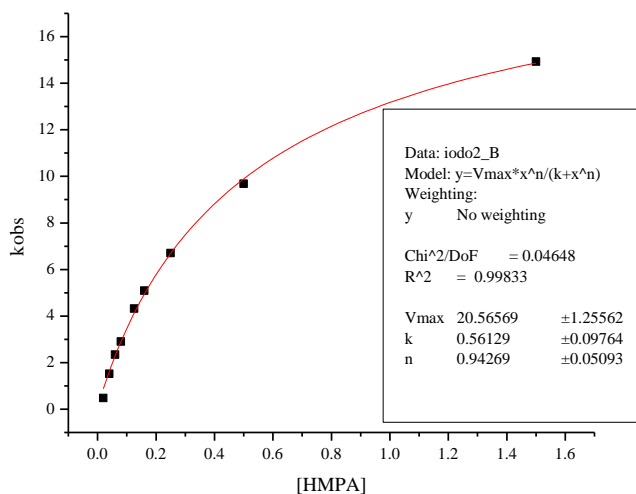


Figure 8.2.3.1 [HMPA] versus k_{obs} for the SBR with **6**. $SmI_2 = 5$ mM; **6** = 25 equiv.; **3** = 25 equiv.; HMPA = 0-300 equiv. Curve fit based on equation 3.11.

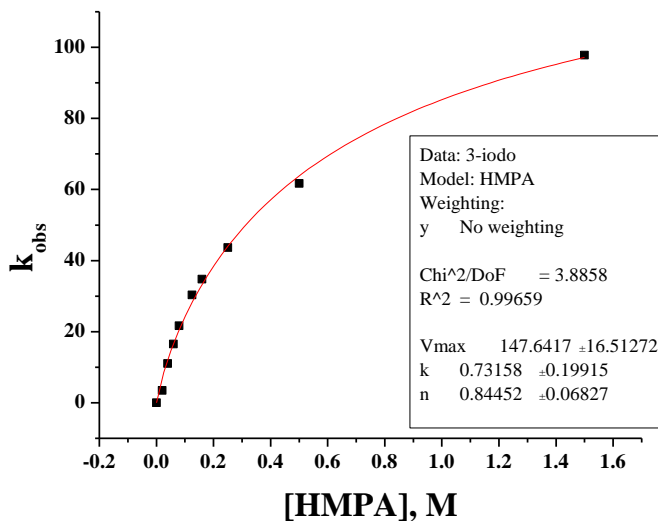


Figure 8.2.3.2 [HMPA] versus k_{obs} for the SBR with **7**. $SmI_2 = 5$ mM; **7** = 25 equiv.; **3** = 25 equiv.; HMPA = 0-300 equiv. Curve fit based on equation 3.11.

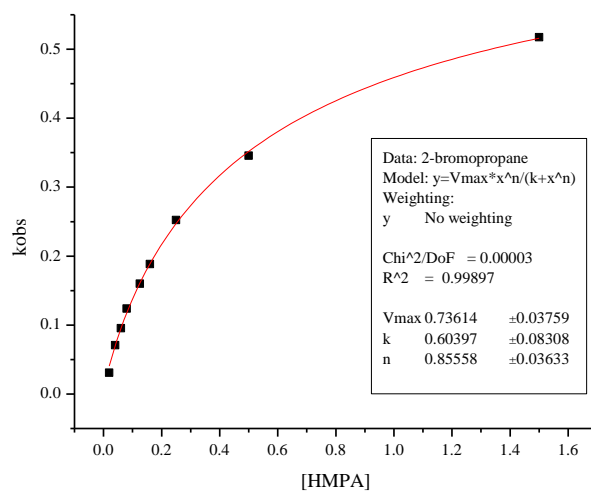


Figure 8.2.3.3 [HMPA] versus k_{obs} for the SBR with **8**. $SmI_2 = 5 \text{ mM}$; **8** = 25 equiv.; **3** = 25 equiv.; HMPA = 0-300 equiv. Curve fit based on equation 3.11.

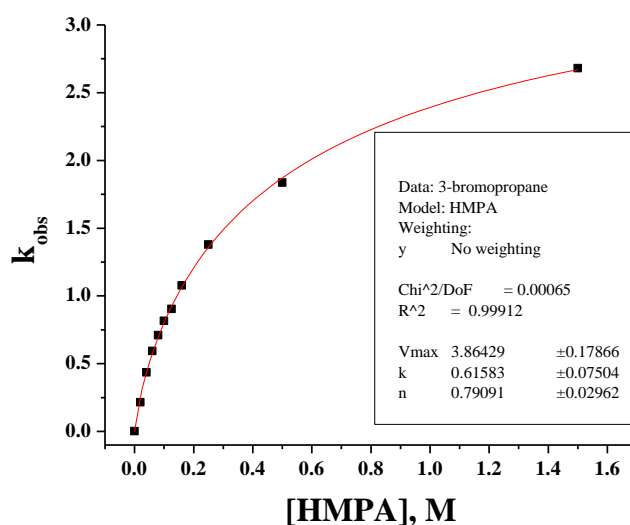


Figure 8.2.3.4 [HMPA] versus k_{obs} for the SBR with **9**. $SmI_2 = 5 \text{ mM}$; **9** = 25 equiv.; **3** = 25 equiv.; HMPA = 0-300 equiv. Curve fit based on equation 3.11.

8.2.4 Computational Calculation Results

Table 8.2.4.1 Absolute energies (Hartree), zero point vibrational energies (ZPVE, kcal/mol), low frequencies (1/cm) and dipole moments (Debye) for structures related to the formation of complex as calculated at the B3LYP/6-31G(d,p) level of theory.

Structures	Absolute energy (Hartrees)	Energy (kcal/mol)	ZPVE (kcal/mol)	Total E. (kcal/mol)	Low freq. (1/cm)	Dipole moment, D
Complex	-3473.917318	-2179917.86	200.94	-2179716.92	11.95	4.47
HMPA	-820.509183	-514877.72	159.09	-514718.63	36.73	3.92
Bromoethane	-2653.402094	-1665036.35	41.26	-1664995.09	259.76	2.31
ΔE (complex – reactants)		-3.79		-3.21		

Table 8.2.4.2 Single-point energies in THF using Onsager model for structures related to the formation of complex as calculated at the B3LYP/6-311+G(d,p) level of theory.

Structures	Absolute energy (Hartrees)	Energy (kcal/mol)
Complex	-3473.918724	-2179918.74
HMPA	-820.510660	-514878.64
Bromoethane	-2653.403552	-1665037.26
ΔE (complex – reactants)		-2.83

Table 8.2.4.3 Mulliken charges on gas phase optimized structures as calculated at the B3LYP/6-311+G(d,p) level of theory.

Mulliken charges	P	O	C1	Br
Complex	0.745	-0.349	-0.254	-0.142
HMPA	0.734	-0.304	-	-
Bromoethane	-	-	-0.262	-0.119

Table 8.2.4.4 Cartesian coordinates of all optimized structures at the B3LYP/6-311+G(d,p)

Bromoethane

C	0.598256	-1.090620	0.000000
H	1.218230	-1.186362	0.888472
H	1.218230	-1.186362	-0.888472
C	-0.573083	-2.051771	0.000000
H	-1.197383	-1.919871	-0.885503
H	-0.192730	-3.079580	0.000000
H	-1.197383	-1.919871	0.885503
Br	0.000000	0.804183	0.000000

HMPA

P	-0.032015	0.487429	0.000000
N	1.548653	-0.116111	0.000000
N	-0.658526	-0.193995	1.414138
N	-0.658526	-0.193995	-1.414138
O	-0.257909	1.962597	0.000000
C	2.355345	0.051839	-1.214088
H	3.143032	-0.708169	-1.229077
H	1.736556	-0.068645	-2.101054
H	2.829948	1.041455	-1.253473
C	2.355345	0.051839	1.214088
H	1.736556	-0.068645	2.101054
H	3.143032	-0.708169	1.229077
H	2.829948	1.041455	1.253473
C	-1.679812	0.538272	2.161946
H	-1.502565	0.418743	3.237062
H	-1.625615	1.596005	1.912160
H	-2.692170	0.170467	1.941300
C	-0.614521	-1.621844	1.705179
H	-0.481349	-1.772638	2.782878
H	-1.538911	-2.137507	1.407945
H	0.226144	-2.091065	1.195240
C	-1.679812	0.538272	-2.161946
H	-1.625615	1.596005	-1.912160
H	-1.502565	0.418743	-3.237062
H	-2.692170	0.170467	-1.941300
C	-0.614521	-1.621844	-1.705179
H	-1.538911	-2.137507	-1.407945

H	-0.481349	-1.772638	-2.782878
H	0.226144	-2.091065	-1.195240

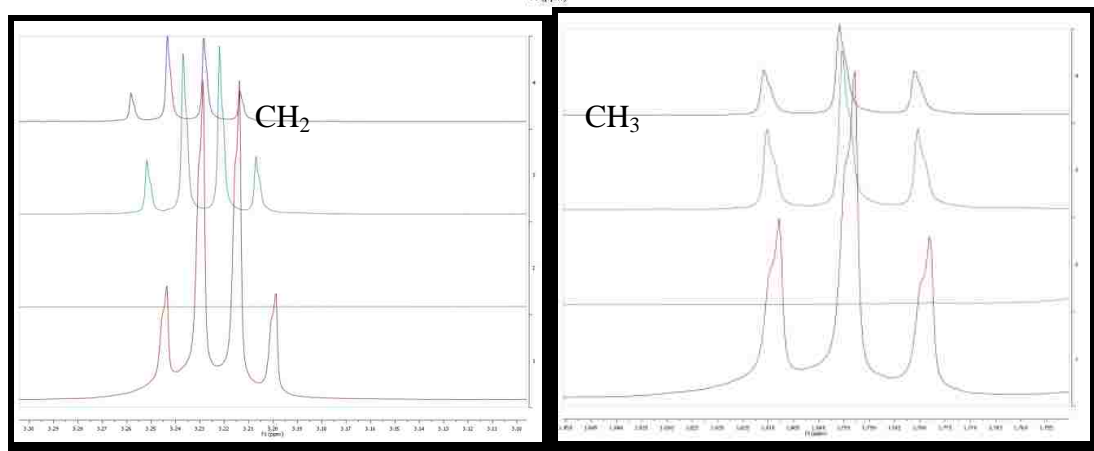
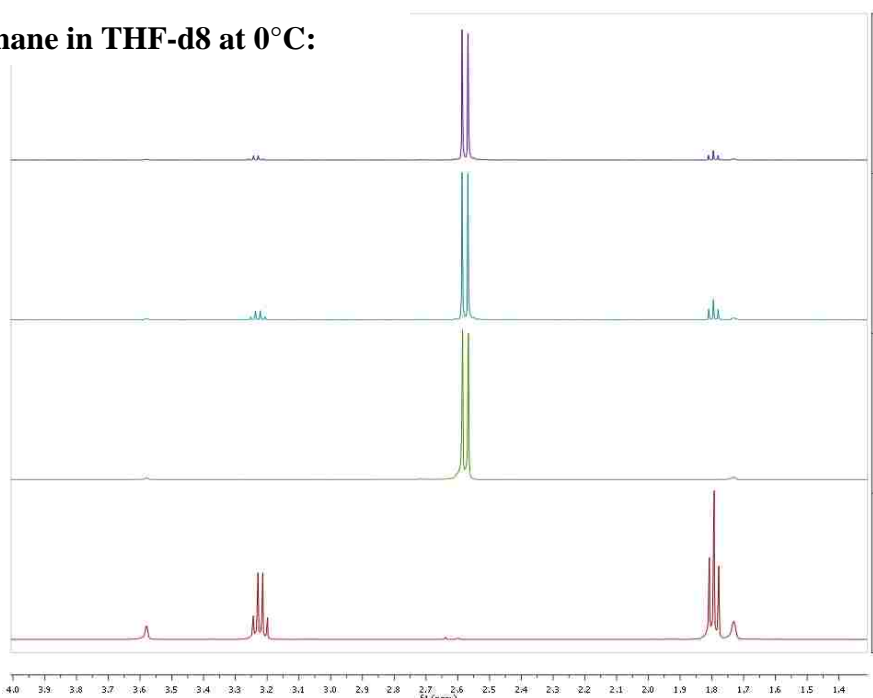
Bromoethane- HMPA –complex

P	1.446144	0.153162	0.121377
N	1.038746	-1.194610	-0.804088
N	2.288762	1.101761	-0.993175
N	2.427571	-0.524897	1.316207
O	0.367162	0.970010	0.761765
C	-2.899183	0.937678	0.942824
H	-3.257632	0.724929	1.947615
H	-1.816215	0.843635	0.895330
C	-3.396094	2.266880	0.415687
H	-4.485826	2.334879	0.436739
H	-2.988962	3.065734	1.046118
H	-3.055674	2.440697	-0.606805
Br	-3.597431	-0.584270	-0.151237
C	2.243339	2.558201	-0.871434
H	3.137261	2.955540	-0.369699
H	2.187130	3.007298	-1.869663
H	1.361488	2.849914	-0.304877
C	3.418154	0.604714	-1.770723
H	3.412117	1.068921	-2.763664
H	4.383385	0.837153	-1.298742
H	3.345962	-0.473918	-1.905035
C	2.448212	0.071048	2.651210
H	1.545269	0.658906	2.802452
H	2.484314	-0.722518	3.406484
H	3.324402	0.718903	2.796551
C	3.581319	-1.366646	1.021273
H	4.521619	-0.797296	1.017769
H	3.668675	-2.150068	1.783054
H	3.463728	-1.852430	0.053394
C	0.401187	-0.990903	-2.112045
H	0.622439	-1.849380	-2.754373
H	-0.687803	-0.899084	-2.019302
H	0.787899	-0.091437	-2.586979
C	0.516902	-2.388498	-0.125186
H	-0.569509	-2.330339	0.013746
H	0.740874	-3.271202	-0.732777
H	0.987114	-2.507514	0.848952

8.2.5 ^1H and ^{13}C NMR

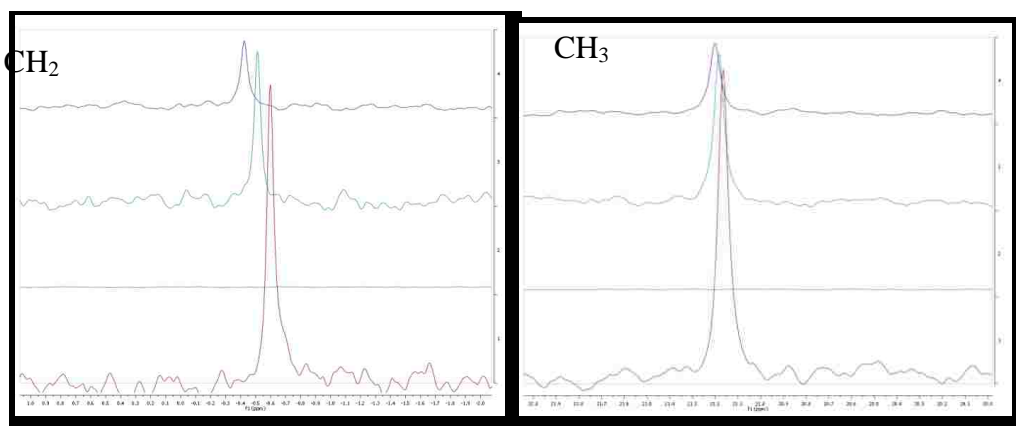
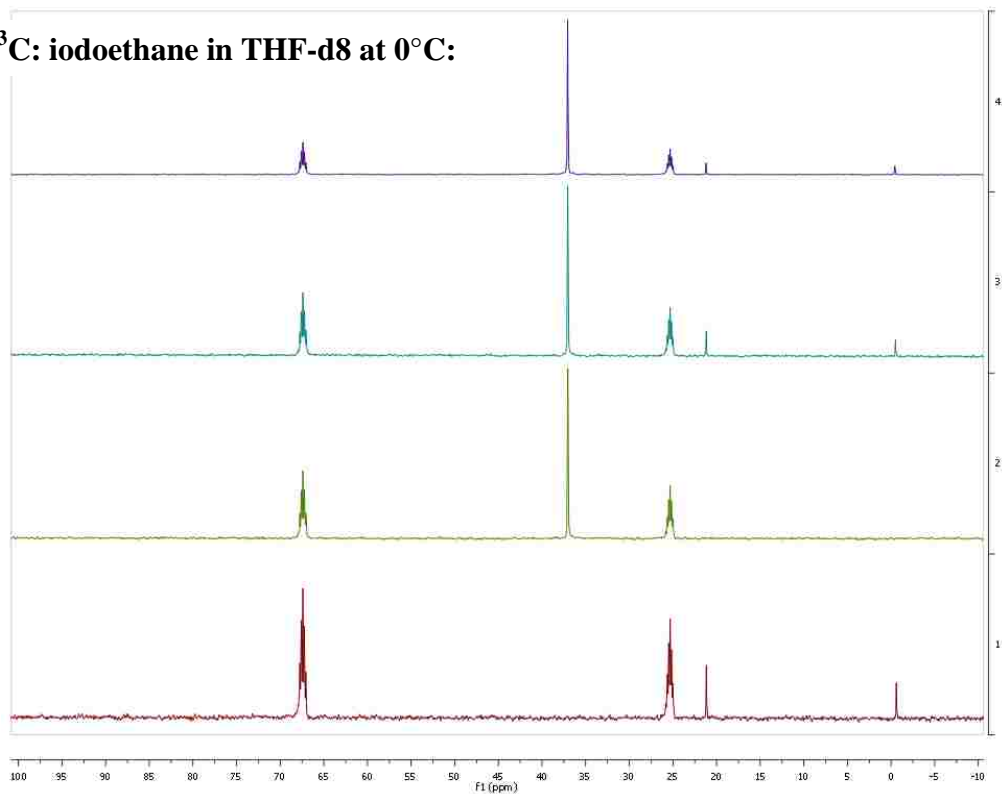
8.2.5.1 Alkyl Halide-HMPA NMR Experiments

^1H : iodoethane in THF-d8 at 0°C :

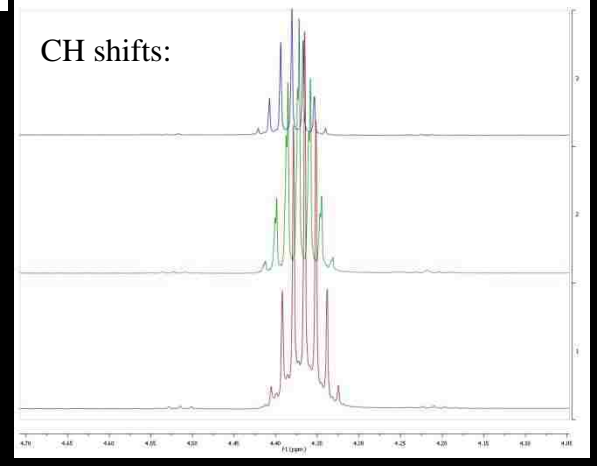
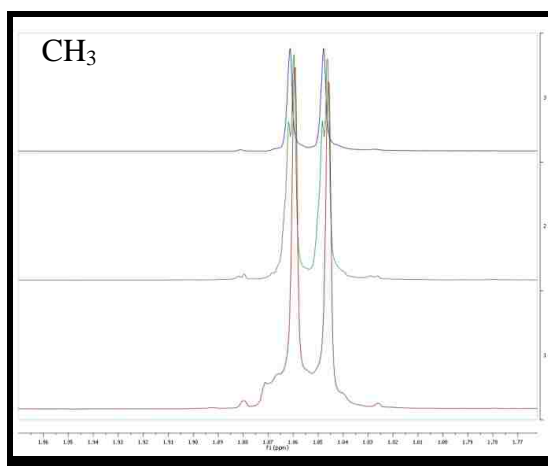
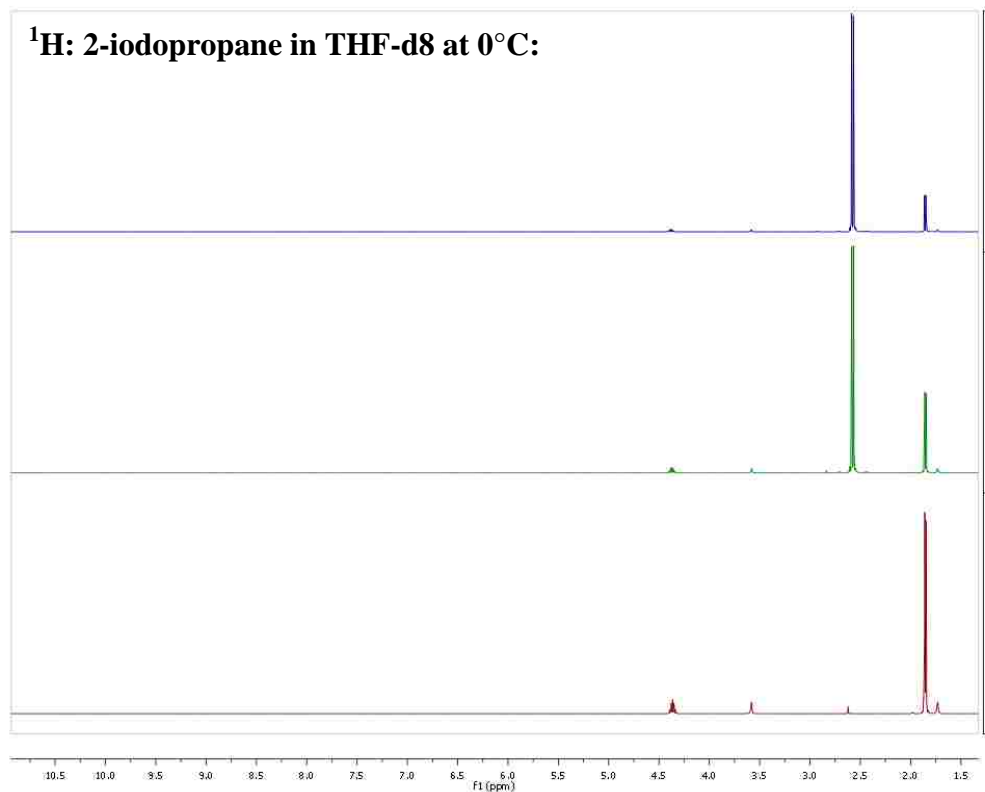


^1H NMR	CH_2	ΔCH_2 ppm	CH_3	ΔCH_3 ppm	HMPA	ΔHMPA ppm
Iodoethane	3.222		1.793			
HMPA					2.576	
Iodoethane + 1equiv. HMPA	3.230	0.008	1.796	0.003	2.578	0.002
Iodoethane + 2equiv. HMPA	3.236	0.014	1.796	0.003	2.576	0.000

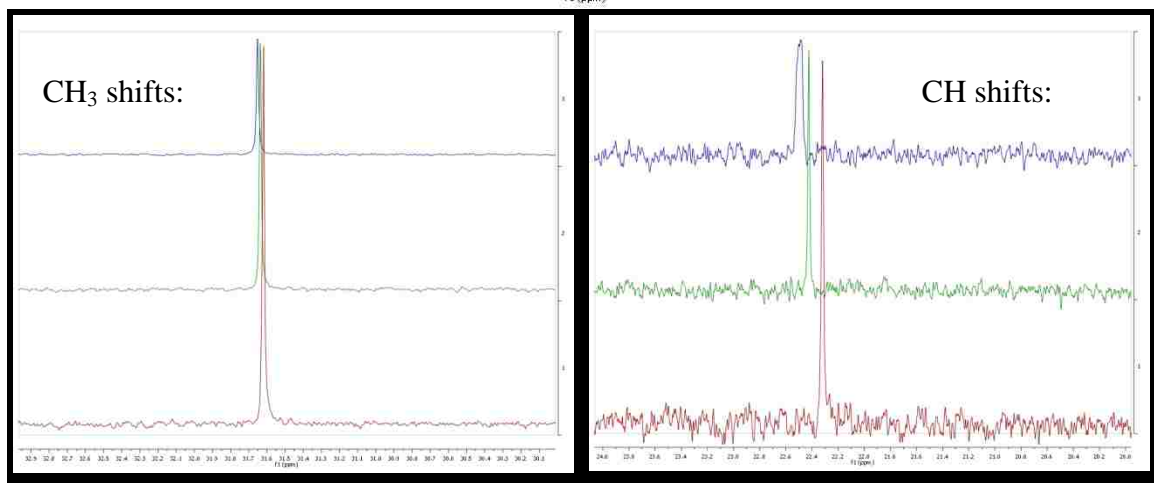
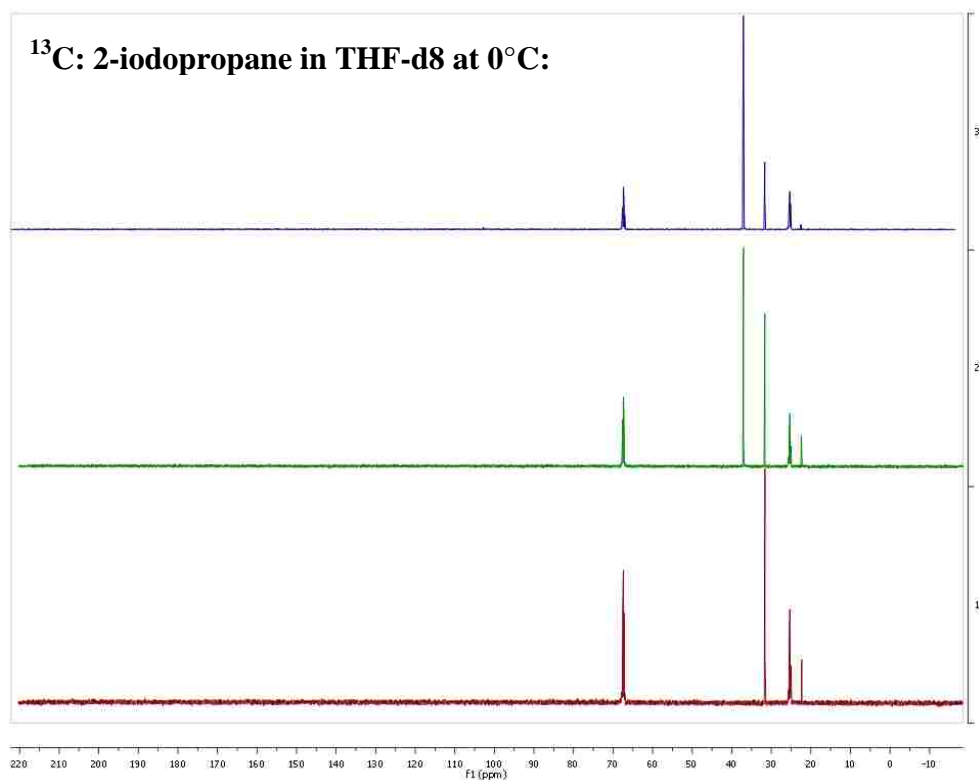
¹³C: iodoethane in THF-d8 at 0°C:



¹³ C NMR	CH ₂	Δ CH ₂ ppm	CH ₃	ΔCH ₃ ppm	HMPA	ΔHMP A ppm
Iodoethane	-0.596		21.169			
HMPA					37.047	
Iodoethane + 1equiv. HMPA	-0.509	0.087	21.186	0.017	37.057	0.010
Iodoethane + 2equiv. HMPA	-0.422	0.174	21.205	0.036	37.064	0.017

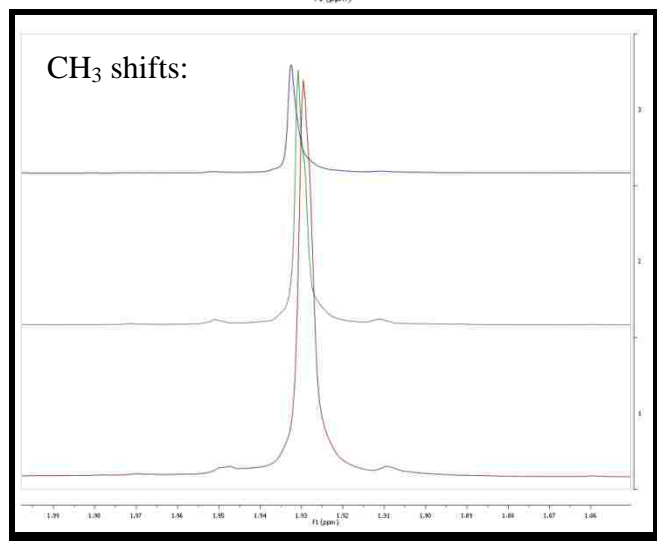
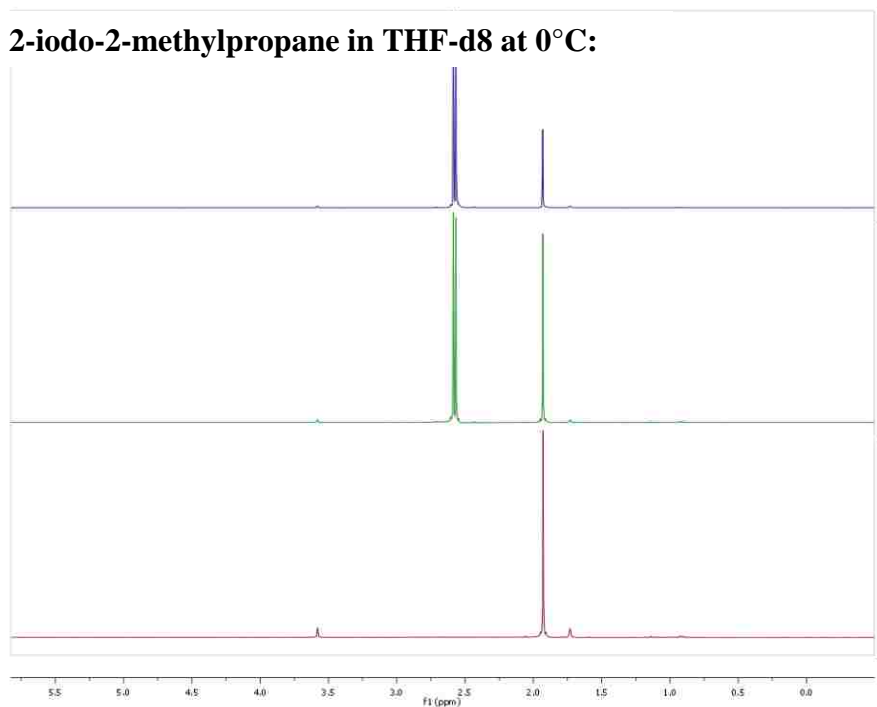


¹ H NMR	CH	Δ CH ppm	CH ₃	ΔCH ₃ ppm	HMPA	ΔHMPA ppm
2-iodopropane	4.365		1.852			
HMPA					2.576	
2-iodopropane + 1equiv. HMPA	4.372	0.007	1.853	0.001	2.575	0.001
2-iodopropane + 2equiv. HMPA	4.381	0.016	1.854	0.002	2.576	0.001



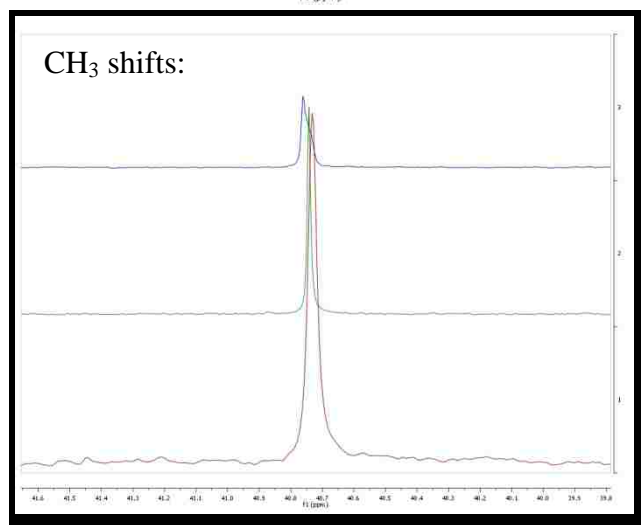
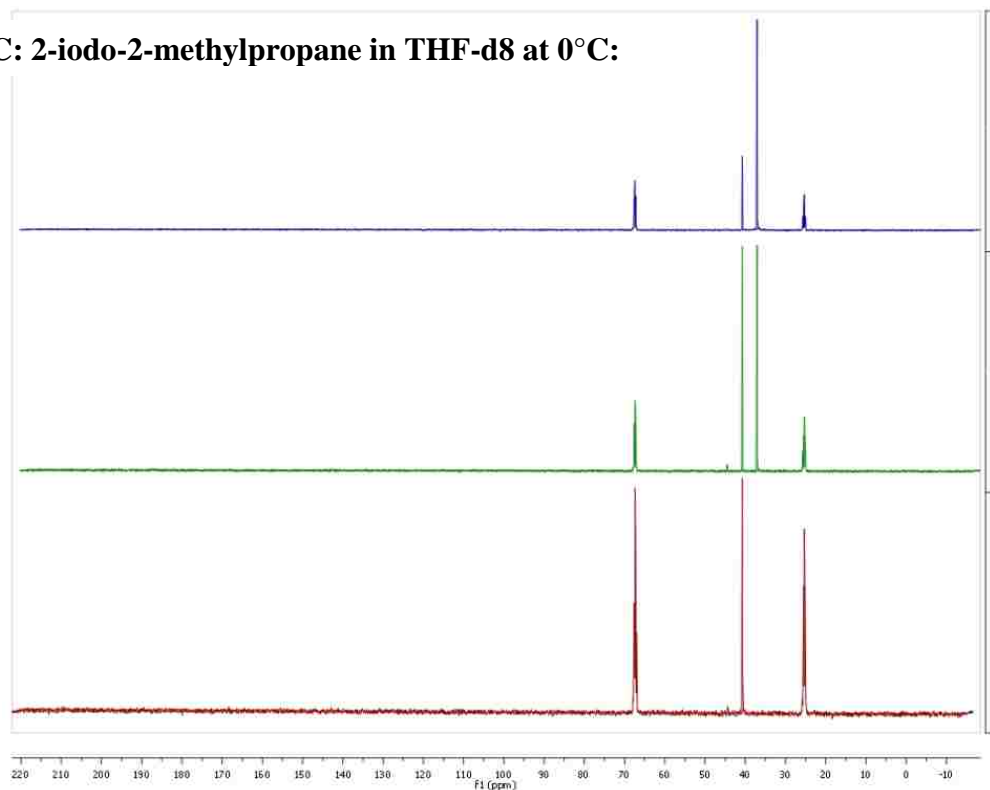
¹³ C NMR	CH	Δ CH ppm	CH ₃	Δ CH ₃ ppm	HMPA	Δ HMPA ppm
2-iodopropane HMPA	22.317		31.616		37.047	
2-iodopropane + 1equiv. HMPA	22.424	0.107	31.635	0.019	37.062	0.015
2-iodopropane + 2equiv. HMPA	22.484	0.167	31.651	0.035	37.069	0.022

¹H: 2-iodo-2-methylpropane in THF-d8 at 0°C:



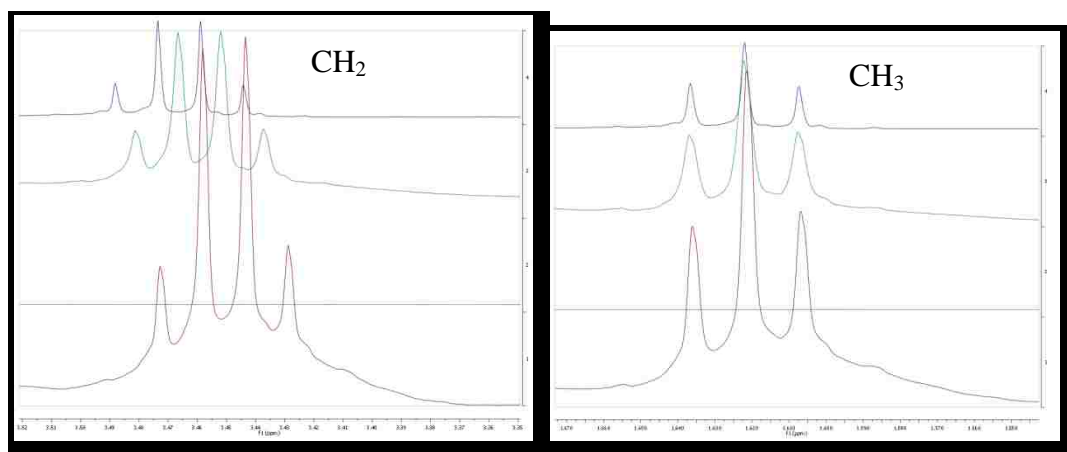
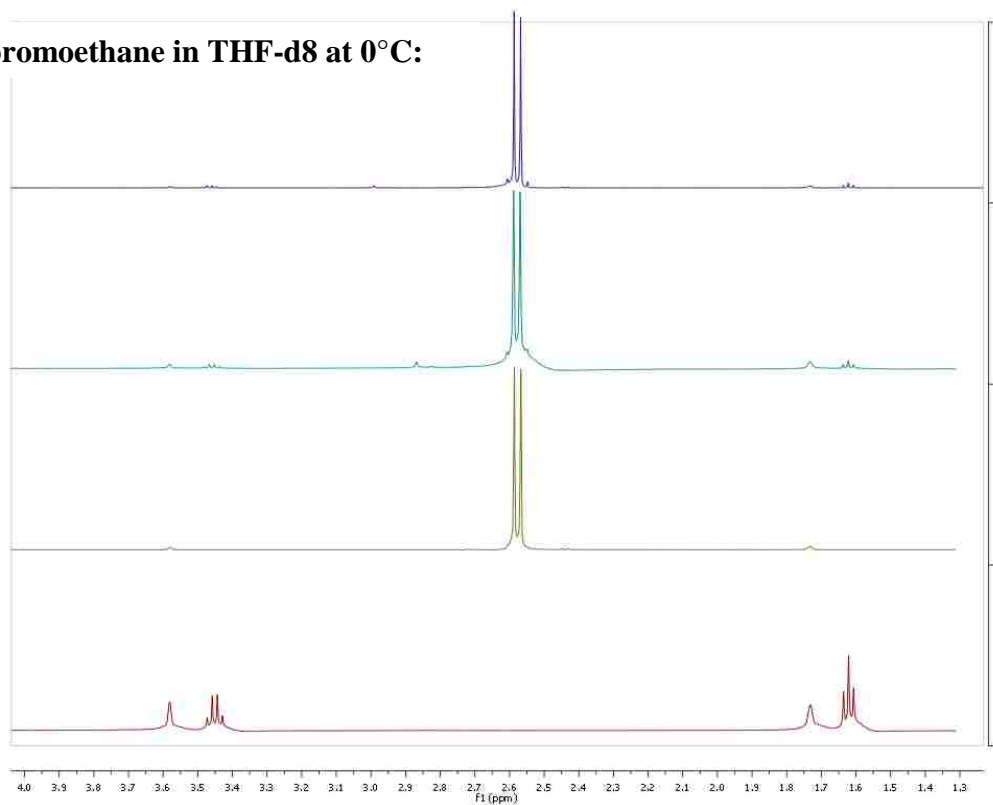
¹ H NMR	CH ₃	ΔCH ₃ ppm	HMPA	ΔHMPA ppm
2-iodo-methyl propane HMPA	1.930		2.576	
2-iodo-methyl propane + 1equiv. HMPA	1.931	0.001	2.577	0.001
2-iodo-methyl propane + 2equiv. HMPA	1.933	0.003	2.577	0.001

¹³C: 2-iodo-2-methylpropane in THF-d8 at 0°C:

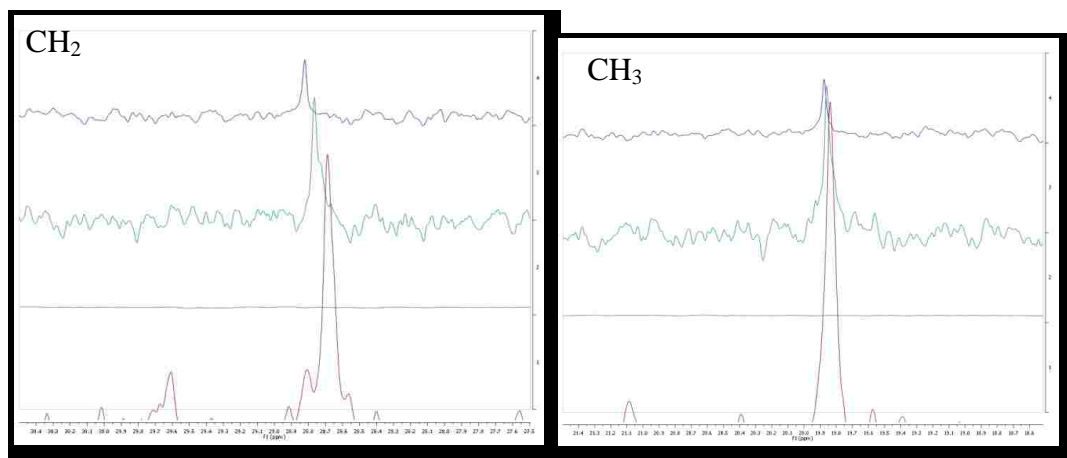
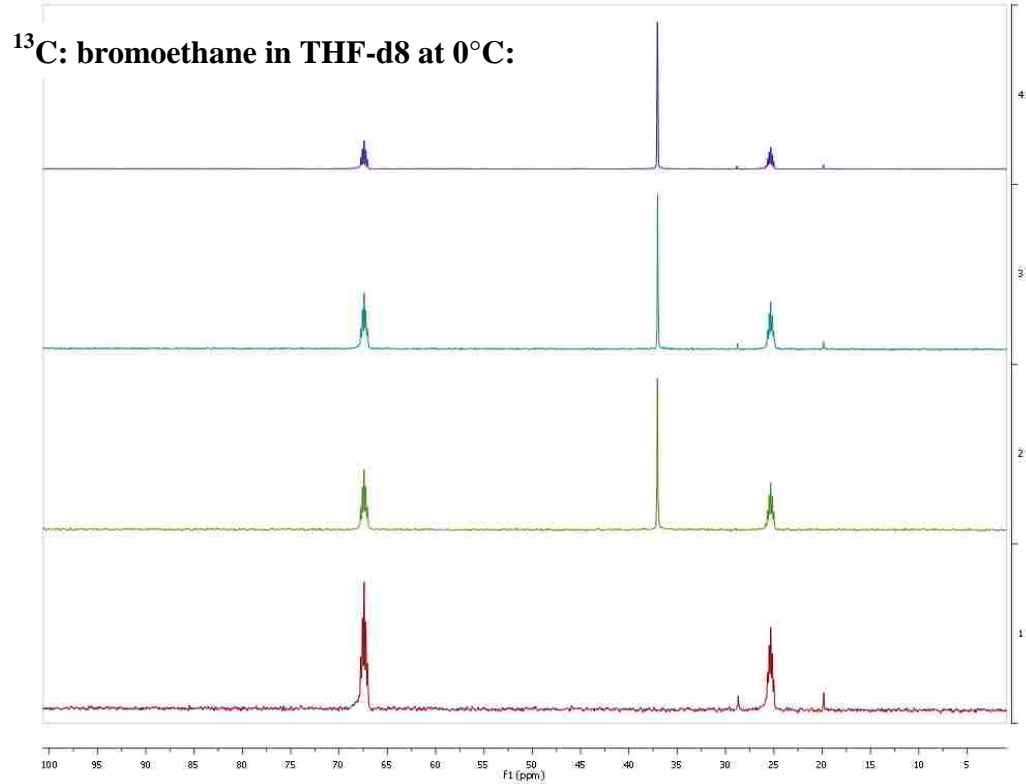


¹³ C NMR	CH ₃	ΔCH ₃ ppm	HMPA	ΔHMPA ppm
2-iodo-methyl propane HMPA	40.732		37.047	
2-iodo-methyl propane + 1equiv. HMPA	40.744	0.012	37.064	0.017
2-iodo-methyl propane + 2equiv. HMPA	40.758	0.026	37.081	0.034

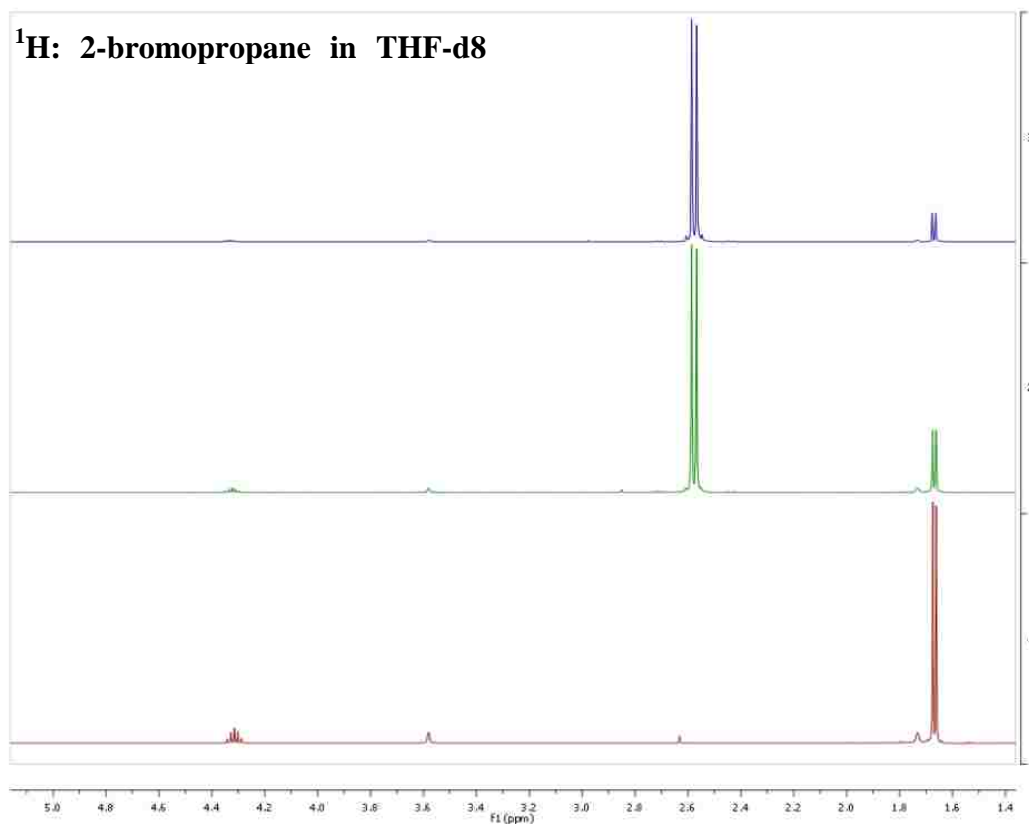
¹H: bromoethane in THF-d8 at 0°C:



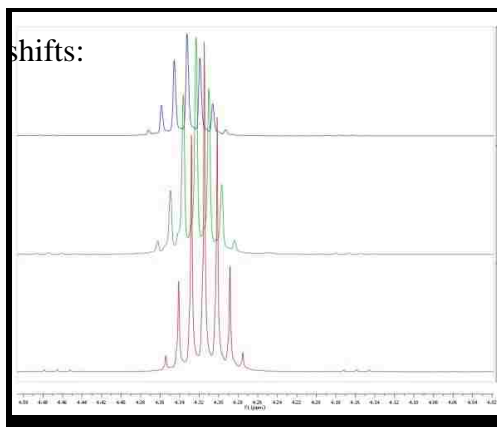
¹ H NMR	CH ₂	Δ CH ₂ ppm	CH ₃	Δ CH ₃ ppm	HMPA	Δ HMPA ppm
Bromoethane	3.450		1.621		2.576	
Bromoethane + 1equiv. HMPA	3.458	0.008	1.622	0.001	2.579	0.003
Bromoethane + 2equiv. HMPA	3.464	0.014	1.619	0.002	2.570	0.006



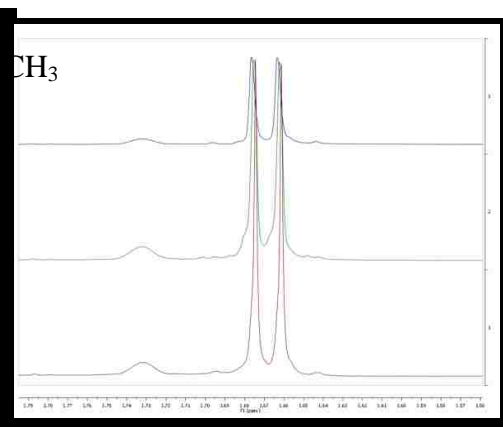
¹³ C NMR	CH ₂	Δ CH ₂ ppm	CH ₃	Δ CH ₃ ppm	HMPA	Δ HMPA ppm
Bromoethane HMPA	28.684		19.833		37.047	
Bromoethane + 1equiv. HMPA	28.760	0.076	19.855	0.022	37.040	0.007
Bromoethane + 2equiv. HMPA	28.816	0.132	19.868	0.035	37.040	0.007



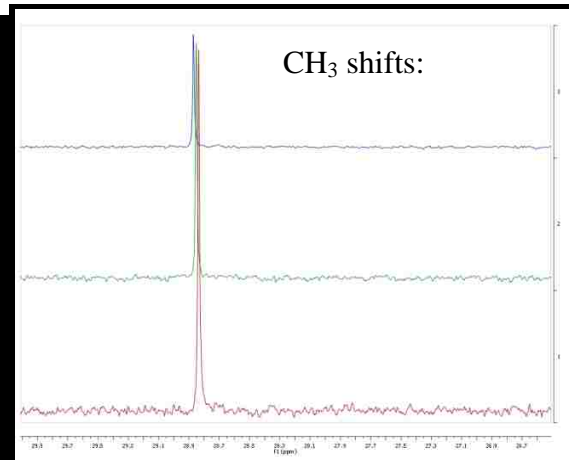
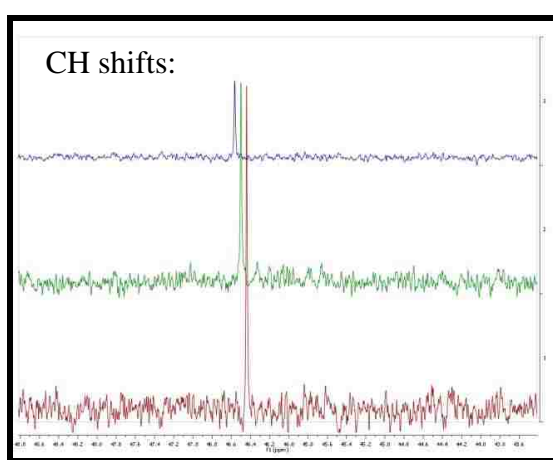
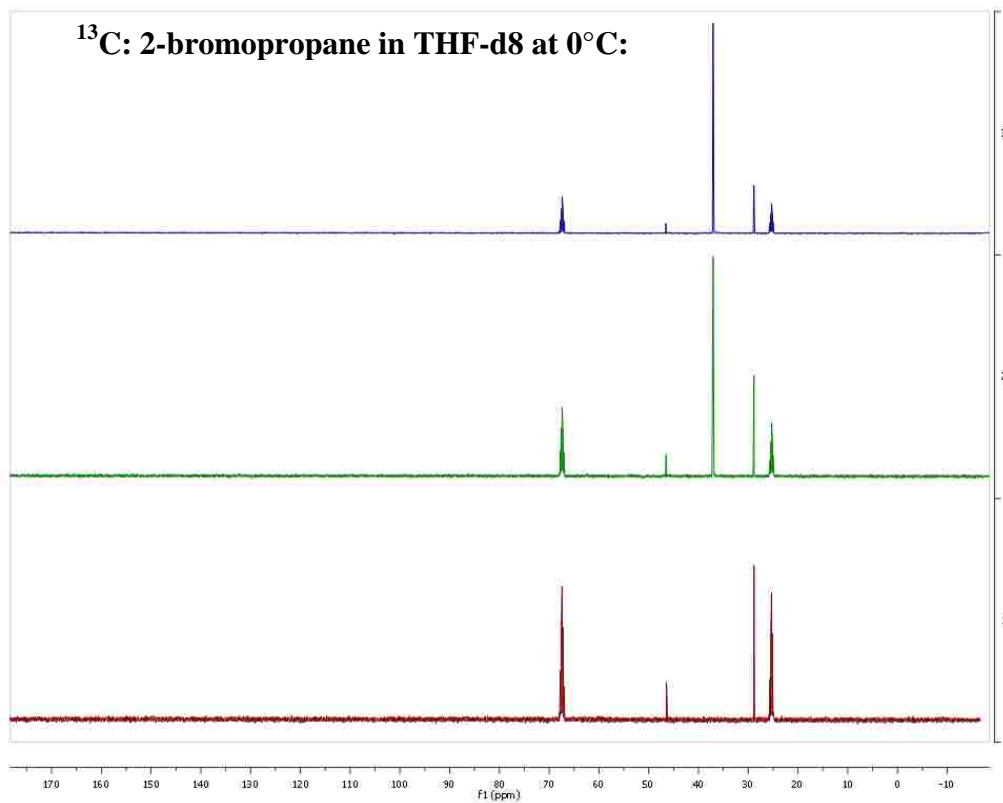
CH shifts:



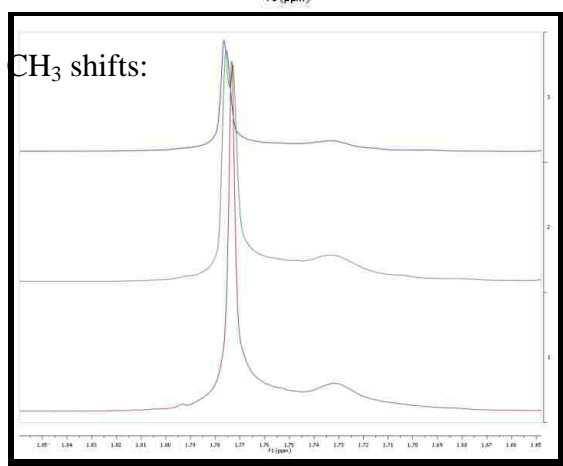
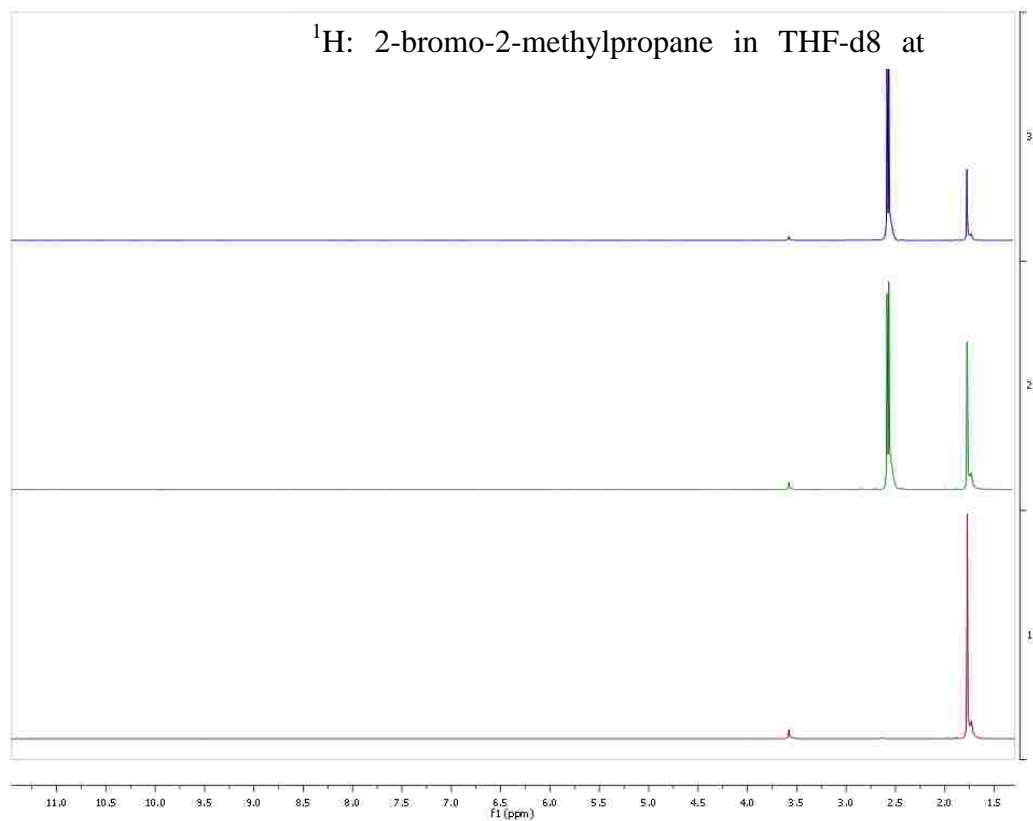
CH₃



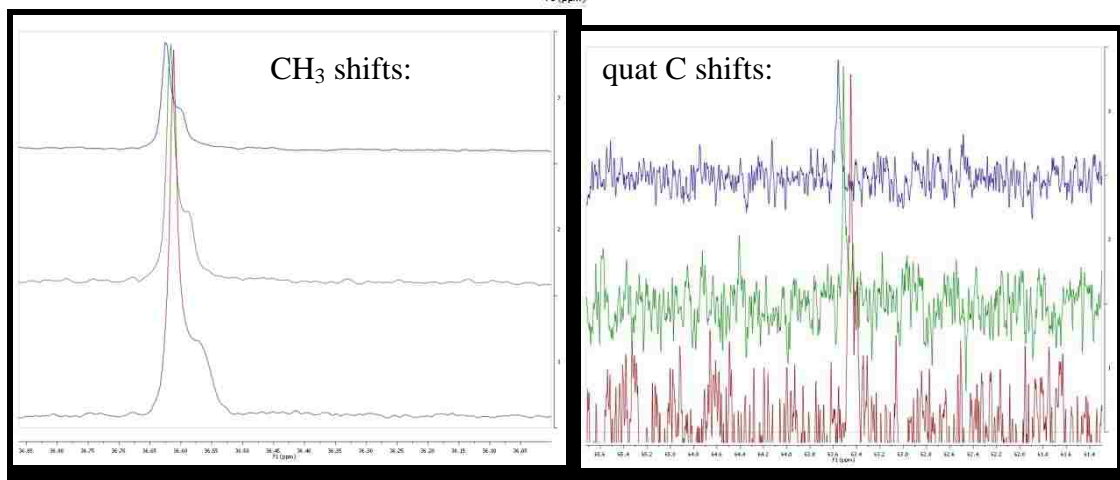
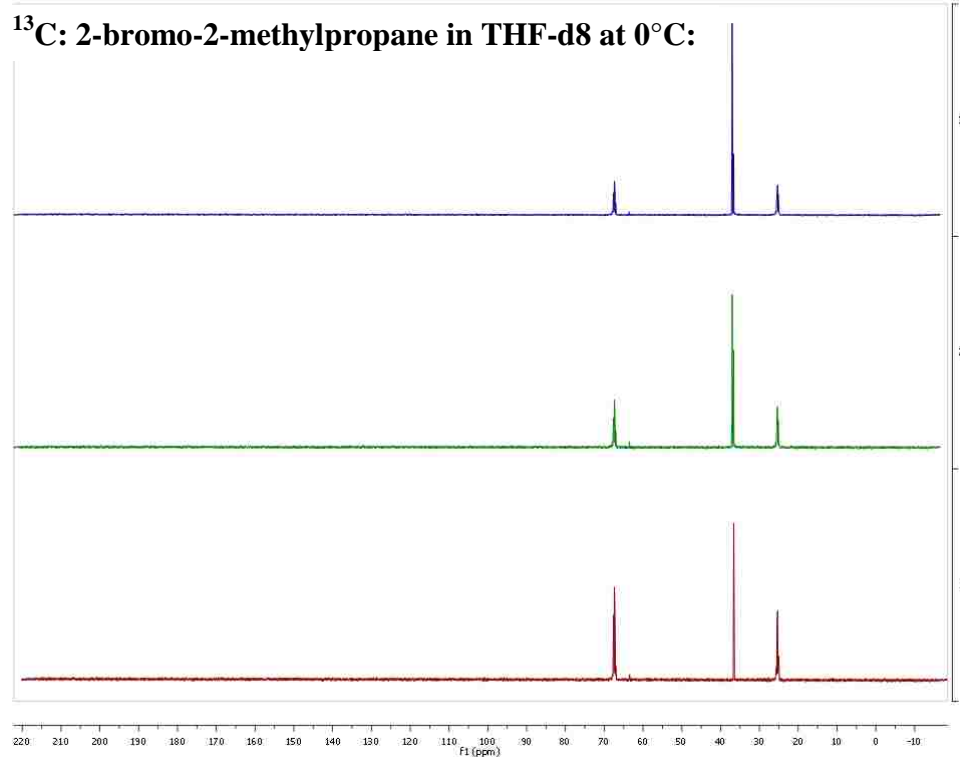
¹ H NMR	CH	Δ CH ppm	CH ₃	Δ CH ₃ ppm	HMPA	Δ HMPA ppm
2-Bromopropane	4.314		1.668			
HMPA					2.576	
2-Bromopropane + 1equiv. HMPA	4.323	0.009	1.669	0.001	2.576	0.000
2-Bromopropane + 2equiv. HMPA	4.333	0.019	1.670	0.002	2.577	0.001



¹³ C NMR	CH	Δ CH ppm	CH ₃	Δ CH ₃ ppm	HMPA	Δ HMPA ppm
2-Bromopropane	46.441		28.836			
HMPA					37.047	
2-Bromopropane + 1equiv. HMPA	46.499	0.058	28.853	0.017	37.053	0.006
2-Bromopropane + 2equiv. HMPA	46.551	0.110	28.873	0.037	37.048	0.001

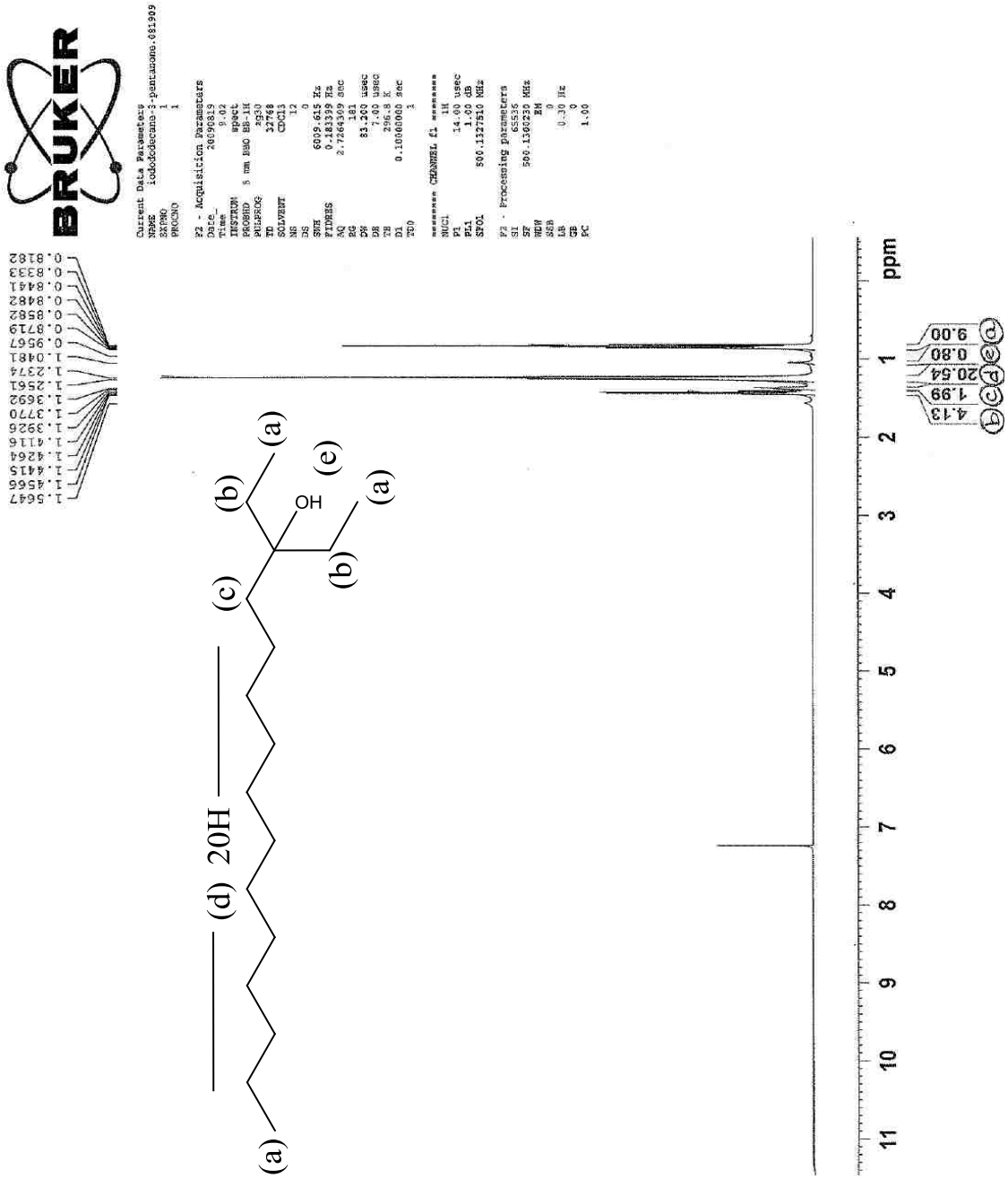


¹ H NMR	CH ₃	ΔCH ₃ ppm	HMPA	ΔHMPA ppm
2-bromo-2-methylpropane HMPA	1.773		2.576	
2-bromo-2-methylpropane + 1equiv. HMPA	1.776	0.003	2.578	0.002
2-bromo-2-methylpropane + 2equiv. HMPA	1.777	0.004	2.577	0.001



¹³ C NMR	C	ΔC ppm	CH ₃	Δ CH ₃ ppm	HMPA	Δ HMPA ppm
2-bromo-2-methylpropane	63.451		36.612			
HMPA					37.047	
2-bromo-2-methylpropane + 1equiv. HMPA	63.513	0.062	36.618	0.006	37.049	0.002
2-bromo-2-methylpropane + 2equiv. HMPA	63.556	0.105	36.623	0.011	37.054	0.007

8.2.5.2 Product Characterization



8.2.5.1 ¹H NMR (4) 3-ethylpentadecan-3-ol



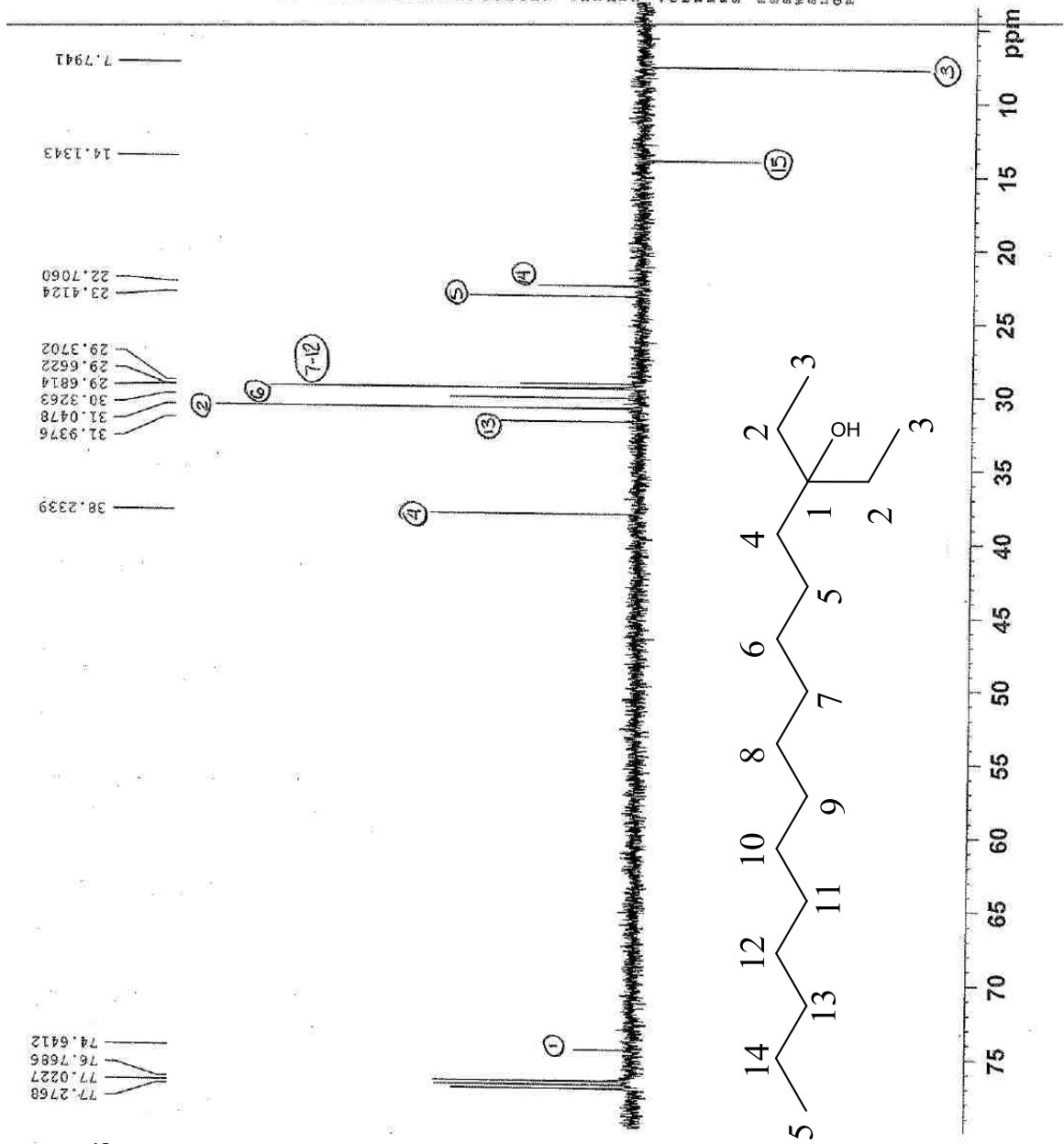
Current Data Parameters
 NAME 8-cyclohexyl-3-pentadecanol.061
 XNAME 2
 PROCNO 1

F2 - Acquisition Parameters
 Date_ 20090815
 Time_ 21:09
 INSTRUM spect
 PROBRD 5 mm BBO BB-1H
 PULPROG zgpg30
 TD 65536
 SOLVENT CDCl3
 NS 126
 DS 4
 SFO1 300.1324 MHz
 SWH 6000.000 MHz
 FIDRES 0.458323 Hz
 AQ 1.0912410 sec
 RG 1.0321.3
 DR 16.650 usec
 DE 7.00 usec
 TEM 297.5 K
 CHST3 145.064900 usec
 CHST11 1.0000000
 D1 2.0000000 sec
 D2 0.06589655 sec
 DELTA 0.00001095 sec
 TDC 1

===== CHANNEL F1 =====
 NUC1 13C
 P1 8.60 usec
 PL 17.20 dB
 PR 1.00 dB
 SFO1 125.7703640 MHz

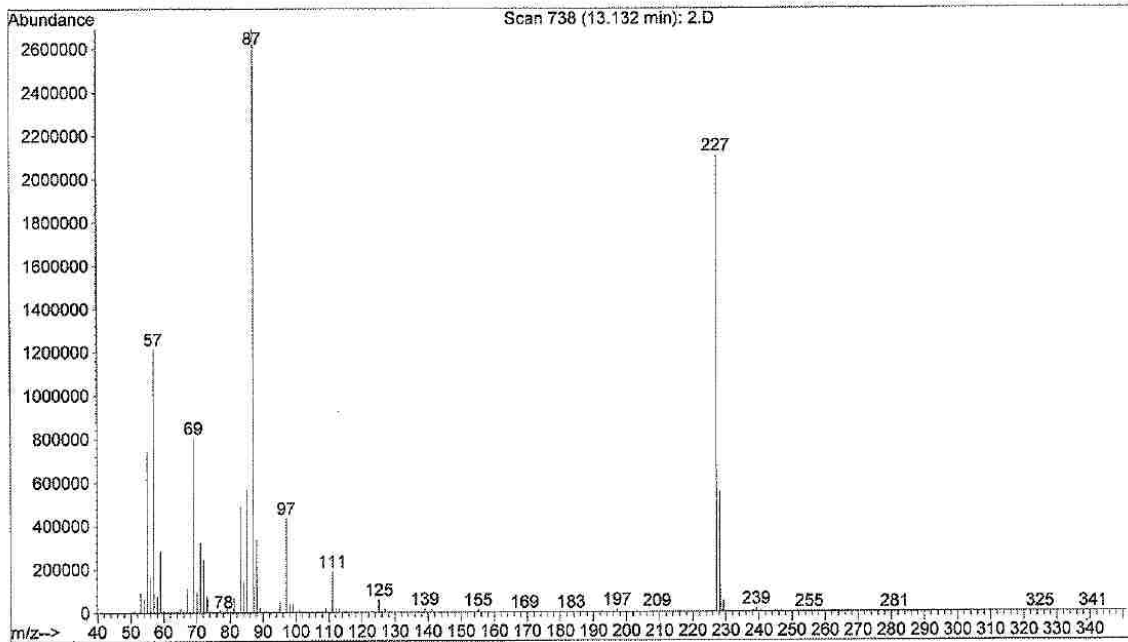
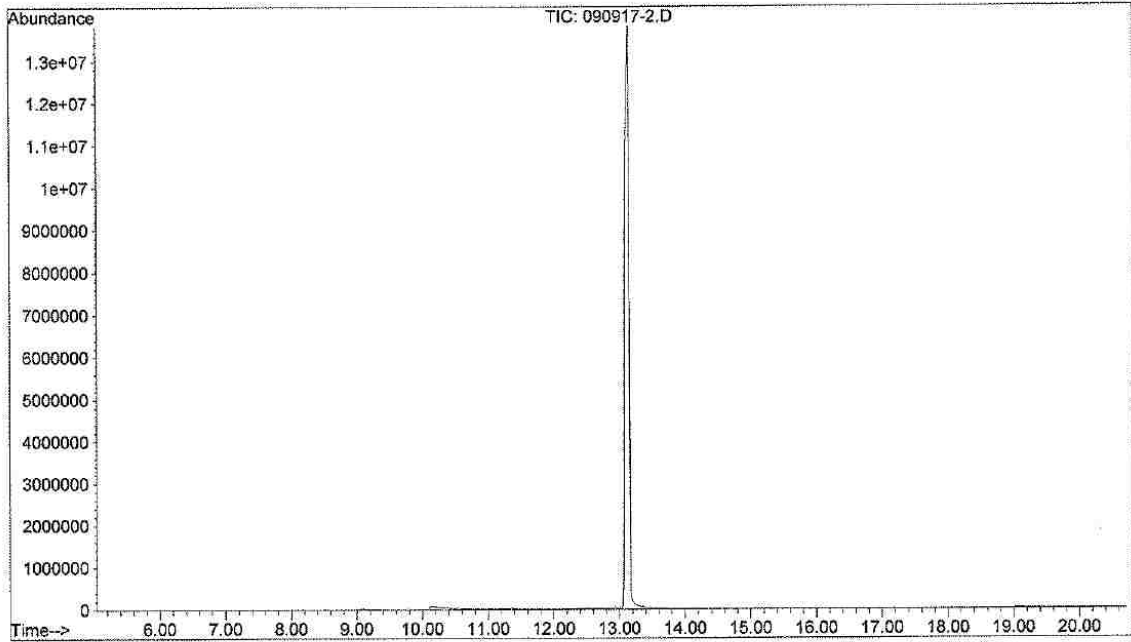
===== CHANNEL F2 =====
 CPDPRG2 waltz16
 NUC2 1H
 P2 100.00 usec
 PL2 1.00 dB
 PR2 17.50 dB
 SFO2 500.1322150 MHz

F2 - Processing parameters
 SI 32768
 SF 125.757890 MHz
 NDN 0
 SSB 0
 GB 0
 EC 1.10



8.2.5.2 ¹³C NMR (4) 3-ethylpentadecan-3-ol

File : C:\HPCHEM\1\DATA\KAT208\090917-2.D
Operator : kim
Acquired : 17 Sep 2009 15:26 using AcqMethod SADA4
Instrument : GC/MS Ins
Sample Name: iododecane-3pentanone-smi2-hmpa
Misc Info :
Vial Number: 1



8.2.5.3 GC-MS (4) 3-ethylpentadecan-3-ol



Current Data Parameters
 NAME SBBAB3.B-CW30.20ent.HRPA.979
 EXPNO 1
 PROCNO 1

F2 - Acquisition Parameters

Date_ 20100707
 Time 5:24
 INSTRUM spect
 PROBEHD 5 mm BBO BB-1H
 PULPROG zg30
 TD 32768
 SOLVENT CTC13
 NS 12
 DS 2
 SWH 6009.515 Hz
 FIDRES 0.183309 Hz
 AQ 2.7264309 sec
 RG 40.3
 DW 85.200 usec
 DE 27.00 usec
 TE 300.2 K
 D1 0.10000005 sec
 TD0 1

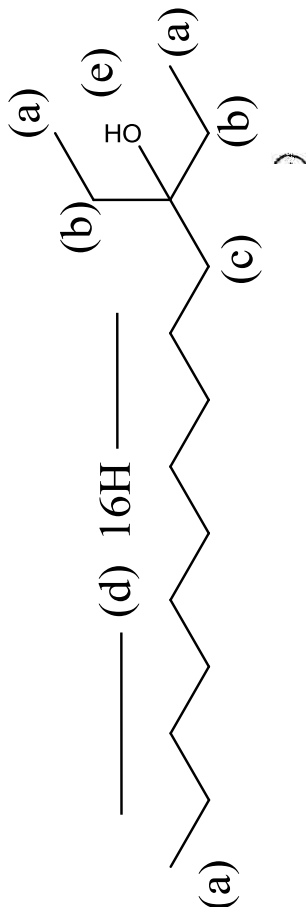
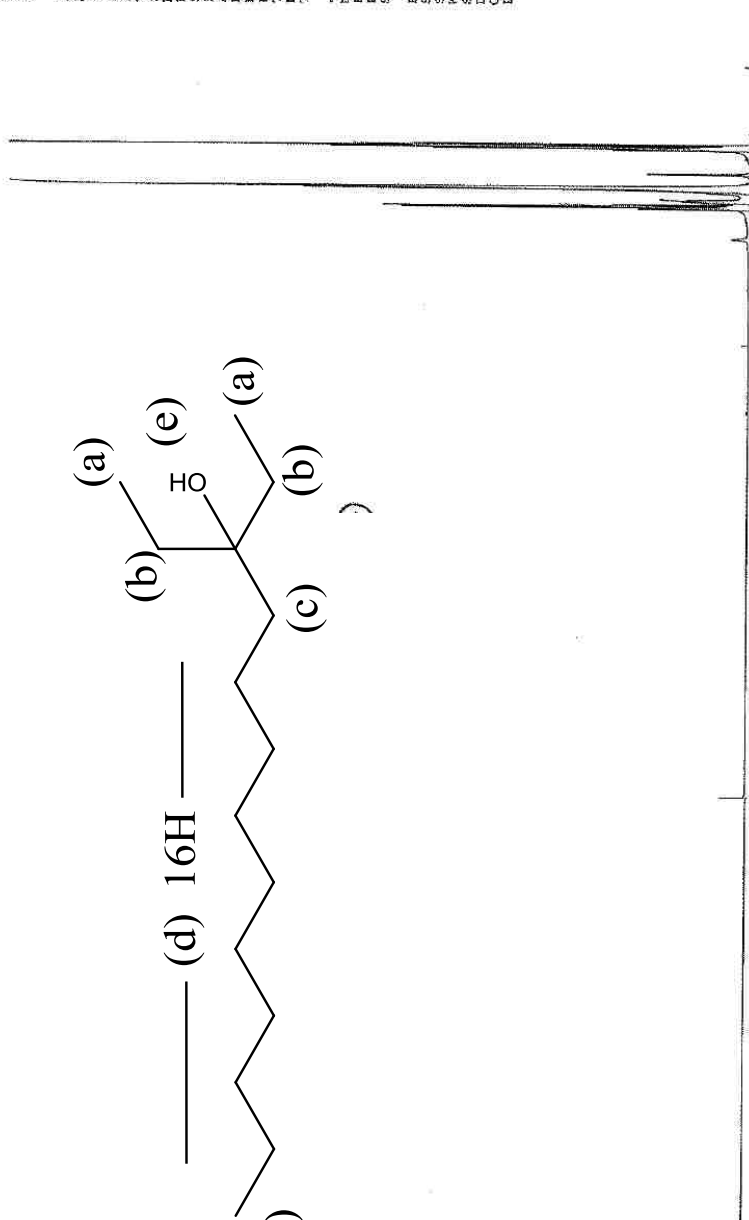
===== CHANNEL f1 =====

NUC1 1H
 P1 14.00 usec
 PL1 0.00 dB
 SFO1 500.1327510 MHz

F2 - Processing parameters

SI 65536
 SF 500.1300231 MHz
 SD 30
 SSB 0
 LB 0.30 Hz
 GB 0
 PC 1.00

1.4468
 1.4319
 1.4168
 1.4015
 1.2669
 1.2475
 1.2320
 1.0981
 0.8626
 0.8495
 0.8385
 0.8237
 0.8086



8.2.5.4 ¹H NMR (5) 3-ethyltridecan-3-ol



Current Parameters:
NAME: 8.2.5.5
SUBSTR: 3-ethyltridecan-3-ol
PROGNO: 1

F2 - Acquisition Parameters
Date: 20180719
Time: 17:02
INSTRUM: spect
PROBHD: 5 mm BBO BB4-1H
PULPROG: zgpg30
TD: 65536
SOLVENT: CDCl3
NS: 103
DS: 4
SWH: 30030.000 Hz
FIDRES: 0.458232 Hz
AQ: 1.0910410 sec
RG: 25890.3
DC: 1.6000000 usec
DE: 7.0000000 usec
TE: 297.1 K
D1: 2.00000000 sec
d11: 1.10000000 sec
d12: 0.03000000 sec
TD0: 1

===== CHANNEL f1 =====
NUC1: 13C
P1: 130 nsec
PL1: 0 dB
SFO1: 125.7603540 MHz

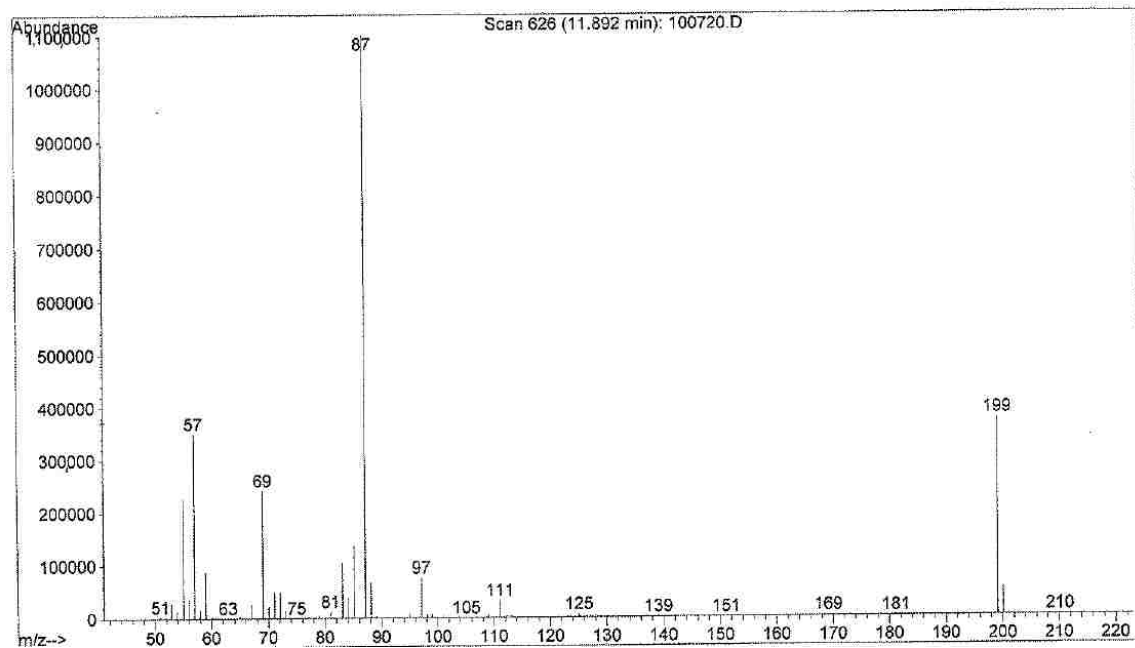
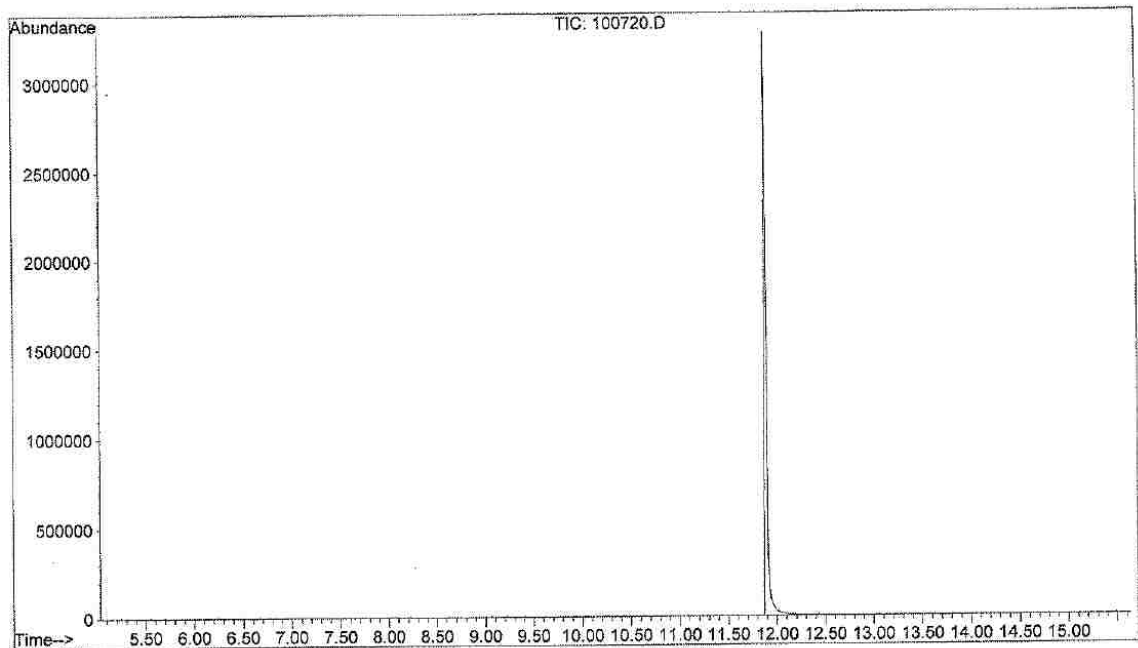
===== CHANNEL f2 =====
NUC2: 1H
P2: 100.00 usec
PL2: 0 dB
SFO2: 500.132239 MHz

F2 - Processing parameters
SI: 32768
SF: 125.757958 MHz
WDW: EM
SSB: 0
LB: 1.00 Hz
GB: 0
PC: 1.40

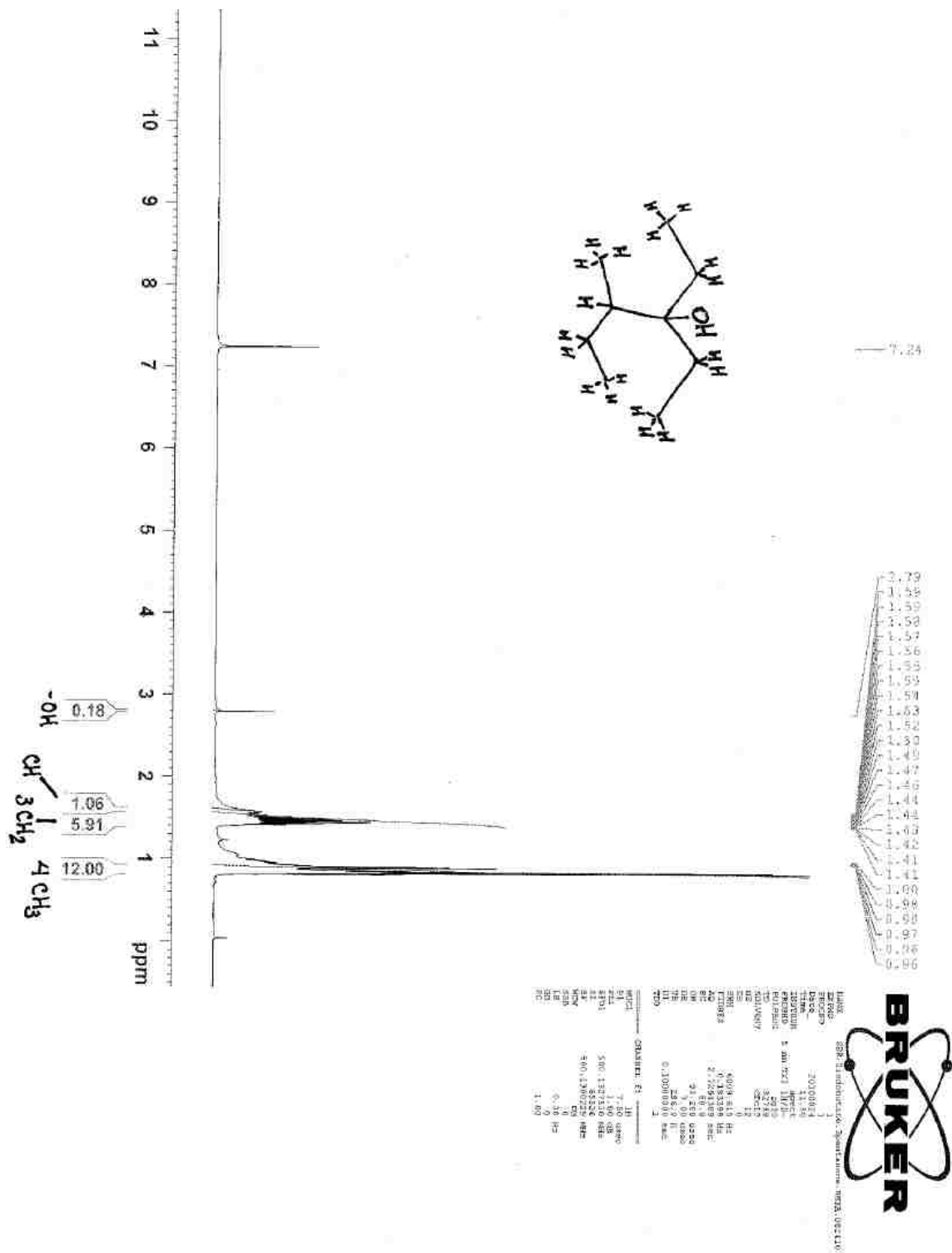


8.2.5.5 ¹³C NMR (5) 3-ethyltridecan-3-ol

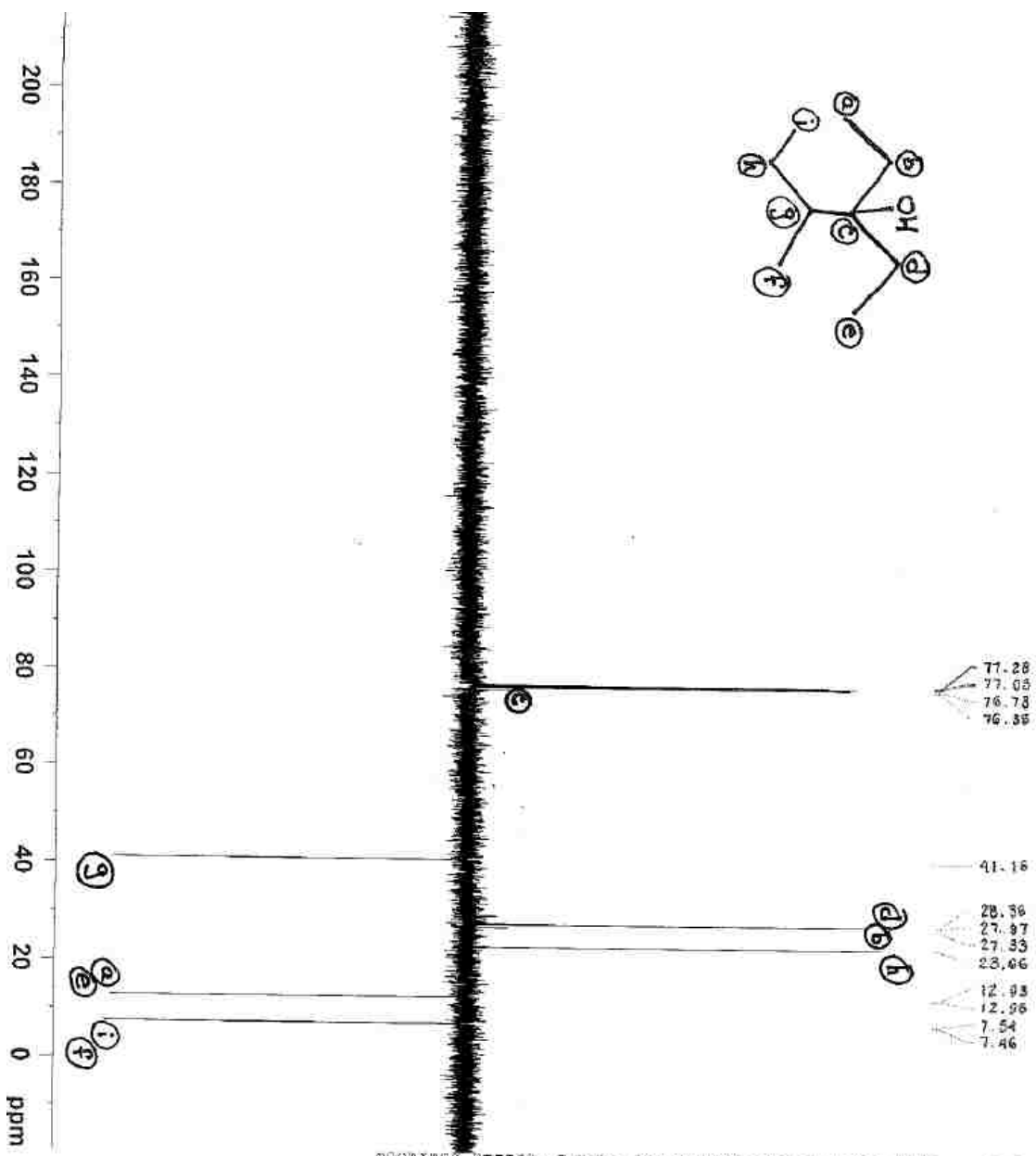
File : C:\HPCHEM\1\DATA\KAT208\100720.D
Operator : kim
Acquired : 20 Jul 2010 9:37 using AcqMethod SADA4
Instrument : GC/MS Ins
Sample Name: SBR-bromo-HMPA
Misc Info :
Vial Number: 1



8.2.5.6 GC-MS (5) 3-ethyltridecan-3-ol



8.2.5.7 ¹H NMR (10) 3-ethyl-4-methylhexan-3-ol



BRUKER

CHANNEL: CH3 F3200MHz
 GAIN: 10.00000000
 SWH: 20000.000000
 RES: 0.10000000
 FID: 1.00000000
 F2: 125.760346 MHz
 CHANNEL: CH2 F3200MHz
 GAIN: 10.00000000
 SWH: 20000.000000
 RES: 0.10000000
 FID: 1.00000000
 F2: 125.760346 MHz
 CHANNEL: CH1 F3200MHz
 GAIN: 10.00000000
 SWH: 20000.000000
 RES: 0.10000000
 FID: 1.00000000
 F2: 125.760346 MHz

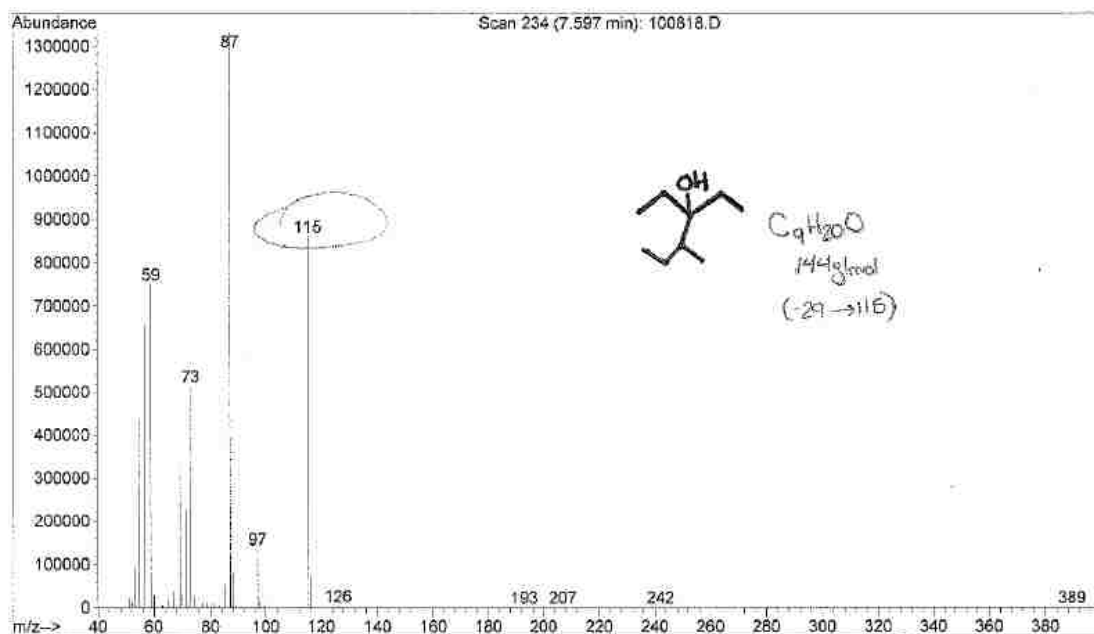
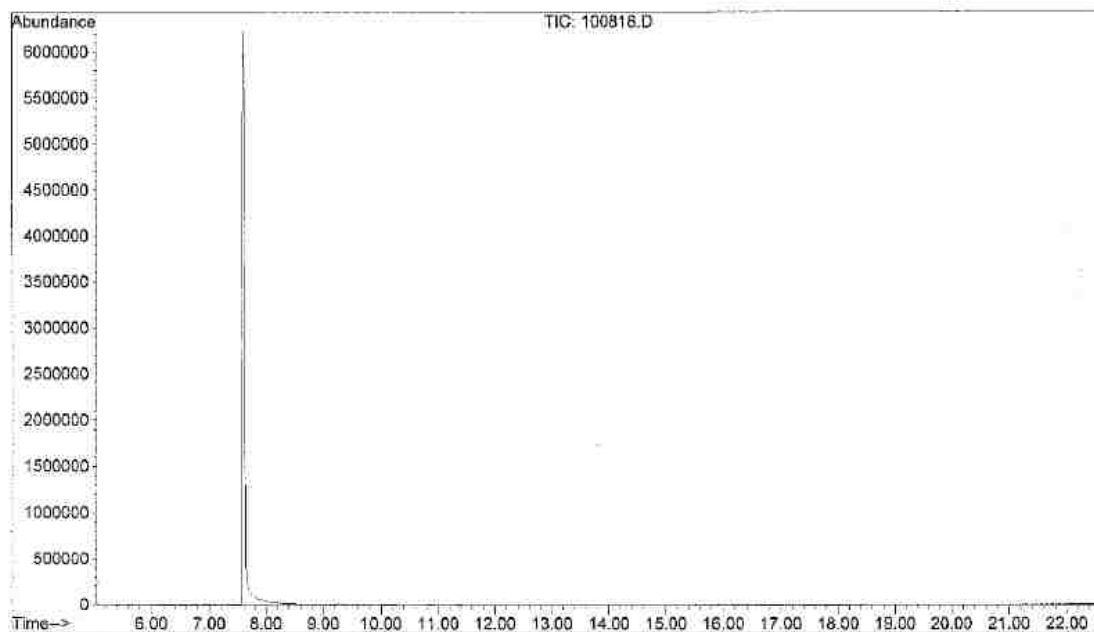
NAME: 3-ethyl-4-methylhexan-3-ol
 LANTHUM: 5 mm HNP SPC-1H
 PULPROG: zgpg30
 TO: 0.00000000
 ACQ: 12.11.2018
 DE: 12.11.2018
 TIME: 12.11.2018 11:54:58
 F2: 125.760346 MHz
 F1: 125.760346 MHz
 F0: 125.760346 MHz
 CH1: 125.760346 MHz
 CH2: 125.760346 MHz
 CH3: 125.760346 MHz
 P1: 1.00000000
 P2: 1.00000000
 P3: 1.00000000
 P4: 1.00000000
 P5: 1.00000000
 P6: 1.00000000
 P7: 1.00000000
 P8: 1.00000000
 P9: 1.00000000
 P10: 1.00000000
 P11: 1.00000000
 P12: 1.00000000
 P13: 1.00000000
 P14: 1.00000000
 P15: 1.00000000
 P16: 1.00000000
 P17: 1.00000000
 P18: 1.00000000
 P19: 1.00000000
 P20: 1.00000000
 P21: 1.00000000
 P22: 1.00000000
 P23: 1.00000000
 P24: 1.00000000
 P25: 1.00000000
 P26: 1.00000000
 P27: 1.00000000
 P28: 1.00000000
 P29: 1.00000000
 P30: 1.00000000
 P31: 1.00000000
 P32: 1.00000000
 P33: 1.00000000
 P34: 1.00000000
 P35: 1.00000000
 P36: 1.00000000
 P37: 1.00000000
 P38: 1.00000000
 P39: 1.00000000
 P40: 1.00000000
 P41: 1.00000000
 P42: 1.00000000
 P43: 1.00000000
 P44: 1.00000000
 P45: 1.00000000
 P46: 1.00000000
 P47: 1.00000000
 P48: 1.00000000
 P49: 1.00000000
 P50: 1.00000000
 P51: 1.00000000
 P52: 1.00000000
 P53: 1.00000000
 P54: 1.00000000
 P55: 1.00000000
 P56: 1.00000000
 P57: 1.00000000
 P58: 1.00000000
 P59: 1.00000000
 P60: 1.00000000
 P61: 1.00000000
 P62: 1.00000000
 P63: 1.00000000
 P64: 1.00000000
 P65: 1.00000000
 P66: 1.00000000
 P67: 1.00000000
 P68: 1.00000000
 P69: 1.00000000
 P70: 1.00000000
 P71: 1.00000000
 P72: 1.00000000
 P73: 1.00000000
 P74: 1.00000000
 P75: 1.00000000
 P76: 1.00000000
 P77: 1.00000000
 P78: 1.00000000
 P79: 1.00000000
 P80: 1.00000000
 P81: 1.00000000
 P82: 1.00000000
 P83: 1.00000000
 P84: 1.00000000
 P85: 1.00000000
 P86: 1.00000000
 P87: 1.00000000
 P88: 1.00000000
 P89: 1.00000000
 P90: 1.00000000
 P91: 1.00000000
 P92: 1.00000000
 P93: 1.00000000
 P94: 1.00000000
 P95: 1.00000000
 P96: 1.00000000
 P97: 1.00000000
 P98: 1.00000000
 P99: 1.00000000
 P100: 1.00000000

CH2 ↑
 CH3 ↑
 CH ↑

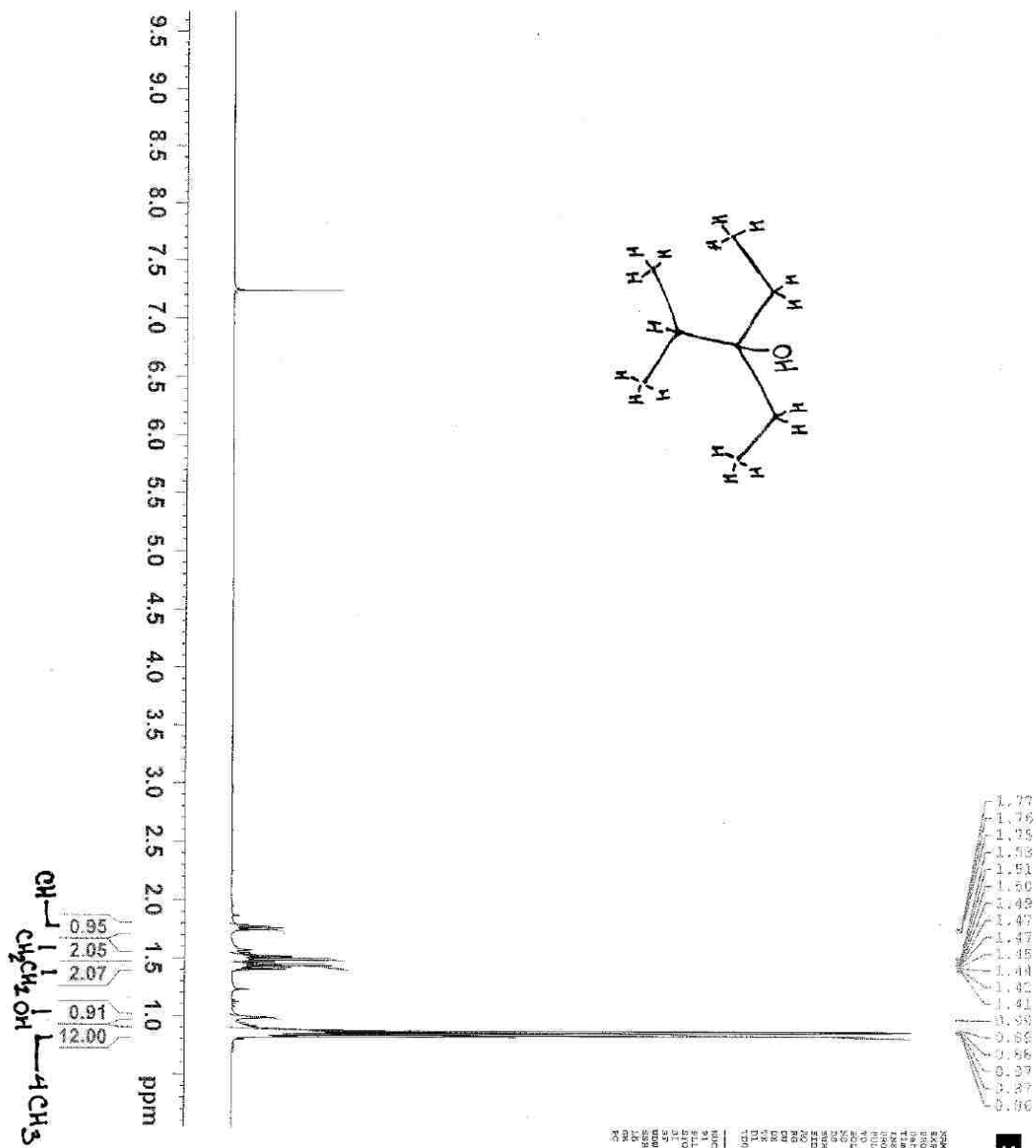
8.2.5.8 ¹³C NMR (10) 3-ethyl-4-methylhexan-3-ol
266

File : C:\HPCHEM\1\DATA\KAT208\100818.D
 Operator : kim
 Acquired : 18 Aug 2010 11:17 using AcqMethod SADA4
 Instrument : GC/MS Ins
 Sample Name: SBR.HMPA.2iodobutane.3-pentanone
 Misc Info :
 Vial Number: 1

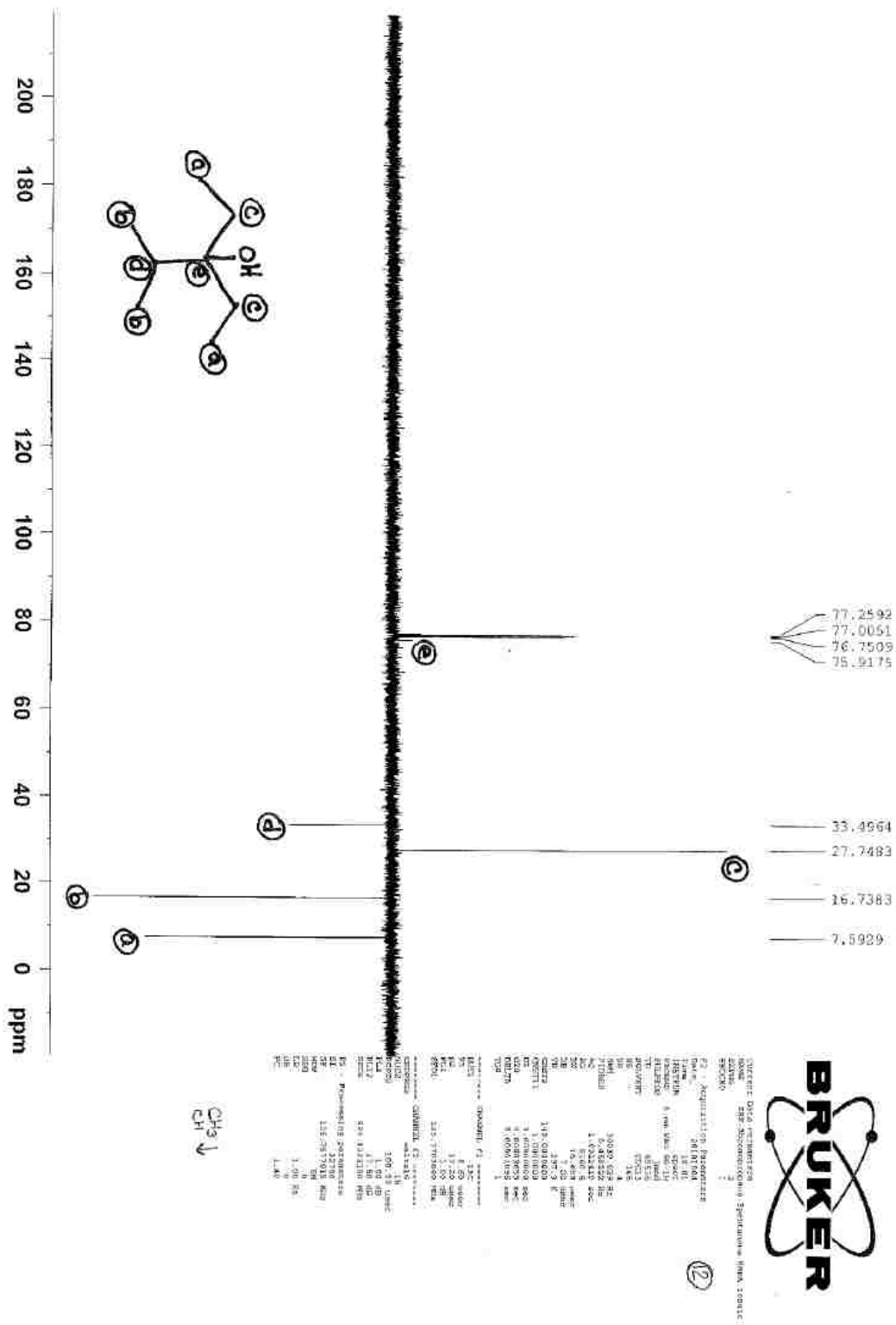
2^o iodo
 (10)



8.2.5.9 GC-MS (10) 3-ethyl-4-methylhexan-3-ol



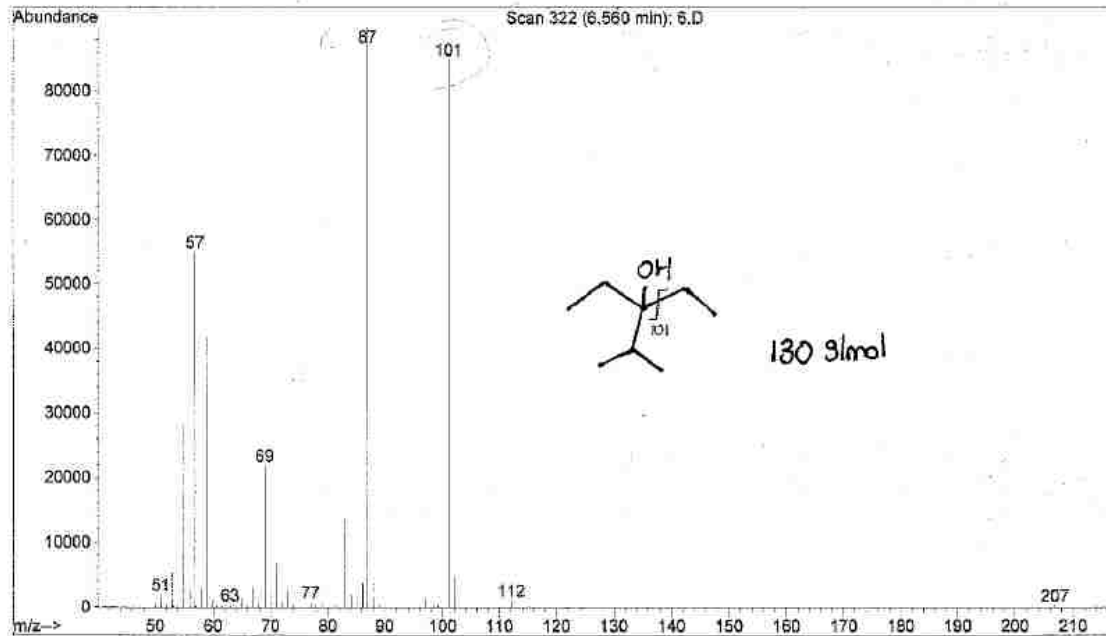
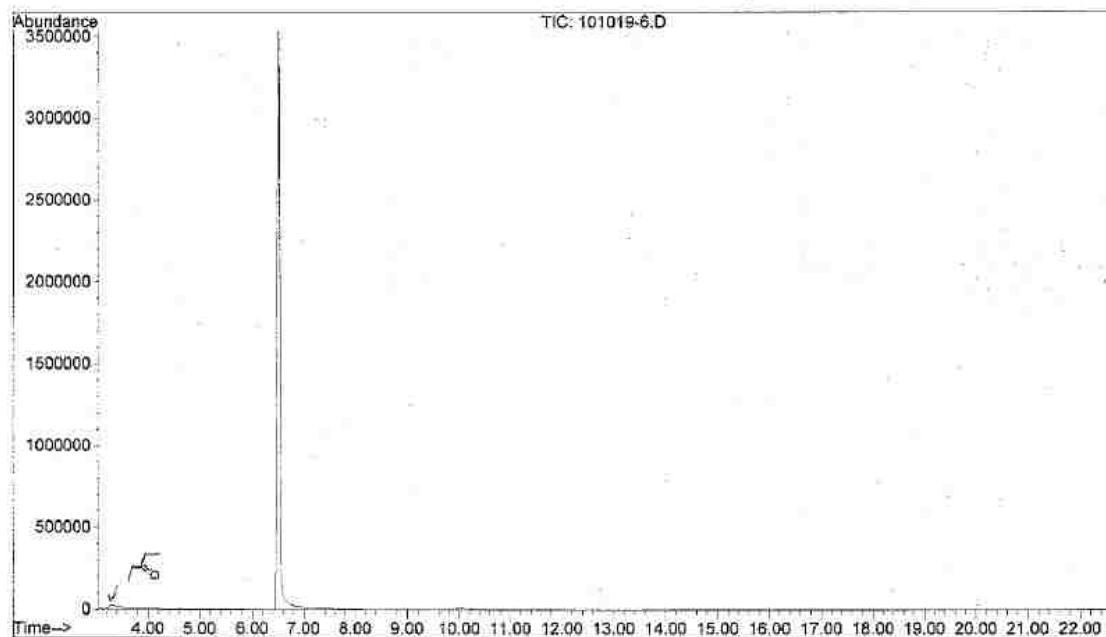
8.2.5.10 ¹H NMR (12) 3-ethyl-2-methylpentan-3-ol



8.2.5.11 ^{13}C NMR (12) 3-ethyl-2-methylpentan-3-ol

File : C:\HPCHEM\1\DATA\KAT208\101019-6.D
Operator : kim
Acquired : 19 Oct 2010 16:02 using AcqMethod SADA1510
Instrument : GC/MS Ins
Sample Name: SBR.2bromopropane
Misc Info :
Vial Number: 1

(12)



8.2.5.12 GC-MS (12) 3-ethyl-2-methylpentan-3-ol

8.3 Catalytic Ni(II) in SmI₂ Reactions: Sm(II) or Ni(0) Chemistry?

8.3.1 Product Identification

8.3.1.1 (6) 3-ethylpentadecan-3-ol ¹H NMR (500MHz, CDCl₃) δ (ppm): 0.8438 (9H, m, 3CH₃); 0.9567 (1H s, OH, peak disappears with the addition of D₂O), 1.2370 (20H br s, 10 CH₂); 1.3922 (2H, m, CH₂); 1.4262 (4H, q, C(2)H₂, CH₃CH₂-C₁₃H₂₆-OH). ¹³C NMR (125MHz, CDCl₃) δ (ppm): 7.7941; 14.1343; 22.7060; 23.4124; 29.3702; 29.6622; 29.6814; 30.3263; 31.0478; 31.9376; 38.2339; 74.6412. GC-MS *m/z* (rel. abundance) 227 (64), 87 (100).

8.3.2 Kinetic Data: Stopped-Flow Plots

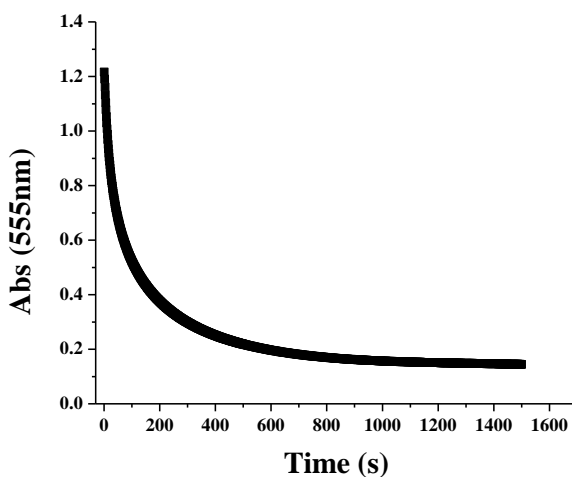


Figure 8.3.2.1. Representative decay trace at 555 nm of SmI₂ (0.02) with 1 mol% Ni(DPPE)₂ (2.0x 10⁻⁴), 0.04M **4**, 0.04M **5**.

Table 8.3.2.2. Conditions of RPKA “same excess” experiment.

	SmI ₂ (mmol)	R-X (mmol)			Ketone (mmol)			Ni(II)	
		measured	needed	excess	measured	needed	excess	mmol	mol %
1	0.100	0.200	0.050	0.150	0.200	0.050	0.150	0.001	1.000
2	0.050	0.175	0.025	0.150	0.175	0.025	0.150	0.001	1.000

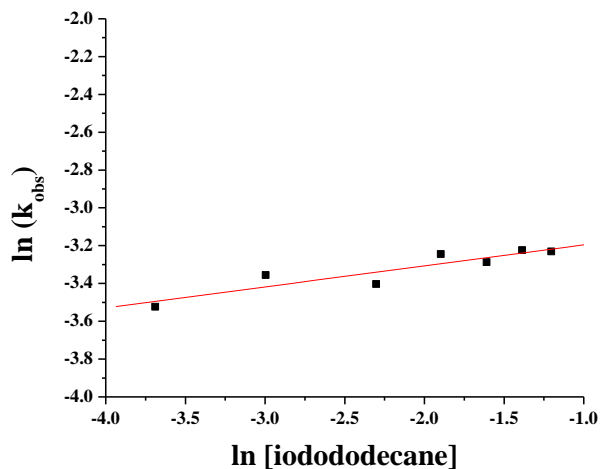


Figure 8.3.2.3. Plot of $\ln[4]$ versus $\ln k_{\text{obs}}$. $\text{SmI}_2 = 5 \text{ mM}$; **5** = 25 equiv.; HMPA = 10 equiv.; **4** = 10-60 equiv. Rate Order = 0.11 ± 0.02

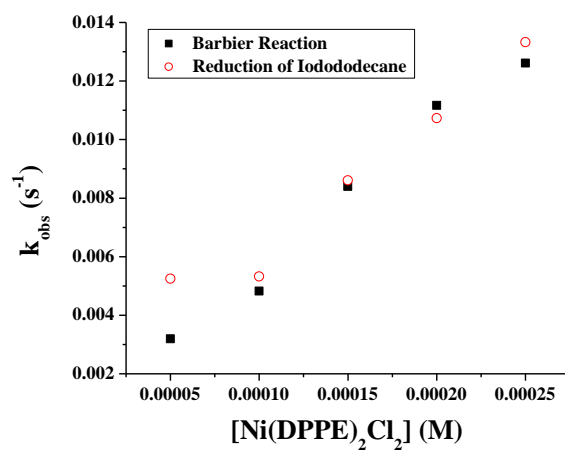


Figure 8.3.2.4. Effect of increasing amounts of $\text{Ni}(\text{DPPE})_2\text{Cl}_2$ on the Samarium Barbier reaction (**4** and **5**) and the reduction of **4**. ■ $\text{SmI}_2 = 5\text{mM}$; **4** = 25 equiv.; **5** = 25 equiv.; $\text{Ni}(\text{DPPE})_2\text{Cl}_2 = 1\text{-}5 \text{ mol\%}$ (5.0e^{-5} - $2.5\text{e}^{-4} \text{ M}$) ○ $\text{SmI}_2 = 5\text{mM}$; **4** = 25 equiv.; $\text{Ni}(\text{DPPE})_2\text{Cl}_2 = 1\text{-}5 \text{ mol\%}$ (5.0e^{-5} - $2.5\text{e}^{-4} \text{ M}$).

8.3.3 ¹H NMR



0.8342
0.8449
0.8491
0.8589
0.8725
1.0411
1.2376
1.2566
1.2765
1.2905
1.3638
1.3695
1.3773
1.3932
1.4123
1.4274
1.4424
1.4575
1.5482

Current Data Parameters
NAME Al(acac)2.1mol%.15ml.tms.107410
EXPERO 1
PROCNO 1

F2 - Acquisition Parameters
Date_ 20101010
Time_ 13:37
INSTRUM spect
PROBHD 5 mm BBO BB-1H
PULPROG zgpg30
TD 32768
SOLVENT CHCl3
NS 3
DS 3
SWH 6000.415 Hz
FIDRES 0.183389 Hz
AQ 2.7254309 sec
RG 256
DE 83.300 usec
TE 296.5 K
D1 0.10000000 sec
TD0 1

===== CHANNEL f1 =====
NUC1 1H
P1 14.00 usec
PL1 1.00 dB
SFO1 500.1327510 MHz
F2 - Processing parameters
SI 65516
SF 500.13000233 MHz
WDW EM
SSB 0
LB 0.30 Hz
GB C
PC 1.00

7.2401

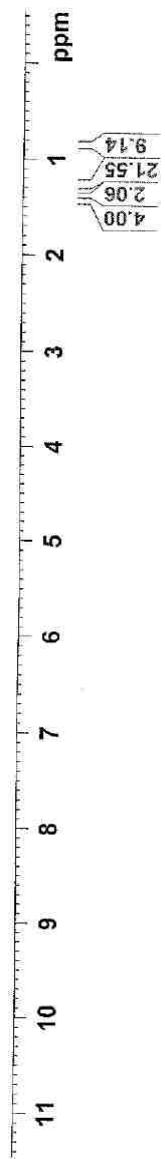


Figure 8.3.3.1. ¹H NMR of 6

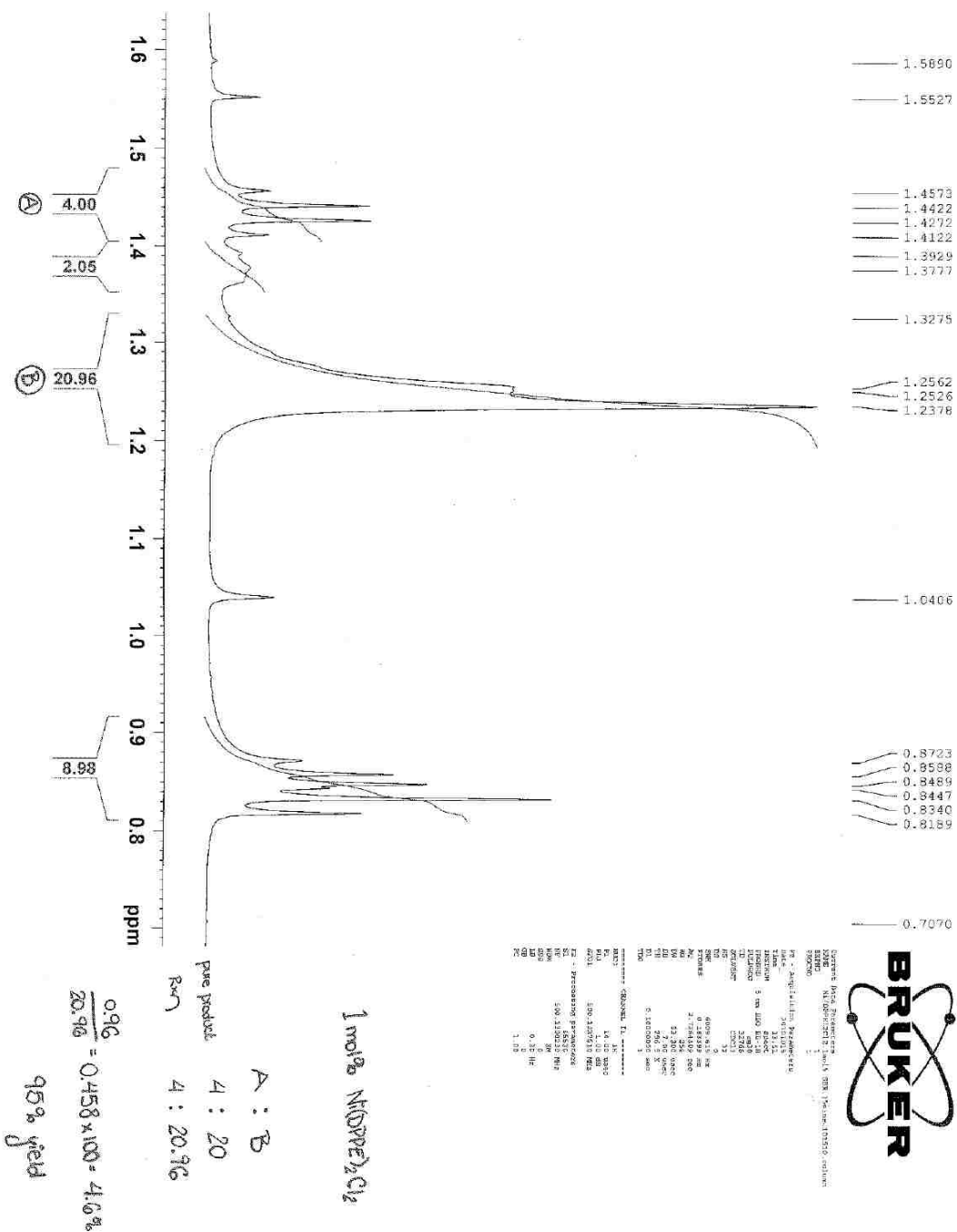


Figure 8.3.3.3. ¹H NMR ratio of **6**: dodecane with 1 mol% Ni(DPPE)₂Cl₂. (Table 4.1, entry 4)

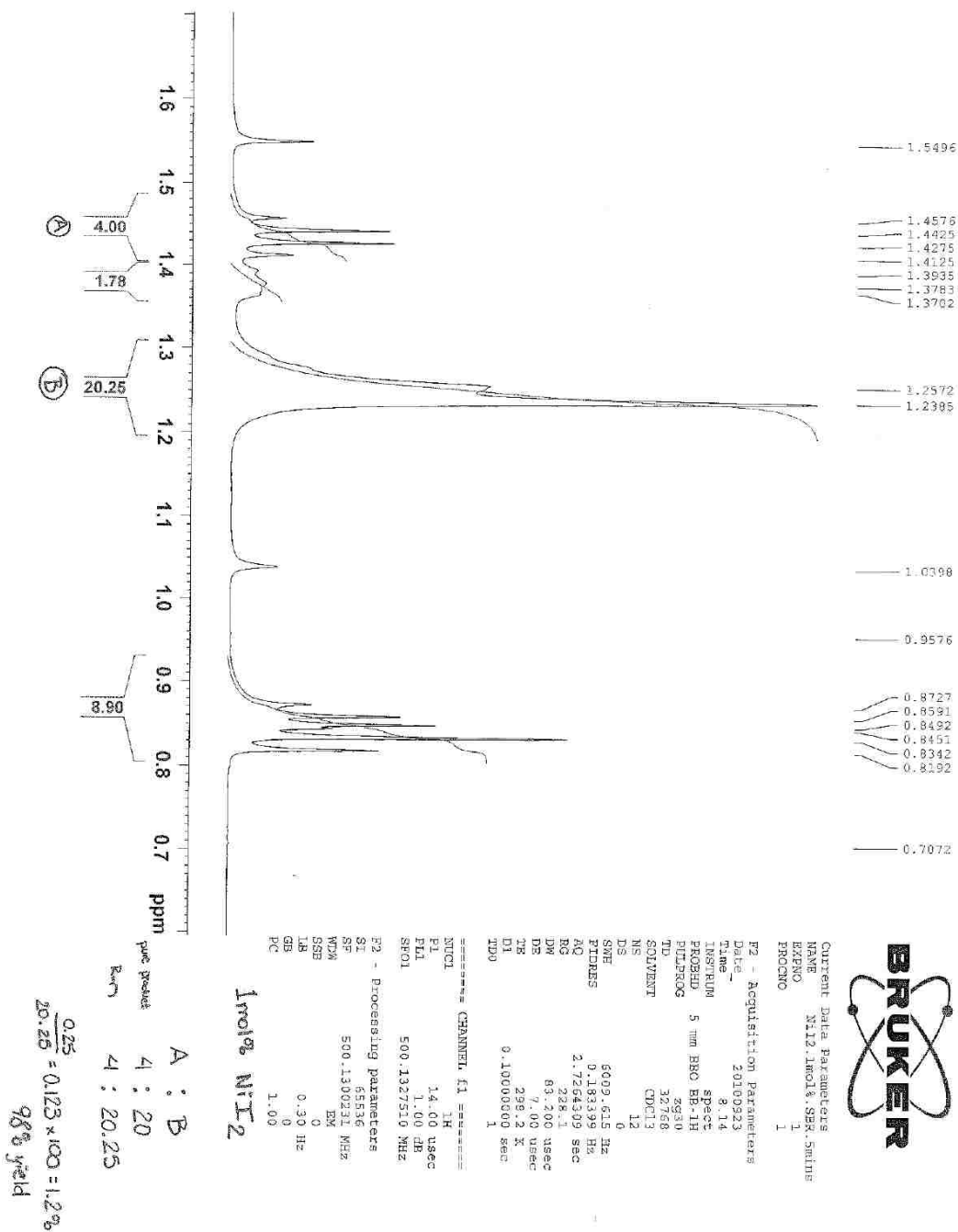
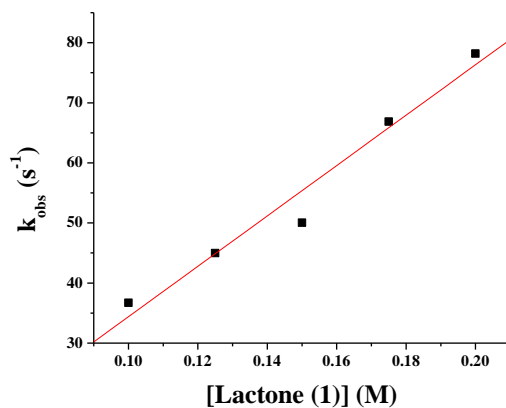


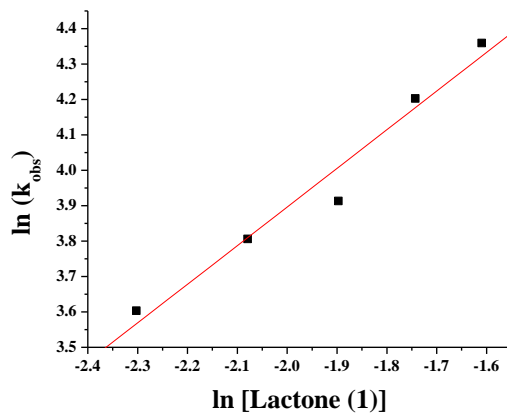
Figure 8.3.3.4. ¹H NMR ratio of **6**: dodecane with 1 mol% NiI₂. (Table 4.1, entry 2)

8.4 Addition of H₂O to SmI₂ Reactions: Reduction of Lactones

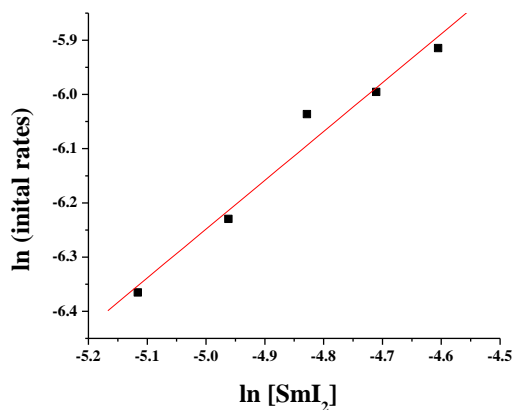
8.4.1 Kinetic Data: Stopped-Flow Plots



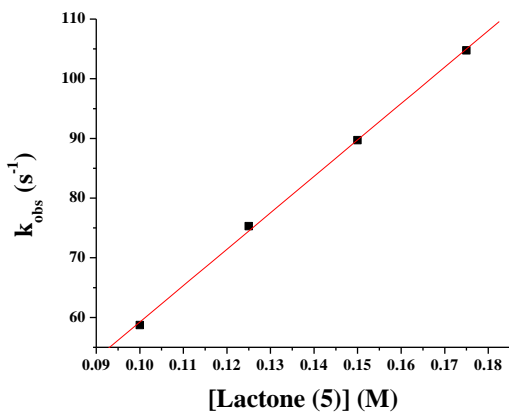
8.4.1.1 Plot of k_{obs} vs [Lactone (1)]. SmI₂ = 10 mM, H₂O = 150 equiv., Lactone (1) = 15-40 equiv. T = 30.0 ± 0.1 °C. Rate Constant = 419 ± 45 M⁻¹s⁻¹.



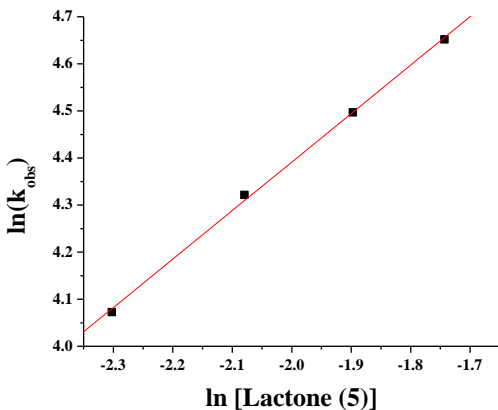
8.4.1.2 Plot of ln(k_{obs}) vs ln[Lactone (1)]. SmI₂ = 10 mM, H₂O = 150 equiv., Lactone (2) = 15-40 equiv. T = 30.0 ± 0.1 °C. Rate Order = 1.09 ± 0.12.



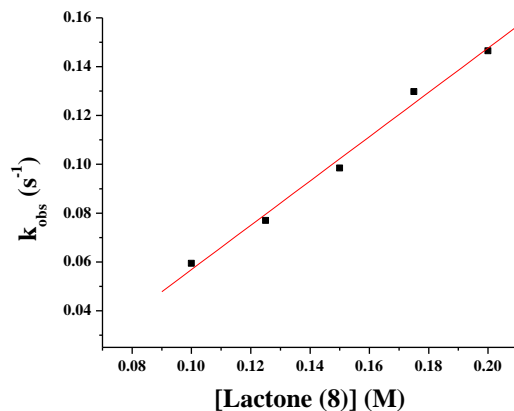
8.4.1.3 Order of SmI₂ by initial rates method. Lactone **1** = 10 mM, H₂O = 10 equiv., SmI₂ = 6-10 mM. SmI₂ order 0.9 ± 0.1



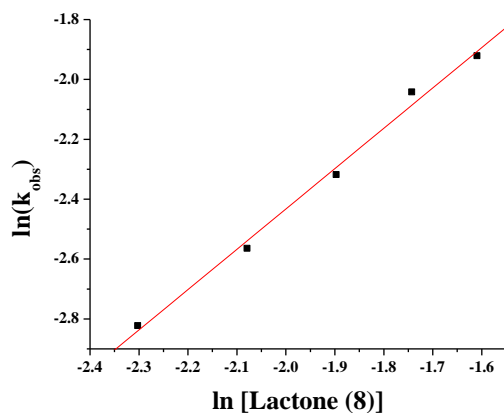
8.4.1.4 Plot of k_{obs} vs [Lactone (**5**)]. SmI₂ = 10 mM, H₂O = 150 equiv., Lactone (**1**) = 10-20 equiv. T = 30.0 ± 0.1 °C. Rate Constant = 610 ± 10 M⁻¹s⁻¹.



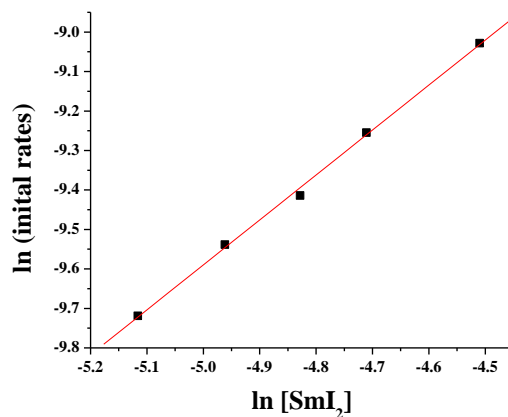
8.4.1.5 Plot of $\ln(k_{obs})$ vs \ln [Lactone (**5**)]. SmI₂ = 10 mM, H₂O = 150 equiv., Lactone (**5**) = 10-20 equiv. T = 30.0 ± 0.1 °C. Rate Order = 1.03 ± 0.02 .



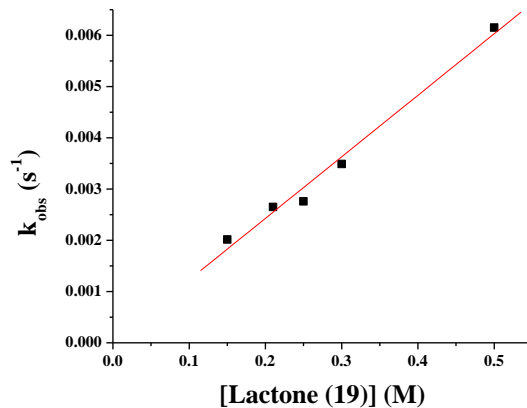
8.4.1.6 Plot of k_{obs} vs [Lactone (8)]. $SmI_2 = 10$ mM, $H_2O = 150$ equiv., Lactone (8) = 10-20 equiv. $T = 30.0 \pm 0.1$ °C. Rate Constant = 0.91 ± 0.05 $M^{-1}s^{-1}$.



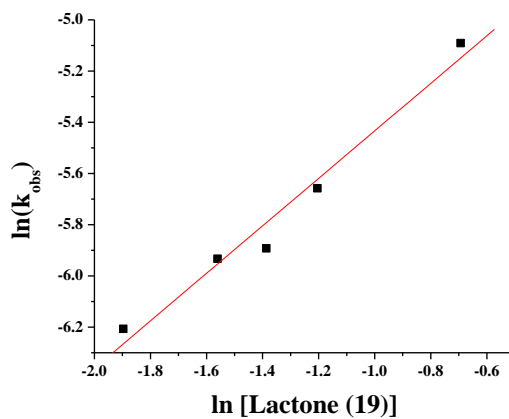
8.4.1.7 Plot of $\ln(k_{obs})$ vs \ln [Lactone (8)]. $SmI_2 = 10$ mM, $H_2O = 150$ equiv., Lactone (8) = 10-20 equiv. $T = 30.0 \pm 0.1$ °C. Rate Order = 1.3 ± 0.1 .



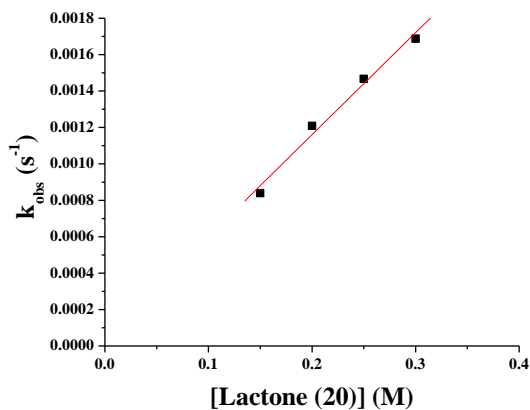
8.4.1.8 Order of SmI_2 by initial rates method. Lactone 8 = 5 mM, $H_2O = 10$ equiv., $SmI_2 = 5$ -10 mM. SmI_2 order 1.1 ± 0.1 .



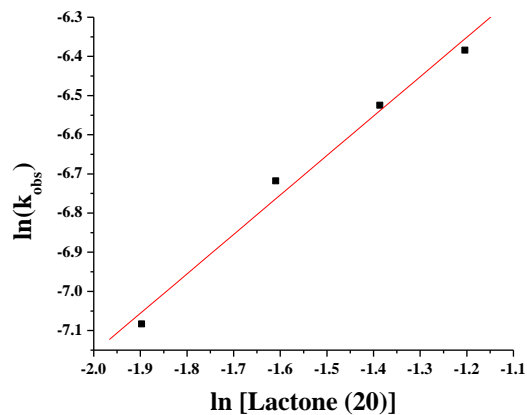
8.4.1.9 Plot of k_{obs} vs [Lactone (19)]. $SmI_2 = 10$ mM, $H_2O = 150$ equiv., Lactone (19) = 15-50 equiv. $T = 30.0 \pm 0.1$ °C. Rate Constant = 0.012 ± 0.001 $M^{-1}s^{-1}$.



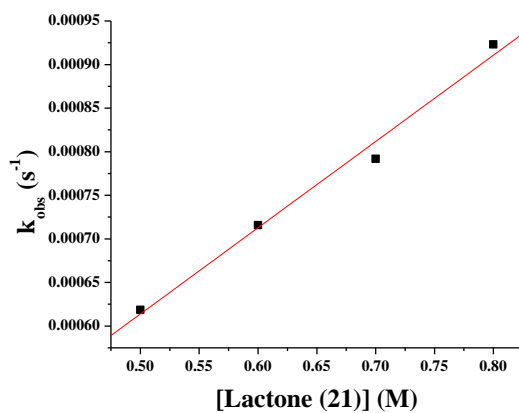
8.4.1.10 Plot of $\ln(k_{obs})$ vs $\ln[\text{Lactone (19)}]$. $SmI_2 = 10$ mM, $H_2O = 150$ equiv., Lactone (19) = 15-50 equiv. $T = 30.0 \pm 0.1$ °C. Rate Order = 0.9 ± 0.1 .



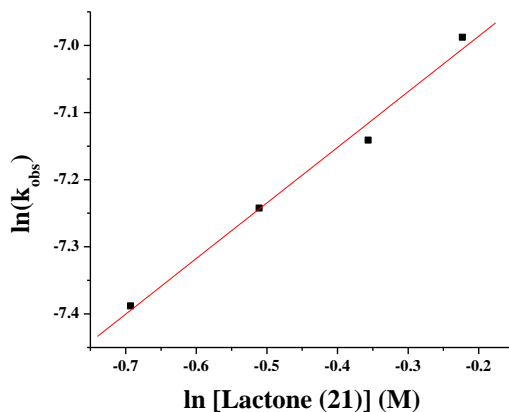
8.4.1.11 Plot of k_{obs} vs [Lactone (20)]. $SmI_2 = 10$ mM, $H_2O = 150$ equiv., Lactone (20) = 15-30 equiv. $T = 30.0 \pm 0.1$ °C. Rate Constant = 0.006 ± 0.001 $M^{-1}s^{-1}$.



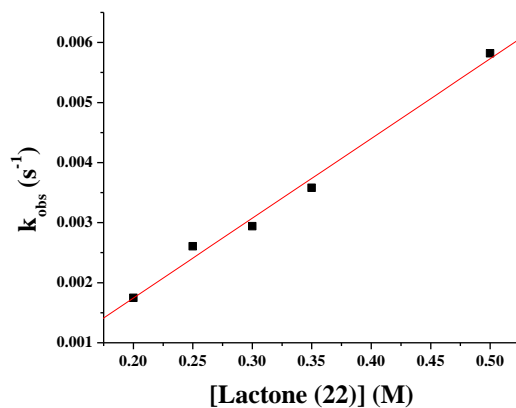
8.4.1.12 Plot of $\ln(k_{obs})$ vs $\ln[\text{Lactone (20)}]$. $\text{SmI}_2 = 10 \text{ mM}$, $\text{H}_2\text{O} = 150 \text{ equiv.}$, Lactone (20) = 15-30 equiv. $T = 30.0 \pm 0.1 \text{ }^\circ\text{C}$. Rate Order = 1.0 ± 0.1 .



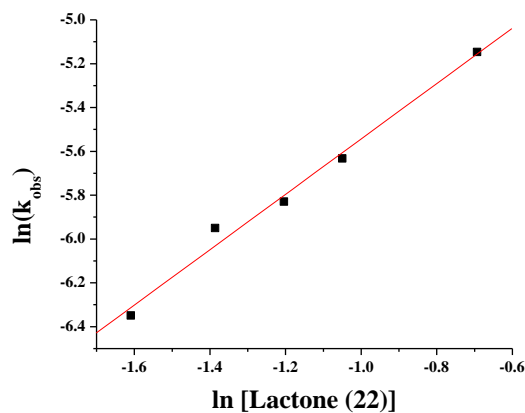
8.4.1.13 Plot of k_{obs} vs $[\text{Lactone (21)}]$. $\text{SmI}_2 = 10 \text{ mM}$, $\text{H}_2\text{O} = 150 \text{ equiv.}$, Lactone (21) = 50-80 equiv. $T = 30.0 \pm 0.1 \text{ }^\circ\text{C}$. Rate Constant = $0.001 \pm 0.001 \text{ M}^{-1}\text{s}^{-1}$.



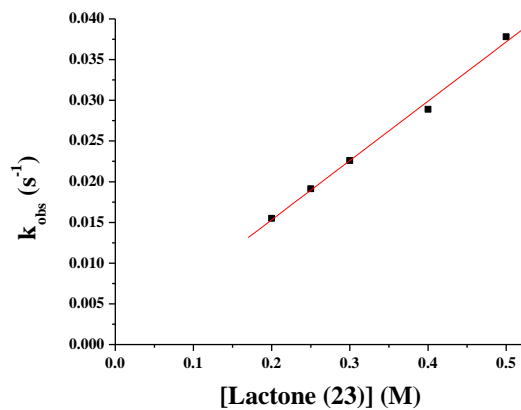
8.4.1.14 Plot of $\ln(k_{obs})$ vs $\ln[\text{Lactone (21)}]$. $\text{SmI}_2 = 10 \text{ mM}$, $\text{H}_2\text{O} = 150 \text{ equiv.}$, Lactone (21) = 50-80 equiv. $T = 30.0 \pm 0.1 \text{ }^\circ\text{C}$. Rate Order = 0.8 ± 0.1 .



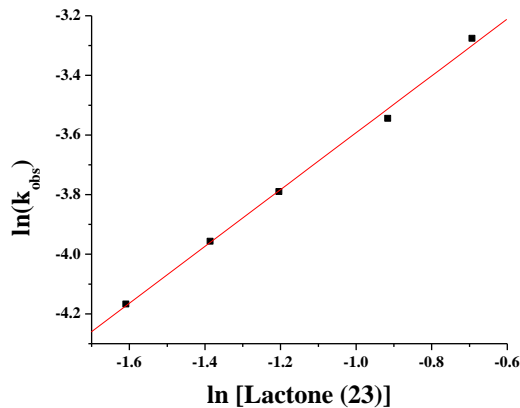
8.4.1.15 Plot of k_{obs} vs [Lactone (22)]. $SmI_2 = 10$ mM, $H_2O = 150$ equiv., Lactone (22) = 20-50 equiv. $T = 30.0 \pm 0.1$ °C. Rate Constant = 0.013 ± 0.001 $M^{-1}s^{-1}$.



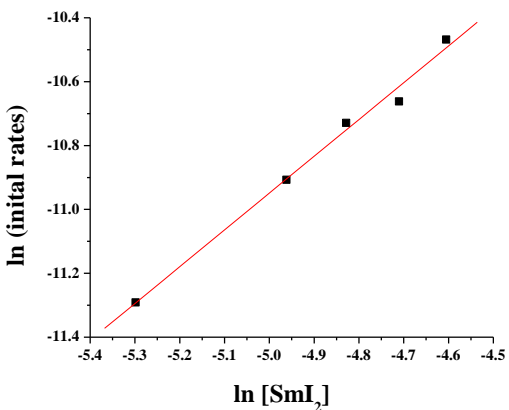
8.4.1.16 Plot of $\ln(k_{obs})$ vs $\ln[\text{Lactone (22)}]$. $SmI_2 = 10$ mM, $H_2O = 150$ equiv., Lactone (22) = 20-50 equiv. $T = 30.0 \pm 0.1$ °C. Rate Order = 1.3 ± 0.1 .



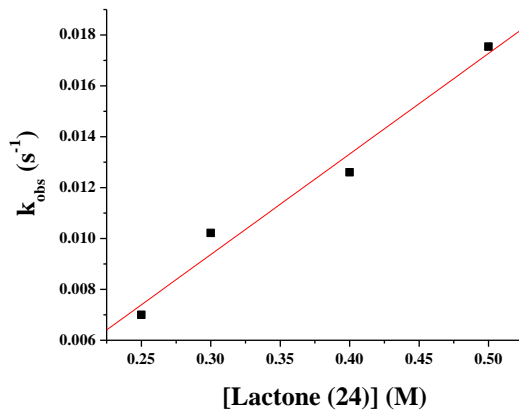
8.4.1.17 Plot of k_{obs} vs [Lactone (23)]. $SmI_2 = 10$ mM, $H_2O = 150$ equiv., Lactone (23) = 20-50 equiv. $T = 30.0 \pm 0.1$ °C. Rate Constant = 0.073 ± 0.001 $M^{-1}s^{-1}$.



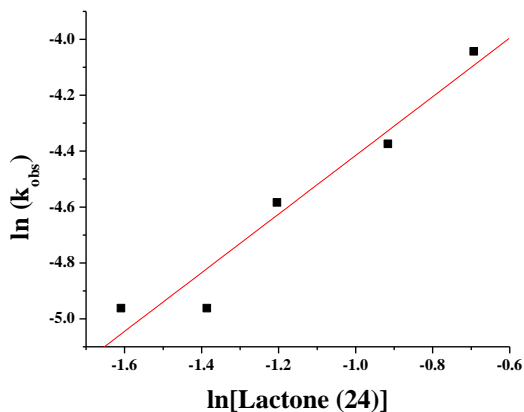
8.4.1.18 Plot of $\ln(k_{obs})$ vs $\ln[\text{Lactone (23)}]$. $\text{SmI}_2 = 10 \text{ mM}$, $\text{H}_2\text{O} = 150 \text{ equiv.}$, Lactone (23) = 20-50 equiv. $T = 30.0 \pm 0.1 \text{ }^\circ\text{C}$. Rate Order = 0.95 ± 0.03 .



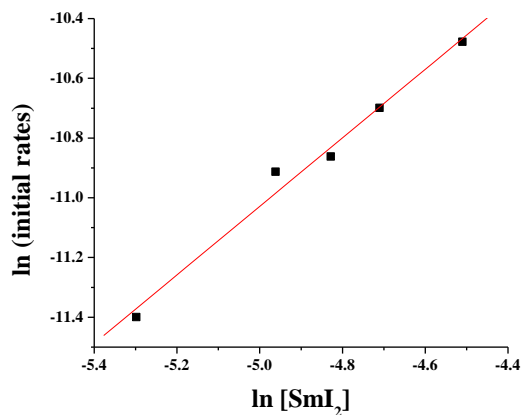
8.4.1.19 Order of SmI_2 by initial rates method. Lactone **23** = 5 mM, $\text{H}_2\text{O} = 10 \text{ equiv.}$, $\text{SmI}_2 = 5\text{-}10 \text{ mM}$. SmI_2 order 1.2 ± 0.1 .



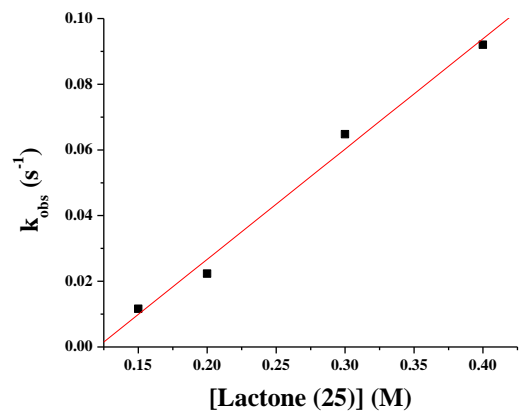
8.4.1.20 Plot of k_{obs} vs $[\text{Lactone (24)}]$. $\text{SmI}_2 = 10 \text{ mM}$, $\text{H}_2\text{O} = 150 \text{ equiv.}$, Lactone (24) = 20-50 equiv. $T = 30.0 \pm 0.1 \text{ }^\circ\text{C}$. Rate Constant = $0.04 \pm 0.01 \text{ M}^{-1}\text{s}^{-1}$.



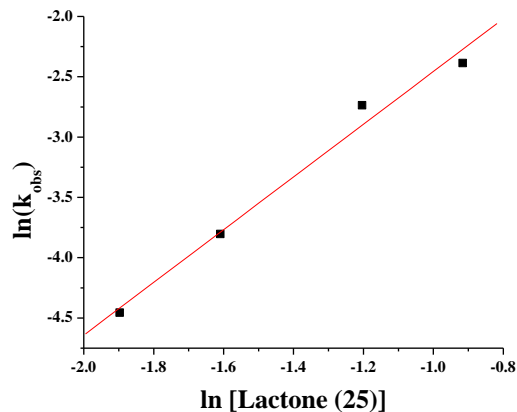
8.4.1.21 Plot of $\ln(k_{obs})$ vs $\ln[\text{Lactone (24)}]$. $\text{SmI}_2 = 10 \text{ mM}$, $\text{H}_2\text{O} = 150 \text{ equiv.}$, Lactone (24) = 20-50 equiv. $T = 30.0 \pm 0.1 \text{ }^\circ\text{C}$. Rate Order = 1.05 ± 0.1 .



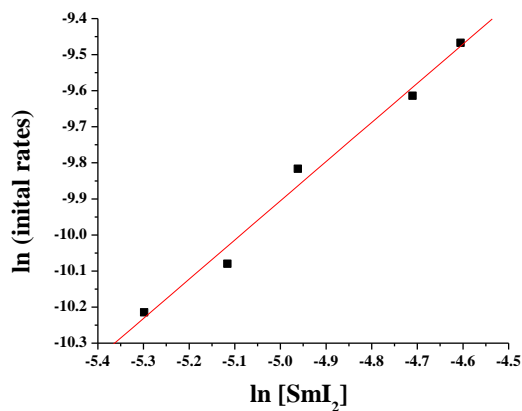
8.4.1.22 Order of SmI_2 by initial rates method. Lactone **24** = 5 mM, $\text{H}_2\text{O} = 10 \text{ equiv.}$, $\text{SmI}_2 = 5\text{-}10 \text{ mM}$. SmI_2 order 1.1 ± 0.1



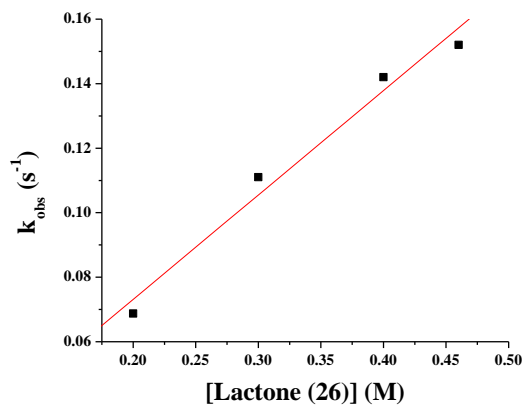
8.4.1.23 Plot of k_{obs} vs $[\text{Lactone (25)}]$. $\text{SmI}_2 = 10 \text{ mM}$, $\text{H}_2\text{O} = 150 \text{ equiv.}$, Lactone (25) = 14-40 equiv. $T = 30.0 \pm 0.1 \text{ }^\circ\text{C}$. Rate Constant = $0.34 \pm 0.03 \text{ M}^{-1}\text{s}^{-1}$.



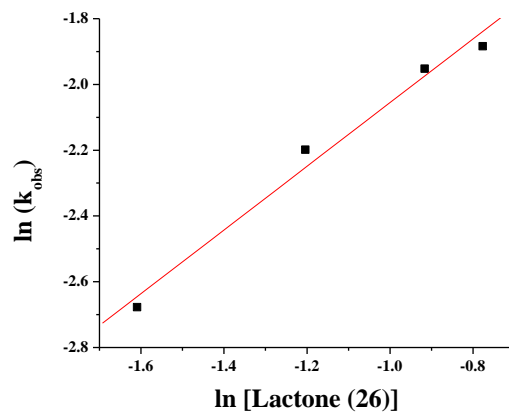
25.4.1.24 Plot of $\ln(k_{obs})$ vs $\ln[\text{Lactone (25)}]$. $\text{SmI}_2 = 10 \text{ mM}$, $\text{H}_2\text{O} = 150 \text{ equiv.}$, Lactone (25) = 15-40 equiv. $T = 30.0 \pm 0.1 \text{ }^\circ\text{C}$. Rate Order = 2.2 ± 0.2 .



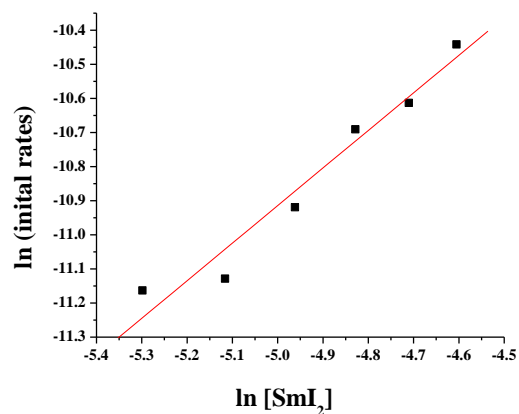
8.4.1.25 Order of SmI_2 by initial rates method. Lactone **25** = 5 mM, $\text{H}_2\text{O} = 10 \text{ equiv.}$, $\text{SmI}_2 = 5\text{-}10 \text{ mM}$. SmI_2 order 1.1 ± 0.1



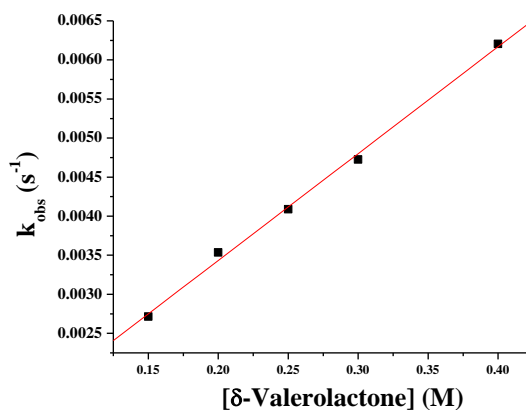
8.4.1.26 Plot of k_{obs} vs $[\text{Lactone (26)}]$. $\text{SmI}_2 = 10 \text{ mM}$, $\text{H}_2\text{O} = 150 \text{ equiv.}$, Lactone (26) = 20-46 equiv. $T = 30.0 \pm 0.1 \text{ }^\circ\text{C}$. Rate Constant = $0.32 \pm 0.03 \text{ M}^{-1}\text{s}^{-1}$.



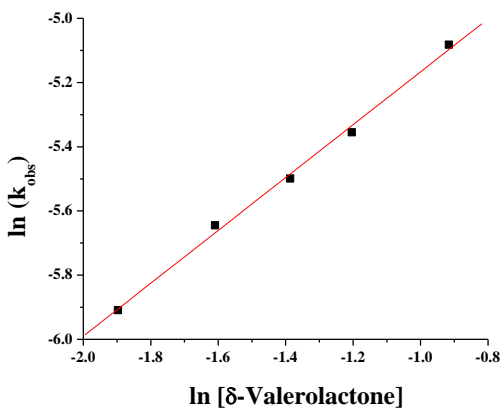
8.4.1.27 Plot of $\ln(k_{obs})$ vs \ln [Lactone (26)]. $\text{SmI}_2 = 10 \text{ mM}$, $\text{H}_2\text{O} = 150 \text{ equiv.}$, Lactone (26) = 15-40 equiv. $T = 30.0 \pm 0.1 \text{ }^\circ\text{C}$. Rate Order = 0.98 ± 0.1 .



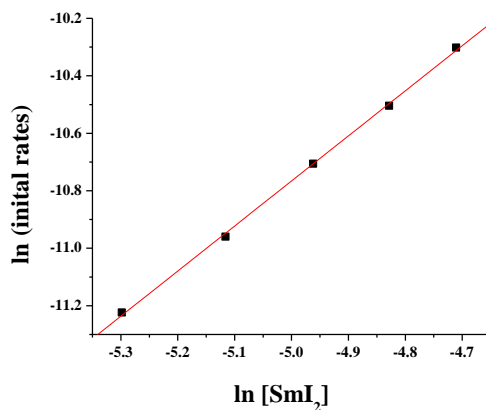
8.4.1.28 Order of SmI_2 by initial rates method. Lactone 26 = 5 mM, $\text{H}_2\text{O} = 10 \text{ equiv.}$, $\text{SmI}_2 = 5\text{-}10 \text{ mM}$. SmI_2 order 1.1 ± 0.1



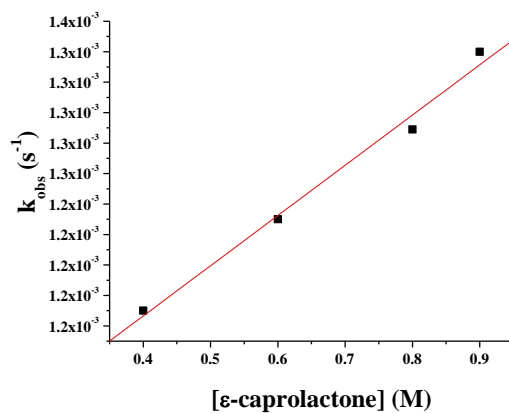
8.4.1.29 Plot of k_{obs} vs [δ -valerolactone] (29). $\text{SmI}_2 = 10 \text{ mM}$, $\text{H}_2\text{O} = 150 \text{ equiv.}$, δ -valerolactone = 15-40 equiv. $T = 30.0 \pm 0.1 \text{ }^\circ\text{C}$. Rate Constant = $0.014 \pm 0.001 \text{ M}^{-1}\text{s}^{-1}$.



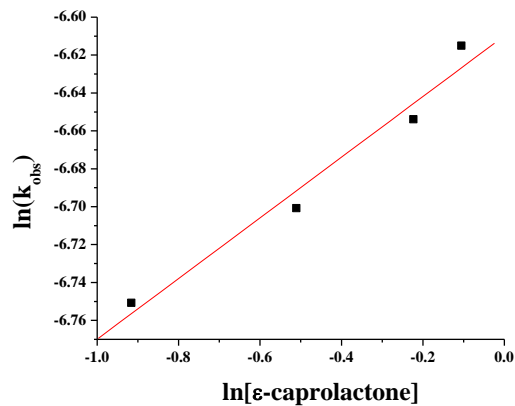
8.4.1.30 Plot of $\ln(k_{obs})$ vs $\ln[\delta\text{-valerolactone}]$ (29). $\text{SmI}_2 = 10 \text{ mM}$, $\text{H}_2\text{O} = 150 \text{ equiv.}$, $\delta\text{-valerolactone} = 15\text{-}40 \text{ equiv.}$ $T = 30.0 \pm 0.1 \text{ }^\circ\text{C}$. Rate Order = 0.82 ± 0.03 .



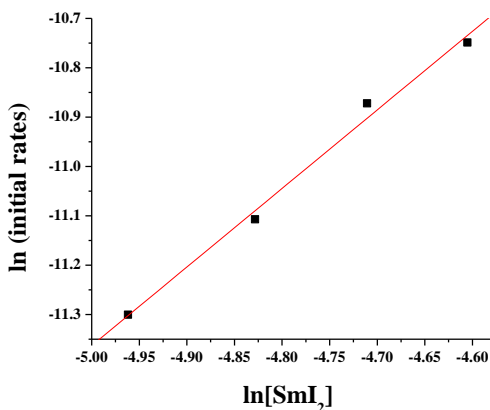
8.4.1.31 Order of SmI_2 by initial rates method. $\delta\text{-valerolactone} = 5 \text{ mM}$, $\text{H}_2\text{O} = 10 \text{ equiv.}$, $\text{SmI}_2 = 5\text{-}10 \text{ mM}$. SmI_2 order 1.5 ± 0.1



8.4.1.32 Plot of k_{obs} vs $[\epsilon\text{-caprolactone}]$ (31). $\text{SmI}_2 = 10 \text{ mM}$, $\text{H}_2\text{O} = 150 \text{ equiv.}$, $\epsilon\text{-caprolactone} = 40\text{-}90 \text{ equiv.}$ $T = 30.0 \pm 0.1 \text{ }^\circ\text{C}$. Rate Constant = $0.0003 \pm 0.00002 \text{ M}^{-1}\text{s}^{-1}$.



8.4.1.33 Plot of $\ln(k_{obs})$ vs $\ln[\epsilon\text{-caprolactone}]$ (31). $\text{SmI}_2 = 10 \text{ mM}$, $\text{H}_2\text{O} = 150 \text{ equiv.}$, $\epsilon\text{-caprolactone} = 40\text{-}90 \text{ equiv.}$ $T = 30.0 \pm 0.1 \text{ }^\circ\text{C}$. Rate Order = 0.16 ± 0.02 .



8.4.1.34 Order of SmI_2 by initial rates method. $\epsilon\text{-caprolactone} = 5 \text{ mM}$, $\text{H}_2\text{O} = 10 \text{ equiv.}$, $\text{SmI}_2 = 5\text{-}10 \text{ mM}$. SmI_2 order 1.5 ± 0.1

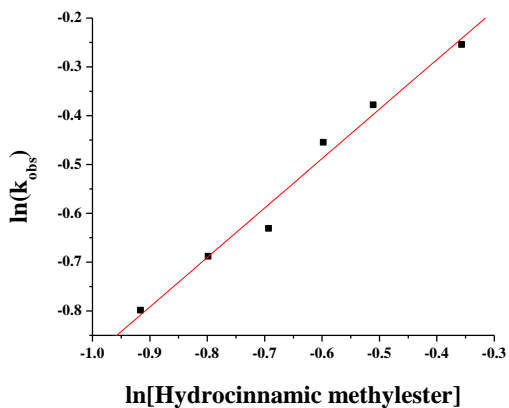
Table 8.4.1.35 Order of SmI_2 : Fractional Times Method

Lactone	$T_{3/4}/T_{1/2}^a$	Order
5	2.2	1
19	2.2	1
20	2.0	1
21	1.9	1
22	2.2	1
28	ref	1
29	2.2	1

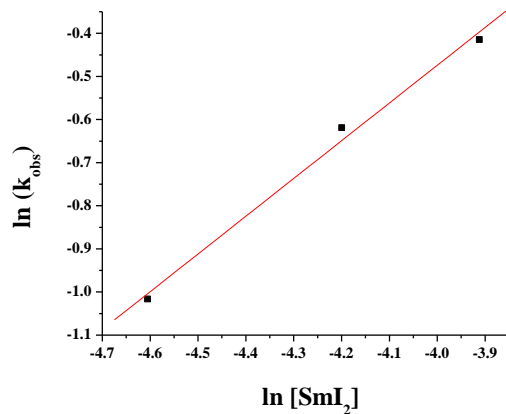
^aaverage of all of the decay plots over the range of concentrations plotted in rate constants plots.

8.5 SmI₂-H₂O-amine system

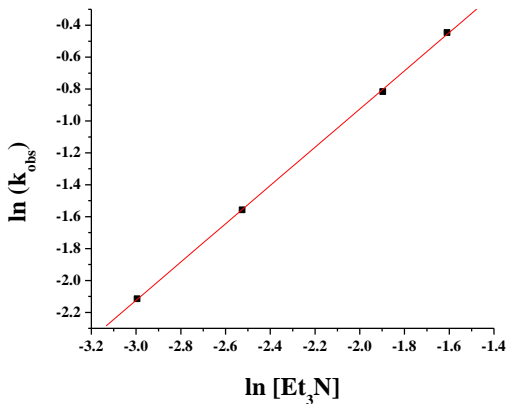
8.5.1 Kinetic Plots—Rate Orders hydrocinnamic acid methyl ester reduction with SmI₂-H₂O-Et₃N at 25 °C



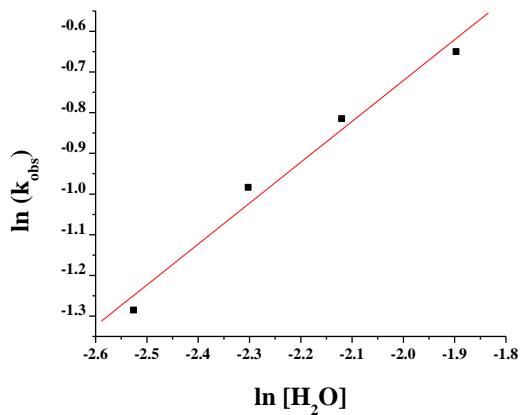
8.5.1.1 Plot of $\ln(k_{obs})$ vs $\ln[\text{hydrocinnamic methylester}]$. SmI₂ = 10 mM, H₂O = 100 mM, Et₃N = 100 mM, methylester = 400-700 mM. T = 25.0 ± 0.1 °C. Rate Order = 1.0 ± 0.1.



8.5.1.2 Plot of $\ln(k_{obs})$ vs $\ln[\text{SmI}_2]$. SmI₂ = 10-20 mM, H₂O = 100 mM, Et₃N = 100 mM, methylester = 500 mM. T = 25.0 ± 0.1 °C. Rate Order = 0.9 ± 0.1.

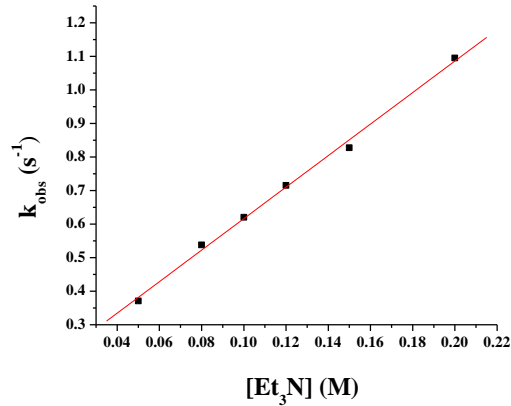


8.5.3.3 Plot of $\ln(k_{\text{obs}})$ vs $\ln[\text{Et}_3\text{N}]$. $\text{SmI}_2 = 10 \text{ mM}$, $\text{H}_2\text{O} = 100 \text{ mM}$, methylester = 500 mM, $\text{Et}_3\text{N} = 50\text{-}200 \text{ mM}$. $T = 25.0 \pm 0.1 \text{ }^\circ\text{C}$. Rate Order = 0.9 ± 0.1 .

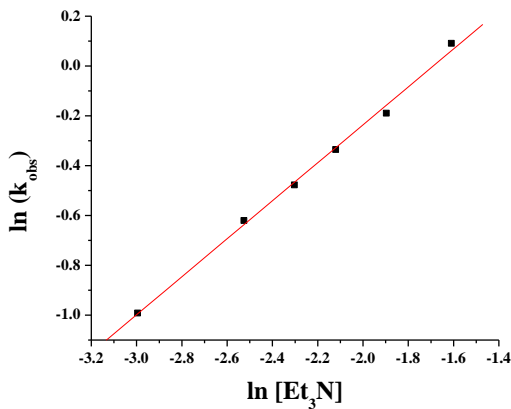


8.5.1.4 Plot of $\ln(k_{\text{obs}})$ vs $\ln[\text{H}_2\text{O}]$. $\text{SmI}_2 = 10 \text{ mM}$, $\text{Et}_3\text{N} = 100 \text{ mM}$, methylester = 500 mM, $\text{H}_2\text{O} = 50\text{-}150 \text{ mM}$. $T = 25.0 \pm 0.1 \text{ }^\circ\text{C}$. Rate Order = 1.0 ± 0.1 .

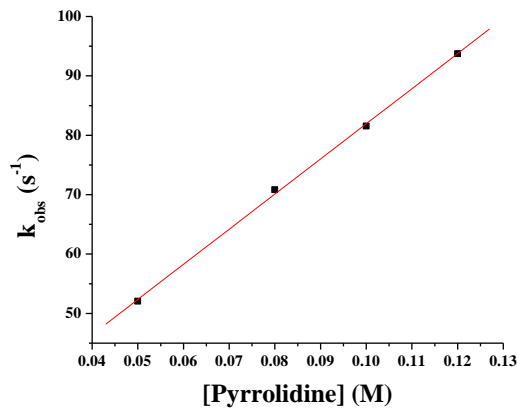
8.5.2 Kinetic Plots—Rate Constants of hydrocinnamic acid methyl ester reduction with $\text{SmI}_2\text{-H}_2\text{O}$ -amines at 0°C



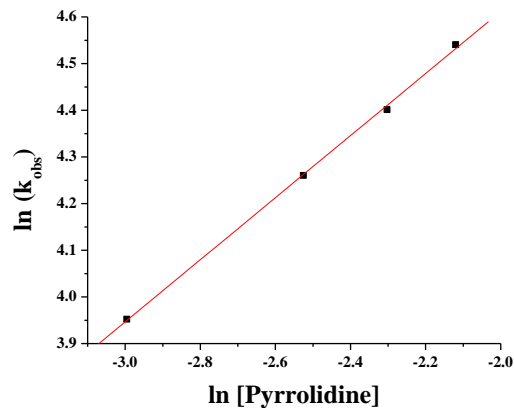
8.5.2.1 Plot of k_{obs} vs $[Et_3N]$. $SmI_2 = 10$ mM, $H_2O = 100$ mM, methylester = 500 mM, $Et_3N = 50-200$ mM. $T = 0.0 \pm 0.1$ °C. Rate Constant = 4.7 ± 0.2 M⁻³s⁻¹.



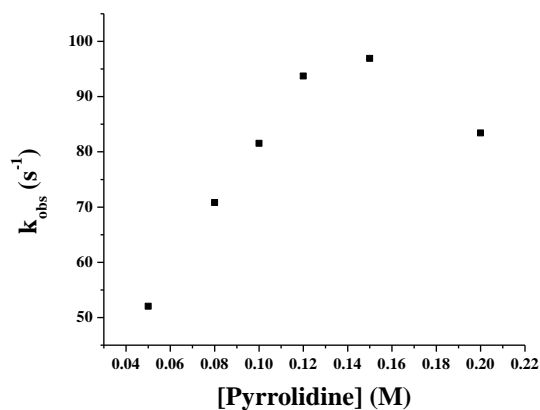
8.5.2.2 Plot of $\ln(k_{obs})$ vs $\ln[Et_3N]$. $SmI_2 = 10$ mM, $H_2O = 100$ mM, methylester = 500 mM, $Et_3N = 50-200$ mM. $T = 0.0 \pm 0.1$ °C. Rate Order = 0.76 ± 0.02 .



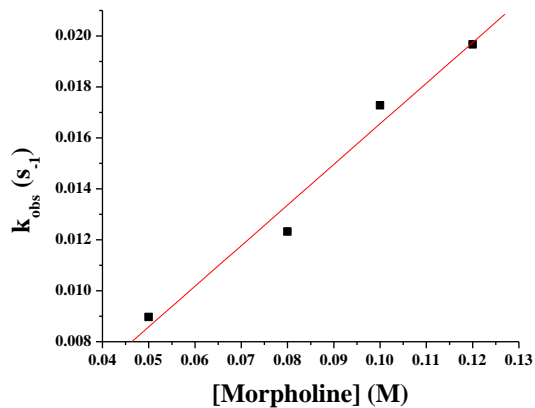
8.5.2.3 Plot of k_{obs} vs [Pyrrolidine]. $SmI_2 = 10$ mM, $H_2O = 100$ mM, methylester = 500 mM, Pyrrolidine = 50-120 mM. $T = 0.0 \pm 0.1$ °C. Rate Constant = 591 ± 12 M⁻³s⁻¹.



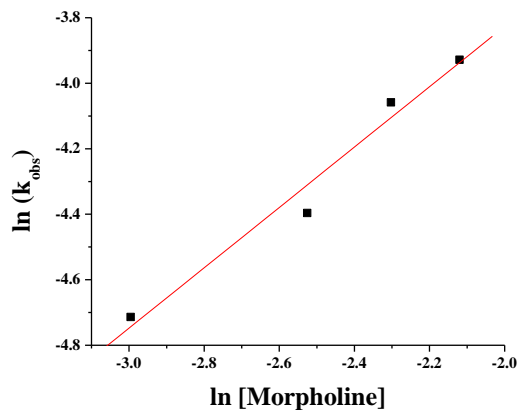
8.5.2.4 Plot of $\ln(k_{obs})$ vs $\ln[\text{Pyrrolidine}]$. $\text{SmI}_2 = 10 \text{ mM}$, $\text{H}_2\text{O} = 100 \text{ mM}$, methylester = 500 mM, Pyrrolidine = 50-120 mM. $T = 0.0 \pm 0.1 \text{ }^\circ\text{C}$. Rate Order = 0.7 ± 0.2 .



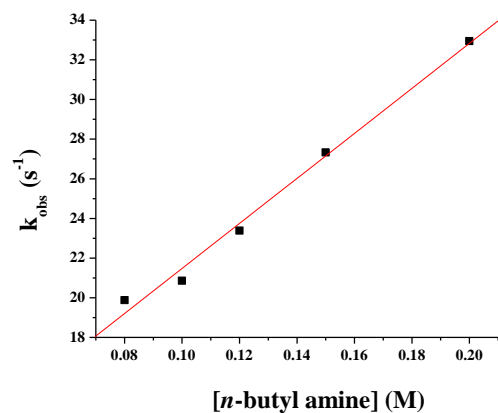
8.5.2.5 Plot of k_{obs} vs [Pyrrolidine]. $\text{SmI}_2 = 10 \text{ mM}$, $\text{H}_2\text{O} = 100 \text{ mM}$, methylester = 500 mM, Pyrrolidine = 50-2000 mM. $T = 0.0 \pm 0.1 \text{ }^\circ\text{C}$.



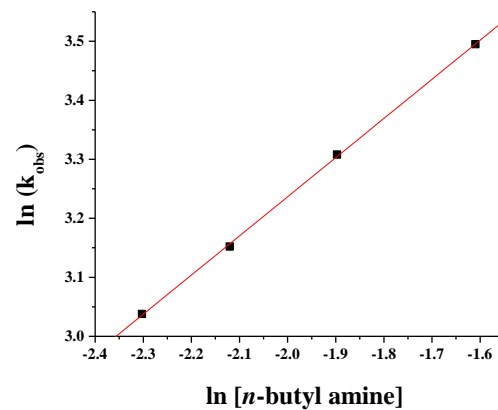
8.5.2.6 Plot of k_{obs} vs [Morpholine]. $\text{SmI}_2 = 10 \text{ mM}$, $\text{H}_2\text{O} = 100 \text{ mM}$, methylester = 500 mM, Morpholine = 50-120 mM. $T = 0.0 \pm 0.1 \text{ }^\circ\text{C}$. Rate Constant = $0.16 \pm 0.02 \text{ M}^{-3}\text{s}^{-1}$.



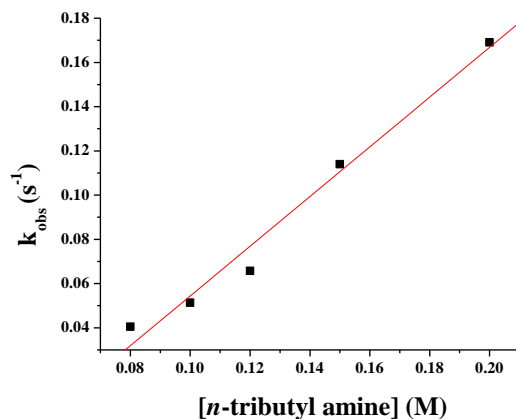
8.5.2.7 Plot of $\ln(k_{obs})$ vs $\ln[\text{Morpholine}]$. $\text{SmI}_2 = 10 \text{ mM}$, $\text{H}_2\text{O} = 100 \text{ mM}$, methylester = 500 mM, Morpholine = 50-120 mM. $T = 0.0 \pm 0.1 \text{ }^\circ\text{C}$. Rate Order = 0.92 ± 0.11 .



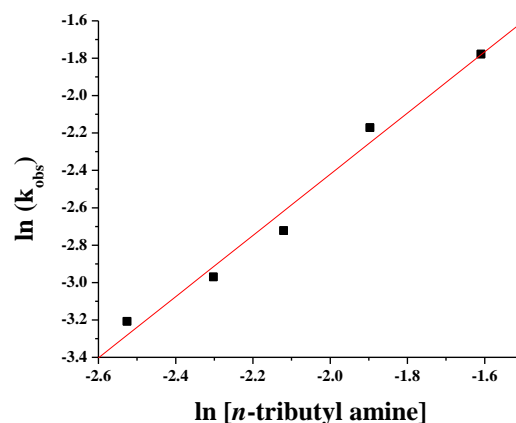
8.5.2.8 Plot of k_{obs} vs $[n\text{-butylamine}]$. $\text{SmI}_2 = 10 \text{ mM}$, $\text{H}_2\text{O} = 100 \text{ mM}$, methylester = 500 mM, $n\text{-butylamine} = 80\text{-}200 \text{ mM}$. $T = 0.0 \pm 0.1 \text{ }^\circ\text{C}$. Rate Constant = $114 \pm 6 \text{ M}^{-3}\text{s}^{-1}$.



8.5.2.9 Plot of $\ln(k_{obs})$ vs $\ln[n\text{-butylamine}]$. $\text{SmI}_2 = 10 \text{ mM}$, $\text{H}_2\text{O} = 100 \text{ mM}$, methylester = 500 mM, $n\text{-butylamine} = 100\text{-}200 \text{ mM}$. $T = 0.0 \pm 0.1 \text{ }^\circ\text{C}$. Rate Order = 0.66 ± 0.01 .

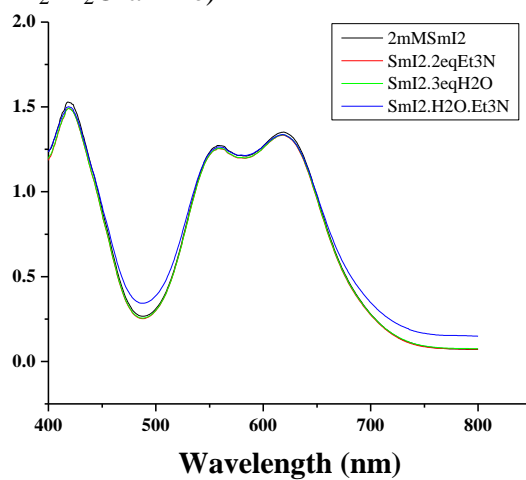


8.5.2.10 Plot of k_{obs} vs [*n*-tributylamine]. $SmI_2 = 10$ mM, $H_2O = 100$ mM, methylester = 500 mM, *n*-tributylamine = 80-200 mM. $T = 0.0 \pm 0.1$ °C. Rate Constant = 1.12 ± 0.09 $M^{-3}s^{-1}$.

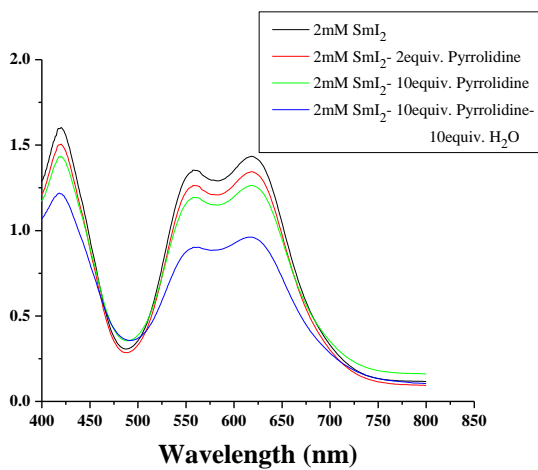


8.5.2.11 Plot of $\ln(k_{obs})$ vs $\ln[n\text{-tributylamine}]$. $SmI_2 = 10$ mM, $H_2O = 100$ mM, methylester = 500 mM, *n*-tributylamine = 100-200 mM. $T = 0.0 \pm 0.1$ °C. Rate Order = 1.63 ± 0.09 .

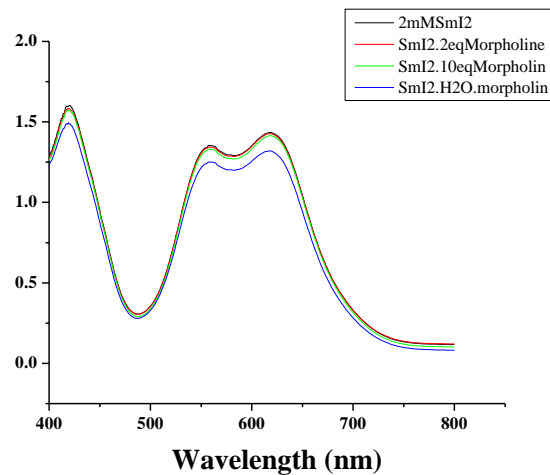
8.5.3 UV-Vis Spectra (SmI₂-H₂O-amine)



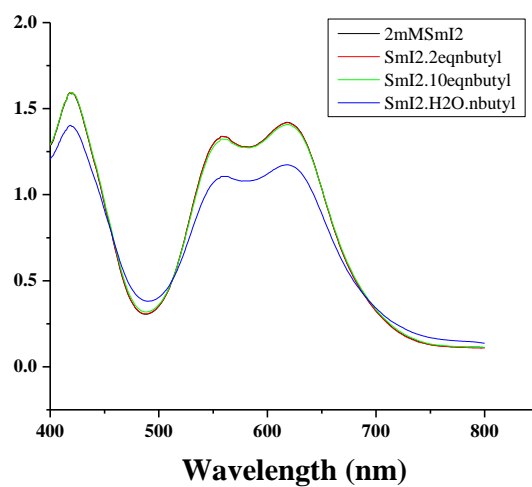
8.5.3.1 UV-Vis of SmI₂ with Et₃N and Et₃N-H₂O.



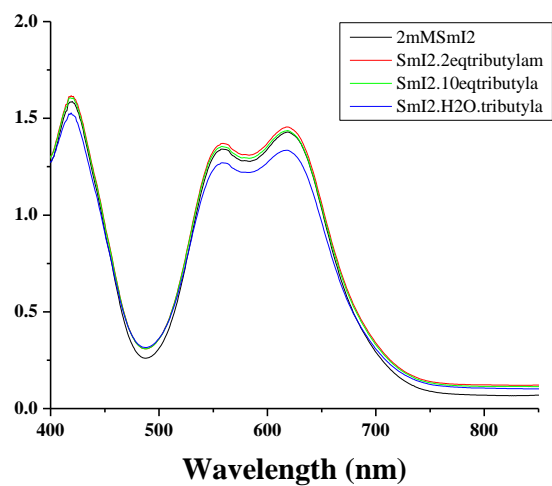
8.5.3.2 UV-Vis of SmI₂ with Pyrrolidine and Pyrrolidine-H₂O



8.5.3.3 UV-Vis of SmI_2 with Morpholine and Morpholine- H_2O



8.5.3.4 UV-Vis of SmI_2 with *n*butylamine and *n*butylamine- H_2O



8.5.3.5 UV-Vis of SmI₂ with *n* tributylamine and *n* tributylamine-H₂O

Kimberly Choquette

kachoquette@gmail.com

Lehigh University Chemistry Department
6 E. Packer Ave. Bethlehem, PA 18015
484-225-4300

Education

Lehigh University

PhD candidate, Department of Chemistry

Thesis: Samarium Diiodide: Mechanistic Investigation of Additives and Reactivity.

Advisor: Dr. Robert Flowers, II

Bethlehem, PA

2008-present

West Chester University

Bachelor of Science, Biochemistry

Independent research projects conducted with Dr. Moran and Dr. Ressler

West Chester, PA

2008

Honors and Awards

Lehigh University Hornor Fellowship

2012-2013

Lehigh University C. Scott Althouse Fellowship

2011-2012

Highlights

- Adept at probing organic reaction mechanisms through kinetic analysis
- Broad knowledge of organic and inorganic synthesis
- Skilled in working with extremely air sensitive reagents and reactions

Research Experience

Lehigh University Department of Chemistry

Advisor: Dr. Robert Flowers, II

Interaction and effect of additives on SmI₂-mediated reactions. 2008-present

- Identified, for the first time, underlying complex formation between alkyl halides and hexamethylphosphoramide (HMPA) which activates the C-H bond.
- Studied formation of Ni nano particles from single electron reduction of Ni(II) salts by SmI₂, allowing for a mild and fast *in situ* preparation of Ni(0) for inorganic catalysis.
- Collaborating with Dr. Procter (University of Manchester, UK) to obtain rate data for single electron reductions by SmI₂/H₂O system for a variety of functional groups.

Bethlehem, PA

- Mechanistic analysis of the roles of H₂O and amines when used in SmI₂ reductions.

West Chester Chemistry Department

West Chester, PA

Advisor: Dr. Michael Moran

Method development for organometallic synthesis.

January-May 2008

- Developed efficient, solvent-free "green" method of purifying tetrasulfur tetranitride, precursor to the electroactive polymer (SN)_x.
- Established new method for preparing ferrocene using only water and small amount of ordinary alcohol as solvents.

Advisor: Dr. Joel Ressler

Organic synthesis development and optimization

June-December 2006

- Explored simplifying elaborate two-step synthesis of classical Gabriel reaction into one pot-reaction.
- Developed technique for ball mill apparatus, maximizing reaction surfaces and improving reaction efficiency.

Techniques

NMR, GCMS, UV-Vis, React IR, CV, Stopped-flow spectroscopy, glove box, Schlenk line

Teaching Experience

Lehigh University

Bethlehem, PA

Advanced Organic Chemistry: Guest Lecturer

Spring, 2010

"Recent Developments in Domino Reactions". Presented background and current applications of Domino reactions in synthetic organic chemistry and its use in natural product and drug development synthesis. (Videotaped for continued use in distance education programs).

Chemical Equilibrium in Aqueous Systems: Teaching Assistant

2009-2010

Concepts, Models and Experiments I & II: Teaching Assistant

2008-2009

Mentored and trained graduate and undergraduate students

2008-present

Internship

Benchmark Analytics Environmental Testing Lab

Center Valley, PA

Radiological Chemistry Department

Summer 2007

- Rapid Gross Alpha testing on drinking water

Publications

Choquette, K.A.; Flowers, R.A., II "Samarium and Ytterbium Reagents" In *Comprehensive Organic Synthesis*, 2nd Ed., Pergamon Press: Oxford. (In press)

"Preparation and Use of Samarium Diiodide (SmI₂) in Organic Synthesis: The Mechanistic Role of HMPA and Ni(II) Salts in the Samarium Barbier Reaction" Choquette, K.A.; Sadasivam, D.V.; Flowers, R.A., II. *J. Vis. Exp.* (72), e4323, doi:10.3791/4323 (2013).

"Study on the coupling of acyclic esters with alkene - the synthesis of 2-(2-hydroxyalkyl) cyclopropanols *via* cascade cyclization using allylsamarium bromide" Yawei Tu, Y.; Zhou, L.; Yin, R.; Lv, X.; Flowers, R.A. II.; Choquette, K.A.; Liu, H.; Niua, Q.; Wang, X. *Chem. Comm.* **2012**, 48, 11026-11028.

"Effect of Crown Ethers on the Ground and Excited State Reactivity of Samarium Diiodide in Acetonitrile" Maity, S.; Choquette, K.A.; Flowers, R.A. II; Prasad, E. *J. Phys. Chem. A.* **2012**, 116, 2154-2160.

"Catalytic Ni(II) In Reaction of SmI₂: Sm(II)- or Ni(0)- Based Chemistry?" Choquette, K.A.; Sadasivam, D.V.; Flowers, R.A., II. *J. Am. Chem. Soc.*, **2011**, 133, 10655-10661.

"Uncovering the Mechanistic Role of HMPA in the Samarium Barbier Reaction" Choquette, K.A.; Sadasivam, D.V.; Flowers, R.A., II. *J. Am. Chem. Soc.*, **2010**, 132, 17396-17398.

Presentations

"Mechanistic Study of Ester Reduction by SmI₂-H₂O-Amine"
2012 ACS National Meeting and Exposition. Philadelphia, PA August 2012

"Mechanistic Investigation of the Role of HMPA in the Samarium Barbier Reaction"
2012 Division of Organic Chemistry Graduate Research Symposium. Bolder, CO
Selected Presenter July 2012

"Investigation of Alkyl Halide and HMPA Complex Formations"
Division of Organic Chemistry Symposium Poster Session. Princeton, NJ.
June 2011

"Catalytic Ni(II) with SmI₂: Expanding Traditional Samarium Chemistry"
2011 ACS National Meeting and Exposition. Anaheim, CA. March 2011

"Kinetic and Mechanistic Study of the Samarium Barbier Reaction"
Lehigh University College of Arts and Sciences Student Research Poster Session. March 2009

References

Dr. Robert Flowers, II (PhD committee chair)
Chair, Department of Chemistry, Lehigh University
(610) 758-4048
Rof2@lehigh.edu

Dr. Ned Heindel (PhD committee member)
Howard S. Bunn Professor of Chemistry, Lehigh University
(610) 758-3464
Ndh0@lehigh.edu

Dr. Michael Moran
Associate Professor Department of Chemistry, West Chester University
(610) 436-2975
Mmoran@wcupa.edu